

# Sheffield Hallam University

*Transport properties of micellar solutions and microemulsions.*

BOSTOCK, Theresa A.

Available from the Sheffield Hallam University Research Archive (SHURA) at:

<http://shura.shu.ac.uk/19372/>

## A Sheffield Hallam University thesis

This thesis is protected by copyright which belongs to the author.

The content must not be changed in any way or sold commercially in any format or medium without the formal permission of the author.

When referring to this work, full bibliographic details including the author, title, awarding institution and date of the thesis must be given.

Please visit <http://shura.shu.ac.uk/19372/> and <http://shura.shu.ac.uk/information.html> for further details about copyright and re-use permissions.

POLYTECHNIC LIBRARY  
POND STREET  
SHEFFIELD S1 1WB

6833

7925307013



**Sheffield City Polytechnic  
Eric Mensforth Library**

**REFERENCE ONLY**

This book must not be taken from the Library

PL/26

R5193

ProQuest Number: 10694253

All rights reserved

INFORMATION TO ALL USERS

The quality of this reproduction is dependent upon the quality of the copy submitted.

In the unlikely event that the author did not send a complete manuscript and there are missing pages, these will be noted. Also, if material had to be removed, a note will indicate the deletion.



ProQuest 10694253

Published by ProQuest LLC (2017). Copyright of the Dissertation is held by the Author.

All rights reserved.

This work is protected against unauthorized copying under Title 17, United States Code  
Microform Edition © ProQuest LLC.

ProQuest LLC.  
789 East Eisenhower Parkway  
P.O. Box 1346  
Ann Arbor, MI 48106 – 1346

TRANSPORT PROPERTIES OF MICELLAR SOLUTIONS  
AND MICROEMULSIONS

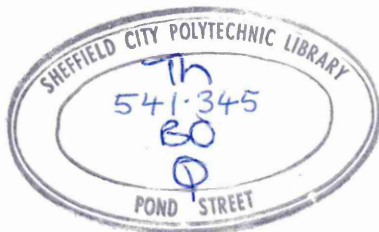
THERESA A. BOSTOCK

Submitted in partial fulfilment of the  
requirements for the degree of Doctor of  
Philosophy awarded by the C.N.A.A.

Sponsoring Establishment :  
Sheffield City Polytechnic

Collaborating Establishment :  
Unilver Research

August 1981.



7925307-01

## ABSTRACT

### TRANSPORT PROPERTIES OF MICELLAR SOLUTIONS AND MICROEMULSIONS

BY THERESA A. BOSTOCK

Binary nonionic surfactant-water systems were studied prior to the more complex nonionic surfactant-water-oil systems. Phase diagrams were determined for the tetraoxyethylene dodecylether ( $C_{12}E_4$ )-water and the Brij 30-water systems; the available hexaoxyethylene dodecylether ( $C_{12}E_6$ )-water phase diagram was confirmed.

Conductivity measurements were made in the isotropic liquid regions of these systems and self-diffusion measurements were made in the isotropic liquid regions of the  $C_{12}E_4$ -water and  $C_{12}E_6$ -water systems, in order to elucidate the structures of these regions. Self-diffusion measurements were made by the NMR spin-echo method with a pulsed field gradient using the nucleus  $^1H$ . The results indicated that the surfactant is aggregated and water plus oxyethylene chains form the continuum up to 100% surfactant.

Phase diagrams were determined for the  $C_{12}E_4$ - $H_2O$ -heptane system and the Brij 30- $H_2O$ -hexane system. Conductivity measurements were made in the isotropic liquid regions. The existence of both water-continuous and oil-continuous isotropic liquid regions is confirmed. The possibility of a percolation mechanism leading to high conductivities in oil-continuous samples is discussed as is phase inversion within the isotropic liquid region, at low water content. The effect of different hydrocarbons on the phase behaviour at low surfactant content was studied by means of phase diagrams and conductivity measurements. The conductivity results at low surfactant content are interpreted in terms of water-continuous and oil-continuous structures and also bicontinuous structures via which phase inversion can occur.

Phase diagrams were determined for  $C_{12}E_4$ - $H_2O$ -triacetin and Brij 30- $H_2O$ -triacetin. The differences between these systems and those with heptane and hexane as third components are explained on the basis of the different structure and polarity of the triacetin molecule.

## CONTENTS

Page No.

1.	INTRODUCTION	1
1.1	The interaction of polyoxyethylene alkyl ethers with water	1
1.1.1	Solubility of the oxyethylene chain in water	1
1.1.2	Micelle formation	1
1.1.3	Cloud point	2
1.1.4	Liquid crystal formation	5
1.2	Emulsions formed by polyoxyethylene alkyl ethers	5
1.2.1	The stability of the emulsions	5
1.2.2	Phase inversion temperature (PIT)	6
1.3	Microemulsions	9
1.3.1	History	9
1.3.2	Uses of microemulsions	9
1.3.3	Types of microemulsion	11
1.3.4	The occurrence of microemulsions formed by polyoxyethylene alkyl ethers	12
1.3.4.1	Solubilization	12
1.3.4.2	Effects of changes in the nonionic surfactant	18
1.3.4.3	Effects of different hydrocarbons	19
1.3.4.4	Triglycerides as the third component	21
1.4	The nature of microemulsions	22
1.4.1	The term microemulsion	22
1.4.2	Solubilized micellar systems	23
1.4.3	Formation of microemulsions	24
1.4.4	Negative interfacial tension	24
1.4.5	Theoretical aspects	26
1.4.6	Particle shape	29
1.4.7	Bicontinuous structures	30
1.4.8	Critical phenomena and metastability	32

1.5	Physical properties and physical methods of investigation	34
1.5.1	Light scattering	34
1.5.2	Viscosity	35
1.5.3	Ultra centrifugation measurements	38
1.5.4	High resolution NMR	39
1.5.5	Self-diffusion	41
1.5.6	Electrical conductivity	43
1.5.7	Percolation	51
1.6	A Summary of microemulsions and the programme of work	58
1.6.1	Summary	58
1.6.2	The proposed programme of work	60
2.	<u>THEORY</u>	63
2.1	Conductivity theory	63
2.1.1	Introduction	63
2.1.2	Conductivity of emulsions	63
2.1.3	Percolation	66
2.2	Self-diffusion measurements	69
2.2.1	Introduction	69
2.2.2	The NMR magnetic-field-gradients, spin-echo experiment	70
2.3	The phase rule	77
3.	<u>EXPERIMENTAL</u>	81
3.1	Materials	81
3.2	Apparatus	81
3.3	The conductance cells	82
3.3.1	The copper cell	82
3.3.2	The platinum cell	84
3.3.3	The standard cell	87

3.4	Determination of phase diagrams	87
3.4.1	Determination of phase diagrams for systems containing Brij 30	87
3.4.2	Determination of phase diagrams for systems containing $C_{12}E_4$ and $C_{12}E_6$	89
3.5	Conductance measurements	91
3.5.1	Conductance measurements with the copper cell	91
3.5.2	Conductance measurements with the platinum cells	92
3.6	Pulsed NMR measurements	94
3.7	Determination of tie lines	96
3.8	Investigation of water soluble impurities in Brij 30	98
3.9	Determination of the sodium in Brij 30	98
4.	<u>RESULTS</u>	100
4.1	Phase diagrams	100
4.1.1	The $C_{12}E_4$ - $H_2O$ phase diagram	102
4.1.2	The $C_{12}E_6$ - $H_2O$ phase diagram	103
4.1.3	The Brij 30- $H_2O$ phase diagram	103
4.1.4	The $C_{12}E_4$ - $H_2O$ -hydrocarbon systems	104
4.1.5	The Brij 30- $H_2O$ -hexane system	106
4.1.6	The $C_{12}E_4$ - $H_2O$ -triacetin system	107
4.2	Conductivity	107
4.2.1	The cell constants	107
4.2.2	Sources of error	109
4.3	High resolution NMR	111
4.4	Viscosity	112
4.5	Self-diffusion	112
4.6	Tie lines	113
4.7	Impurities in Brij 30	113
4.7.1	Sodium in Brij-30	113

4.7.2	Water soluble impurities in Brij 30	113
	<u>FIGURES</u>	114
	<u>TABLES</u>	172
5.	<u>DISCUSSION</u>	193
5.1	Surfactant-water systems	193
5.1.1	$C_{12}E_6$ -Water	193
5.1.1.1	The phase diagram	193
5.1.1.2	Conductivity	194
5.1.1.3	Self-diffusion in the $C_{12}E_6$ - $H_2O$ system	199
5.1.2	$C_{12}E_4$ -water	208
5.1.2.1	The phase diagram	208
5.1.2.2	Conductivity in the $C_{12}E_4$ - $H_2O$ system	209
5.1.2.3	Self-diffusion in the $C_{12}E_4$ - $H_2O$ system	216
5.1.3	Brij 30 - water	221
5.1.3.1	The phase diagram	221
5.1.3.2	Conductivity	221
5.1.3.3	Viscosity in the Brij system	224
5.1.4	Conclusions concerning the $C_{12}E_n$ -water systems	225
5.2	Surfactant-hydrocarbon systems	230
5.2.1	$C_{12}E_4$ -heptane	230
5.2.1.1	The phase diagram	230
5.2.1.2	Conductivity in the $C_{12}E_4$ -heptane system	231
5.2.2	Brij 30 - hexane	232
5.2.2.1	The phase diagram	232
5.2.2.2	Conductivity in the Brij-hexane system	232
5.3	Surfactant-water-hydrocarbon systems	233

5.3.1	$C_{12}E_4$ -H <sub>2</sub> O-heptane	233
5.3.1.1	The phase diagram	233
	The $\alpha$ -region	233
	The $\delta$ -region	234
	The $\gamma$ -region	236
	The $\epsilon$ -region	236
	The $\zeta$ -region	237
5.3.1.2	Conductivity in the $C_{12}E_4$ -H <sub>2</sub> O-heptane system	238
	The $\delta$ -region	238
	The $\gamma$ -region	240
	The $\epsilon$ -region	254
	The $\zeta$ -region	255
5.3.2	Water-hydrocarbon mixtures with added surfactant $C_{12}E_4$ -water-heptane	256
5.3.2.1	The phase diagram	256
5.3.2.2	The conductivity of samples 7 and 11 in the $C_{12}E_4$ -H <sub>2</sub> O-heptane system	257
5.3.3	Water-hydrocarbon mixtures with added surfactant- $C_{12}E_4$ -water-n-decane	260
5.3.3.1	The phase diagram	260
5.3.3.2	The conductivity of samples of 60% n-decane 40% water plus $C_{12}E_4$	262
5.3.4	Water-hydrocarbon mixtures with added surfactant- $C_{12}E_4$ -water-n-hexadecane	263
5.3.4.1	The phase diagram	263
5.3.4.2	The conductivity of samples of 60% water-40% n-hexadecane plus $C_{12}E_4$	263
5.3.5	The importance of the hydrocarbon in the formation of bicontinuous structures in ternary systems	267
5.3.6	The Brij-30-H <sub>2</sub> O-hexane and heptane systems	269
5.3.6.1	The phase diagram of Brij 30 - H <sub>2</sub> O - hexane	269

5.3.6.2	The phase diagram of the Brij 30-H <sub>2</sub> O-heptane system	271
5.3.6.3	Conductivity in the Brij 30-H <sub>2</sub> O-hexane system	272
5.4	Surfactant-triacetin systems	278
5.4.1	C <sub>12</sub> E <sub>4</sub> -triacetin	278
5.4.2	Brij 30 - triacetin	278
5.5	Surfactant-water-triacetin systems	279
5.5.1	C <sub>12</sub> E <sub>4</sub> -H <sub>2</sub> O-triacetin	279
	The $\alpha$ -region	279
	The $\gamma$ -region	281
	The $\epsilon$ -region	282
	The $\delta$ -region	283
5.5.2	The Brij 30-H <sub>2</sub> O-triacetin system	284
	The $\gamma$ -region	284
	The $\zeta$ -region	285
	The $\alpha$ -, $\delta$ -, and $\epsilon$ -regions	286
5.6	<u>CONCLUSIONS</u>	287
	<u>REFERENCES</u>	

## ABSTRACT

### TRANSPORT PROPERTIES OF MICELLAR SOLUTIONS AND MICROEMULSIONS

BY THERESA A. BOSTOCK

Binary nonionic surfactant-water systems were studied prior to the more complex nonionic surfactant-water-oil systems. Phase diagrams were determined for the tetraoxyethylene dodecylether ( $C_{12}E_4$ )-water and the Brij 30-water systems; the available hexaoxyethylene dodecylether ( $C_{12}E_6$ )-water phase diagram was confirmed. Conductivity measurements were made in the isotropic liquid regions of these systems and self-diffusion measurements were made in the isotropic liquid regions of the  $C_{12}E_4$ -water and  $C_{12}E_6$ -water systems, in order to elucidate the structures of these regions. Self-diffusion measurements were made by the NMR spin-echo method with a pulsed field gradient using the nucleus  $^1H$ . The results indicated that the surfactant is aggregated and water plus oxyethylene chains form the continuum up to 100% surfactant.

Phase diagrams were determined for the  $C_{12}E_4$ - $H_2O$ -heptane system and the Brij 30- $H_2O$ -hexane system. Conductivity measurements were made in the isotropic liquid regions. The existence of both water-continuous and oil-continuous isotropic liquid regions is confirmed. The possibility of a percolation mechanism leading to high conductivities in oil-continuous samples is discussed as is phase inversion within the isotropic liquid region, at low water content. The effect of different hydrocarbons on the phase behaviour at low surfactant content was studied by means of phase diagrams and conductivity measurements. The conductivity results at low surfactant content are interpreted in terms of water-continuous and oil-continuous structures and also bicontinuous structures via which phase inversion can occur.

Phase diagrams were determined for  $C_{12}E_4$ - $H_2O$ -triacetin and Brij 30- $H_2O$ -triacetin. The differences between these systems and those with heptane and hexane as third components are explained on the basis of the different structure and polarity of the triacetin molecule.

## 1. INTRODUCTION

The nonionic surfactants which will be discussed here are the polyoxethylene alkyl ethers,  $C_n H_{2n+1} (OCH_2 CH_2)_m OH$ , which will be abbreviated to  $C_n E_m$ .

### 1.1 THE INTERACTION OF POLYOXYETHYLENE ALKYL ETHERS WITH WATER

#### 1.1.1 SOLUBILITY OF THE OXYETHYLENE CHAIN IN WATER

The structure of the molecule renders it amphiphilic in nature, the hydrocarbon chain being soluble in oil whilst the oxyethylene chain is soluble in water. The solubility in water of the oxyethylene chain is partly explained by hydrogen bonding to the ether oxygens (1) That other factors are involved is indicated by the lower solubility of corresponding polyoxymethylene compounds (2). It has been suggested (1) that there is a relationship between the helical conformation of the oxyethylene chain in water and the structure of the water itself, which may partly explain this high solubility. Other authors have suggested that the oxyethylene chain exists in water as interrupted helices (3) or in a randomly coiled configuration (4); this does not necessarily preclude a relationship between the solubility and the water structure.

#### 1.1.2 MICELLE FORMATION

These surfactants only exist as monomer solutions in water at very low concentrations: the critical micelle concentrations (cmc's) are very low.  $C_{12}E_7$  has a cmc of  $5 \times 10^{-5} \text{ mol dm}^{-3}$ . Above the cmc there is aggregation of the surfactant to form micelles, the hydrophobic

### 1.1.2 Cont'd.

hydrocarbon chains forming the interiors of the micelles.

When the surfactant molecules have come together to form micelles, the oxyethylene chains will be hydrated; a maximum of two water molecules will be hydrogen bonded to each ether oxygen; close to the hydrocarbon core geometrical constraints may reduce the number of hydrogen bonded water molecules to well below the theoretical maximum. In addition water molecules will be trapped between the oxyethylene chains and this will be greater the longer the oxyethylene chains. For a range of commercial surfactants, from  $C_{16}E_{17}$  to  $C_{16}E_{63}$ , the micellar hydration has been reported to vary from 5.2 to 10.6 water molecules per ether oxygen (5). Schott reports that the number of water molecules per ether linkage varies from 0.4 to 6.3 (6).

These micelles are not necessarily spherical. Tanford et al (4) have concluded that a disklike shape is in agreement with experimental evidence and theoretical predictions for the  $C_{12}E_m$  series where m ranges from 8 to 23. For surfactants with very long oxyethylene chains (eg  $C_{16}E_{63}$  and  $C_{16}E_{44}$ ) a spherical shape is possible.

### 1.1.3 CLOUD POINT

When a dilute aqueous micellar solution of a nonionic surfactant of this type, is heated, a point comes when the hydrogen bonding of the oxyethylene chains is in-

### 1.1.3 Cont'd.

sufficient to maintain the stability of a single phase. The system clouds as it separates into two phases and the temperature at which this occurs is known as the "cloud point." Although the cloud point is frequently quoted for a 1% solution, the phenomenon occurs over a range of concentrations above the cmc.

The currently held view is that on approach to the cloud point secondary aggregation of small micelles occurs (8); at the cloud point water containing surfactant below the cmc separates from the secondarily aggregated system; this surfactant-rich phase still contains a very large proportion of water (as much as 97% in some cases).

The cloud point depends on concentration and also on the lengths of the hydrocarbon and oxyethylene chains. For a given hydrocarbon chain length the longer the oxyethylene chain the higher the temperature required to reduce the hydrophilic properties of the molecule sufficiently for phase separation to occur and hence the higher the cloud point.

Some systems such as the  $C_{12}E_5-H_2O$  system (Fig. 1.1) cloud then clear again at a higher temperature before clouding a second time. This phenomenon is referred to as a "double cloud point."

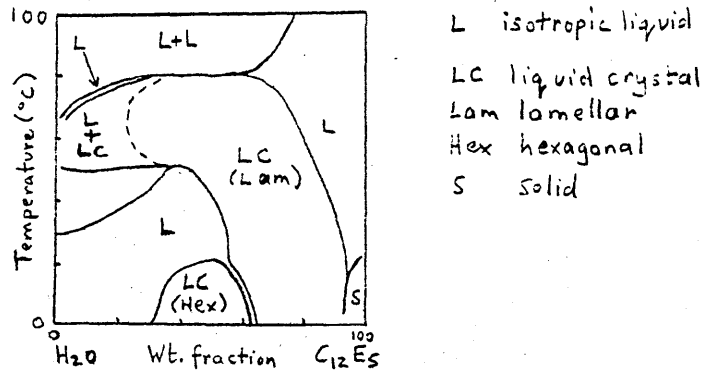


Fig. 1.1. The phase diagram of  $C_{12}E_5-H_2O$ . (from ref.7).

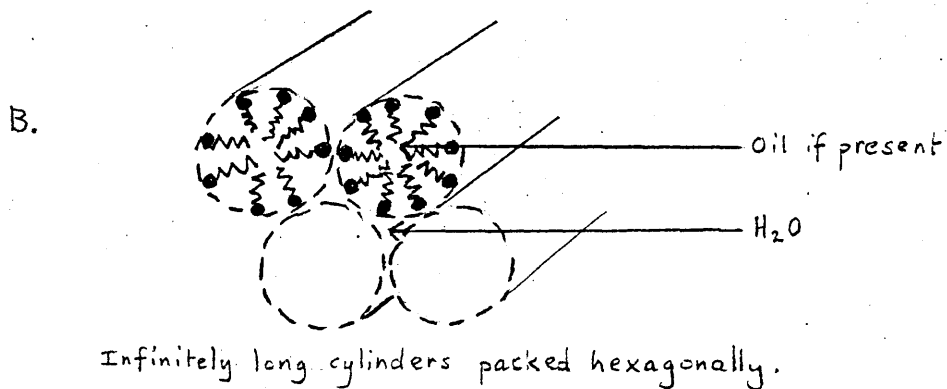
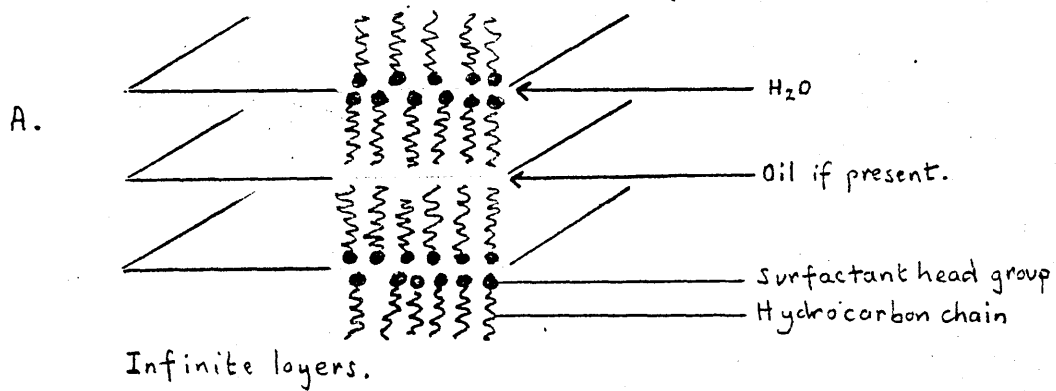


Fig. 1.2. Lamellar (A) and hexagonal (B) liquid crystals.

#### 1.1.4 LIQUID CRYSTAL FORMATION

At higher concentrations in water the polyoxyethylene alkyl ethers form liquid crystals over appreciable ranges of composition and temperature. In the series  $C_{12}E_3$ - $C_{12}E_8$  hexagonal, lamellar and viscous isotropic liquid crystalline phases occur to varying extents (9). Fig. 1.1 shows the hexagonal and lamellar phases in the  $C_{12}E_5$ - $H_2O$  system. It has since been shown that the isotropic region occurring between the hexagonal and lamellar phases is a viscous isotropic liquid crystalline phase (10).

Hexagonal and lamellar phases are birefringent and their structures are well-defined (Fig. 1.2). The viscous isotropic phase has a high viscosity and is not birefringent (hence the name); the structure is not well-defined and the term viscous isotropic phase covers more than one type of structure (9).

### 1.2 EMULSIONS FORMED BY POLYOXYETHYLENE ALKYL ETHERS

#### 1.2.1 THE STABILITY OF THE EMULSIONS

An emulsion is a system of one liquid phase dispersed in another liquid phase which is thermodynamically unstable and will separate into two phases, albeit in some cases extremely slowly.

Surface active agents stabilize emulsions by forming a surface monolayer on the emulsion droplets which

### 1.2.1 Cont'd.

presents a barrier to coalescence. In the case of ionic surface active agents stabilizing oil-in-water (O/W) emulsions the droplets are charged and so there is an electrical force of repulsion opposing coalescence of the droplets. The stability of emulsions stabilized with nonionic surface active agents has been ascribed to some sort of mechanical barrier opposing coalescence imposed by heavily hydrated polyoxyethylene chains or by the formation of a liquid crystal, either as a layer around the droplet itself or by the coming together of surfactant layers when two droplets approach. Becher and Tahara (11) have found that the droplets of O/W emulsions made using mixtures of the commercial surfactants Span 60 and 80 and Tween 60 and 80 are charged. The emulsifiers were used without further purification. No details of possible impurities are given, and hence no indication of any part they might play in producing a charge. The explanation given of the charge, is that it is due to hydrogen-bonding at the ether oxygens of the polyoxyethylene chains and subsequent ionisation of a number of these hydrogen-bonded water molecules to give oxonium ions and hydroxide ions.

### 1.2.2 PHASE INVERSION TEMPERATURE (PIT)

A hydrocarbon, non-ionic surfactant, and water can be mixed to form an O/W emulsion at a low temperature,

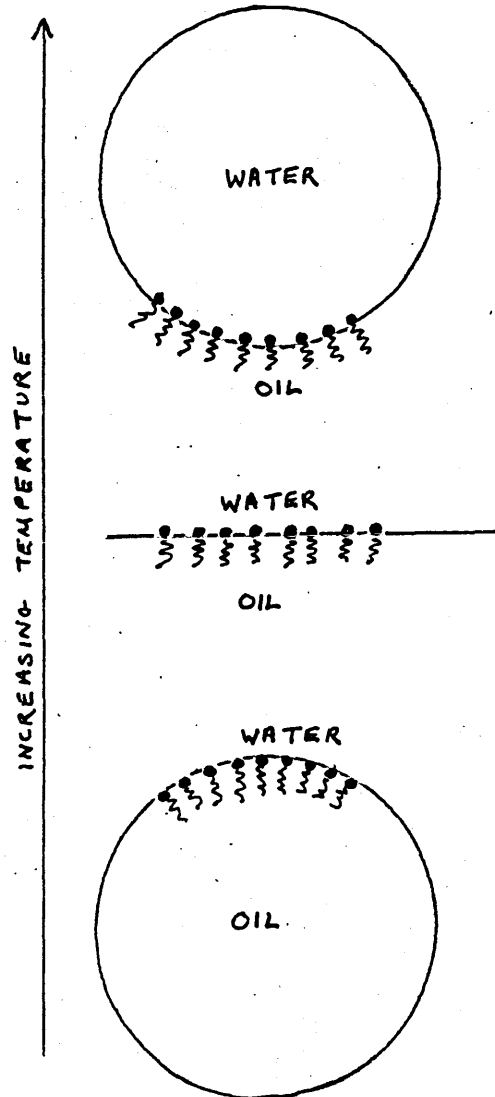


Fig. 1.3. Phase inversion.

### 1.2.2 Cont'd.

the actual temperature depending on the surfactant and also the hydrocarbon used. Initially the surfactant monolayer surrounding the hydrocarbon droplets is convex towards the water (Fig. 1.3). As the temperature is increased the hydrophilicity of the surfactant is reduced. The curvature of the surfactant monolayer decreases, until the surfactant layer becomes planar when the hydrophilic and oleophilic tendencies balance, at which point the surface areas occupied by the hydrocarbon and oxyethylene chains are equal. Above this temperature the surfactant layer becomes concave towards the water and convex towards the oil, the hydrophilic tendency now being weaker. A water in oil (W/O) emulsion results. Mixing may be required to prevent phase separation. The temperature at which the surfactant layer becomes planar and the emulsion changes from O/W to W/O is known as the "Phase inversion temperature" (PIT).

Various factors affect the PIT (12,13):

- i) The surfactant itself - the relative lengths of the hydrocarbon and oxyethylene chains and in the case of a commercial surfactant the oxyethylene chain length distribution,
- ii) the concentration of the surfactant,
- iii) the nature of the oil e.g. whether it is an aliphatic or aromatic hydrocarbon.
- iv) the ratio of the oil phase to the water phase,
- v) the presence of additives or impurities in the three components.

### 1.2.2 Cont'd.

Since the PIT depends on the surfactant (i) it is related to the cloud point: the PIT increases with increasing surfactant cloud point (12).

## 1.3 MICROEMULSIONS

### 1.3.1 HISTORY

The term "microemulsion" was first used by Schulman in 1959 (14) to describe a transparent, isotropic system obtained from an emulsion of hydrocarbon and water stabilized by a soap, by the addition of an alcohol of medium chain length, such as pentanol. Systems of this type, containing high percentages of both oil and water with a smaller percentage of emulsifier mixture, but remaining transparent or translucent had been known for many years as commercial preparations (15) such as self-polishing floor waxes and stable cutting oil emulsions for machine tools. Schulman had observed the systems which he later came to call microemulsions as early as 1943 (16);

### 1.3.2 USES OF MICROEMULSIONS

One of the attractions of microemulsions commercially is their stability, which may be measured in years and is generally much greater than that of conventional emulsions, although they can contain large proportions of the "disperse" phase. Pharmaceutical preparations,

### 1.3.2. Cont'd.

domestic and industrial cleaners and dry-cleaning fluids may be microemulsions (17). Microemulsions are of interest commercially not only because of their present uses but because of their potential uses which include oil extraction (18,19). After the primary drilling when oil comes to the surface under its own pressure the well may be flushed with water; a considerable amount of oil still remains in the rock - estimates suggest a third of the total quantity. Injection of a suitably chosen microemulsion into the reservoir can result in the extraction of a significant quantity of the remaining oil.

Microemulsions may be used in catalysis to bring water soluble substances into closer contact with oil soluble substances and as a means of adding water soluble substances to petrol and diesel fuel in order to improve combustion so as to reduce knock and to reduce pollution (19). Where mixtures of surfactants, water and lipids occur in industrial processes and effluents, it is important to determine the extent to which microemulsions are formed in these mixtures. Perhaps one of the most obvious uses for microemulsions is in detergency where their occurrence and stability is important for soil removal and prevention of redeposition.

### 1.3.3 TYPES OF MICROEMULSION

Microemulsions may be divided into two classes according to the emulsifier used. One class is that into which Schulman's microemulsions fall: an ionic surfactant is used with a cosurfactant, normally a medium chain length alcohol such as pentanol. Such microemulsions require relatively large quantities of emulsifier: as much as 25% by weight for one of Schulman's systems, though this can be reduced by careful choice of surfactant and cosurfactant to about 15% for a water: hydrocarbon ratio of 1:1 (20). These microemulsions also have large stability ranges versus temperature. Nonionic surfactants give rise to a second class of microemulsions. Large amounts of both water and hydrocarbon can exist as a microemulsion with the addition of much smaller amounts of surfactant, about 5% by weight (19,20), but the range of temperature over which these systems are stable is small. Polyoxyethylene alkyl ethers are the nonionic surfactants commonly used. 1-propanol and 2-propanol not normally regarded as emulsifiers have been found to produce microemulsions with hexane and water in the absence of other emulsifiers (21). Microemulsions have also been produced using mixtures of nonionic surfactants with small amounts of ionic surfactants (22).

Within these broad classes the microemulsions may be oil-continuous or water-continuous, or of an as yet indeterminate structure (see section 1.4.7)(1).

### 1.3.4 THE OCCURRENCE OF MICROEMULSIONS FORMED BY POLYOXYETHYLENE ALKYL ETHERS

#### 1.3.4.1. SOLUBILIZATION

Organic compounds that are insoluble or sparingly soluble in water can often be dissolved in an aqueous solution of a suitable surfactant. This phenomenon is known as solubilization. Below the cmc there is little or no uptake of solubilizate indicating that uptake depends on the micelles. In the case of nonionic surfactant micelles there are three possible modes of incorporation of solubilizate into micelles (Fig. 1.4) Non polar molecules are located in the micellar core where the hydrocarbon chains of the surfactant form the solvent; paraffins fall into this category. Amphiphilic molecules, such as long chain alcohols, are located in the micelle in such a way as to allow the hydrocarbon chain to mingle with the other hydrocarbon chains in the core, whilst the more hydrophilic group, such as the OH group, protrudes into the polyoxyethylene outer layer. A third group of substances which have an affinity for polyoxyethylene may be located in the outer layer of the micelle amongst the hydrated polyoxyethylene chains. Phenols fall into this category and have been shown to form complexes with polyethylene glycol, probably by binding of the phenolic hydroxy group with an ether oxygen of the polyoxyethylene (23).

Of particular interest here are hydrocarbons. Fig.1.5

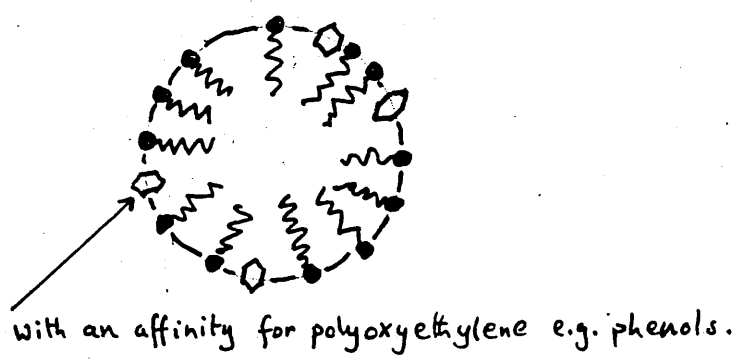
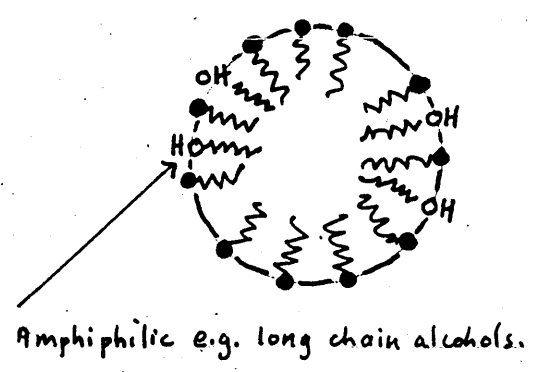
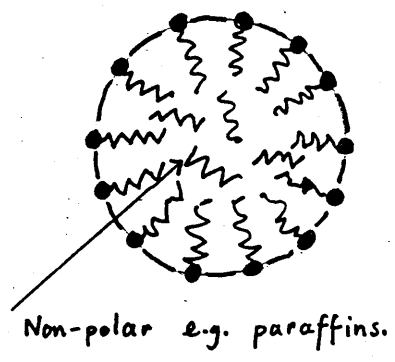


Fig. 1.4. The location of the solubilize in micelles.

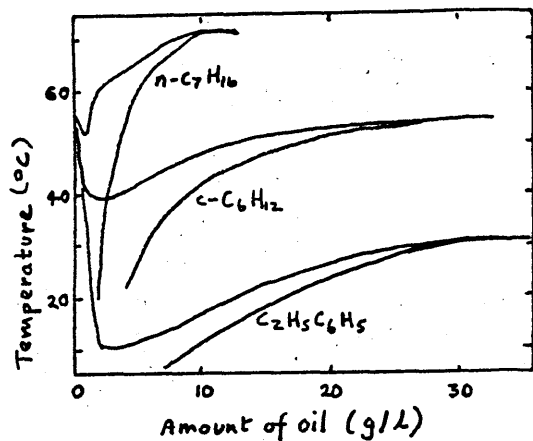


Fig. 1.5. The solubilization of n-heptane, cyclohexane, and ethylbenzene in 1% aqueous solution of polyoxyethylene (9.7) nonylphenyl ether. The upper boundary is the cloud point; the lower boundary is the solubilization end point. (from ref.24).

D denotes surfactant rich phases.

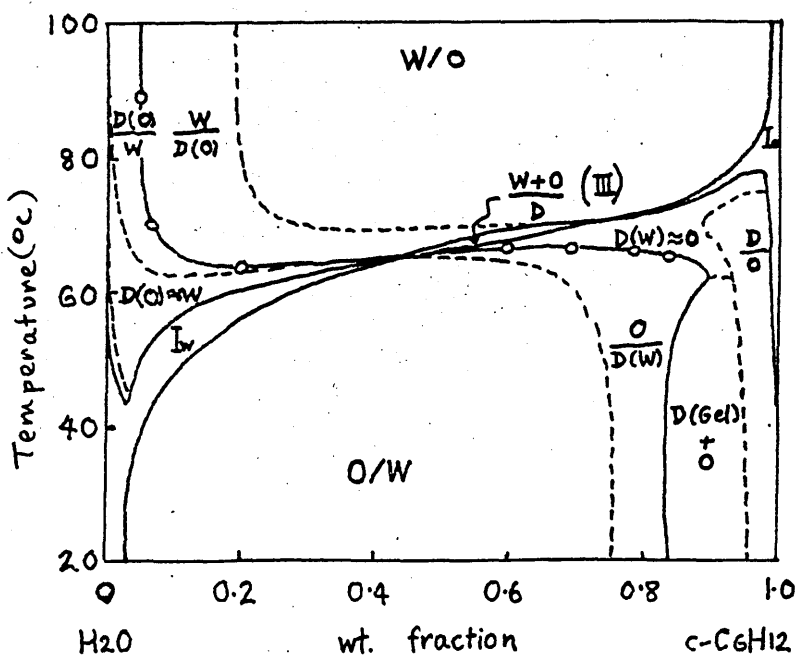


Fig. 1.6. The effect of temperature and composition on the dispersion types of the system composed of water, cyclohexane and polyoxyethylene(9.7) nonylphenylether (7 wt% system). (from ref.26).

#### 1.3.4.1. Cont'd.

shows the effect of adding small amounts of different hydrocarbons to a 1% aqueous solution of polyoxyethylene (9.7) nonylphenyl ether. For n-heptane there is a small (about 3°C) initial decrease in the cloud point on adding heptane, followed by a sharp rise; for ethylbenzene the decrease is large (about 45°C) and the subsequent increase gradual; cyclohexane produces an intermediate effect (24). The difference in behaviour between the straight chain aliphatic and the aromatic hydrocarbon may be due to the fact that the aromatic hydrocarbon is more polarisable and can be partly solubilized in the polyoxyethylene shell as well as in the core of the micelle.

Close to the cloud point the solubilization may increase considerably (Figs. 1.5 and 1.6) and where appreciable quantities of hydrocarbon are solubilized the system may be termed a microemulsion. Similarly the hydrocarbon solution of the nonionic surfactant may solubilize water; this solubilization increases near the haze point (equivalent to the cloud point in aqueous solution). Maximum solubilization occurs at a higher temperature than in aqueous solution. Again the highly solubilized system may be termed a microemulsion (24,25). As can be seen from Fig. 1.6 for a given surfactant at a given concentration, the maximum solubilization of hydrocarbon (water) in aqueous (hydrocarbon) solution, occurs over a very narrow temperature range.

#### 1.3.4.1. Cont'd.

Fig. 1.6 shows the phases present in the two and three phase regions, in addition to the isotropic liquid phases of the micellar solutions and microemulsions. It is clear that the maximum solubilization i.e. the microemulsion formation, occurs in the region of the phase inversion temperature.

In the system polyoxyethylene (9.7) nonyl phenylether (7% bywt), water and cyclohexane, at low cyclohexane content and above the cloud point, two phases exist - water containing surfactant below the cmc and a phase richer in surfactant and containing some cyclohexane known as the surfactant phase. At high cyclohexane content, below the microemulsion region oil (containing a small amount of surfactant) separates from a phase richer in surfactant and containing some water, also known as the surfactant phase. This phase richer in surfactant can dissolve large amounts of both water and cyclohexane. In the central three phase region the phases are water, oil and surfactant phase. Fig. 1.7 shows schematically the effect of temperature on the volume fractions of water, oil and surfactant phases for a system composed of equal quantities (by wt.) of water and oil plus a small percentage of surfactant (e.g. water plus cyclohexane plus 3% by wt. of polyoxyethylene (8.6) nonylphenylether)(27). It can be seen that the low temperature water phase changes continuously to the surfactant phase which then changes continuously

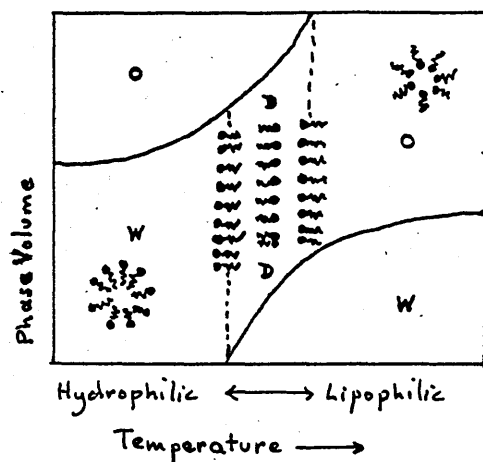


Fig. 1.7. Schematic diagram of water, surfactant (D), and oil phases after the complete phase separation of the system composed of equal quantities (by wt.) of water and cyclohexane plus 3% by wt. of polyoxyethylene(8.6) nonylphenyl ether. The phase inversion region is exaggerated. (from ref.27).

#### 1.3.4.1. Cont'd.

to the oil phase at high temperature, and that this change occurs in the region of the phase inversion temperature. The surfactant phase in the three phase region contains large amounts of both oil and water.

The phase diagrams of many polyoxyethylene alkyl ether-water-hydrocarbon systems are similar to that shown in Fig. 1.6 for surfactant concentrations in the range 0-10% (24). They are shifted to higher or lower temperature according to the PIT of the system.

#### 1.3.4.2. EFFECTS OF CHANGES IN THE NONIONIC SURFACTANT

For optimum solubilization at a given temperature the surfactant chosen should have a hydrocarbon:oxyethylene chain length ratio such that solubilization is taking place close to the PIT with the oil in question.

Solubilization is larger when the nonionic surfactant is pure than when the distribution of hydrophilic chain length is broad as in a commercial material (20). As the oxyethylene chain length distribution becomes sharper solubilization is increased.

A greater degree of solubilization is obtained with a nonionic surfactant having a larger hydrocarbon chain. If a surfactant with a longer hydrocarbon chain is used and solubilization is required at a specific temperature then the oxyethylene chain length also needs to be longer in order to keep the PIT constant (28). In order to act

#### 1.3.4.2. Cont'd.

as a solubilizer a surfactant has finally to be in micellar form in solution, so that the hydrophilic group of the surfactant must have a certain minimum size, which will depend on the size and characteristics of the hydrophobic group. Within this limit, a surfactant, of which the hydrophilic portion is smaller, seems more efficient for solubilizing hydrocarbons (24). For example, in 1% aqueous solutions of polyoxyethylene (n) nonyl phenyl ethers the maximum amount of n-heptane solubilized increases from  $11\text{g/dm}^3$  to  $17\text{g/dm}^3$  when n decreases from 11.4 to 7.4, n being the average number of oxyethylene groups in the surfactant mixture.

#### 1.3.4.3 EFFECTS OF DIFFERENT HYDROCARBONS

Just as the PIT depends on the hydrocarbon so the solubilization at a given temperature depends on the hydrocarbon, and very considerable differences can occur (Fig. 1.5)(1). The maximum solubilization, at whatever temperature this occurs may also change considerably.

The previous discussion of microemulsion has considered phase diagrams in surfactant-water-hydrocarbon systems at a given surfactant concentration, with temperatures as ordinate. These are sections of the complete system; the three component system can be plotted on a triangular diagram at a given temperature. Friberg and Lapczynska have determined the triangular phase diagrams

### 1.3.4.3. Cont'd.

for several hydrocarbons at various temperatures with tetrethylene glycoldodecyl ether as surfactant (Figs. 5.1) (29). These show that a surfactant phase can exist in the absence of other phases, taking it to be a phase of approximately equal amounts of oil and water and a relatively low surfactant concentration, about 10%. It can be seen in the diagrams for hexadecane and decane. For a straight chain aliphatic hydrocarbon a reduction in the chain length from sixteen to ten carbon atoms produces similar phase diagrams but at a temperature  $10^{\circ}\text{C}$  lower. Reducing the chain length further, to six carbon atoms, has a similar effect, the similar isotropic liquid regions appearing in the phase diagrams but  $10^{\circ}\text{C}$  below the temperatures for the hydrocarbon with the ten carbon chain (29). However, closer scrutiny of the phase diagrams for hexadecane and decane reveals that the manner in which the surfactant phase unites with the isotropic liquid phase which extends along the surfactant oil axis is not exactly the same, the union taking place close to the oil corner of the decane diagram but close to the centre of the hexadecane diagram.

A change in the hydrocarbon from aliphatic to aromatic, causes a marked reduction in the PIT (1). The net result is that the phase diagrams are shifted to lower temperatures. Since dodecyl-benzene gives rise to

#### 1.3.4.3. Cont'd.

solubilization similar to that of benzene, in spite of the fact that its molecular size is similar to that of hexadecane, the effect of aromaticity is not simply an effective reduction in chain length (29). The difference is at least partly due to the higher polarizability of the aromatic molecules. At room temperature and below surfactant does not dissolve in benzene and dodecylbenzene, whereas it is soluble in the aliphatic hydrocarbons considered. Up to about 60% of these aromatic hydrocarbons can be dissolved by  $C_{12}E_4$  at these temperatures.

#### 1.3.4.4. TRIGLYCERIDES AS THE THIRD COMPONENT

The discussion, given by Prince (30) of micro-emulsion formation, or rather the the lack of it, by triglycerides using two component emulsifiers - surfactant plus cosurfactant - is also applicable to systems with nonionic emulsifiers. Triglycerides, because of their polarity, do not reside in the centre of micelles with the hydrocarbon tails of the surfactant molecules, but at the interface, with the glyceride heads in the water phase. This tends to expand the film but because of the nature of the triglyceride molecule with its three ester linkages, the film fails to remain coherent so greatly reducing any possibility of microemulsification.

Friberg and Rydhag (31) found that tricaprylin and a nonionic emulsifier (an alkyl aryl polyethylene glycol)

#### 1.3.4.4. Cont'd.

were completely soluble in each other, and that this combination dissolved a weight of water roughly proportional to the weight of emulsifier and reaching a maximum of about 20%, when there was very little tricaprylin present. They did succeed in solubilizing tricaprylin, up to a maximum of about 15%, in an aqueous solution of sodium xylene sulphonate and monocaprylin.

### 1.4 NATURE OF MICROEMULSIONS

#### 1.4.1 THE TERM MICROEMULSION

When Schulman first observed his transparent W/O dispersions he called them oleopathic hydromicelles (16). Later he called them oleophilic hydromicelles and the O/W dispersions hydrophilic oleomicelles (32). In 1959 examples of these systems were photographed directly by electron microscopy after staining with osmium tetroxide, and shown to consist of spherical droplets of oil or water dispersed in the appropriate continuous phase (14). Schulman applied the term "micro emulsion" to these systems. Microemulsions were thought to be emulsions of very small droplet size (14) and to differ from true emulsions only with respect to the droplet size which was sufficiently small for them to be transparent (droplet diameter  $< \frac{1}{4}\lambda$ ) or translucent, scattering light in the Tyndall range.

#### 1.4.1 Cont'd.

Since the recognition of these systems there has been considerable investigation of their occurrence and discussion of their structure, formation and stability. The precise use of the term "microemulsion" varies between authors. Generally it refers to systems which contain large amounts of both oil and water and a smaller amount of surfactant mixture and which are transparent and which show long-term stability. Many of these systems are now regarded as micellar systems characterised by extremely high solubilization ratios and as such are thermodynamically stable (33). This has led some authors to refer to them as "so-called microemulsions." On this basis the term microemulsion may cover systems which vary from crystal clear to densely turbid.

#### 1.4.2. SOLUBILIZED MICELLAR SYSTEMS

There is no dividing line between micellar systems containing solubilized material and microemulsions of this type (section 1.3.4.1). The systems may be micellar or inverse micellar, oil forming the continuous medium. It is possible to prepare Schulman's microemulsions from the pure hydrocarbon via the addition of alcohol, followed by the addition of water and soap. No phase transition is observed during this process indicating that the system is still one-phase rather than a two-phase emulsion (28).

Zulauf and Eicke (34) make a distinction on the basis of results from the system Aerosol-OT<sup>†</sup>-water-isooctane,

<sup>†</sup> Aerosol-OT is sodium di-2-ethylhexylsufosuccinate.

#### 1.4.2. Cont'd.

studied by photon correlation spectroscopy. In the oil-continuous region they found that below a certain water content the aggregates behaved as rigid macromolecules and they interpreted this as meaning that the water in the interior of the aggregates was highly structured by hydrogen bonds. This they regarded as a micellar solution. At higher water contents they observed less rigidly bound water in the aggregates separated from the continuous phase by a well defined surfactant monolayer. This they regarded as a microemulsion.

#### 1.4.3. FORMATION OF MICROEMULSIONS

Unlike ordinary emulsions which require an expenditure of energy (e.g. vigorous shaking in the simplest case) to form them, microemulsions are usually formed on gentle mixing of the components. This should be so if the systems are thermodynamically stable and if all the components are liquid (more agitation may be required to break down liquid crystalline material within a reasonable length of time). Spontaneous emulsification is thought to occur by one of three processes or by a combination of them. These are interfacial turbulence, diffusion and stranding and a process resulting from negative interfacial tension (35,36).

#### 1.4.4. NEGATIVE INTERFACIAL TENSION

Much interest has centred on interfacial tension. It was thought to be a factor in the formation of microemulsions when these were regarded as thermodynamically

#### 1.4.4. Cont'd.

unstable systems as well as when they were regarded as thermodynamically stable systems (37,38). A negative interfacial tension between the oil phase and the aqueous phase will cause an increase in interfacial area until the interfacial tension reaches zero; the increase in interfacial area is produced by a breakdown of one of the phases into smaller and smaller drops, resulting in a microemulsion. Negative interfacial tensions have not been measured but extrapolation of measurements which can be made tend to indicate such negative interfacial tensions in the systems under consideration. These measurements have been made on systems where an ionic surfactant plus a cosurfactant has been employed (36). In the case of nonionic surfactants interfacial tensions which are very low and at a minimum have been found close to the PIT when a surfactant phase (1.3.4.1) is formed containing large amounts of both oil and water (36).

Consideration of interfacial tensions between the two phases led to a consideration of the nature of the interface itself. Where an ionic surfactant and an alcohol are used the interfacial film consists of these two components appropriately orientated with hydrophilic ends in the aqueous phase and oleophilic ends in the oil phase. In the case of the nonionic surfactant the interfacial film is of surfactant again appropriately

#### 1.4.4. Cont'd.

orientated. The interfacial film, which is also referred to as the interphase has been considered as a duplex film, with different tensions on either side of it (39). If the surfactant-oil tension and surfactant-water tension are different in the flat film then curvature of the film is required to equalise them (c.f. section 1.2.2), the side having the higher tension becoming convex. This can occur where there is a net negative interfacial tension in the flat film.

#### 1.4.5. THEORETICAL ASPECTS

A negative interfacial tension is not necessarily a condition for obtaining a microemulsion. The free energy of the system is not only a function of the surface energy, but also of other parameters such as the chemical potentials of the components and entropy.

A negative interfacial tension or a very small positive interfacial tension will favour microemulsion formation.

Microemulsion systems have been considered both from the points of view of thermodynamics (40) and of statistical mechanics (41). Phase inversion from one type of microemulsion to the other has been predicted (40) as well as phase separation (42). Theories have become more extensive and more detailed; Robbins (43) has developed a model which quantitatively predicts phase behaviour in microemulsions. This model treats the

#### 1.4.5. Cont'd.

interface between a droplet and its contacting external phase as a duplex monolayer of oriented surfactant molecules. The respective hydrophilic heads and lipophilic chain sides of the interface are treated as independent interphases, water interacting with the heads and oil with the chains. Direction and degree of curvature are imposed by a lateral stress gradient in the interface which is expressed in terms of surfactant molecular volume, interfacial tension and compressibility which are physically measurable quantities. Phase behaviour, expressed in terms of water and oil uptake, is described on an idealized ternary phase diagram. The theory, assuming monodispersity, predicts droplet size and interfacial concentrations of adsorbed surfactant in terms of molecules per droplet.

Talmon and Prager (44) have proposed a statistical mechanical model for microemulsions which suggests that over certain ranges of the model parameters it is possible for a bicontinuous phase (1.4.7) to coexist with an O/W and a W/O microemulsion; such three-phase equilibria have been reported (45). Also the results imply that a very thin layer of the bicontinuous phase can reduce the interfacial tension between a W/O and an O/W microemulsion by several orders of magnitude.

Ruckenstein (42) has also attempted to explain the low values of the interfacial free energy between two

#### 1.4.5. Cont'd.

microemulsion phases in equilibrium using a thermodynamic treatment.

Gerbacia et al (46) considered microemulsion as thermodynamically unstable systems, distinct from thermodynamically stable swollen micellar solutions. The long term stability of such systems was assumed to arise from the presence of the surfactant-cosurfactant-solvent film surrounding the droplets. A theory was developed to explain the stability. This work was based on evidence by Rosano (47) using a surfactant plus a cosurfactant that mixing the components in one order produces stable microemulsions but mixing them in a different order produces no emulsion. This is contrary to the bulk of the evidence concerning microemulsion formation.

Microemulsions are generally regarded as thermodynamically stable systems and theories have been developed to explain their thermodynamic stability.

Theories concerned with microemulsions formed with nonionic surfactants do not have to take into account the effects of the charged surfactant head groups and the cosurfactant molecules involved in the interface that are present in microemulsions formed by a surfactant plus a cosurfactant.

Most theories consider monodisperse spherical droplets of the disperse phase; these have been observed. If the interfacial tension is zero then there would appear to be no requirement for spherical droplets (48) but this is not necessarily so. For an ionic surfactant, the microemulsion droplet contains most of its soap ions in the interface and very few in the bulk. A small deformation will increase the surface area so reducing the adsorption density. Further adsorption from the bulk to compensate for this decrease would lead to a rather large decrease in the bulk concentration and to a strong rise in the interfacial tension, so driving the shape back to spherical (49). It would appear possible that this effect could occur in systems containing nonionic surfactant, thus ensuring spherical droplets.

Rosoff and Giniger demonstrated, by light scattering, micellar clustering in microemulsions as phase boundaries were approached, (50). The micellar clusters differed in size and structure depending on their location within the phase diagram.

Whilst nonionic surfactants form typical W/O and O/W swollen micellar solutions with the expected spherical droplets, phases are also formed of an indeterminate structure. A representative composition of surfactant phase is 10% surfactant and equal quantities of hydrocarbon and water. Shinoda and Sagitani show some sort of lamellar structure for the surfactant phase in their

#### 1.4.6. Cont'd.

schematic diagram (27). Since the phase is an isotropic liquid a regularly layered structure is excluded.

Friberg and Rydha'g considered a non-regular structure in which both oil and water are dispersed and continuous; they do not think it probable, on the basis of calculations concerning the energy involved when the layers are bent.

#### 1.4.7 BICONTINUOUS STRUCTURES

Scriven has considered the possibility of bicontinuous structures arising in liquids, (51). These would be analogous to porous media where one subvolume is solid or semi solid e.g. sandstone and sponge. An interspersion of two phases is bicontinuous only if each phase is connected across the specimen. Scriven suggests that such structures could occur in microemulsions containing comparable amounts of water and hydrocarbon. The surfactant would form the partitioning surface between oil and water. Periodic minimal surfaces exist such as the Neovius minimal surface, which has simple cubic symmetry. The surface curvature varies continuously throughout the structure; a positive curvature in one direction is balanced by a negative curvature at right angles to it so that almost every point is a saddle point (9). The problems associated with the wide variation in curvature of the interface which occur in some proposed structures are avoided. The Neovius minimal surface would not produce a birefringent structure because of the

#### 1.4.7. Cont'd.

cubic symmetry but it would be a very viscous structure. It has been suggested that certain cubic liquid crystal phases could have this structure (51,9)(1.1.4). The much less viscous microemulsion cannot have such a highly ordered structure. Thermal fluctuations can alter lattice distance and symmetry in periodic bicontinuous structures. As the temperature rises periodicity and symmetry can be destroyed by the increasing deviations from its original shape of the partitioning surface. In microemulsions this is likely to cause fluctuations in connectivity as necks are pinched off and rewelded. As the temperature rises this can gradually destroy the continuity of one of the sub volumes until it becomes a dispersion of discrete droplets. This type of behaviour may explain how microemulsions can continuously evolve into water-continuous solutions of oil-swollen micelles on addition of water or oil-continuous solutions of water swollen micelles on the addition of oil (51). This continuous evolution from water-continuous to oil-continuous is shown clearly in Fig. 1.7.

Lalanne et al (52) and Larche et al (53) also describe bicontinuous structures and continuous evolution from oil-continuous to water continuous systems. These are discussed in sections 1.5.2, Viscosity and 1.5.5, Self-diffusion.

#### 1.4.8 CRITICAL PHENONEMA AND METASTABILITY

Skoulios and Guillon (54) propose that critical phenomena may account for the stability of micro-emulsions in some regions of their occurrence on the phase diagram. They consider that tricritical or other polycritical points can occur in systems of water, oil and emulsifier. In the neighbourhood of such a point the state of the system is governed by the competition between two order parameters. For microemulsions the authors refer to these as micellar ordering and osmotic demixing. There are local fluctuations between micellar and emulsion structures and if the rate of emulsion coalescence is slow and the rate of micelle formation rapid, under the influence of these order parameters then the system can behave as though it is stable, whilst constantly renewing itself. It is possible that this dynamic stability may exert an influence over an extended region of the phase diagram.

It has been suggested (50,55) that metastable states may occur in parts of the microemulsion regions shown on phase diagrams, in the vicinity of phase separation areas. Such states would be analogous to supercooled liquids, where nucleation can take an increasingly long time as the critical point is reached.

Rosoff and Giniger (50) have studied systems containing water, sodium dodecyl sulphate and pentanol with

#### 1.4.8. Cont'd.

hexadecane and benzene. In samples containing hexadecane it was found that it was possible to mix two solutions, giving the required final composition, which did not clear on vigorous shaking but only on mild sonication. Heating such a "microemulsion" caused turbidity but on cooling the system cleared again showing reversibility. They concluded that metastable states were involved since the expected transition did not always take place. They suggested that a liquid crystalline phase might be involved, producing a kinetic barrier to the formation of the W/O micelles which is not overcome by ordinary mixing.

Ahmad, Shinoda and Friberg (56) found certain "solutions" which appeared to be microemulsions in the sodium dodecyl sulphate pentanol, water, benzene system. These "solutions" occurred near the boundary of a lamellar liquid crystalline phase. Separation was achieved by ultracentrifugation at 30,000g for 1hr. The bulk birefringence of these "solutions" is not mentioned.

## 1.5 PHYSICAL PROPERTIES AND PHYSICAL METHODS OF INVESTIGATION

### 1.5.1 LIGHT SCATTERING

Microemulsions are normally translucent, scattering light in the Tyndall range, appearing bluish by reflected light and yellowish when the transmitted light is observed. They may also be transparent or turbid depending on the precise definition of microemulsion which is assumed.

Light scattering depends on:

1. The particle size: as this decreases systems go from turbid to translucent to clear.
2. the difference in refractive index of the continuous and disperse phases
3. the droplet size distribution: the scattering by a few large droplets may mask that due to many smaller ones
4. particle shape

Droplet size distribution is not usually important in microemulsion systems since these systems are not likely to exhibit a high degree of polydispersity. Where the droplets or aggregates are extremely uniform in size, colours other than blue and yellow can be seen when the sample is viewed from different angles to the incident beam of light (57). The spectral colours are purer for a higher degree of monodispersity.

### 1.5.1. Cont'd.

Light scattering can be used to determine particle size and also to give information about particle shape. Ballaro et al (58) used it to show that particles in their four component system (using a surfactant plus a cosurfactant) were spherical in the microemulsion and emulsion regions but rods and possibly lamellar in the intervening liquid crystalline regions. The microemulsion droplet size changed on traversing the regions; for both types of microemulsion it increased on approaching the liquid crystalline phase.

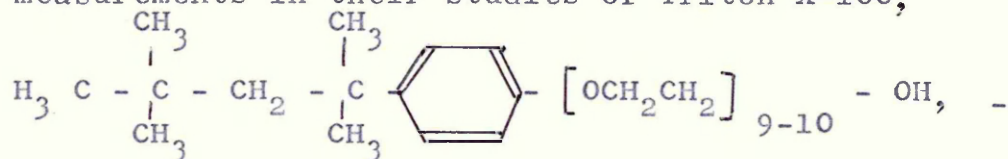
### 1.5.2. VISCOSITY

When dispersed aggregates are other than spherical they offer more resistance to flow than when they are spherical, so that the viscosity of the system is greater. In systems in which microemulsions occur liquid crystals often occur also. These exhibit a high viscosity; a large increase in viscosity as composition or temperature is changed is usually one indication of the formation of a liquid crystalline phase. Falco et al (59) measured viscosities in the system potassium oleate, hexanol, water and hexadecane as a function of the water to oil phase volume ratio. They found low viscosity W/O and O/W microemulsions separated by a high viscosity liquid crystalline region. The viscosity of the W/O microemulsion measured as a function of increasing water content indicated spherical aggregates which then changed to cylindrical aggregates as the liquid crystalline phase

1.5.2. Cont'd.

was approached. It would appear from their evidence that formation of cylindrical aggregates precedes the actual formation of the liquid crystalline phase.

Kumar and Balasubramanian (60) used viscosity measurements in their studies of Triton X-100,



alcohol-water-cyclohexane systems (section 1.5.6). They found systems of spherical reverse micelles exhibiting Newtonian viscosity. For a surfactant: alcohol ratio of 4:1 on adding water to the initial reverse micellar system they obtained an optically anisotropic phase in which there was a considerable rise in the relative viscosity as the water content was increased and which exhibited thixotropy. The viscosity increased still further on adding more water to obtain macroemulsions.

Lalanne et al (52) studied the viscosity in the system sodium dodecyl sulphate, n-butanol, water and toluene and considered their results in conjunction with nmr spin-lattice relaxation time ( $T_1$ ) measurements (Fig.1.8). They found evidence for spherical micelles of O/W and also of W/O; these regions (E,H) exhibited low viscosity but a high "microviscosity" (their interpretation of  $T_1$ ) for the disperse phase and a low viscosity for the continuous phase. Between these regions, region I

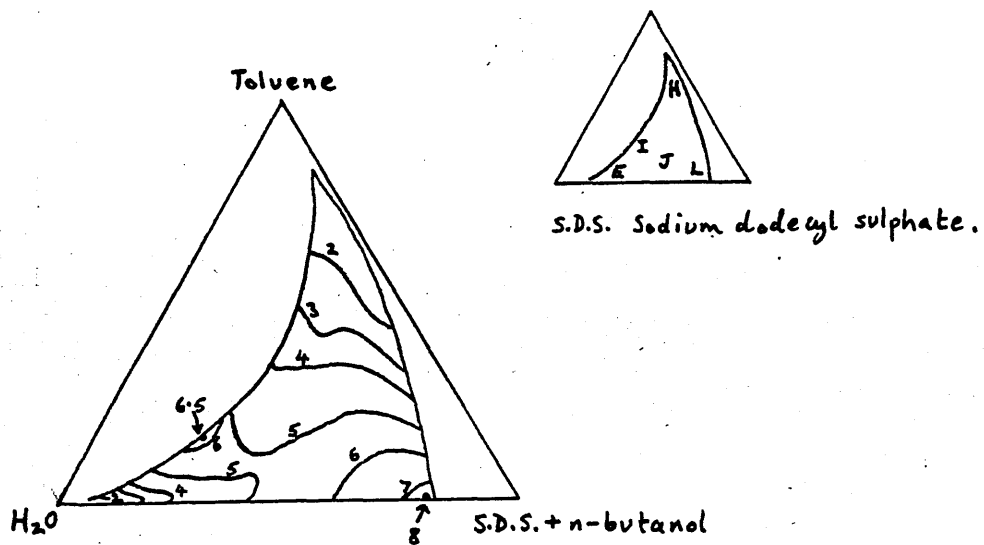


Fig.1.8. The sodium dodecyl sulphate - n-butanol -water -toluene system with lines of isoviscosity, and the maximum viscosities in zones I and L indicated. (from ref. 52).

### 1.5.2. Cont'd.

exhibited a low "microviscosity" for both oil and water but the highest macroscopic viscosity. They suggested that in this region there was a progressive phase inversion from water continuous to oil-continuous. Their suggestion for the structure, admittedly stylized and hence "not satisfactory", was of networks of micelles of oil and water overlapping and separated by surfactant. Region L close to the surfactant corner of the phase diagram showed a high "microviscosity" for both oil and water and a high macroscopic viscosity. They suggested that this was compatible with water in a "pseudo oil" consisting mainly of surfactant and co-surfactant with a small amount of oil.

Region J was intermediate between regions I and L in its properties.

### 1.5.3. ULTRA CENTRIFUGATION MEASUREMENTS

The ultracentrifuge has been used to investigate microemulsions. Smith et al (61) used it to look at samples from the ternary system 2-propanol, water and hexane. Microemulsion samples showed some sedimentation after ultracentrifugation but returned to homogeneity on standing. Other samples which were not regarded as microemulsions showed no sedimentation. They also found some samples which were unstable to the high centrifugal forces and classified these as metastable microemulsions.

### 1.5.3. Cont'd.

Hwan et al (62) used ultracentrifugation to investigate phase continuity and drop size in microemulsions containing synthetic petroleum sulphonate surfactants, an alcohol cosurfactant, sodium chloride brine and an oil.

Dvolaitzky et al (63) used ultracentrifugation in conjunction with neutron scattering in their studies of water in cyclohexane microemulsions produced using sodium dodecyl sulphate and 1-pentanol. The volume fraction of the dispersed phase was very low (1-4%) which is much lower than in many microemulsion systems.

### 1.5.4. HIGH RESOLUTION NMR

High resolution NMR has been used in the investigation of the structure of microemulsion systems. Changes in the chemical shifts of the constituent groups of the components of the system give information concerning the different chemical environments of these groups; the bandwidths of the resonances give an indication of the mobility of the groups concerned.

Kumar and Balasubramanian (64,65) used  $^1\text{H}$  NMR to investigate systems formed by adding water to Triton X-100 plus hexanol in cyclohexane. They found that the initial addition of water led to the formation of reverse micelles with a decrease in the mobility of the ethylene oxide chains. At low concentrations most of the water was bound to the ethylene oxide groups. This surfactant

#### 1.5.4. Cont'd.

hydration increased as water was added levelling off to a value suggesting a limiting ratio of one molecule of water bound per two oxyethylene units. This is a much lower value than that which has been found in most cases for normal micelles (section 1.1.2). As the water concentration increased "free" water pools were formed indicated by a change in the chemical shift of the -OH signal from its initial high value of  $5.8 \tau$  to the normal bulk water value of around  $5.0 \tau$ .

Detergentless microemulsions can be formed from hexane, water and 2-propanol;  $^1\text{H}$  NMR showed that "bulk" water was present in these systems (66).

Hansen and Mast investigated the system sodium dodecylbenzenes sulphonate, water and xylene using  $^1\text{H}$  NMR. This showed that xylene was solubilized in surfactant micelles, initially distributed along the surfactant molecules and only above a certain higher concentration accumulating in the core of the micelle. Surfactant line width variations were attributed to increased mobility of the surfactant chains when xylene molecules were distributed between them. The surfactant and xylene chemical shifts showed no discontinuity in going from the one-phase solubilized system to the two-phase macroemulsion, indicating continuity of the molecular environment.

Shah used NMR in studying the system hexadecane,

#### 1.5.4. Cont'd.

potassium oleate and hexanol, with added water (67, 68,69). He measured chemical shift and band width for the water, methylene and methyl protons as a function of the ratio of water to oil. As the water content was increased there was a transition from a W/O microemulsion to a reversed hexagonal liquid crystal phase, then to a lamellar liquid crystal phase and then to an O/W microemulsion. The chemical shift of the water protons changed significantly and by different amounts in the two liquid crystalline phases. The bandwidth increased in the liquid crystalline phases for all the protons measured, though by different amounts due to the reduced mobility.

#### 1.5.5. SELF-DIFFUSION

The pulsed field gradient NMR technique for measuring self diffusion coefficients is outlined in section 2.2. Lindman et al (70) have used this technique and also a tracer technique using radioactive labelling, to measure self diffusion coefficients in isotropic liquid regions of the systems  $C_{12}E_4$ -water-hexadecane and sodium octylbenzene sulphonate-pentanol-sodium chloride-water-decane. In the nonionic surfactant system at high water contents they found diffusion coefficients typical of a normal micellar solution; in the ionic surfactant system normal micelles only appeared to occur to a very limited extent at very high water contents. Diffusion coefficients

### 1.5.5. Cont'd.

typical of reversed micellar solutions were found in the nonionic surfactant system at high hexadecane contents and in the ionic surfactant system only at very high decane contents. Both systems exhibited large regions at high concentrations of both hydrocarbon and water where diffusion coefficients indicated bicontinuous structures with high self-diffusion coefficients for both hydrocarbon and water. No distinct transition from a normal to a reversed structure was found.

Larche et al (53) used self-diffusion measurements (made by the open-ended capillary tube method with radioactive tracers) and conductivity measurements in their study of the system sodium p-octylbenzene sulphonate-1-pentanol-water (+0.3wt% NaCl) - decane. By maintaining a constant alcohol: surfactant ratio (2.1) they worked in a pseudo-ternary system which exhibited a large isotropic liquid region. At high water content similarly low values of surfactant and decane self-diffusion coefficients and a high value for the sodium ion self-diffusion coefficient were in agreement with an O/W microemulsion. At low water content the sodium ion, chloride ion, water and surfactant exhibited similarly low self-diffusion coefficients (of the order of  $1 \times 10^{-10} \text{ m}^2 \text{ s}^{-1}$ ) whilst the decane had a higher self-diffusion coefficient ( $8 \times 10^{-10} \text{ m}^2 \text{ s}^{-1}$ ) in agreement with a W/O microemulsion structure. At intermediate volume fractions of water all the diffusion coefficients were

#### 1.5.5. Cont'd.

greater than the surfactant diffusion coefficient which remained almost constant; there was a continuous change from values appropriate to an O/W structure to those of a W/O structure. The authors suggest an intermediate bicontinuous structure comparing the instantaneous structure with that of porous media. The continuous variation of the conductivity from low values ( $< 0.05 \text{ Sm}^{-1}$ ) in the W/O region to high values ( $\sim 1.0 \text{ Sm}^{-1}$ ) in the O/W region is in agreement with this,

#### 1.5.6. ELECTRICAL CONDUCTIVITY

Conductivity measurements have been used in the investigation of several microemulsion systems, both oil-continuous and water-continuous. Such measurements can be a convenient way of determining the nature of the continuous phase.

Kumar and Balasubramanian (60) measured conductivity in the Triton X-100-alcohol-water cyclohexane system. The water was doped with potassium chloride for these measurements; the alcohols used were pentanol, hexanol and octanol, similar results being obtained for all. The conductivity was measured for increasing amounts of water added to a fixed volume of solution of surfactant and alcohol in cyclohexane. For a Triton X-100: alcohol ratio of 3:2 the initial low conductivity of about  $0.5 \text{ m Sm}^{-1}$  remained virtually the same until just before phase

#### 1.5.6. Cont'd.

separation occurred to form macroemulsions, when it rose steeply. The authors state that there is no appreciable barrier to conduction in the macroemulsions which would be the case if these are O/W emulsions. The conductivity changed by a factor of about 100 from the initial oil-continuous phase to the final macroemulsion.

For the surfactant:alcohol ratio 4:1 the variation of conductivity with added water is more complex (Fig.1.9). The initial low conductivity of about  $0.5 \text{ m Sm}^{-1}$  (as before) rose prior to the phase transition to the anisotropic phase. The conductivity then fell, the explanation given being that the effect of the increase in the medium viscosity outweighs the effect of the relatively easy conduction pathways in the lamellar/cylindrical micellar configuration; however, the viscosity of the medium is not necessarily related to the conductivity. Beyond the anisotropic region macroemulsions were again formed and the conductivity rose as in the system with the surfactant;alcohol ratio of 3:2.

Smith et al (61) measured conductivity in their investigation of the system 2-propanol-water-hexane, which they found to exhibit an oil-continuous microemulsion region. They proposed structures for regions covering most of the phase diagram on the basis of conductivity and ultracentrifugation data. The conductivity increased steadily through the microemulsion region as the propanol content was increased; this behaviour was ascribed to an increasing amount of water in the continuous

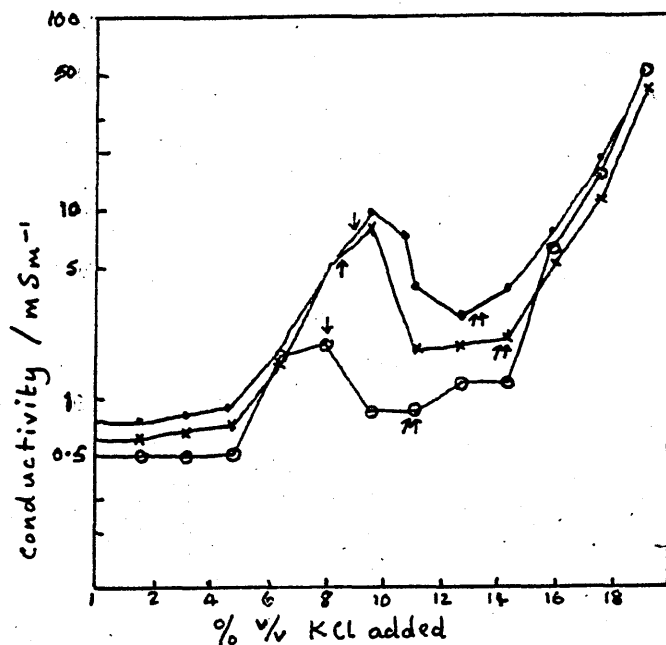


Fig. 1.9. Variation of the conductivity of the micellar dispersion as a function of aqueous KCl uptake into a 20% solution of Triton X-100 - alcohol (ratio 4:1) in cyclohexane. Single arrow indicates transition to anisotropic phase and double arrow indicates region of phase separation. .... pentanol; x x x x hexanol; o o o o octanol. (from ref.60.)

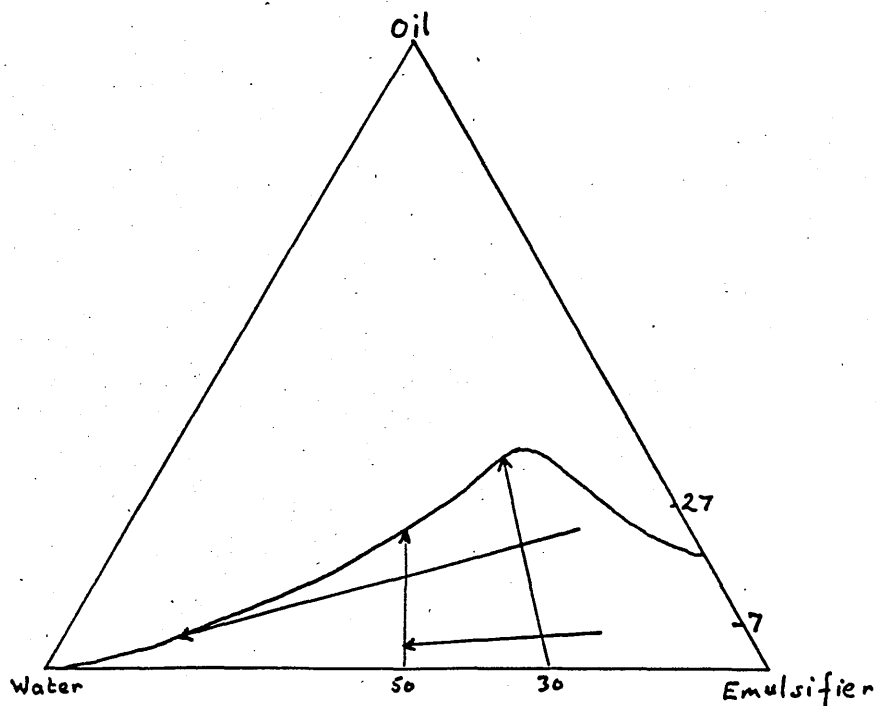


Fig. 1.10. The pseudo three component phase map of Tween 60-n-pentanol-water-hexadecane. The arrows denote compositions employed for the conductivity measurements. (from ref.71).

### 1.5.6. Cont'd.

phase (rather than in the reverse micelles). The conductivities measured in this region ranged from about  $10 \mu\text{Sm}^{-1}$  to about  $200 \mu\text{Sm}^{-1}$  according to the water content and propanol content of the sample.

Mackay and Agarwal (7) have measured the conductivity of a number of O/W microemulsions containing added electrolyte in the systems surfactant-n-pentanol-water-oil where the oil was hexadecane or Nujol and the nonionic surfactants were various Tweens. They studied the Tween 60-n-pentanol-water-hexadecane system in more detail. They replaced the water with 0.1M sodium chloride solution for the conductivity measurements. For a constant emulsifier:oil ratio (see Fig. 1.10) they found that the equivalent conductance ( $\Lambda$ ) obeyed the relation

$$\Lambda = \Lambda^0 (1 - a \phi_{\text{comp}})^n \quad \text{-- 1.1}$$

where  $\phi_{\text{comp}}$  is the disperse phase volume estimated from the composition and density of the microemulsion and 'a' and 'n' are parameters to be found for the system. The systems obeyed the relation well except at the highest values of  $\phi_{\text{comp}}$ . The clear region extends to the emulsifier-oil axis so it is suggested that these deviations from the linearity of the above expression are a result of a transition from the O/W micellar solution (i.e. the microemulsion) to some other isotropic phase. The maximum values of  $\phi_{\text{comp}}$  were 0.80 and 0.85;

### 1.5.6. Cont'd.

the maximum disperse phase volume for monodisperse hard spheres in 0.74 so that it is not surprising if the microemulsion breaks down at these phase volumes.

The 'a' values were generally found to be about 1.2. Mackay and Agarwal discussed the meaning of the 'a' term and thought the most likely possibility to be that the effective phase volume with respect to conductivity measurements differed from  $\phi_{\text{comp}}$  and was in fact larger than  $\phi_{\text{comp}}$  so that  $\phi = a \phi_{\text{comp}}$  where  $\phi$  is the effective phase volume. This could be accounted for on the basis that some of the water should be included as part of the drop, in the form of water of hydration of the ethylene oxide groups. If the bound water/surfactant ratio is constant then constant 'a' values result. Calculations of the quantity of water involved gave values of 1-2 moles of water per ethylene oxide group. The authors suggest that the presence of pentanol in the system may account for the constancy of the 'a' value for different Tweens.

The 'n' values were constant at constant emulsifier: oil ratios but decreased on increasing the oil concentrations ranging from about 1.5 to 1.1. A tentative explanation of the change in 'n' values is given, based on the behaviour of the alcohol in the system.

The results were compared with theoretical equations for macroemulsions (the Maxwell and Bruggeman equations - chapter 2) and also with the usual behaviour of macroemulsions. The conductivity measured in the present system was considerably lower than that which would be expected if the theoretical equations were obeyed or if the system behaved as a macroemulsion. Converting the equation 1.1 to the same form as the Bruggeman equation (Equation 2.1) gives:

$$\frac{K}{K_m} = (1-\phi)^{2.5} \quad - \quad 1.21$$

where  $K$  is the conductivity of the emulsion and  $K_m$  the conductivity of the continuous phase;  $\phi$  is the disperse phase volume. The exponent is 2.5 instead of 1.5 as in the Bruggeman equation.

No mention is made of the impurities occurring in the commercial surfactants used and whether these are likely to affect the results in any way.

Roux and Viillard (72) measured conductivity in dilute (0.002M) aqueous solutions of nonionic surfactants (polyoxyethylene nonylphenyl ethers of varying oxyethylene chain length), to which methyl benzoate was added. At about 0.5% (v/v) ester transparent solutions were obtained which they described as a microemulsions. Sedimentation velocity measurements indicated the presence of large aggregates. The location of the

### 1.5.6. Cont'd.

ester in the aggregates is not discussed. These microemulsions are much more dilute than many systems so described.

Conductivity was related to changes in viscosity in the micellar solutions and the emulsions (occurring at lower ester concentration) and the microemulsions.

Shah et al have measured electrical resistance (reciprocal of conductance) in the same systems for which they recorded the NMR (67,68,69) (Section 1.5.4.). Since their system contained an ionic surfactant, doping with a salt was not necessary. Electrical resistance was measured as water was added to the mixture of hexadecane, hexanol and potassium oleate. The resistance dropped initially as water was added to the system. (Fig 1.11). They accounted for this on the basis of "molecular solubilization" of water in the hexadecane - hexanol-potassium oleate mixture, NMR supporting this interpretation. The resistance then remained fairly constant throughout the W/O microemulsion region, in which the interface between the oil and water is the main barrier controlling ion transport between the electrodes.

The resistance then dropped abruptly as the system became birefringent on the formation of a liquid crystalline region. The sharp decrease in resistance within the birefringent region appears to coincide with the change from a reversed hexagonal to a lamellar phase

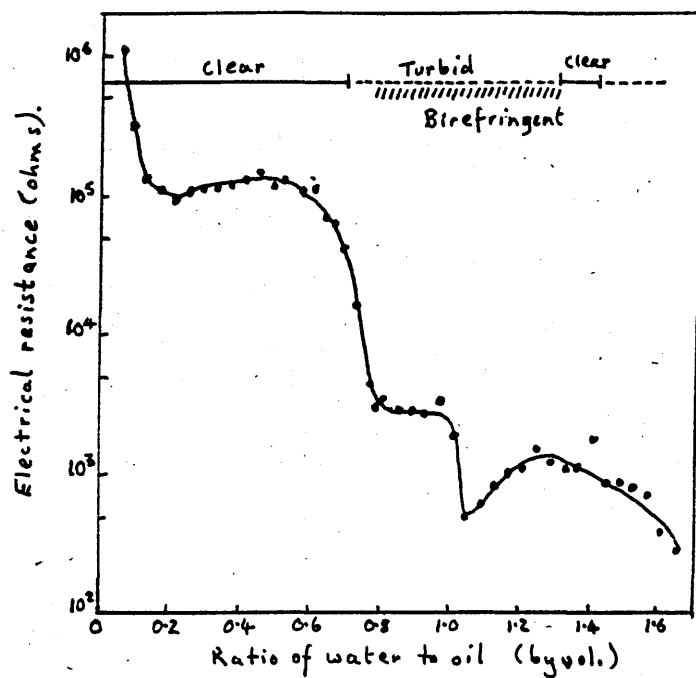


Fig. 1.11. Variation in electrical resistance, optical clarity, and birefringence of a system consisting of 1cm<sup>3</sup> of hexadecane, 0.4cm<sup>3</sup> of hexanol and 0.2g of potassium oleate as water is added. (from ref.69).

### 1.5.6. Cont'd.

which the authors discuss in relation to their NMR data. The resistance then increases again; this is attributed to the disruption of lamellar structures. It then decreases as the O/W microemulsion is formed. Throughout this system the resistance changes by a factor of  $10^4$ ; the difference between the resistance of the W/O and the O/W microemulsions is a factor of between  $10^2$  and  $10^3$ .

### 1.5.7. PERCOLATION

The conductivity variation with composition, which has been observed in some microemulsions, is of a form typical of a percolation mechanism as described in chapter 2.

Lagues et al (73) have studied microemulsions consisting of sodium dodecylsulphate, 1-pentanol, water and cyclohexane, using neutron scattering and conductivity measurements. They titrated each mixture with alcohol. A maximum in the value of the conductivity was observed at the clearing point and was considered as the conductivity of the microemulsion. The compositions of the samples are not stated. A plot of conductivity versus the volume fraction of water ( $\phi_W$ ) in the microemulsion shows a dramatic increase in conductivity (two orders of magnitude) between  $\phi_W = 0.06$  and  $\phi_W = 0.09$ . The results are found to agree satisfactorily with percolation theory: in the expression:-

$$K(\phi_W) = K_0 (\phi_W - \phi_c)^t$$

### 1.5.7. Cont'd.

$t$  is found to be  $1.55 \pm 0.1$ , in agreement with the theoretical value of 1.6;  $\phi_c$  is found to be 0.078 which is the water volume fraction at the threshold. This yields a value of 0.14 for the total volume fraction occupied by the droplets (this includes the soap and some alcohol). This agrees with the theoretical threshold value of 0.15 obtained for site percolation on various lattices (74). Models more appropriate to real systems yield higher threshold values (0.25, 0.29) but these are again based on static models (appropriate to solids). A "stirred percolation" model has been presented(75) which is applicable to conducting droplets undergoing Brownian motion in an insulating medium but no threshold value is quoted.

Below the threshold the conductivity is not zero and the authors compare it with theory for non-zero conductivity in this region; they account for the discrepancy on the basis of the mobility of the droplets - the theory is valid for fixed conducting elements. They suggest that the droplets are charged to the extent of one ion for 600 molecules of soap in the interfacial film.

The neutron scattering results indicate a structure modification at a water content which coincides with the break in the conductivity curve at  $\phi_w = 0.33$  (Fig.1.12). The volume of the droplets agrees with the random packing

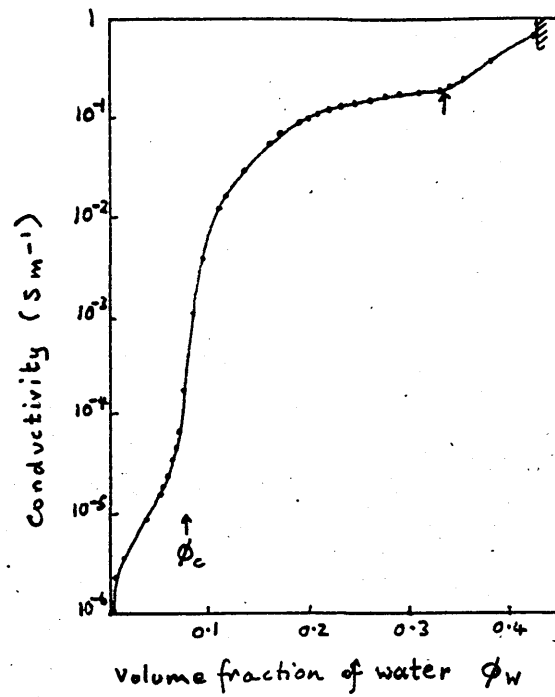


Fig. 1.12. Variation of conductivity with water concentration in a W/O microemulsion composed of sodium dodecyl sulphate, 1-pentanol, water and cyclohexane. (from ref.73).

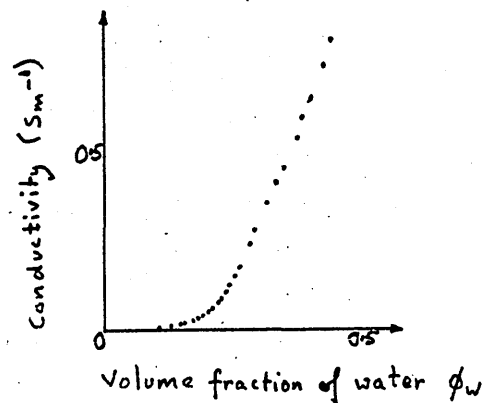


Fig. 1.13. Variation of conductivity with disperse water volume fraction in a W/O microemulsion composed of potassium oleate, butanol, water and toluene. (from ref. 76).

### 1.5.7. Cont'd.

volume for hard spheres (0.637). The authors compare the conductivity with that of a sodium chloride solution and finding it to be low, propose that conduction in the interfacial films is the principal mechanism between the threshold and  $\phi_W = 0.33$ . Neutron scattering results show that the aqueous cores of the droplets are not connected in this range. They suggest that the increase of conductivity above  $\phi_W = 0.33$  could arise from progressive connection of the aqueous phase, related to the structural inversion which is observed by neutron scattering.

Lagourette et al (76) measured changes in conductivity with increasing water content, in oil-continuous micro-emulsions consisting of water, toluene, potassium oleate and butanol which were said to be characteristic of percolative conduction. The potassium oleate:butanol ratio was kept constant at 0.5. Measurements were made for several series of samples in each of which the mass fraction of emulsifier (potassium oleate plus butanol) was kept constant as the water fraction was increased. Plots of conductivity versus the phase volume of water ( $\phi_W$ ) showed a sharp increase as  $\phi_W$  passed a critical value. The percolation threshold  $\phi_c$  was determined in terms of water volume fraction by plotting  $K^{1.6}$  versus  $\phi_W$  ( $K(\phi_W) \propto (\phi_W - \phi_c)^{1.6}$ ). The value of 0.176 obtained was somewhat different to that of Lagues et al; however, a

1.5.7. Cont'd.

comparison of this value with an appropriate theoretical threshold value of 0.29 yielded the ratio of the disperse globule external radius to the water core radius of 1.18, which is in excellent agreement with that obtained by Lagues et al by neutron scattering.

The plot of  $K$  versus  $\phi_W$  (Fig. 1.13) is quite different from that of Lagues et al (Fig. 1.12), the conductivity continuing to increase steeply instead of increasing more gradually after the rapid increase; the ranges of  $\phi_W$  are similar extending to values just over 0.4.  $K(\phi_W) \propto (\phi_W - \phi_c)^{1.6}$  is applicable in the vicinity of  $\phi_c$ , then for higher values of  $\phi_W$  the relation

$$\frac{K}{K_1} = \frac{3}{2} (\phi - \frac{1}{3})$$

where  $\phi$  is the volume fraction of the disperse phase (water cores plus shells of combined surface active agents) and  $K_1$  is the conductivity of the disperse phase itself, becomes applicable. For values of  $\phi > 0.4$  there is excellent agreement with theory both with respect to slope and intercept.

For values of  $\phi_W$  below the threshold value the conductivity is not zero as it would be were a rigorous percolative conduction exhibited by the system; it is suggested that electrophoretic movement of the droplets could account for this.

Lagourette et al also regard the conduction mechanism as interfacial on the basis of the fact that for a fixed mass fraction of combined surface active agents  $K$  increases with  $\phi$  whilst  $K_1$  remains constant and that  $K_1$  increases in proportion to the amount of surfactant and that  $K_1$  values are considerably lower (e.g. about  $\frac{1}{3}$ ) than those of an aqueous solution containing the same molar fraction of solubilized KCl.

They suggest that the droplet interlinking and clustering process suggested by the percolative behaviour of the microemulsion conductivity might precede phase inversion from W/O to O/W via a bicontinuous structure.

Lagues and Sauterey (75) also studied W/O microemulsions consisting of sodium dodecyl sulphate, 1-pentanol, water and cyclohexane. They studied systems with different water: soap ratios and also with added sodium chloride. Their conductivity curves as a function of the water content of the system are of a similar form to that of Lagues et al (above). At low water content ( $\phi_w \leq 0.05$ ) they explain the conductivity on the basis of the motion of charged droplets. They estimate the charge to be equivalent to one ion per  $\sim 500$  molecules of soap but do not explain its origin.

At higher concentrations of the disperse phase they use a "stirred" percolation model to account for the variation in conductivity with water content. This makes allowance for the Brownian motion of droplets in

1.5.7. Cont'd.

microemulsion systems which is not present in the static systems for which percolation models have previously been developed. They develop an expression which appears to be:

$$\frac{K}{\phi} \propto (\phi_c - \phi_w)^{-1.2} \quad \phi_w < \phi_c$$

For three of their microemulsions the exponent is found to be 1.4, 1.3 and 1.1; it is not determined for the other microemulsion investigated.

This "stirred" percolation model is not used to predict a threshold value. These values were determined experimentally and varied from 0.10 to 0.26 for the "hard-sphere" volume of the droplets. The authors suggest that the variations may be due to variations in the interactions of the droplets in the different microemulsion systems, polydispersity and nonsphericity.

For values of  $\phi > \phi_c$  the expression used was the same as that used by Lagues et al (73) and Lagourette et al (76):

$$K \propto (\phi_w - \phi_c)^t$$

where theory gives  $t=1.6$ . Values of 1.6, 1.6, 1.4 and 1.8 were obtained for the exponent.

These authors also determined an inversion (from W/O to O/W microemulsions) concentration of droplets of around 0.60 "hard-sphere" droplet volume, in agreement with the previous work (73).

## 1.6 A SUMMARY OF MICROEMULSIONS AND THE PROGRAMME OF WORK

### 1.6.1 SUMMARY

The term microemulsion covers a wide range of systems, even if solubilized systems containing relatively small amounts of oil (in water) or water (in oil) (say  $< 5\%$ ) are excluded. Such a dividing line is entirely arbitrary in the case of water continuous systems since there is a continuous evolution from surfactant micelles to surfactant micelles containing solubilized oil to surfactant "micelles" containing larger amounts of solubilized oil which can be described as microemulsion droplets (Section 1.4.2). In the case of oil-continuous systems there may be a dividing line below which all the water is bound to the hydrophilic groups of the surfactant and above which "free" water pools exist. Within these limits the term microemulsion covers systems whose structures are:-

1. just what the name implies (i.e. micro-droplets of oil (or water) surrounded by a surfactant film and dispersed in water (or oil))
2. bicontinuous (though the exact structures of such phase remain to be determined) (Section 1.4.7) or
3. as yet undetermined.

The currently held view is that microemulsion systems are thermodynamically stable. Metastable states may be confused with microemulsions in some systems (section 1.4.8).

### 1.6.1 Cont'd.

Various theories have been proposed to account for the occurrence and stability of microemulsions. These are usually based on micro emulsion structures. Solubilized systems and the microemulsions stemming from them at slightly higher concentrations of the disperse phase are generally regarded as extensions of micellar systems. There does not appear to be any one generally accepted theory for the occurrence and stability of microemulsions; indeed a complex theory would be required to cover the whole range of microemulsions.

A variety of methods of investigation of microemulsion structures has been used. Of particular interest here are conductivity and self-diffusion measurements. Conductivity measurements are relatively easy to make but their interpretation can be difficult (sections 1.5.6 and 1.5.7). Self-diffusion measurements have only recently been used in two microemulsion systems (section 1.5.5). Other methods include light-scattering, NMR and viscosity measurements.

Microemulsions are important commercially in many fields (Section 1.3.2). Microemulsions formed with hydrocarbons are important in tertiary oil recovery. Animal and vegetable fats and oils are composed mainly of triglycerides; thus, these are important in industrial processes using these raw materials in food processing and also in the domestic wash process, where they form part of the soil. Triglycerides are not readily solubilized

### 1.6.1. Cont'd.

(section 1.3.4.4) and have not been observed to form microemulsions.

### 1.6.2 THE PROPOSED PROGRAMME OF WORK

Nonionic surfactants were chosen for use since the alternative ionic surfactants also require a cosurfactant in order to form microemulsions and this introduces another variable.  $C_{12}E_4$  was known to form extensive microemulsion regions with hydrocarbons (29) so this was chosen as the nonionic surfactant. Brij 30 was a convenient commercial surfactant of this type with a nominal average oxyethylene chain length of four units. This had the advantage of being available in larger quantity than the pure surfactant, and so was useful for preliminary measurements as well as being of interest for the purposes of comparison with the pure material.

It was decided to investigate the binary surfactant-water phase diagrams prior to the microemulsion systems, in the hope that some knowledge of the structures occurring in the isotropic liquid regions of the binary systems might help in the elucidation of the structures occurring in the ternary systems. The  $C_{12}E_4-H_2O$  phase diagram had not previously been determined. The  $C_{12}E_6-H_2O$  phase diagram was available in the literature (77); an isotropic liquid region extends from 0-100%  $C_{12}E_6$ . In the  $C_{12}E_4-H_2O$  system the isotropic liquid regions found were not continuous from 0-100%  $C_{12}E_4$  so it was decided to investigate the  $C_{12}E_6-H_2O$  system also.

### 1.6.2. Cont'd.

Conductivity and self-diffusion were the methods used to study the isotropic liquid regions. Conductivity measurements can be a convenient way of distinguishing between water-continuous and oil-continuous systems; the latter were expected to occur in the ternary systems to be investigated but also possibly in the binary systems if all the water was enclosed within inverted surfactant micelles with the surfactant hydrocarbon chains forming the continuum. It was hoped that self-diffusion measurements would distinguish between micellar and continuous phases and so give further information concerning the structures of the systems.

Hexane was chosen as the hydrocarbon for the first ternary system, Brij 30-H<sub>2</sub>O-hexane to be studied; a short chain aliphatic paraffin was required, as a simple third component prior to investigations of more complex third components such as triglycerides. Short chain aliphatic paraffins were known to form micro-emulsions with C<sub>12</sub>E<sub>4</sub>. Hexane has a freezing point below 0°C so that problems due to crystallisation of the oil would not be encountered. However, the high volatility of hexane (b.p. 69°C) was a disadvantage particularly when studying the system at higher temperatures (~50°C) so heptane (b.p. 98°C) was used for studies with the pure surfactant, C<sub>12</sub>E<sub>4</sub>. Phase diagrams were determined to locate the isotropic liquid regions which were to be studied by conductivity measurements.

### 1.6.2. Cont'd.

The data available in the literature (29) showed a different phase behaviour for hexane and hexadecane in the  $C_{12}E_4$ - $H_2O$ -oil system. Partial phase diagrams were determined to confirm this and then conductivity measurements were made in the isotropic liquid regions. It was decided to make limited studies of the equivalent decane and octadecane systems.

Studies were to be made of the ternary systems for  $C_{12}E_4$  and Brij with different triglycerides as the third component. Triacetin was the first member of this series, for which phase diagrams were to be determined. An attempt was to be made to elucidate the reasons for the lack of microemulsion formation by triglycerides.

## 2. THEORY

### 2.1 CONDUCTIVITY THEORY

#### 2.1.1 INTRODUCTION

The systems studied consisted of three components - water, pure nonionic surfactant or commercial nonionic surfactant and an aliphatic hydrocarbon. The water was doped with sodium chloride. Water itself is a relatively poor conductor ( $K = 10^{-4} - 10^{-6} \text{ Sm}^{-1}$ ) but the addition of ions in the form of sodium chloride produces a highly conducting solution ( $K = 0.1 \text{ Sm}^{-1}$  for 0.01M NaCl solution). It is not appropriate here to discuss the theory of electrolytic conductance applicable to such a solution; this is reviewed by Fuoss (78). The pure nonionic surfactant is also a poor conductor ( $K = 10^{-7} \text{ Sm}^{-1}$ ). The aliphatic hydrocarbon is an insulator ( $K = 10^{-10} \text{ Sm}^{-1}$  for hexane (79)).

#### 2.1.2 CONDUCTIVITY OF EMULSIONS

Various theoretical equations have been developed expressing the conductivity of an emulsion in terms of the conductivity of its constituents and the phase volumes. For an O/W emulsion the conductivity of the oil is so low, compared to that of the water, that it can be neglected. According to Mackay and Agarwal (71) polydisperse O/W emulsions are best described by the Bruggeman equation:

$$\frac{K}{K_m} = (1 - \phi)^{3/2} \quad 2.1$$

where  $K$  and  $K_m$  are the specific conductivities of the emulsion and the continuous phase, respectively, and

$\phi$  is the phase volume of the disperse phase. For monodisperse systems the data lie between the Bruggeman and the Maxwell equations:

$$\frac{K}{K_m} = \frac{2(1 - \phi)}{2 + \phi} \quad 2.2$$

The analogous equation to equation 2.1, for W/O emulsions, where the conductivity of the oil is very much less than that of the aqueous phase, is:

$$\frac{K}{K_m} = \frac{1}{(1-\phi)^3} \quad 2.3$$

where the symbols have the same meaning as above with regard to continuous phase and disperse phase. (80).

These equations were developed for emulsion systems where the disperse phase consists of spherical droplets and any surfactant forming an interfacial film is neglected. De la Rue and Tobias (81) developed an empirical formula from the Bruggeman equation:

$$\frac{K}{K_m} = (1 - \phi)^n \quad 2.4$$

where  $n$  is chosen to fit the data. For suspensions of spherical glass beads, irregular sand particles and polystyrene cylinders in electrolyte solutions they found values of  $n$  close to 1.5 as in the Bruggeman equation.

A parallel set of equations exists for the dielectric constants of emulsions. Hanai (80) has re-

viewed the work which has been done to compare the measured dielectric constants and conductivities with the theoretical equations. Several of these systems are so unlike oil and water emulsions that (e.g. dog blood suspensions and bakelite hemispheres in tap water) that any agreement with the theoretical equations is irrelevant to the present work. Hanai et al measured the conductivities of emulsions of nujol-carbon tetrachloride mixtures in 0.05N aqueous potassium chloride solutions prepared with the nonionic surfactants, Span 20, Tween 20 and polyoxyethylene glycol cetylolether. Good agreement with the Bruggeman equation for dielectric constant at high frequency, was found for W/O emulsions consisting of water in a nujol-carbon tetrachloride mixture using the surfactants Arlacel 83, Span 20 and Tween 60, and for water in kerosene, transformer oil and terpene using surfactants such as polyoxyethylene oleates, polyoxyethylene nonyl phenyl ethers and zinc stearate.

Chapman (82) measured dielectric constants for W/O emulsions consisting of water in paraffin oil using magnesium stearate as emulsifier and found good agreement with the Bruggeman equation.

Clause et al (83) measured the conductivity (and also dielectric constants) of "microemulsions" of benzene in water produced using the nonionic emulsifiers Tween 20 and Span 20. Although described as microemulsions

### 2.1.2. Cont'd.

these systems were metastable emulsions (creaming after three or four days) with a very small droplet size. The conductivity results were in agreement with the Bruggeman equation.

The system most akin to those studied in the present work is that of Mackay and Agarwal (section 1.5.6).

### 2.1.3. PERCOLATION

Percolation is a conduction phenomenon which may be relevant to some microemulsions. A hypothetical static system, consisting of an insulator (e.g. a hydrocarbon oil) and a conductor (e.g. water containing dissolved ions) dispersed in it, will be considered first. When there are only a few water droplets dispersed in the oil there will be no connection between them and the medium will still behave as an insulator. As the number of water droplets is increased (by adding more water), a point will come when some start to touch each other and as the number is increased further sufficient droplets will touch each other for a conduction channel to be formed through the system. On further increase in the number of droplets the number of conduction channels will increase rapidly. The result of this is that conduction will not occur below a certain droplet concentration; when this threshold concentration is reached conduction will occur and then there will be a rapid increase in conduction as the droplet concentration

### 2.1.3. Cont'd.

is increased further. In real systems of two liquids like that above, the water droplets will not be static so that conduction channels will be established through them by means of their collisions, at a lower droplet concentration than in the static system.

Various models have been used in order to derive theoretical equations for percolation (74). A model in which the conducting medium consists of identical spheres, permitted to overlap with centres distributed at random, gives a threshold volume fraction for the conducting medium, of 0.29. Other models used for deriving the threshold volume fraction are less appropriate to microemulsions. Derivation of the behaviour of the conductivity near the threshold has proved more difficult. Kirkpatrick (74) has derived an expression

$$K(n) \approx K(n - n_c)^{1.6} \quad 2.5$$

where  $K$  depends on the model chosen and  $n$  refers to the number of sites in the model and  $n_c$  the number at the threshold. He suggests that this should be accurate to about 20% near the threshold. For a microemulsion this would be expressed as:

$$K(\phi) \propto (\phi - \phi_c)^{1.6} \quad 2.6$$

where  $\phi_c$  is the threshold volume fraction.

### 2.1.3. Cont'd.

At higher values of  $\phi$  ( 0.4) the following equation is applicable

$$\frac{K}{K_1} = \frac{3}{2} (\phi - \frac{1}{3}) \quad 2.7$$

where  $K$  is the conductivity of the system,  $K_1$  the conductivity of the conducting constituent. (76, 84). The equation is of the form  $K(\phi) \propto (\phi - \phi_c)$  so that  $\phi_c$  appears to be  $\frac{1}{3}$  but this is an overestimate. Equations 2.6 and 2.7 would suggest that the Bruggeman equation (2.1) for oil-continuous emulsions is only applicable to emulsions of low (less than about  $\frac{1}{3}$ ) disperse phase volume. This assumes that the only barrier to percolation is too small a disperse phase volume.

It would appear that if the conductivity of an oil continuous microemulsion system can be described by these percolation equations then the microemulsion is exhibiting percolation. However, if the equations do not fit although the general form appears to be that of percolative conduction (sharp rise in conductivity after a threshold value of  $\phi_w$  is reached), then percolation may still be a likely explanation of the results.

## 2.2 SELF-DIFFUSION MEASUREMENTS

### 2.2.1 INTRODUCTION

Self-diffusion may be studied directly by the NMR spin-echo technique (section 2.2.2)(85). This method of measurement detects diffusion occurring over a time period between a few milliseconds and a few seconds in most of the systems to which it can be applied. The distances traversed in these times are comparable to the dimensions of colloidal structures. Hence, the observed diffusion will depend whether colloidal structures restrict the diffusional motion. The effect will be most pronounced when the distance diffused is of the same order of magnitude as the dimensions of the restricting structure; the diffusion measured will depend on the time during which diffusion is observed.

The spin-echo method has been used to investigate self-diffusion in a wide variety of systems e.g. yeast cells, vermiculite crystals, liquid-liquid emulsions (85) and surfactant liquid crystals (both lamellar and cubic) (86,87).

Although  $^1\text{H}$  is the nucleus often used in these experiments, other nuclei can be used e.g.  $^2\text{H}$ ,  $^7\text{Li}$ ,  $^{19}\text{F}$ . Where more than one diffusing species contains the same nucleus, separate diffusion coefficients can be obtained (without having to make a substitution such as  $^2\text{H}$  for  $^1\text{H}$ ) if they are of sufficiently different magnitude.

The sample is placed in a magnetic field which is as near to homogeneous as possible. The net magnetisation,  $\underline{M}$ , of the ensemble of nuclear spins, is parallel to this static field,  $H_0$ . Application of a small rotating field, at the resonance frequency of the nuclear spins of interest, in the form of a radiofrequency pulse, tips the magnetisation vector  $\underline{M}$ , away from the preferred direction parallel to  $H_0$ , and it then precesses about  $H_0$  at the Larmor frequency until components perpendicular to  $H_0$  decay by relaxation or other means. It is convenient at this point to consider the rotating frame in which  $\underline{M}$  is static. By use of a radiofrequency pulse of appropriate magnitude and duration, it is possible to tip  $\underline{M}$  through  $90^\circ$  so that it is perpendicular to  $H_0$  (Fig. 2.1). After the pulse the magnetisation,  $\underline{M}$ , returns to the preferred direction, parallel to  $H_0$ , at a rate determined by the relaxation processes and the static field inhomogeneity. Components of  $\underline{M}$  "fan out" in the xy plane (due to slightly different precession rates) reducing the net component of  $\underline{M}$  in this plane.

Since  $\underline{M}$  is in fact precessing about  $H_0$ , the component of  $\underline{M}$  perpendicular to  $H_0$  can produce a signal in an appropriately placed coil. This signal decays as the component of  $\underline{M}$  in the xy plane decays. This signal is known as the "free induction decay."

If a pulse of appropriate duration and magnitude to cause reversal of the spins ( $180^\circ$  pulse) is now applied the

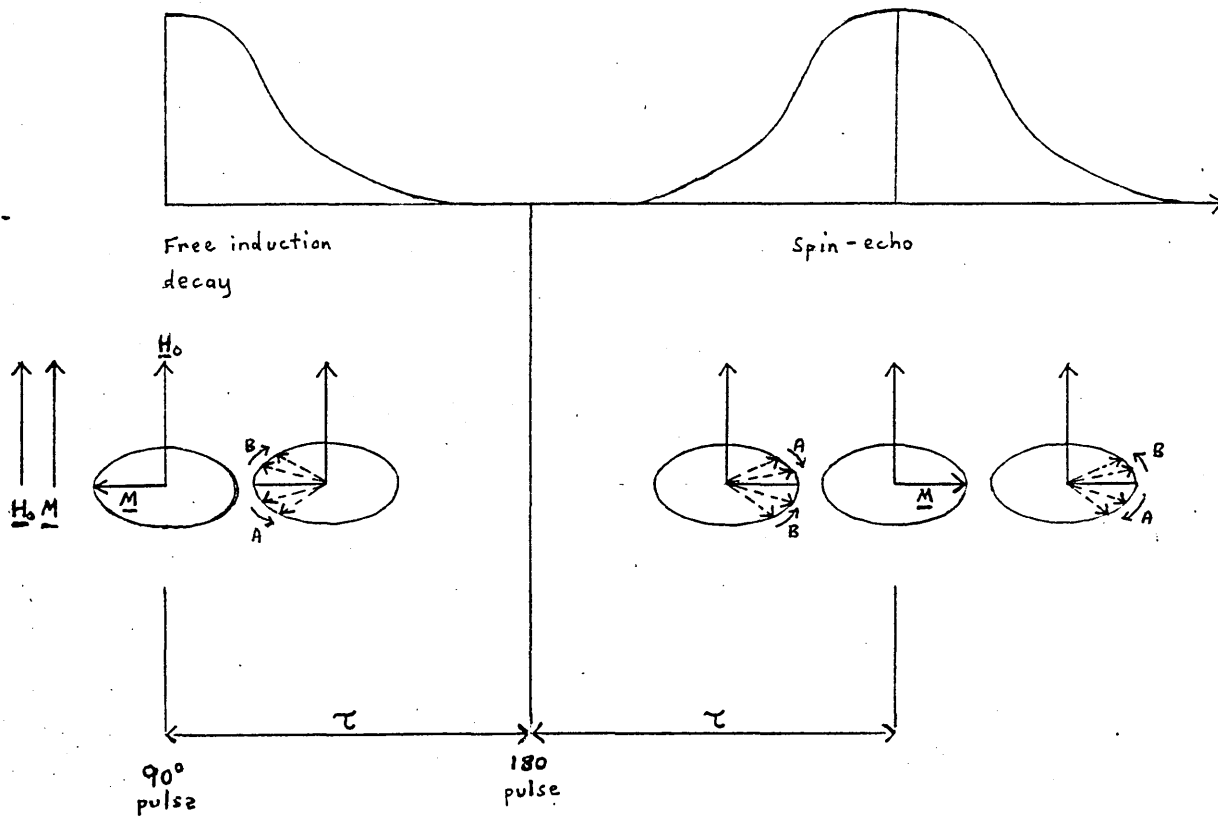


Fig.2.1. The nmr spin-echo experiment.

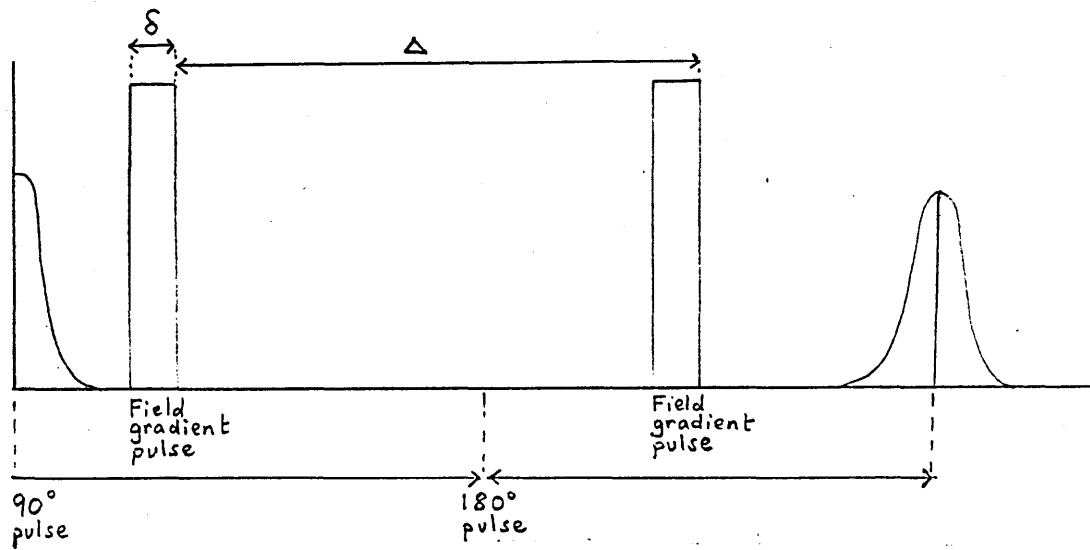


Fig.2.2. Pulse sequence used in self-diffusion measurements.

components of  $\underline{M}$  in the xy plane will gradually refocus (Fig. 2.1). They will then fan out again as before.

This results in an increase in the signal up to a maximum and then a decrease in the signal as before (in fact two free induction decay signals back to back); this signal is known as a "spin-echo". If the  $180^\circ$  pulse is at a time  $\tau$  after the  $90^\circ$  pulse, then refocussing is complete at  $2\tau$  and the spin-echo occurs at  $2\tau$ . The movement of molecules to slightly different values of  $H_0$  (possible because of inhomogeneities in the field) produces some irreversible defocussing of components of  $\underline{M}$  so that exact refocussing does not occur and the echo is therefore a smaller signal than the first free induction decay after the  $90^\circ$  pulse; the longer  $\tau$  the smaller the echo.

A pulsed magnetic field gradient is applied in the experiment to measure self-diffusion. A field gradient pulse is applied after the  $90^\circ$  pulse (Fig. 2.2). This causes a loss of phase coherence as different parts of the sample are exposed to different magnetic fields; thus the spin-echo is reduced in intensity (in the experiment its height on the oscilloscope screen is reduced to zero. A second field gradient pulse is applied after the  $180^\circ$  pulse which is equal (in magnitude and duration) and opposite to the first pulse; this counteracts the effects of the first pulse, restoring the echo to its full height, provided there has been no movement of spins

### 2.2.2. Cont'd.

within the sample. If diffusion is occurring the spins move between the times of application of the two pulses and so they do not experience an equal and opposite field when the second magnetic field gradient pulse is applied. Thus the effect of the first pulse is not completely counteracted, resulting in incomplete refocussing of the components of  $\underline{M}$  and a smaller echo. The decrease in the echo size will depend on how much diffusion has occurred between the times of application of the magnetic field gradient pulses and on the magnitude of the field gradient pulses used.

The relationship between the loss of echo height and the magnetic field gradient pulses applied is given by the following equations:

$$\frac{h}{h_0} = - D \cdot L \quad 2.8$$

where  $h$  is the echo height and  $h_0$  the echo height in the absence of field gradient pulses.

$$L = \nu^2 \int^2 \left( \Delta - \frac{\int}{3} \right) G_t^2 \quad 2.9$$

where  $\nu$  is a constant, the gyromagnetic ratio of the nucleus concerned ( $^1\text{H}$  in this experiment),  $\int$  the duration of the field gradient pulses,  $\Delta$  the time between them and  $G_t$  their strength.

$$G_t \propto \nu \quad 2.10$$

where  $V$  is the voltage used in the production of the pulses.

The echo height is observed as  $G_t$  is varied. For samples with one species containing protons all of which diffuse at the same rate, a plot of  $\ln \frac{h}{h_0}$  against  $V^2$  is a straight line from the gradient of which  $D$  can be calculated if the constants are known. Water is used for calibration since its diffusion coefficient is known; this is much easier than determining  $G_t$  itself. In order that a reasonable rate of decrease in  $\ln h$  is obtained over a convenient range of  $G_t$ ,  $\delta$  and  $\Delta$  are altered according to the sample, larger values being used for samples with slower rates of self-diffusion.

If the sample contains a number of species  $i$ , with self-diffusion coefficients  $D_i$ , then the echo height is given by equation 2.11.

$$h_g = \sum_i h_{i0} e^{-LD_i} \quad 2.11$$

where  $h_{i0}$  is the contribution to  $h_0$  of species  $i$ .

For a system where two diffusion coefficients are observed (such as the surfactant -  $H_2O$  systems) the graph obtained is not linear (Fig. 2.3). Where one component diffuses much faster than the other (water diffuses much faster than surfactant) at high values of  $G_t$

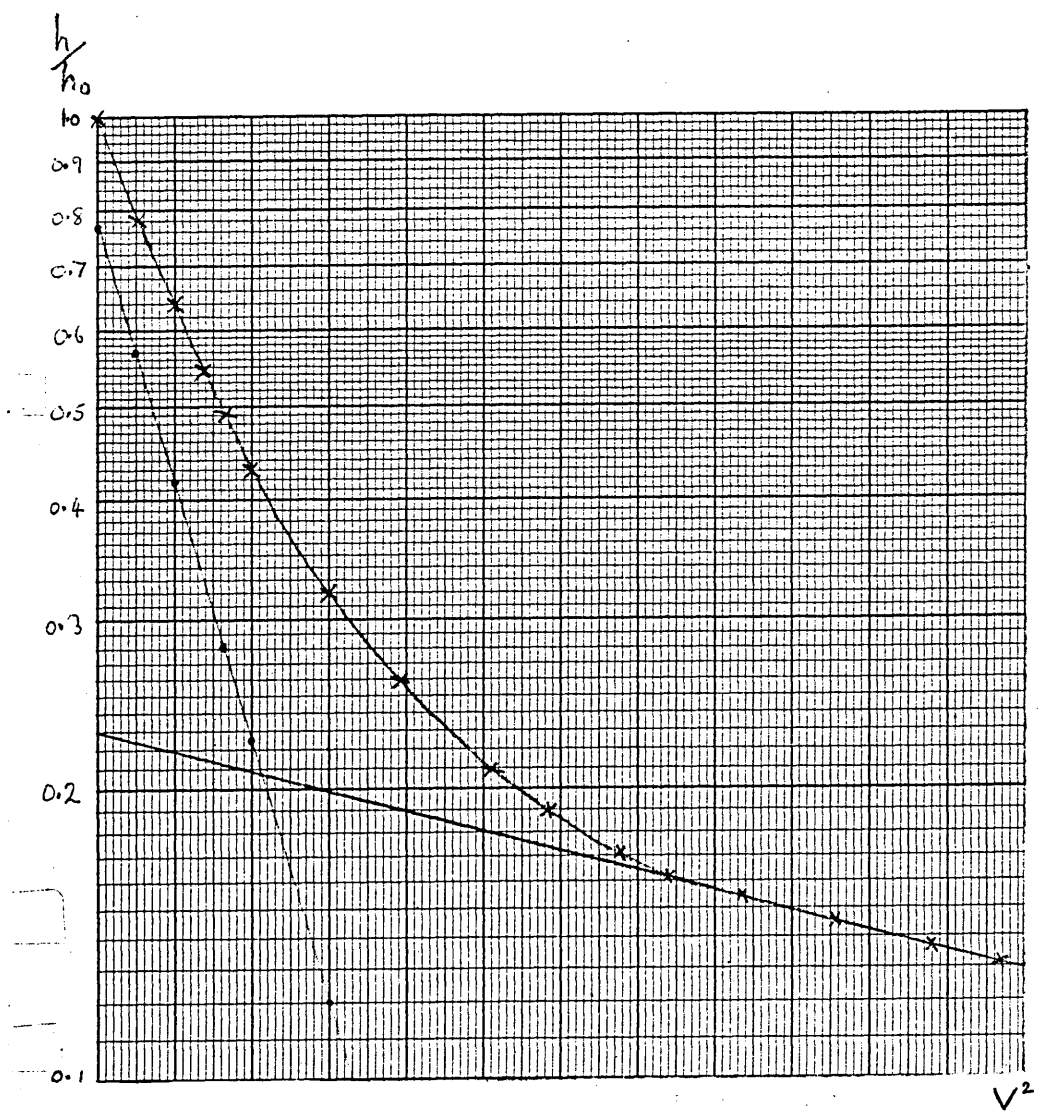


Fig.2.3. Example of graph obtained when measuring self-diffusion coefficients in surfactant-H<sub>2</sub>O samples.

### 2.2.2 Cont'd.

the contribution of the fast-moving component to the echo height measured is negligible. In the present case surfactant -  $D_2O$  samples give a straight line (using the  $^1H$  nucleus) so that it is possible to extrapolate the straight line obtained at high values of  $G_t$ , for surfactant  $H_2O$  samples, back to the h-axis.

If log-linear graph paper is used this line can be subtracted from the original curve to give the  $H_2O$  contributions to h, which are linear with  $V^2$ . The self-diffusion coefficient of the water in the surfactant system can be calculated from this second line. In cases where the graph is inadequate at high values of  $G_t$  it is possible to use the surfactant self-diffusion coefficient determined for the equivalent surfactant -  $D_2O$  sample and draw the line such that when it is subtracted from the curve a straight line is obtained for the water in the sample. The large difference between the self-diffusion coefficients of water and surfactant means that accurate values cannot usually be obtained for both from the same set of measurements. When obtaining values for water, the gradient of the surfactant part of the graph is usually close to unity and consequently there is a large error in it. Nevertheless, because it is so much smaller than the gradient of the water line, it is quite adequate for subtraction from the original curve, to obtain the water line.

### 2.3 THE PHASE RULE

The Gibbs phase rule provides a general relationship between the degrees of freedom of  $f$ , the number of phases,  $p$ , and the number of components,  $c$ :

$$f = c - p + 2 \qquad 2.12$$

The number of degrees of freedom,  $f$ , is equal to the number of intensive variables required to describe the system, minus the number that cannot be independently varied.

It is convenient to study many systems at atmospheric pressure and to regard this pressure as constant (the variations occurring having little effect where vapour phases are not involved). This leaves temperature and compositions as the intensive variables.

For a two-component system the concentration of only one component is required in order to specify the composition of the system. Thus there are two degrees of freedom (at constant pressure) and the system can be described by a two-dimensional diagram (Fig. 2.4). The maximum number of phases present in a given area of the diagram is two:

$$\begin{aligned} p &= c + 2 - f \\ &= 2 + 2 - 2 \end{aligned}$$

Single phase regions can also exist. It is possible for three-phase regions to exist but only along a line in the diagram, temperature and composition no longer being

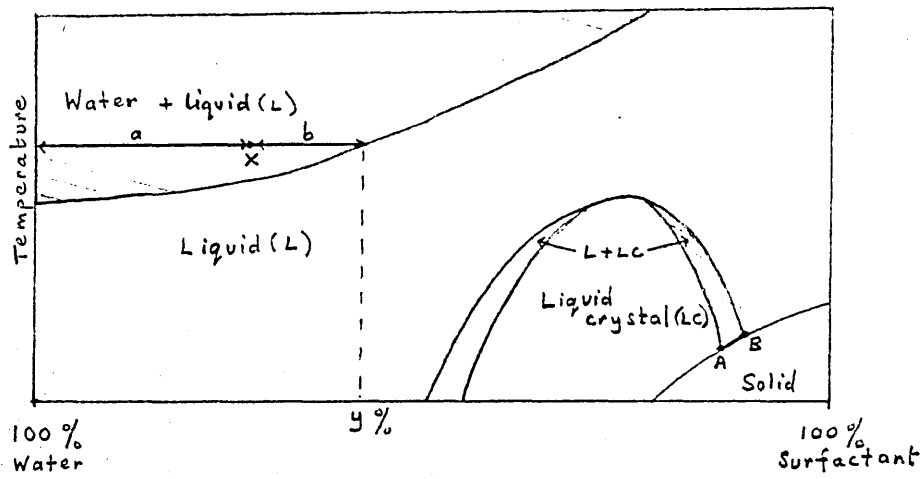


Fig.2.4. Phase diagram for a 2-component system (hypothetical).

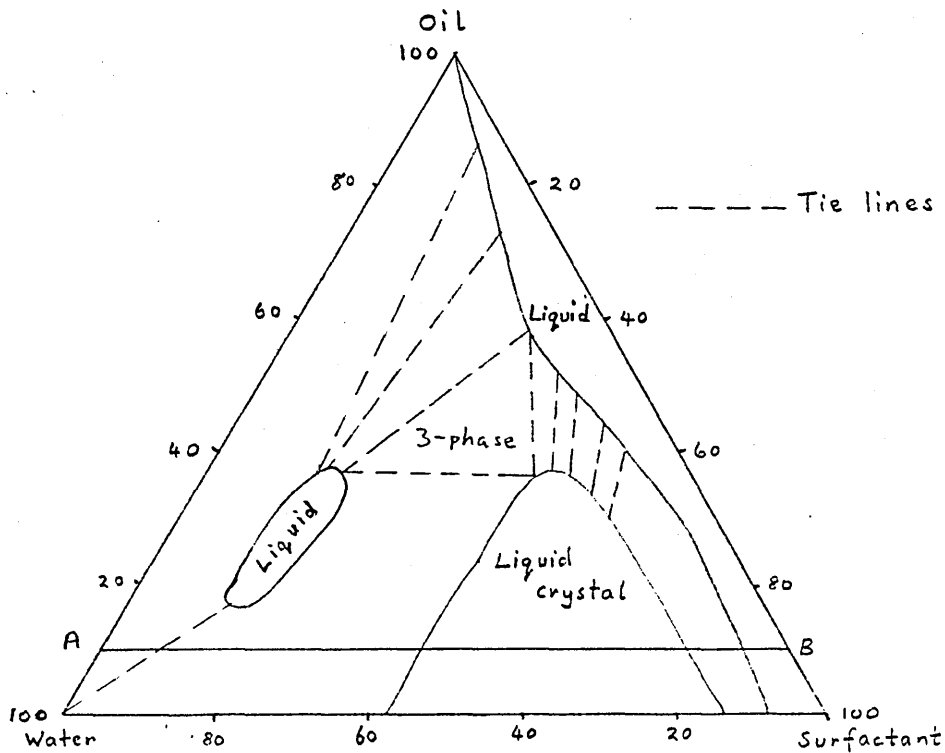


Fig.2.5. Phase diagram for a 3-component system (hypothetical).

### 2.3 Cont'd..

independent so that there is only one degree of freedom. AB in Fig. 2.4 is such a line; liquid, liquid crystal and solid are in equilibrium at compositions and temperatures specified by this line.

The proportions of the two separate phases at a point in the two phase region can be deduced from the tie line - this line links the two single phase regions at constant temperature (Fig. 2.4). The proportions of the two phases are in inverse ratio to the distance of the point (e.g. X) from the edge of the single phase regions (measuring along the tie line).

At X:

$$\frac{\text{proportion of water}}{\text{proportion of isotropic liquid of composition } y} = \frac{1}{a} / \frac{1}{b}$$

For a three-component system at constant pressure there are three degrees of freedom: the concentrations of two of the components and the temperature are required to specify a point in the system. This results in a three-dimensional phase diagram. Phase diagrams for such systems are frequently drawn at constant temperature, to be stacked on a vertical temperature axis. The composition diagrams at constant temperature are triangular (Fig. 2.5); each corner represents a composition of 100% of a particular component; each side represents compositions of binary mixtures. A line drawn parallel to the surfactant water axis (line AB for example) represents

a constant oil content.

In such systems at constant pressure and temperature one-, two- and three-phase regions occur, over areas of the phase-diagram. In theory four phases can be present at compositions specified by a line in the phase diagram:

$$f = 1$$

$$p = c + 2 - f$$

$$= 3 + 2 - 1$$

The three-phase regions are triangular in shape, the corners being points on the phase boundaries of single phase regions (Fig. 2.5). The relative proportions of the three phases are in inverse ratio to the distance of the point under consideration, from the corners of the triangle.

Where two-phases are in equilibrium tie-lines between the two single-phase regions have to be determined experimentally - they are not parallel to the composition axis as in the binary system. As before the proportions of the components are in inverse ratio to the distances of the point from the single-phases measured along the tie-line.

### 3. EXPERIMENTAL

#### 3.1 MATERIALS

The nonionic surfactants used were the commercially available "Brij 30" (Honeywill-Atlas Ltd.), which is a mixture of polyoxyethylene dodecyl ethers with an average oxyethylene chainlength of four units, and pure tetraoxyethylene dodecyl ether ( $C_{12}E_4$ ) (Nikkol, Japan) and pure hexaoxyethylene dodecyl ether ( $C_{12}E_6$ ) (Nikkol, Japan); all were used as received. The tetraethylene glycol ( $E_4$ ) (Aldrich Chemical Co. Limited) was used as received. Distilled deionised water was used. The following hydrocarbons were used as received: n-hexane, spectrographic grade (Fisons Ltd.); n-heptane, laboratory reagent grade (99.5%, BDH Chemicals Ltd.); n-decane, laboratory reagent grade (99.5%, BDH Chemicals Ltd.); n-hexadecane, puriss grade (99% Koch Light); n-octadecane, laboratory reagent grade (99% BDH Chemicals Ltd.). The triacetin was approximately 99% (Sigma Chemical Co.). The dekalin was a cis/trans mixture of laboratory reagent grade (BDH Chemicals Ltd.). Sodium chloride and potassium chloride were Analar grade.

#### 3.2 APPARATUS

The polarising microscope used was a Reichert instrument with heating and cooling stages.

Conductance was measured with a Wayne Kerr Universal Bridge, model number B224, operating at 1592 Hz.

### 3.2 Cont'd..

The self-diffusion coefficient measurements were made using a Bruker-Physik pulsed nmr spectrometer (B-KR 322s) operating at 60 MHz, with the Bruker-Physik field gradient unit accessory (B-KR-300 Z18).

High resolution nmr measurements were made at 60MHz using a JEOL C-60 HL spectrometer with variable temperature facilities.

An MSE High Speed 18 centrifuge with a variable temperature facility and a heated centrifuge constructed from an MSE Minor centrifuge contained in an air thermostat with a Laboratory Thermal Equipment temperature control unit were used in tie line determinations. Polypropylene tubes were used in the MSE High Speed 18 centrifuge and glass tubes were used in the MSE Minor centrifuge.

Viscosity measurements were made using an Ostwald viscometer with a time of passage for water at 25°C of 75s.

Sodium in Brij was determined using a Perkin Elmer AA 360 atomic emission spectrometer.

### 3.3 THE CONDUCTANCE CELLS

#### 3.3.1 THE COPPER CELL

Preliminary measurements were made using a cell consisting of two 0.8mm thick copper plates set into a piece of teflon and secured with a nylon screw and nylon nut (Fig. 3.1). The plates were cleaned briefly in concentrated

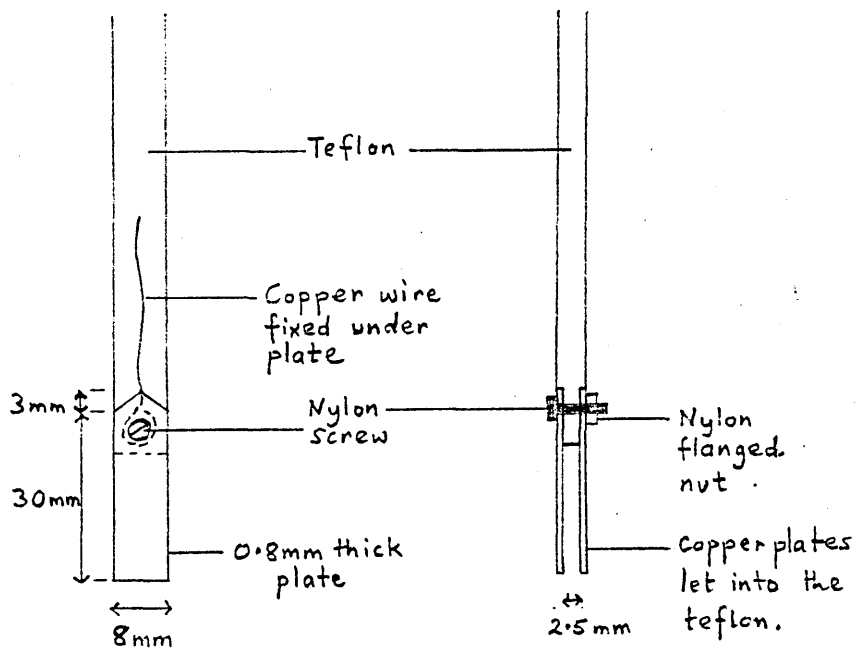


Fig.3.1. The copper cell.

### 3.3.1 Cont'd..

nitric acid before the cell was assembled. The distance between the plates was fixed at 2.5mm. The cell was used in stoppered test tubes (stoppered to facilitate the storage of samples between measurements), 100mm long, and having an internal diameter of 15mm. A volume of sample of 5cm<sup>3</sup> was sufficient to cover the plates. An increase in sample volume to, say, 6cm<sup>3</sup>, did not affect the conductance measured.

This cell had a number of drawbacks; these included:-

1. The susceptibility to oxidation of the copper,
2. the fact that the position of the cell in the sample tube was not fixed, leading to a small variation in the cell constant from one measurement to another,
3. the presence of tiny spaces between the copper plates and the teflon support and between the nylon screw in its hole and the teflon support; aqueous solution could be retained in these spaces when the conductivity of a non-aqueous sample was being measured and by providing a route for conduction through this aqueous channel lead to an erroneously high value of the conductance measured.

### 3.3.2 THE PLATINUM CELL

The platinum and glass cell was designed to eliminate these problems, and to minimise the volume of solution used, whilst retaining a suitable cell constant for the

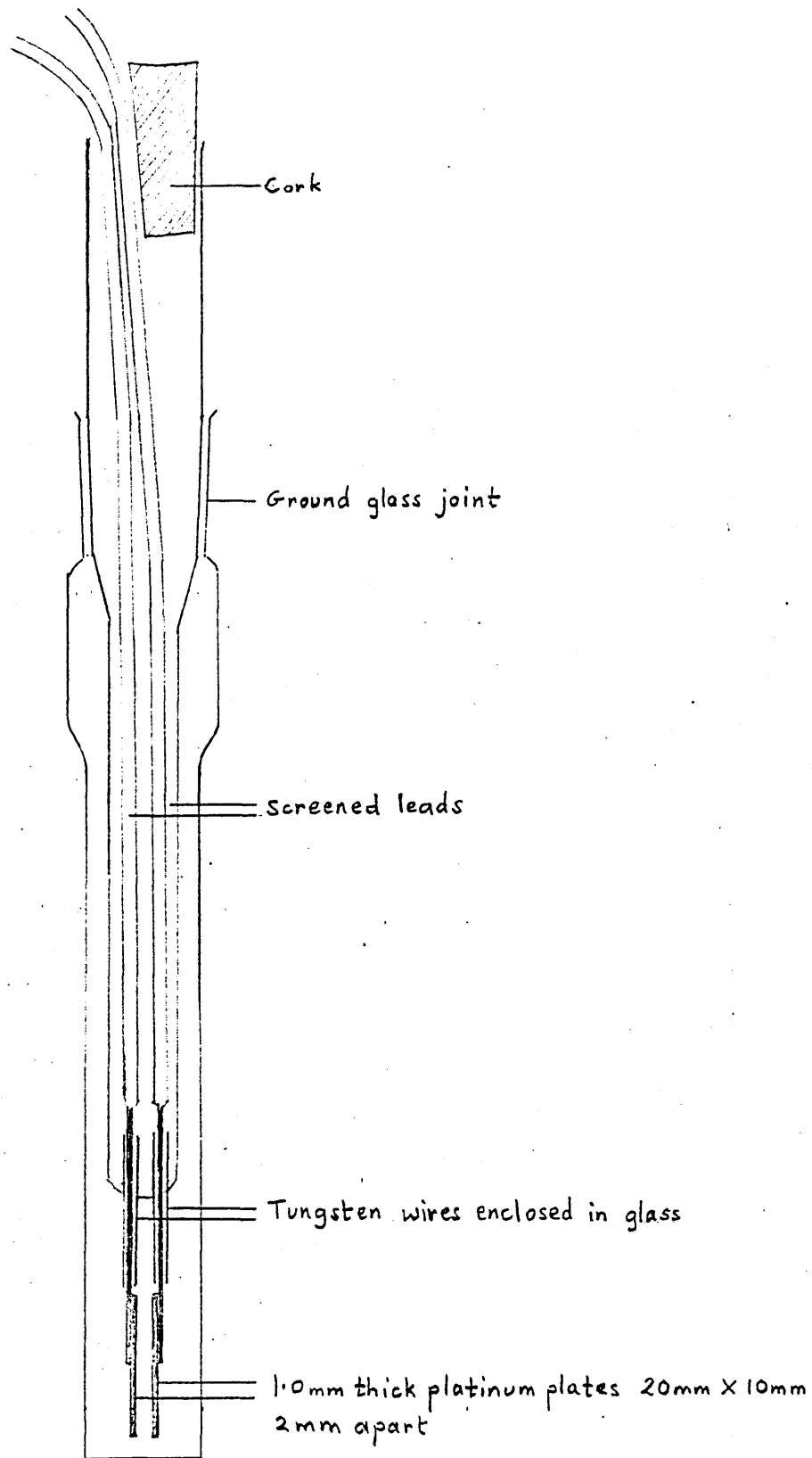


Fig.3.2. The platinum cell.

### 3.3.2 Cont'd..

conductivities to be measured. The cell also needed to be easily cleaned since liquid crystalline material was likely to be left on it after some measurements.

Two cells of the design shown in Fig. 3.2 were made. Bright platinum plates 20mm by 10mm and 1.0mm thick were soldered onto tungsten wires of 1mm diameter; these were sheathed in glass and set into the glass stem. Tungsten wires were used since platinum wires of a thickness sufficient to make the cell robust enough, could not be sealed in the glass satisfactorily because of the different coefficients of expansion of platinum and glass. The plates were fixed 2mm apart. The leads inside the stem were screened and the screening was connected to the screening of the leads of the conductance bridge, during measurements. The screening of the leads inside the stem was necessary because of the Parker effect; in the absence of screening this led to conductances being recorded, for poorly conducting nonaqueous samples, which were higher than the true values.

The top of the stem was a ground glass joint so that the cell fitted into the flat bottomed tubes, 155mm long with an external diameter of 17mm. A line was marked on the top edge of each tube so that the line on the cell could be aligned with it. In this way small variations in cell constant due to different alignments of the cell in

### 3.3.2 Cont'd..

each tube were avoided; these occurred because neither the cell nor the tubes were perfectly symmetrical. A sample volume of  $3.75\text{cm}^3$  was sufficient in all the tubes. Above this value the conductance measured was independent of the sample volume.

Before use for the first time these cells were cleaned with dilute hydrochloric acid and with acetone to remove any grease and soaked in water overnight. The cells were stored in water.

### 3.3.3 THE STANDARD CELL

A Mullard cell, type E7591/B, which is a glass cell with platinised platinum electrodes was also used for standardisation measurements in conjunction with the copper cell.

## 3.4 DETERMINATION OF PHASE DIAGRAMS

### 3.4.1 DETERMINATION OF PHASE DIAGRAMS FOR SYSTEMS CONTAINING BRIJ 30.

The Brij was stored at room temperature. It was shaken before use to suspend the traces of crystalline material present in it at room temperature. The Brij and water or Brij, water and hydrocarbon or triacetin, were weighed into stoppered test tubes; a total weight of 5g was used. In the binary systems samples were made up at 10% (composition by weight) intervals; additional samples were then made up, where necessary, to delineate the

### 3.4.1 Cont'd..

isotropic liquid region more precisely. In the ternary systems thirty-six samples at 10% intervals were examined, so covering the whole diagram Fig. 4.0 (p115). Extra samples of intermediate composition were made up as in the binary systems. Cross sections through the phase diagrams were determined by adding a third component in aliquots to an initial binary mixture.

The samples were observed whilst being stirred with a thermometer (-10 to 110 °C) as they were heated and cooled, usually in a water bath. The temperatures between which the single phase liquid regions existed were thus determined. Where appropriate a sleeve was used with the thermometer to reduce evaporation of volatile components at higher temperatures. Observation of any birefringence in the bulk samples (with the exception of Brij-H<sub>2</sub>O samples) aided the determination of the phase boundaries of the isotropic liquid regions. A box, having opposite faces of polaroid sheet, 25mm apart, was used; the pieces of polaroid sheet were crossed; the tube containing the sample was placed within the box. When the box was held up to the light it could be seen whether the sample was birefringent. Streaming birefringence, when present, could be observed with the same device when the thermometer was moved briskly up and down.

Daylight was used, in most cases, for the observation of the clarity or otherwise, of the samples and the presence

### 3.4.1 Cont'd..

or absence of birefringence. This was particularly important in the observation of samples which were blue translucent; blue translucence was not easily observed in artificial light.

Since the commercial surfactant, Brij 30, is a mixture of polyoxyethylene chain lengths, the transitions to and from single phase liquid regions were in some cases very poorly defined; in some samples the second phase was very slow to form or to dissolve at the transition. The temperature of the transition was estimated from the temperatures obtained on cooling and the temperatures obtained on heating the sample; a weighted average was taken.

Long term stability studies were not carried out on the samples.

Some observations of liquid crystalline samples were made on the variable temperature stage of the polarising microscope in order to identify the types of liquid crystal present.

### 3.4.2 DETERMINATION OF PHASE DIAGRAMS FOR SYSTEMS CONTAINING $C_{12}E_4$ and $C_{12}E_6$

The  $C_{12}E_4$  and  $C_{12}E_6$  were stored in a refrigerator; they were warmed to melt them before use and weighed out in the liquid state. The  $C_{12}E_4-H_2O$  and  $C_{12}E_6-H_2O$  systems

### 3.4.2. Cont'd.

were investigated using series of samples made up by dilution of the initial samples with water, up to a maximum of about 8g; above this sample size stirring was inadequate. The  $C_{12}E_4 - H_2O$  - heptane system was studied using the set of thirty-six samples at 10% intervals (Fig. 4.0 ); samples of a total weight of 2g were used. Additional samples were made up, where necessary, to delineate the isotropic liquid regions more precisely. The  $C_{12}E_4 - H_2O$  - triacetin system was studied using series of samples made by diluting initial  $C_{12}E_4$ -triacetin samples with water; again additional samples were made where necessary.

Cross sections through the phase diagrams were obtained by diluting initial binary mixtures with the third component. Only partial diagrams obtained in this way were determined for  $C_{12}E_4$  ternary systems with decane, hexadecane and octadecane as the third component.

The determination of the phase boundaries of the isotropic liquid regions was carried out as for the Brij systems (3.4.1.). In general the phase boundaries were more sharply defined with the pure surfactants. At low temperature and low surfactant content the phase transitions in  $C_{12}E_4 - H_2O$  - heptane and  $C_{12}E_4 - H_2O$ -decane samples took place only slowly; for this reason some of these samples were observed over periods of several hours at 0, 4 and 6 °C.

### 3.5 CONDUCTANCE MEASUREMENTS

#### 3.5.1 CONDUCTANCE MEASUREMENTS WITH THE COPPER CELL

This cell was stored dry so that the nylon screw would not stretch as it was liable to do when wet. Before use and before storage the cell was washed thoroughly with deionised water and dried with a tissue. When the plates became tarnished they were cleaned by placing the cell in deci-normal nitric acid; such cleaning did not significantly change measured conductances (except in the case of potassium chloride solution - see below). Between measurements with different samples the cell was dipped in acetone, then washed with water and dried with a tissue. The acetone was needed to remove the liquid crystalline coating which often formed on the cell when it was removed from the sample.

The cell constant could not be determined directly with potassium chloride solution because this tended to react with the copper plates, giving widely varying results and drifting readings on the conductance bridge. The cell constant of the Mullard cell was determined with 0.01 molar potassium chloride solution. The conductivities of Brij-H<sub>2</sub>O and Brij-H<sub>2</sub>O-hexane mixtures, which gave isotropic liquid phases at room temperature, were determined with the calibrated Mullard cell. Measurements were then made with these mixtures and the copper cell; hence its cell constant was determined. This was only determined at room temperature.

### 3.5.1. Cont'd..

Conductivities of samples containing Brij were measured with this cell. 5g samples were used, made up as for the phase diagram determinations. The larger volumes of samples containing high proportions of hexane or heptane did not affect the measurements. Initially the conductance of the water used to make up these samples was measured before use and water distilled within a few days was used, provided that its conductance remained sufficiently low. This procedure was later disregarded when the ionic impurity in the Brij was discovered, since any conductivity due to the water would have been negligible compared to that due to the ions from the Brij itself.

Conductance measurements were made at varying temperatures by placing the cell in a thermostated water bath.

### 3.5.2 CONDUCTANCE MEASUREMENTS WITH THE PLATINUM CELLS

The cells were stored in distilled deionised water. After an initial thorough cleaning with dilute hydrochloric acid and acetone no further cleaning of the plates was required except washing with acetone to remove the sample material. The cell was cleaned and dried with acetone between samples.

The cell constants were determined directly using 0.01 normal potassium chloride solution at  $25.0 \pm 0.2^\circ\text{C}$ .

### 3.5.2. Cont'd..

The cell constants were determined daily at 25.0°C when conductance measurements were being made. A series of measurements made at temperatures ranging from 0 to 75°C enabled the change in cell constant with temperature to be determined.

Samples of a minimum weight of 3.75g were used.

These were made up as for the phase diagram determinations except that for samples containing  $C_{12}E_4$  and  $C_{12}E_6$  0.01M sodium chloride solution was used instead of distilled deionised water. This solution was made up from Analar sodium chloride and distilled deionised water. The use of sodium chloride swamped errors due to traces of electrolyte contaminating the samples and gave a more convenient range of conductance for measurement.

The narrow salient region ( $\zeta$ ) in the  $C_{12}E_4-H_2O$ -heptane system has only a very small temperature range of occurrence for a given composition and only a narrow range of composition at a given temperature. Therefore, the following procedure was used to measure conductance in this region at specific temperatures. Binary mixtures of  $C_{12}E_4$  and water were made; heptane was added gradually, reducing the temperature of occurrence of the  $\zeta$ -region. When the desired temperature of occurrence was reached the conductance was measured. Further heptane was then added for another measurement to be made at a lower temperature. Up to four measurements were made in this way with each initial sample.

### 3.5.2. Cont'd..

A series of thermostatted water baths was used so that a cell could be placed in a given sample and measurements made at several temperatures without removing the cell from the sample. It was necessary to loosen the stopper to allow the pressure within the cell to return to atmospheric as the temperature was changed. Care was needed when making measurements at higher temperatures to ensure that the whole of the tube was in the water bath, so that evaporation of the more volatile components of the mixture and subsequent condensation in the cooler top of the tube did not occur; this could lead to alterations in sample composition and to inhomogeneity in the sample. With the exception of the refrigerated baths used for measurements below room temperature, the baths were of glass so that the state of the samples could be easily observed.

### 3.6 PULSED NMR MEASUREMENTS

Pulsed nmr was used to measure self-diffusion coefficients in the  $C_{12}E_4$ -water and  $C_{12}E_6$ -water systems.

The samples were made up by weight (about 0.4g) in the nmr tubes, which were then sealed. When not in use these samples were stored in a deep freeze. The samples were homogenized prior to use by heating or cooling to the temperature of the isotropic liquid phase and shaking. Since the temperature of the probe could

### 3.6 Cont'd..

only be altered by increments of one degree, obtaining the isotropic liquid phase throughout the sample was difficult when this phase had only a narrow temperature range as in the case of the higher temperature isotropic liquid phase in the  $C_{12}E_4$  - water system. Possible small differences in temperature within the probe itself may also have contributed to the problem.

The proton resonance was observed at 60MHz, small adjustments away from this frequency being made, when necessary, to avoid local interference. A  $90^\circ$ - $180^\circ$  pulse sequence was employed; the interval between the  $90^\circ$  and  $180^\circ$  pulses was  $\tau$ ; this produced an echo. The signal was observed on an oscilloscope screen. Field gradient pulses were applied (see section 2.2) and the echo height on the screen was observed as a function of the strength of the field gradient pulses ( $G_t$ ); the applied voltage which is proportional to  $G_t$ , was the property recorded. Water was used for calibration since its self diffusion coefficient was known (106). In order that a convenient range of  $G_t$  would be used the duration of the field gradient pulses ( $\sigma$ ) and the time between them ( $\Delta$ ) were altered according to the sample, larger values being used for samples with slower rates of self-diffusion.

Typical operating conditions were:

### 3.6 Cont'd..

for water diffusion:

$\tau$  20ms

$\delta$  3ms

$\Delta$  20ms

for surfactant diffusion:

$\tau$  40ms

$\delta$  5ms

$\Delta$  50ms

$90^\circ$  pulses  $3\mu\text{s}$ .

### 3.7 DETERMINATION OF TIE LINES

In order to confirm that certain isotropic liquid regions found in the  $\text{C}_{12}\text{E}_4\text{-H}_2\text{O}$ -heptane and  $\text{C}_{12}\text{E}_4\text{-H}_2\text{O}$ -hexadecane systems were genuine single phases and not metastable states, tie lines were investigated. In choosing compositions of samples an attempt was made to obtain two-phase liquid-liquid mixtures one phase being that under investigation; three-phase regions also occurred in these three-component systems.

A sample of  $\text{C}_{12}\text{E}_4$ , water and hexadecane was made up in a glass tube, homogenized at the required temperature (by vigorous shaking) then centrifuged in the heated centrifuge for 10mins at approximately 650rpm. Two layers were obtained which were analysed by high resolution nmr. The nmr was run at the same required temperature so that the samples remained as single phases; calculation

### 3.7 Cont'd.

of the relative amounts of the three components present, from the nmr spectrum, was only possible if no liquid crystalline material was present to give a broad line.

3g (approx) samples of  $C_{12}E_4$ , water and heptane were made up in stoppered polypropylene tubes for use with the MSE High Speed 18 centrifuge. These were homogenized where possible by heating or cooling from a single phase since vigorous shaking was not effective with these more viscous samples. The samples were maintained at the required temperature before centrifuging. 3 mins at 7,000 rpm was sufficient to separate some samples at  $12^{\circ}C$ ; 10mins at 10,000 rpm did not separate some at  $4^{\circ}C$  - these were highly viscous, possibly due to the presence of liquid crystalline material. Since the phases being investigated have only small temperature ranges of occurrence, fluctuations in the temperature of the centrifuge during its operation were a problem. The samples were separated and analysed by high resolution nmr as in the case of the  $C_{12}E_4-H_2O$ -hexadecane samples.

### 3.8 INVESTIGATION OF WATER SOLUBLE IMPURITIES IN BRIJ 30

A mixture of Brij and water (73% Brij) was heated until it formed an isotropic liquid, being mixed thoroughly and then heated further so that it separated into two layers. The lower aqueous layer was separated from the upper surfactant layer, which contains some water, at this temperature (about 90°C). Further water was added to the surfactant layer and the process repeated. Three extractions were done. The conductivities of the extrants were measured.

Further mixtures of about two parts of Brij to one part of water, or D<sub>2</sub>O were treated similarly. Only one extraction of each was carried out; these extracts were used in further tests for impurities in the Brij, (see section 4.7 ). The high resolution nmr spectra of D<sub>2</sub>O extracts were obtained.

### 3.9 DETERMINATION OF THE SODIUM IN BRIJ 30

The amount of sodium in the Brij was measured by atomic emission spectroscopy. 0.5%, 1%, 1.5% and 2% mixtures of Brij in water were made up and shaken well, before being measured in the spectrometer (a Perkin Elmer AA 360). At these concentrations the mixtures were not isotropic solutions; they were cloudy and a thin upper layer of surfactant tended to separate out. The ionic material would have been expected to be in the bulk aqueous layer though. The spectrometer was calibrated with standard sodium solutions. To check that surfactant

3.9 Cont'd.

did not interfere in any way, such as by altering the rate of solution uptake, 1% and 2% of deionised Brij was added to a 40 ppm standard solution. No difference in the reading was found.

## 4. RESULTS

The bulk of the results are presented in the form of phase diagrams, graphs and tables at the end of this chapter. The following is a description of those points which cannot be shown adequately in the diagrams and graphs. All percentage compositions quoted in these results are weight/weight.

### 4.1 PHASE DIAGRAMS

Figs. 4.1-4.26 show binary and ternary phase diagrams; fig. 4.0 shows the numbering system used for three component samples. The partial phase diagrams for three components are drawn at constant temperature (triangular diagrams) or at a constant ratio of two of the components (and thus at varying temperature).

Isotropic liquid regions are shown in all the phase diagrams. In the surfactant-water diagrams narrow two-phase liquid plus liquid crystal regions are not shown and are included in the liquid crystalline regions on the edges of which they occur. The boundaries between liquid crystalline and solid phases are not shown. In the ternary diagrams only the boundaries of the isotropic liquid regions are shown precisely. The approximate location of the liquid crystalline region is indicated on some of the diagrams.

The isotropic liquid regions include those samples which are clear but exhibit streaming birefringence (but not static birefringence). Streaming birefringence is

#### 4.1 Cont'd.

only indicated in the isotropic liquid regions although it can occur in other parts of the phase diagrams. The method of observing streaming birefringence was crude, where it is shown in the diagrams it occurs but it may occur to a greater extent than indicated. Also the onset of streaming birefringence when traversing the phase diagrams is very gradual so that its limits cannot be located precisely.

The isotropic liquid region also include samples which are blue-translucent (rather than colourless) by reflected light and yellowish-brown by transmitted light. In some cases a sharp boundary was found between blue-translucent regions and obviously two-phase (or three-phase) regions. In other cases there is not a sharp boundary. Where the boundary is very indistinct this is indicated.

Phase boundaries are located more precisely in the binary diagrams than in the ternary diagrams since observation of a given composition as a function of temperature gives points on the binary diagram but only gives points on the ternary diagram if the phase changes occur at the actual temperatures for which the diagrams are drawn; the phase boundary is extrapolated from the behaviour of the compositions studied.

Birefringence in the samples was observed by means of crossed polars using white light. Whilst many samples containing liquid crystalline material showed the normal

#### 4.1 Cont'd..

birefringence transmitting white light through the crossed polars other samples exhibited rainbow colours when viewed through crossed polars; the sizes of the rainbow patterns in the samples varied from one sample to another. These effects were more pronounced with the pure surfactants. They normally occurred in fairly fluid samples containing liquid plus liquid crystalline material. It was not determined whether "rainbow birefringence" could occur in single liquid crystalline phases where these were less viscous.

##### 4.1.1 THE $C_{12}E_4$ - $H_2O$ PHASE DIAGRAM (Fig. 4.1)

Different batches of  $C_{12}E_4$  produced small differences in the temperature of occurrence of the phase changes but the diagram was otherwise unchanged.  $C_{12}E_4$ - $D_2O$  samples showed the same phase changes but  $2^\circ C$  lower than the  $C_{12}E_4$ - $H_2O$  samples, using the same  $C_{12}E_4$ .

Below 16%  $C_{12}E_4$  the samples in the upper clear region are blue-translucent and become more so with decreasing surfactant content. Samples in this region are stable above about 2%; below this concentration it is still possible to obtain blue translucent samples at about the same temperature but they separate out in a few minutes.

No streaming birefringence was observed in the upper clear region on either side of the break in this region

#### 4.1.1 Cont'd.

between about 54 and 63%  $C_{12}E_4$ . There were slight variations ( $\sim 3\%$ ) in the length of the break and its composition of occurrence according to the batch of  $C_{12}E_4$ .

$C_{12}E_4$  in air, saturated with water vapour at  $35^\circ\text{C}$ , absorbs water until the sample composition reaches about 70%  $C_{12}E_4$ . At this composition and temperature the sample is a lamellar liquid crystal.

#### 4.1.2 THE $C_{12}E_6$ - $H_2O$ PHASE DIAGRAM (Fig. 4.2)

As in the  $C_{12}E_4$ - $H_2O$  system small differences were found between the phase diagrams according to the batch of surfactant used.

The isotropic region between the hexagonal and lamellar liquid crystalline phases, was found to be highly viscous and glassy clear. It has been shown (10) that this is a viscous isotropic liquid crystalline phase.

#### 4.1.3 THE BRIJ 30 - $H_2O$ PHASE DIAGRAM (Fig. 4.3)

The Brij itself is a commercial surfactant and contains a mixture of surfactant chain lengths. At room temperature it is a cloudy liquid; by about  $28^\circ\text{C}$  it is clear but the clearing point is not sharp. The phase changes in the Brij system are not as sharp as with the pure surfactants.

#### 4.1.3. Cont'd.

The clear region in the Brij-H<sub>2</sub>O system becomes blue-translucent below about 16% Brij, and becomes progressively more so as the Brij concentration decreases. A continuation of this region exists below about 10.5% Brij, but is not stable: the blue translucent liquid is only obtained on heating from room temperature or below and is only stable for about 3 minutes.

Streaming birefringence is not observed in the narrow part of the clear region, even in the region of maximum viscosity at 55% Brij.

Repetition of the investigation of the Brij-water phase diagram after 12 months showed that it was of the same form but that the temperature of occurrence of the narrow part of the clear region was 1½°C lower. The Brij had been stored at room temperature in a plastic can.

#### 4.1.4 THE C<sub>12</sub>E<sub>4</sub>-H<sub>2</sub>O-HYDROCARBON SYSTEMS

Only the heptane system (Figs. 4.5, 4.6 and 4.7) has been investigated in detail. The boundaries of the low temperature isotropic liquid region ( $\delta$ ) which is joined to the water corner at the lowest temperatures are difficult to locate precisely; at the lowest temperatures the samples tend to be viscous presenting problems with stirring and metastable states seem to be readily formed. The isotropic regions are formed only

#### 4.1.4. Cont'd.

slowly from cloudy (possibly birefringent) states and clear isotropic samples can take hours to become cloudy; similarly long times can be required for cloudy samples to clear. Blue-translucent states also occur throughout the temperature range and there is no clear boundary between the blue-translucent samples and cloudy samples on the low surfactant side of the region. The drawing of this boundary was therefore somewhat arbitrary.

The problem with the blue-translucent samples also occurred, to some extent, on the low surfactant side of the  $\epsilon$ -region.

In the  $C_{12}E_4$ - $H_2O$ -decane and -hexadecane systems (Figs. 4.11 and 4.12) metastable states again occurred adjacent to the  $\delta$ -region on its low temperature boundary. The low-surfactant content boundaries of the  $\delta$ - and  $\epsilon$ -regions of the decane system, where blue-translucent solutions occurred, were similarly ill-defined.

In the  $C_{12}E_4$ - $H_2O$ -heptane system blue-translucent solutions also occurred in the extension of the high temperature clear region, which occurred as heptane was added, at similar compositions to those at which the blue-translucence occurred in the binary system.

In the  $C_{12}E_4$ - $H_2O$  system the break in the high-temperature clear region between 54 and 63%  $C_{12}E_4$  disappears

#### 4.1.4. Cont'd.

on addition of heptane; about 2% is sufficient.

Many of the samples in this system ( $C_{12}E_4$ - $H_2O$ -heptane) which were birefringent due to the presence of liquid crystalline material exhibited rainbow colours when viewed between crossed polars with white light. A glassy clear liquid region existed at compositions around 10%  $C_{12}E_4$ , 10%  $H_2O$  plus 80% heptane below  $10^\circ C$ ; below about  $2^\circ C$  the sample became more viscous but remained clear. This clear liquid exhibited rainbow birefringence and so was not included in the isotropic liquid regions delineated; it did not appear to be connected to these.

#### 4.1.5 THE BRIJ 30- $H_2O$ -HEXANE SYSTEM (Figs 4.8 and 4.9)

The phase boundaries in this system are less well defined because of the mixture of chain lengths present in the Brij. At room temperature and below it is not possible to draw the phase boundary close to the Brij-hexane axis because cloudiness develops so gradually with changes in composition and also to some extent with time.

Samples of compositions close to 10% Brij, 40% water and 50% hexane are blue-translucent.

No detailed investigation has been made of the liquid crystalline phases. A lamellar phase has a large area of occurrence but other liquid crystalline phases may also be present. Samples of 50% Brij, 40% water, 10% hexane and 60% Brij, 30% water and 10% hexane show a

#### 4.1.5. Cont'd.

viscous isotropic phase between 40°C and 41.5°C, and between 40°C and 45°, respectively. This is a very viscous, glassy clear phase which is not birefringent until prodded with the thermometer when a flash of birefringence is seen.

#### 4.1.6 THE C<sub>12</sub>E<sub>4</sub>-H<sub>2</sub>O-TRIACETIN SYSTEM (Figs.4.23 and 4.24)

Again blue-translucent solutions occur where the high temperature clear region extends on the addition of triacetin.

The limit of compositions exhibiting birefringence (due to the presence of liquid crystalline material) is shown approximately at 0°C; liquid crystal, as a single phase or a component of a two-or-three-phase system, does not occur for water: surfactant ratios greater than about 50:50.

### 4.2 CONDUCTIVITY

Conductivity results are shown graphically in Figs. 4.5 - 4.9 on the phase diagrams, Figs. 4.27 - 4.46 and in tables 4.1 - 4.9.

#### 4.2.1 THE CELL CONSTANTS

The cell constant of the copper cell was  $8.3^{\pm} 0.2 \text{ m}^{-1}$  at 22°C. The cell constant of the Mullard cell was  $151 \text{ m}^{-1}$  (error  $< 1 \text{ m}^{-1}$ ) at 25°C.

#### 4.2.1. Cont'd.

The cell constants measured for the first platinum cell at  $25.0 \pm 0.2^\circ\text{C}$  were as follows:

6.92	$\text{m}^{-1}$
6.83	$\text{m}^{-1}$
$7.15 \pm 0.04$	$\text{m}^{-1}$

The first two values refer to a small number of measurements made on two days with the new cell. After this one platinum plate dropped off due to inadequate soldering; its replacement resulted in a slightly different cell constant.

The cell constants measured for the second platinum cell at  $25.0 \pm 0.2^\circ\text{C}$  were:

$7.62 \pm 0.04$	$\text{m}^{-1}$
$7.69 \pm 0.04$	$\text{m}^{-1}$

The difference arose because the tube in which the cell constant was measured was changed. Correction factors (cell constant for cell in tube y = cell constant measured in tube x multiplied by the correction factor) were determined for the different tubes and varied between 0.995 and 1.035. These correction factors were different for the two cells.

The variation of the cell constants with temperature was estimated to be  $0.003 \text{m}^{-1} \text{ }^\circ\text{C}^{-1}$ , the cell constants increasing with increasing temperature. Values of the conductivity of potassium chloride solution at varying temperature, obtained from The International Critical Tables, were used.

#### 4.2.2 SOURCES OF ERROR

Except at very low conductivities instrumental error was outweighed by other factors. Below 10nS conductance readings could only be obtained to two figures on the Wayne Kerr conductance bridge. Below 1nS only one approximate figure was obtained which served only as an indication of order of magnitude.

Errors arose due to changes in sample composition: part of the volatile hydrocarbon component could be lost at higher temperatures (above  $\sim 50^{\circ}\text{C}$ ); part of the water component could be lost at the highest temperatures in the binary systems (above  $\sim 80^{\circ}\text{C}$ ); the sample could absorb water particularly at higher temperatures, because of the humid atmosphere above the water baths used. Although the stoppered tubes reduced these problems they were opened and closed several times in the course of measurements so that these changes could occur. Slight changes in the water content of samples containing only a small proportion of water could cause significant changes in conductivity; this was particularly so for the pure surfactants which tended to absorb water.

For certain samples, in the  $\text{C}_{12}\text{E}_4\text{-H}_2\text{O}$ -hydrocarbon systems, very small temperature variations ( $<0.1^{\circ}\text{C}$ ) caused large changes in conductivity (e.g. sample number 7). Some of these samples were studied in detail in a thermostatted water bath with a high degree of temperature stability (temperature change on  $0.1^{\circ}\text{C}$  thermometer too

small to observe over 4hr.). Figs. 4.42 and 4.43 show these results. Others on the edges of the  $\epsilon$  and  $\gamma$  - regions were not studied in detail and the conductivities quoted could have been considerably different at temperatures only very slightly different.

The conductivities of samples in the Brij-H<sub>2</sub>O and Brij-H<sub>2</sub>O-hexane systems were measured with the copper cell. Measurements in the ternary system at 10% water content were repeated with the platinum cell. The results from measurements with the copper cell are subject to rather more error due to the design of the cell (section 3.3.1).

To exclude the possibility of changes in conductivity being due to the presence of sodium chloride, the conductivities of the following samples were also measured in the absence of sodium chloride (the samples were made up with distilled deionised water):

	<u>maximum K</u>	<u>minimum K</u>
sample number 6	8.0 $\mu\text{Sm}^{-1}$ (153)	2.7 $\mu\text{Sm}^{-1}$ (21.3)
sample number 11	1.2 $\text{mSm}^{-1}$ (20.9)	0.38 $\mu\text{Sm}^{-1}$ (0.58)
15.0% C <sub>12</sub> E <sub>4</sub> - 51.0%H <sub>2</sub> O - 34.0% decane	1.5 $\text{mSm}^{-1}$ (23.2)	11 $\mu\text{Sm}^{-1}$ (145)

The conductivity versus temperature curves for these samples were of the same form as those of samples doped with sodium chloride. The maximum and minimum values of conductivity measured in the clear regions are quoted, with values for the equivalent samples containing sodium chloride, in brackets (in the same units).

### 4.3 HIGH RESOLUTION NMR

High resolution nmr spectra were obtained for samples of 20%, 30% and 40%  $C_{12}E_4$  in water below  $25^{\circ}C$ . Table 4.14 shows the line widths (at half height) for the hydrogens of the oxyethylene chains and the hydrocarbon chains. Above the temperature of occurrence of the isotropic liquid region the 20% and 30% samples are cloudy and birefringent; the 40% sample is almost clear but birefringent. The surfactant lines are so broad that they are virtually indistinguishable; only the water lines are clear at these temperatures ( $> 21^{\circ}C$ ).

Within the isotropic liquid region the oxyethylene line in each sample is sharper than the hydrocarbon chain line and broadens only slightly with decreasing temperature. The hydrocarbon chain line broadens considerably so that at the lowest temperatures its width cannot be measured, the  $CH_2$  and  $CH_3$  lines forming one broad line. There is no measurable change in the width of the water line in this region. No sharp changes occur in line widths, in keeping with the gradual development of streaming birefringence with decreasing temperature. In this single phase liquid region stirring with a glass rod shows that, qualitatively, there is a marked increase in viscosity as the  $C_{12}E_4$  concentration is increased.

#### 4.4 VISCOSITY

Figs. 4.47 and 4.48 show viscosity in the Brij-water system, in the narrow high temperature isotropic liquid region. Absolute values of viscosity have not been determined. The viscometer was calibrated at 25°C with water; the measurements were made at around 67°C. The change in the dimensions of the viscometer was not allowed for but this error will be almost the same for most measurements, since most were made over small temperature ranges, of about 5°C, though the range was 16°C in one case. The density of the samples also needs to be known to calculate the viscosity from the present measurements. A value the same as that of water at 25°C was assumed although the true density is likely to be a little lower than this, considering the temperature and the density of the Brij used (0.943 gcm<sup>-3</sup> at 25°C). However, it is variations between the samples and with temperature which are of greater importance; changes in density of the same order of magnitude as changes in the viscosity would have produced noticeable volume changes in the samples.

#### 4.5 SELF-DIFFUSION

Self-diffusion measurements are subject to considerably more error than the conductivity measurements, as indicated by the scatter on some of the graphs. Error bars, where these are shown, are estimated from the

#### 4.5 Cont'd.

plots of  $\ln h$  versus  $V^2$ ; there is a considerable variation in the errors estimated in this way, due in part to the conditions for measuring the self-diffusion coefficient, in some samples being closer to the instrumental limits. This does not account for the scatter in some of the graphs (Figs. 4.49 - 4.55). A large error may have arisen in some cases because the sample was not a single isotropic phase; the problems in achieving this state are described in the experimental section (section 3.6).

#### 4.6 TIE LINES

Two tie lines were determined in the  $C_{12}E_4-H_2O$ -heptane system and one in the  $C_{12}E_4-H_2O$ -hexadecane system. In each case only one determination was made. Table 4.16 gives the compositions of the initial and separated samples.

#### 4.7 IMPURITIES IN BRIJ-30

##### 4.7.1 SODIUM IN BRIJ-30

A concentration of sodium of  $0.060 \text{ mol dm}^{-3}$  was found.

##### 4.7.2 WATER SOLUBLE IMPURITIES IN BRIJ 30

The high resolution nmr spectra of  $D_2O$  extracts are consistent with the organic matter in the extracts being polyethylene glycol : the peaks in the spectrum are at 3.80 and 4.85 $\tau$ .

4.7.2. Cont'd.

The conductivities of three successive extracts were as follows:

conductivity of first extract	=	28	$\text{mSm}^{-1}$
" " second "	=	12	$\text{mSm}^{-1}$
" " third "	=	5	$\text{mSm}^{-1}$

The nature of the anion present was not determined. Tests on the first extract for chloride and sulphate were negative, indicating that if these anions were present their concentrations were insufficient to give positive test results (with silver nitrate solution or barium chloride solution).

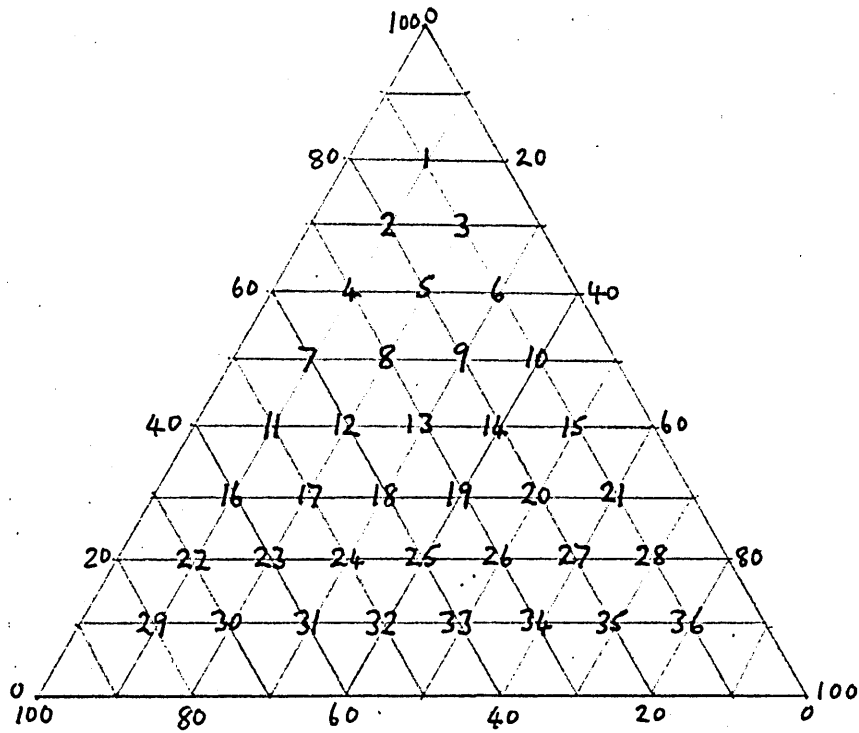


Fig. 4.0. The numbering system used for samples in the ternary systems.

Key to symbols used in the phase diagrams



Blue translucence (not shown in all diagrams)



or

Streaming birefringence



Phase boundary which could not be located precisely,  
or boundary of metastable region.



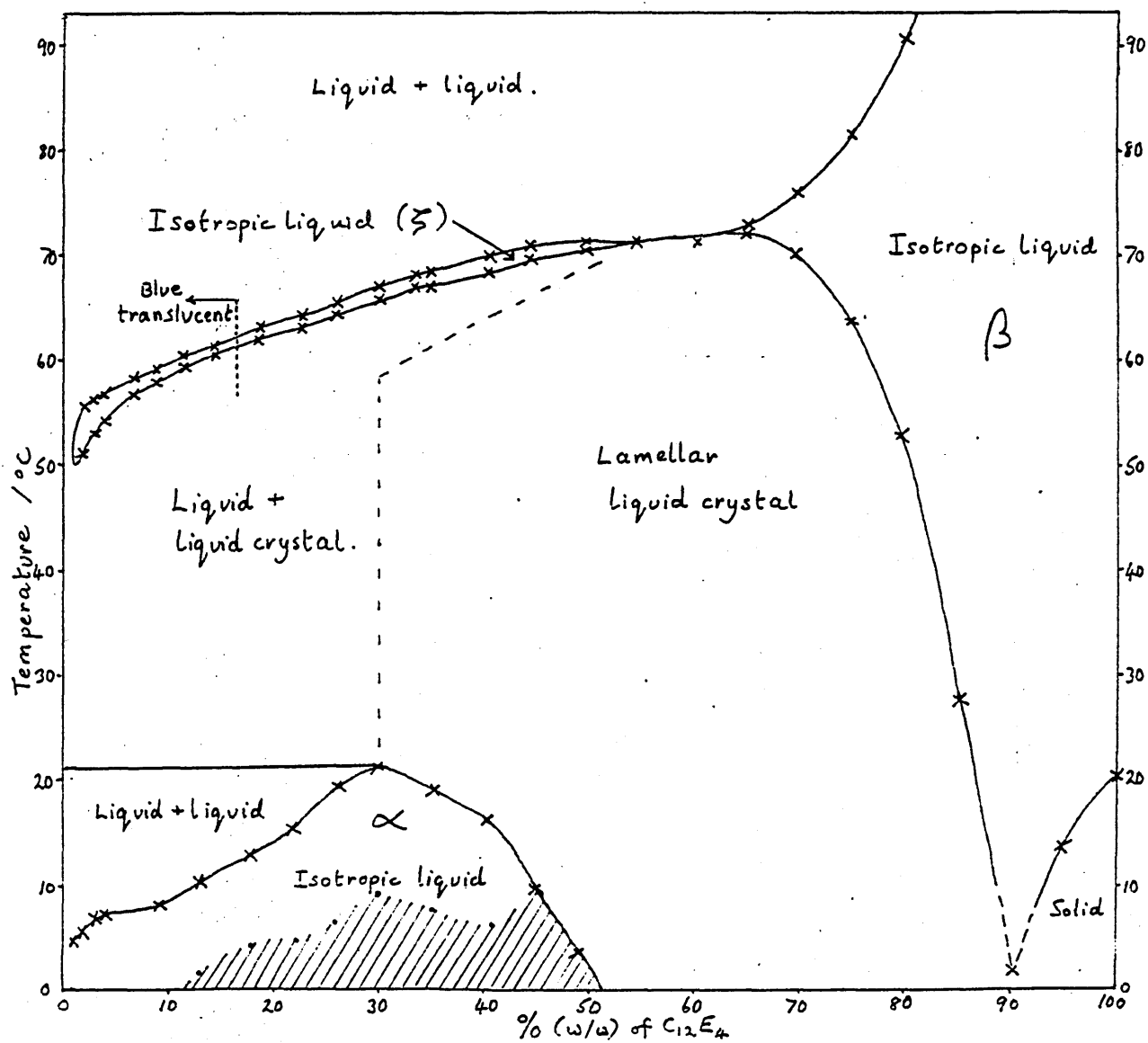


Fig. 4.1. Phase diagram of C<sub>12</sub>E<sub>4</sub>-water.

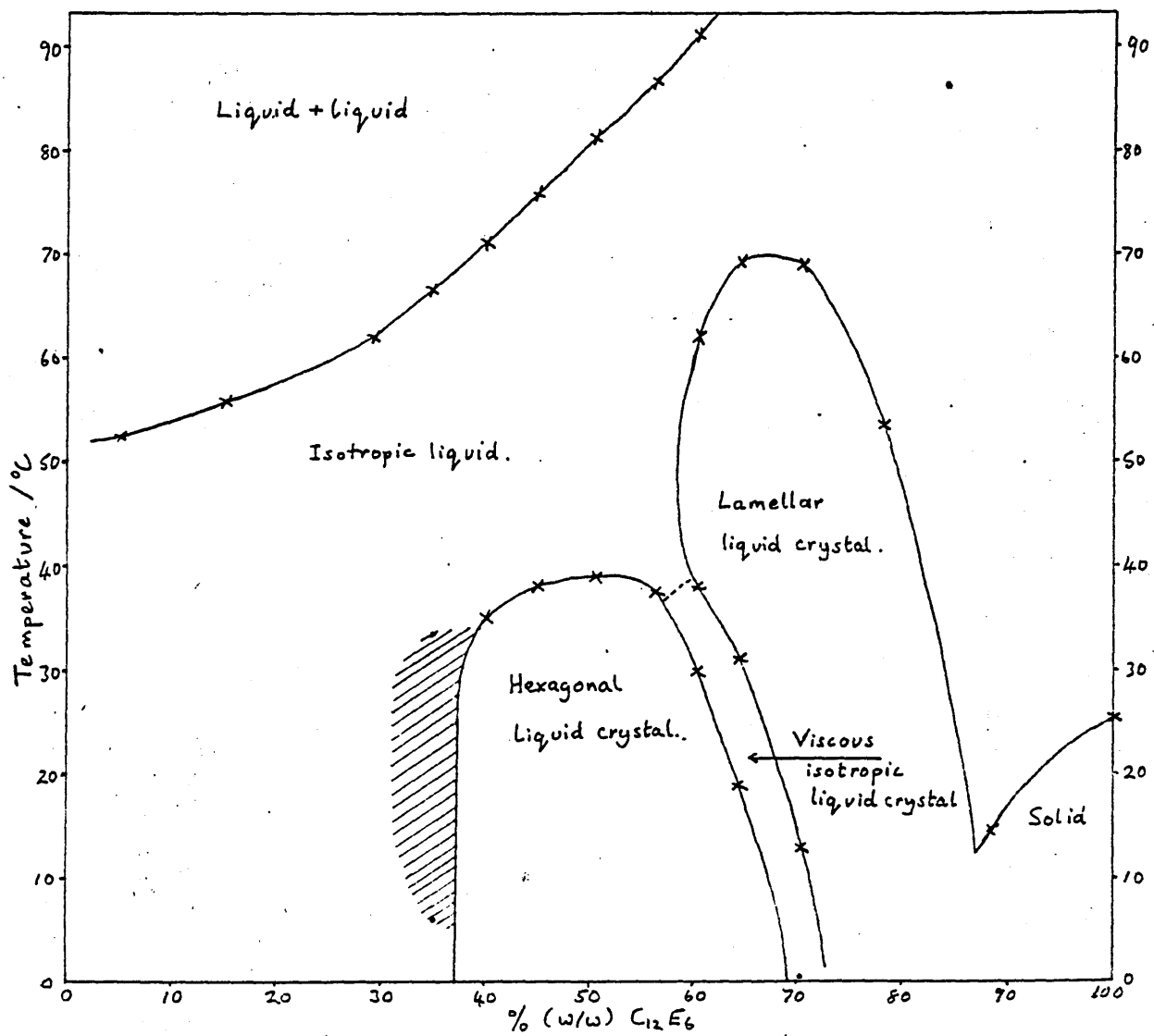


Fig. 4.2. Phase diagram of C<sub>12</sub>E<sub>6</sub>-water.

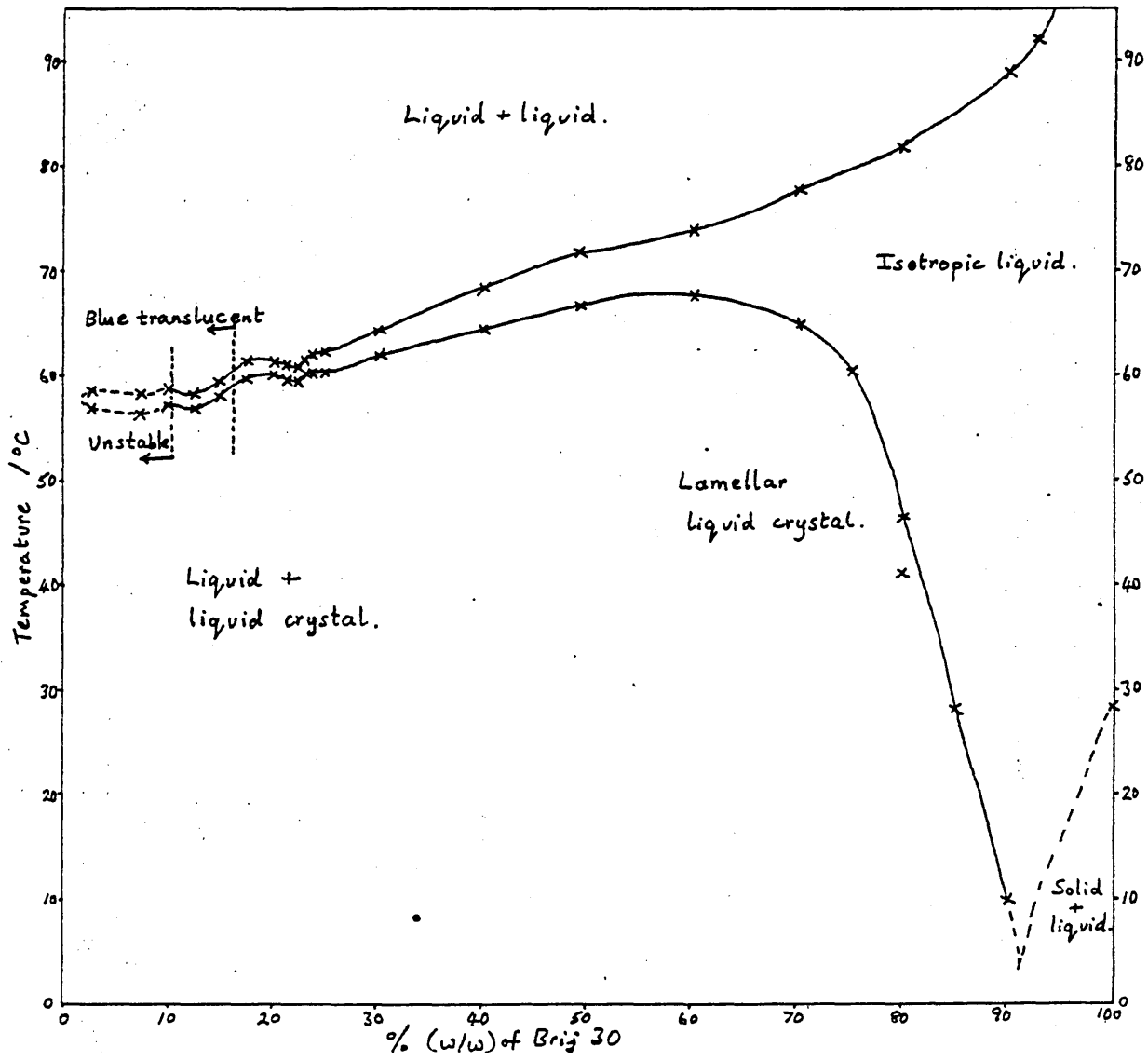


Fig. 4.3. Phase diagram of Brij-water.

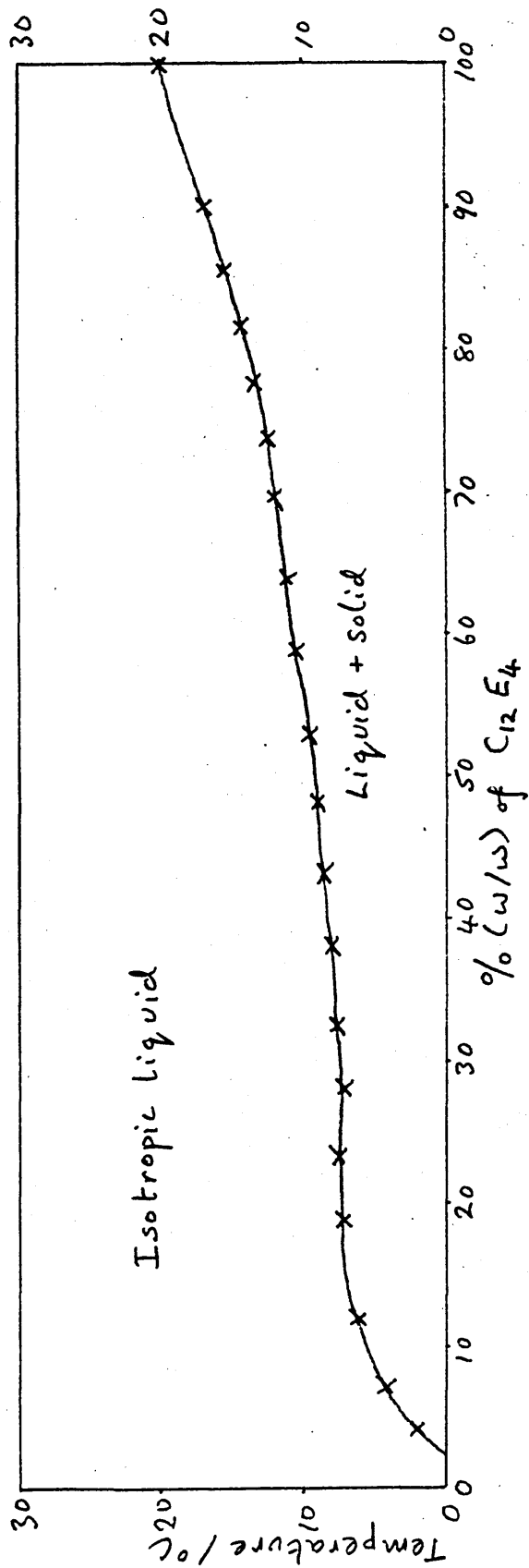


Fig. 4.4. Phase diagram of C<sub>12</sub>E<sub>4</sub>-heptane.

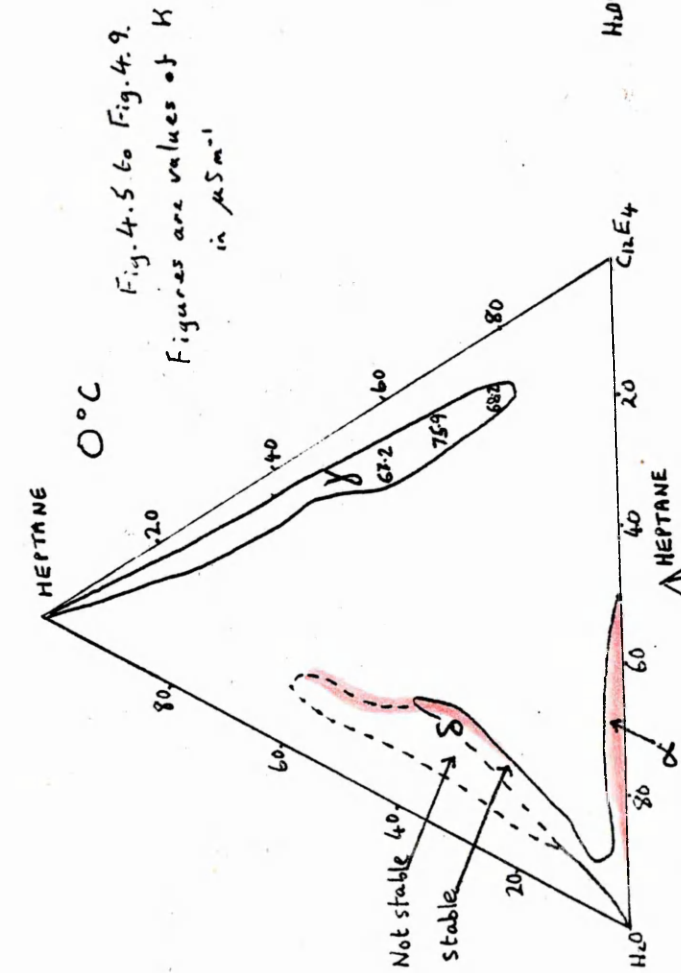


Fig. 4.5 to Fig. 4.9.  
Figures are values of  $K$   
in  $\mu\text{S}\cdot\text{m}^{-1}$

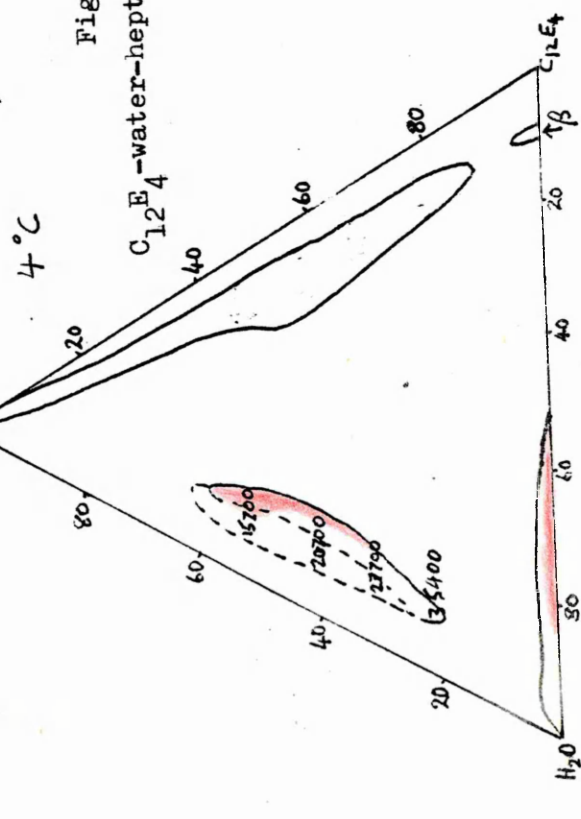
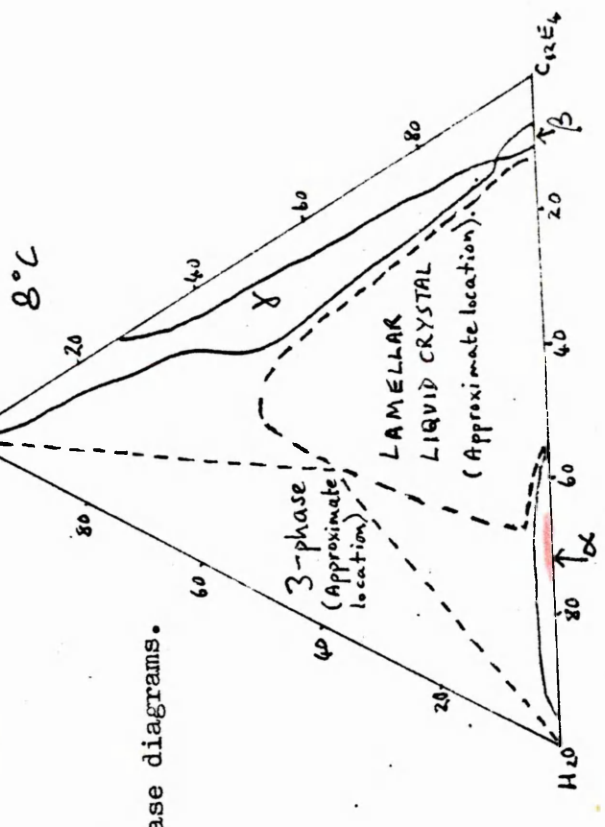
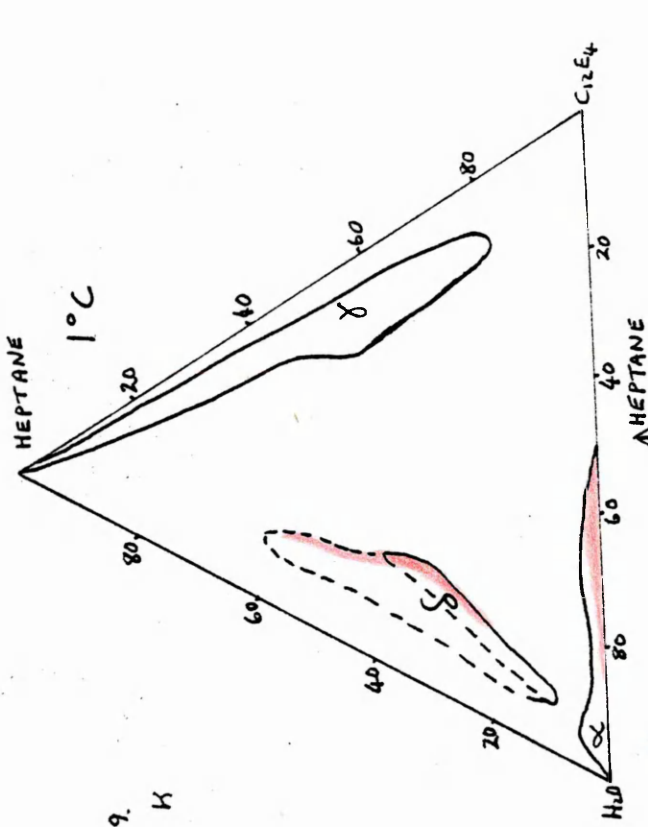
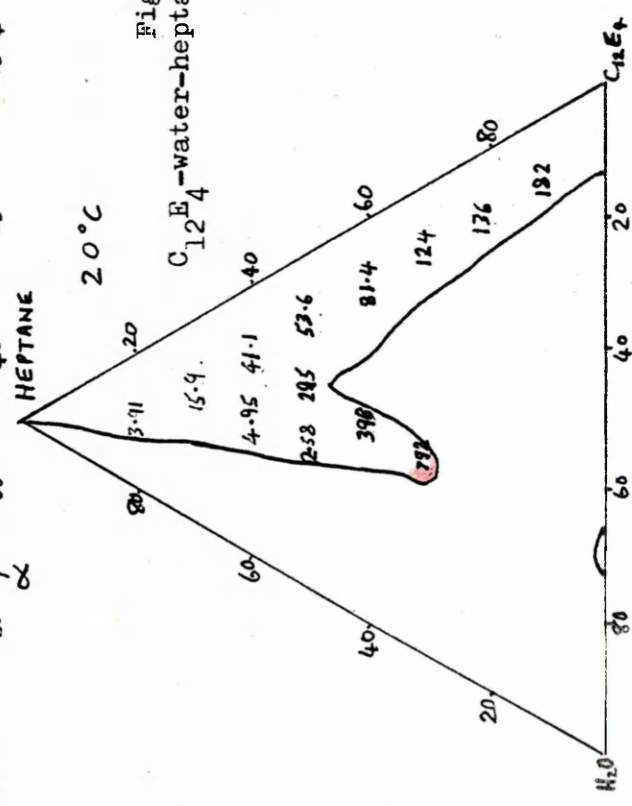
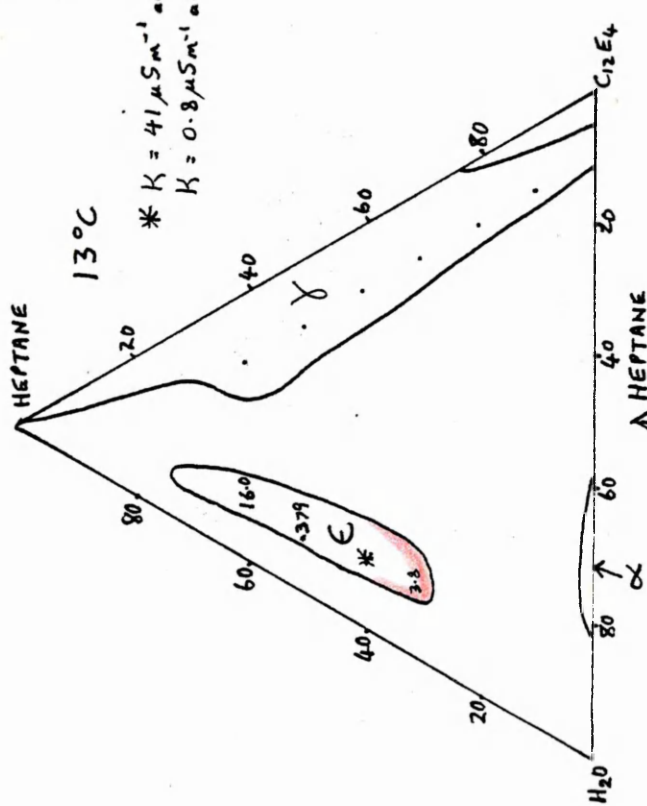
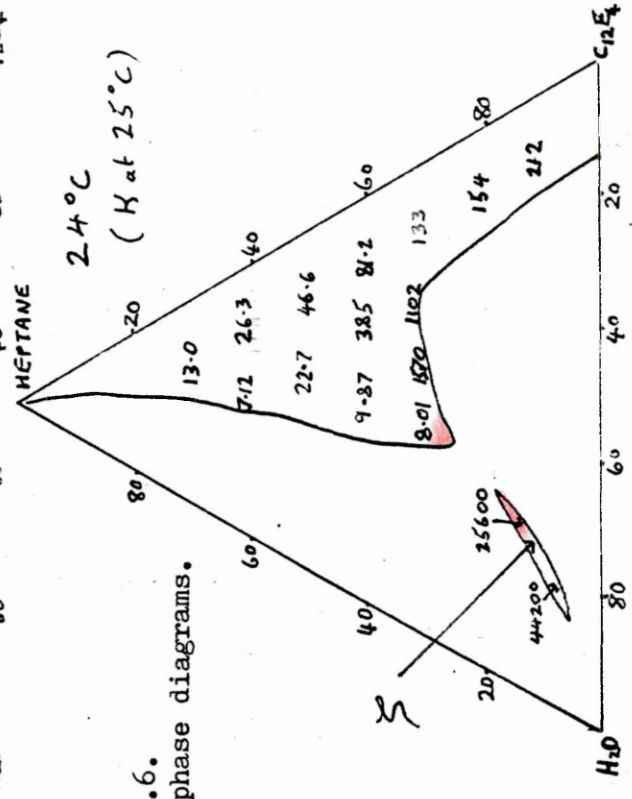
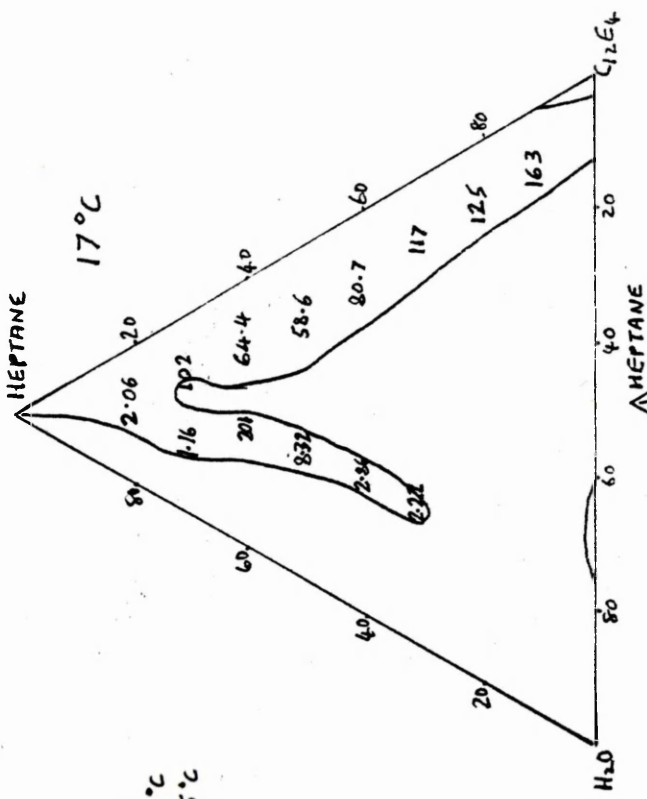


Fig. 4.5.

$C_{12}E_4$ -water-heptane phase diagrams.





\*  $K = 41 \mu\text{Sm}^{-1}$  at  $12.1^\circ\text{C}$   
 $K = 0.8 \mu\text{Sm}^{-1}$  at  $12.5^\circ\text{C}$

Fig. 4.6.  
 $\text{C}_{12}\text{E}_4$ -water-heptane phase diagrams.

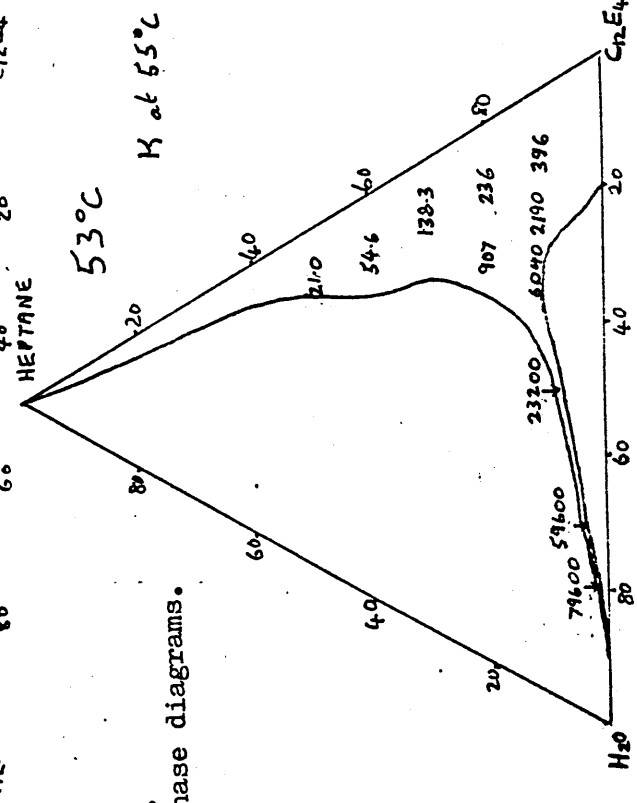
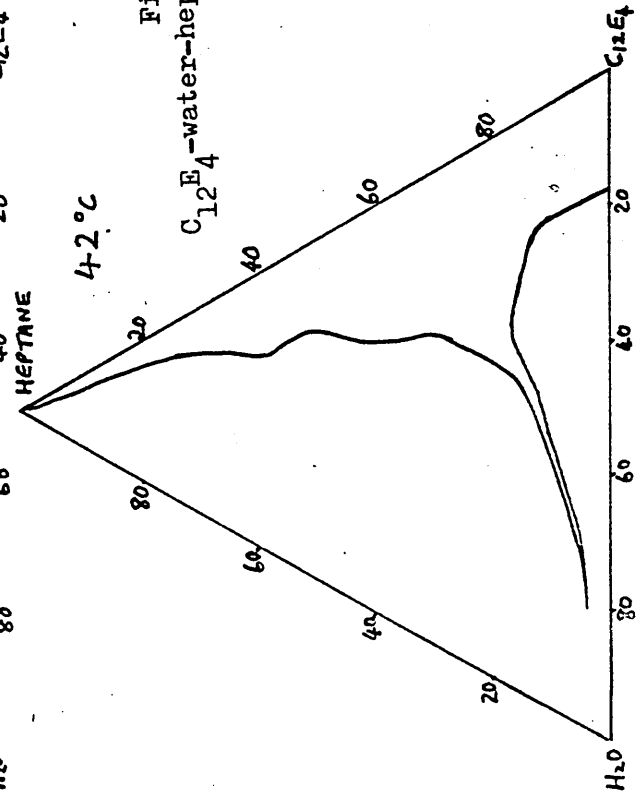
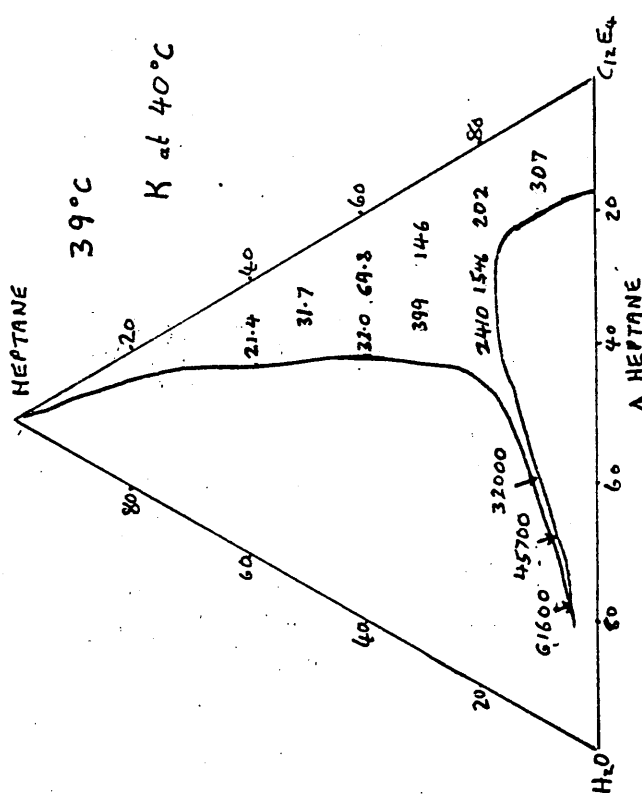
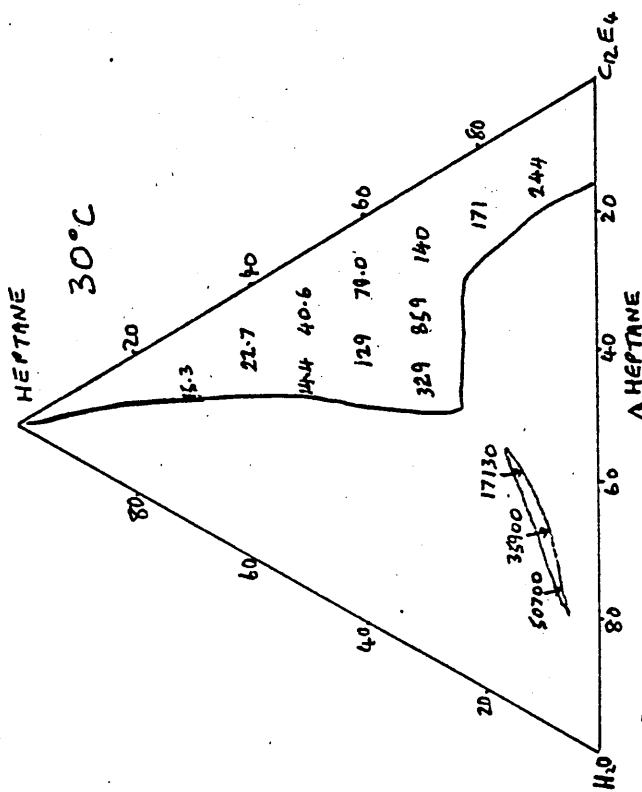


Fig. 4.7.  
C<sub>12</sub>E<sub>4</sub>-water-heptane phase diagrams.

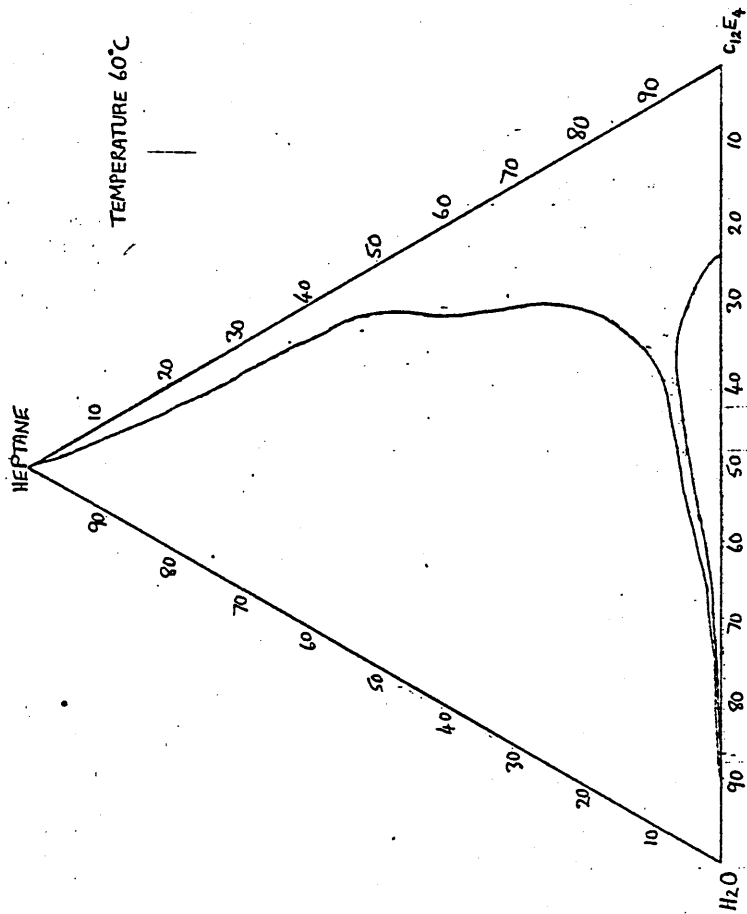


Fig.4.7.continued.  
 C<sub>12</sub>E<sub>4</sub>-water-heptane phase diagrams.

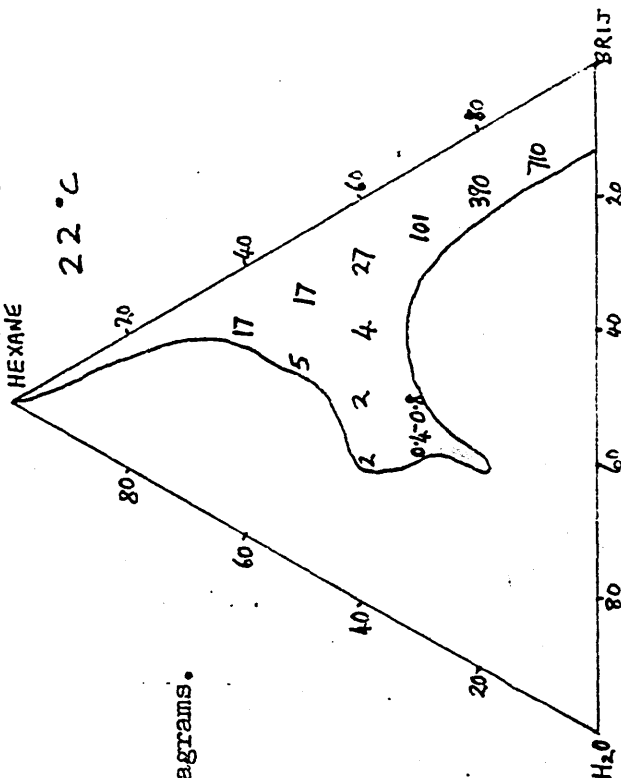
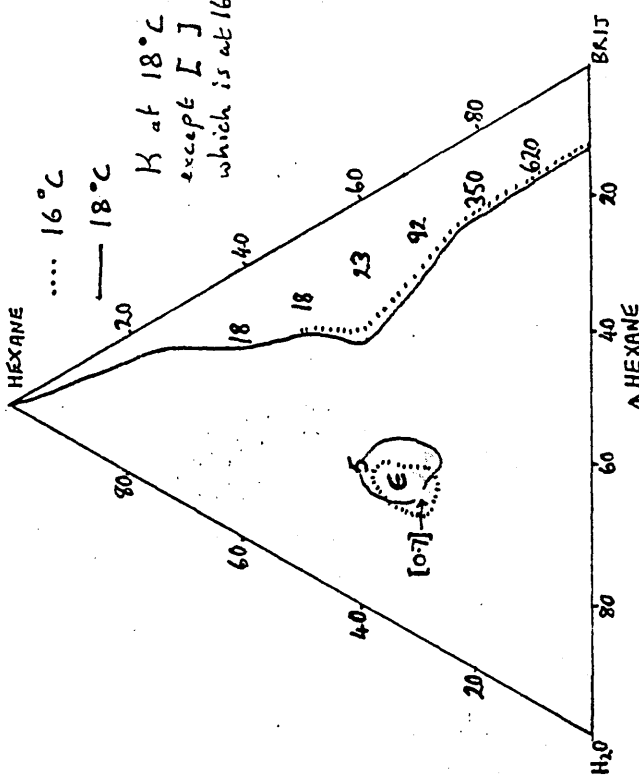
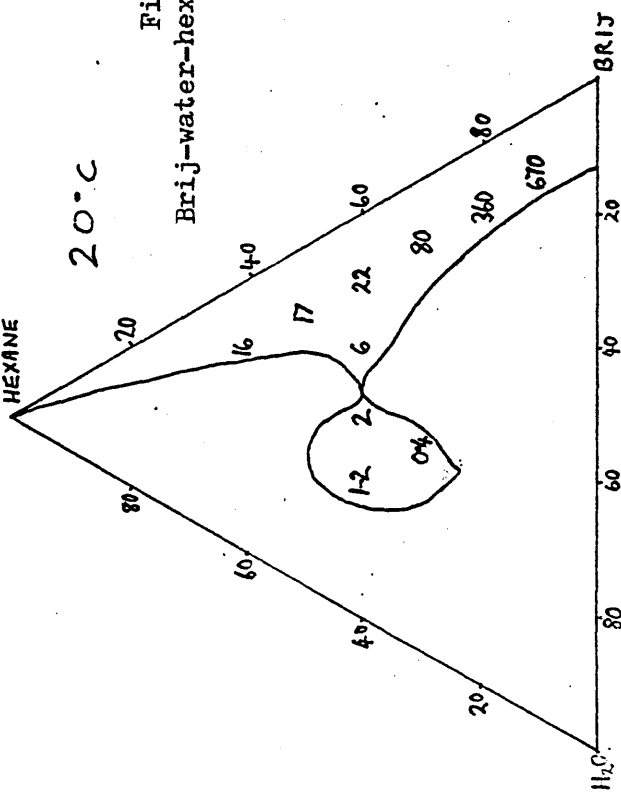
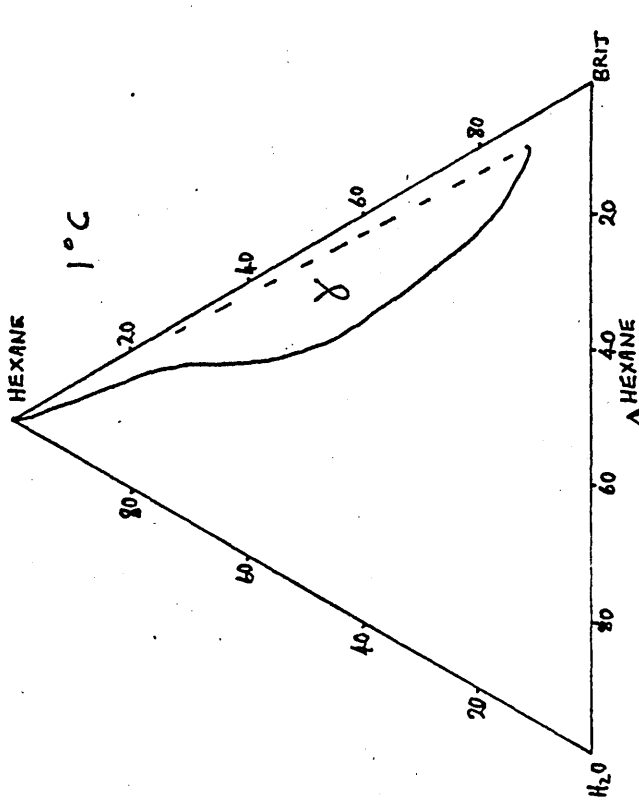


Fig. 4.8.  
Brij-water-hexane phase diagrams.

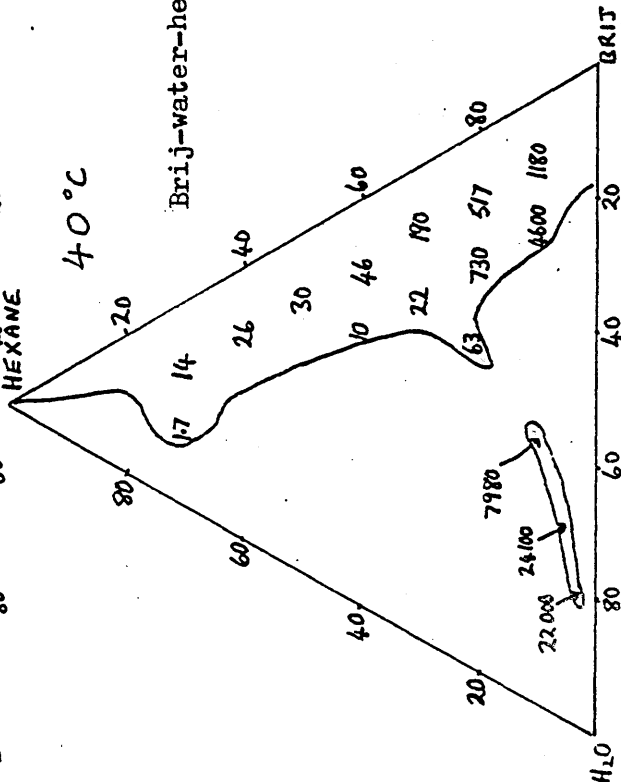
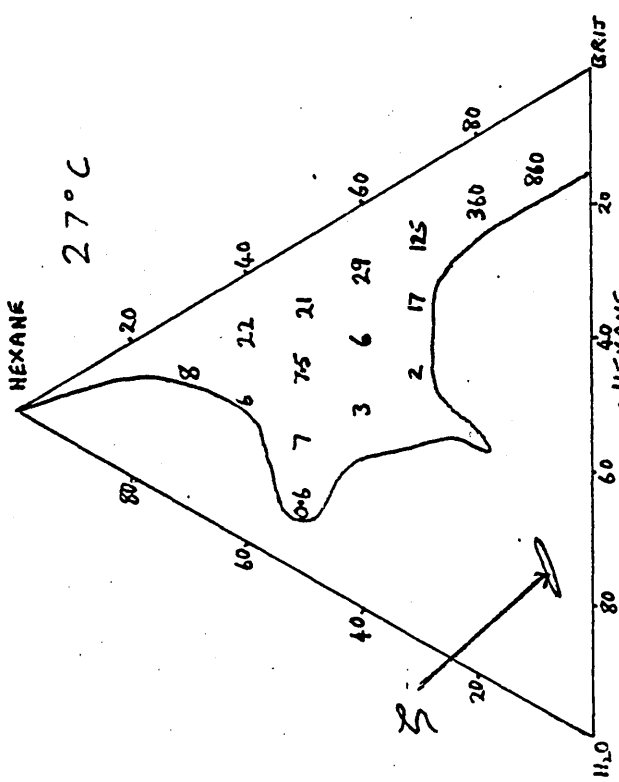
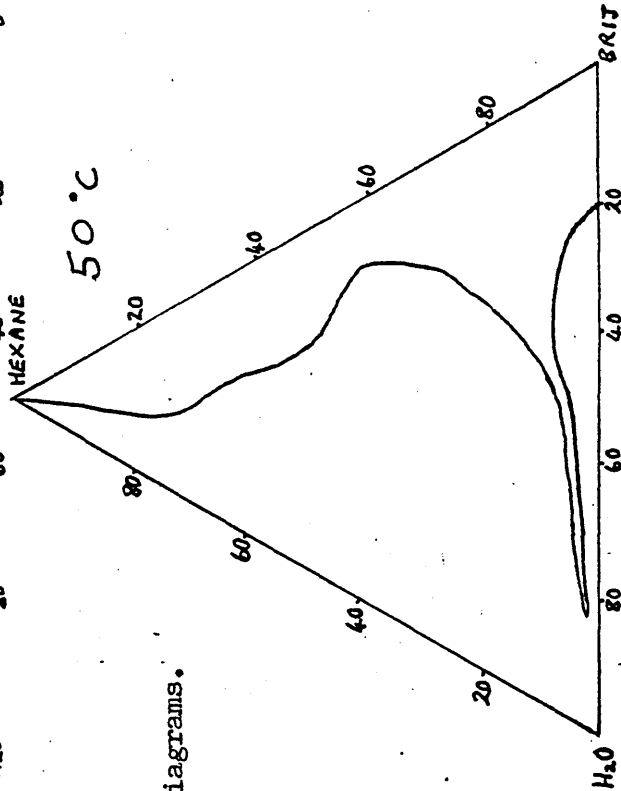
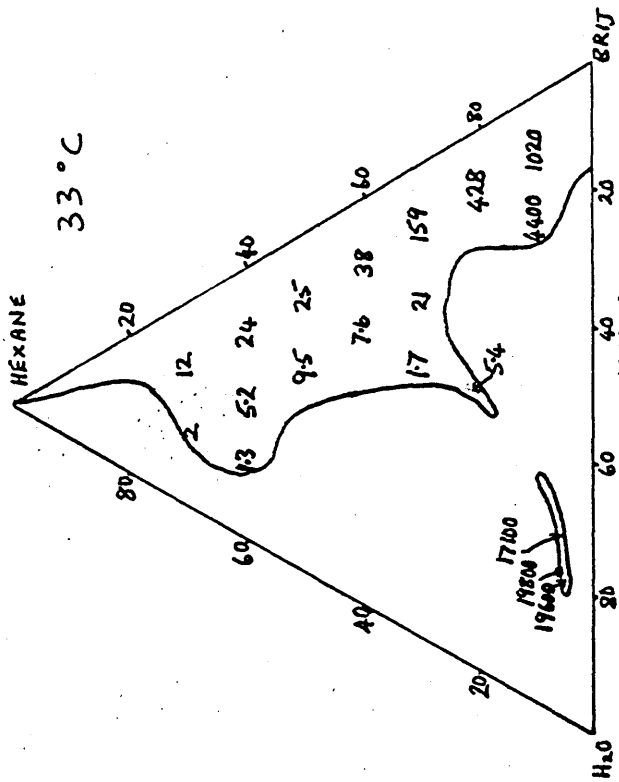


Fig. 4.9.  
Brij-water-hexane phase diagrams.

Fig. 4.10. Phase diagram obtained on adding  $C_{12}E_4$  to 59.7% water-40.3% heptane.

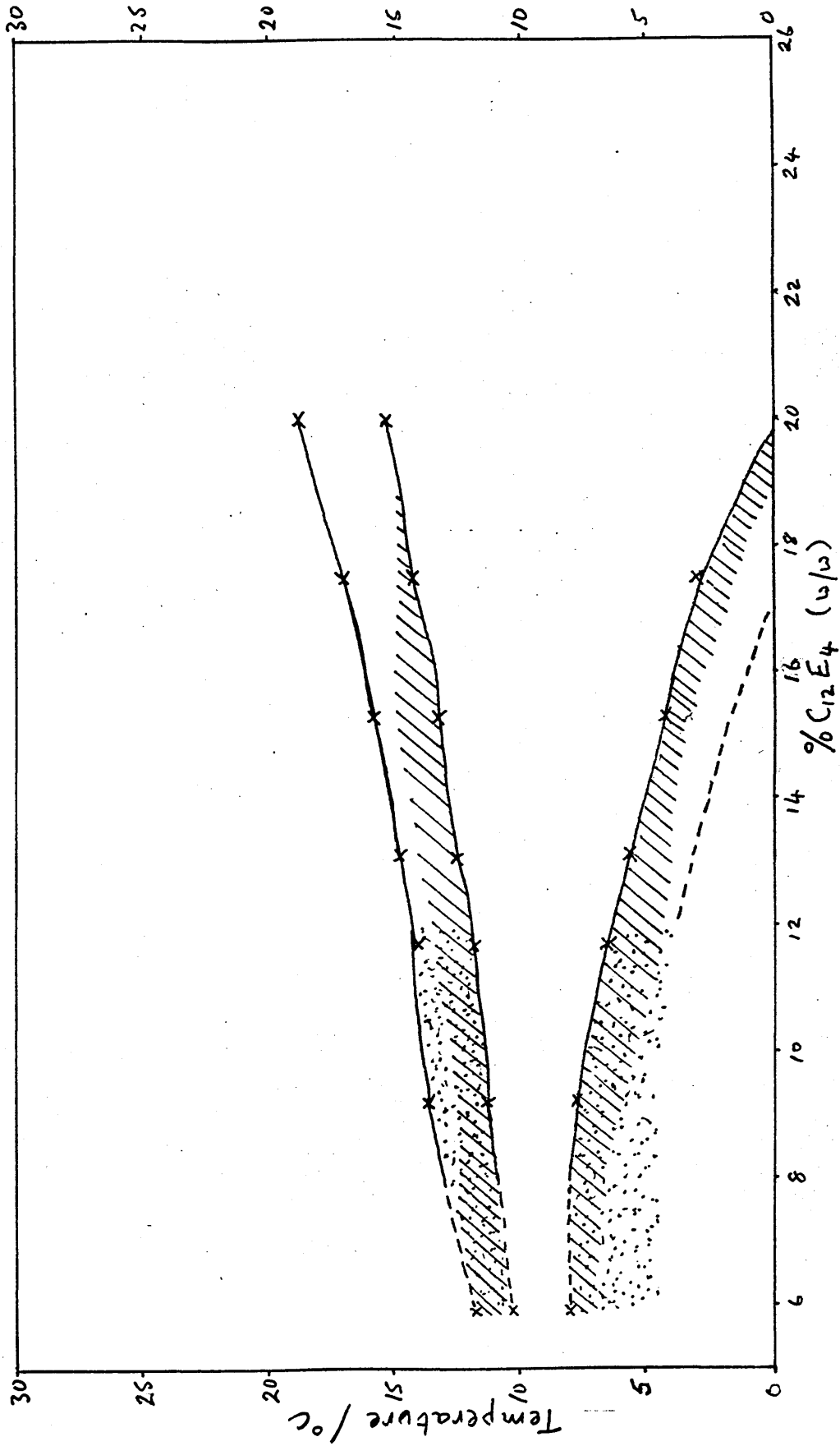
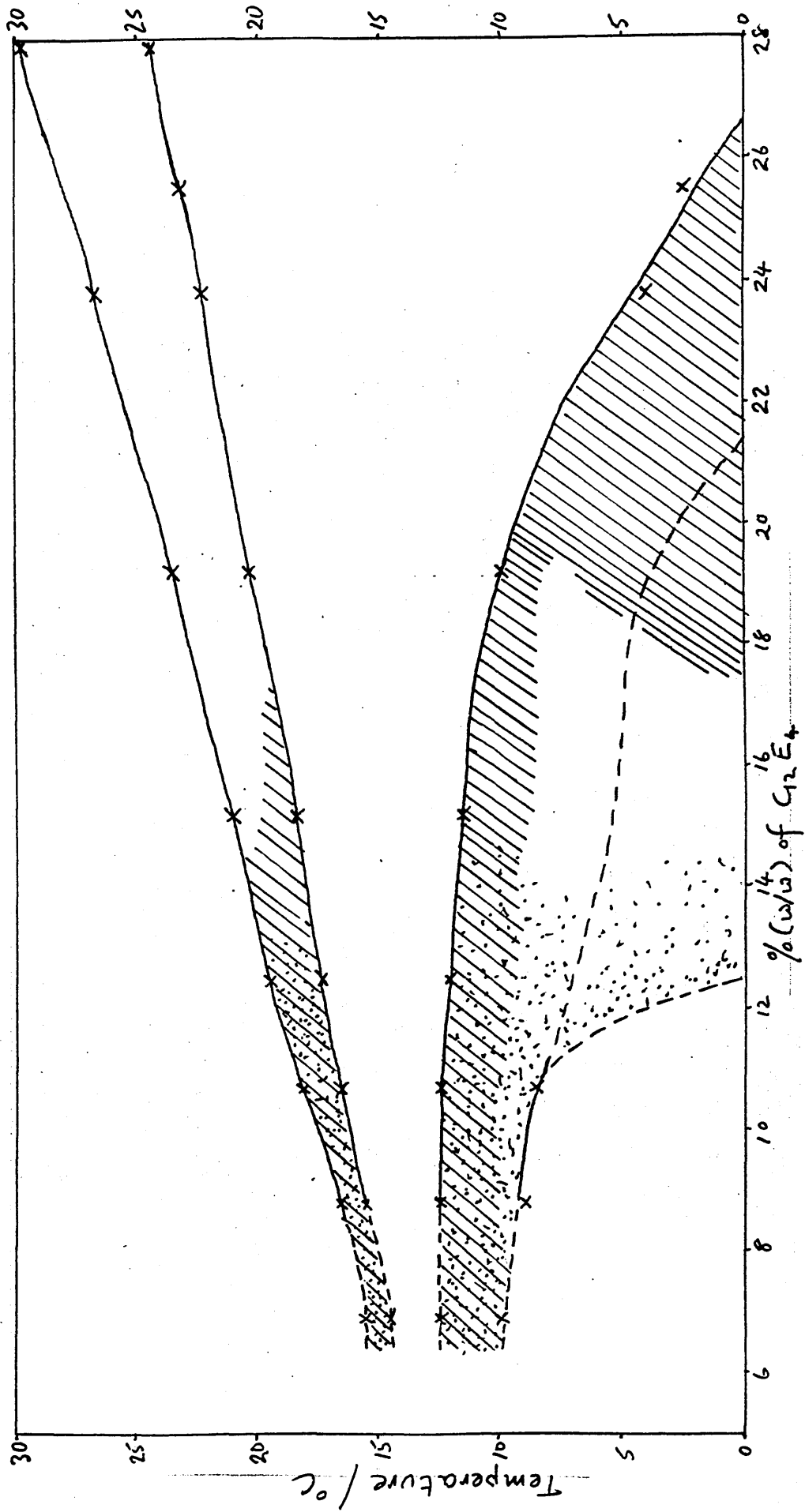
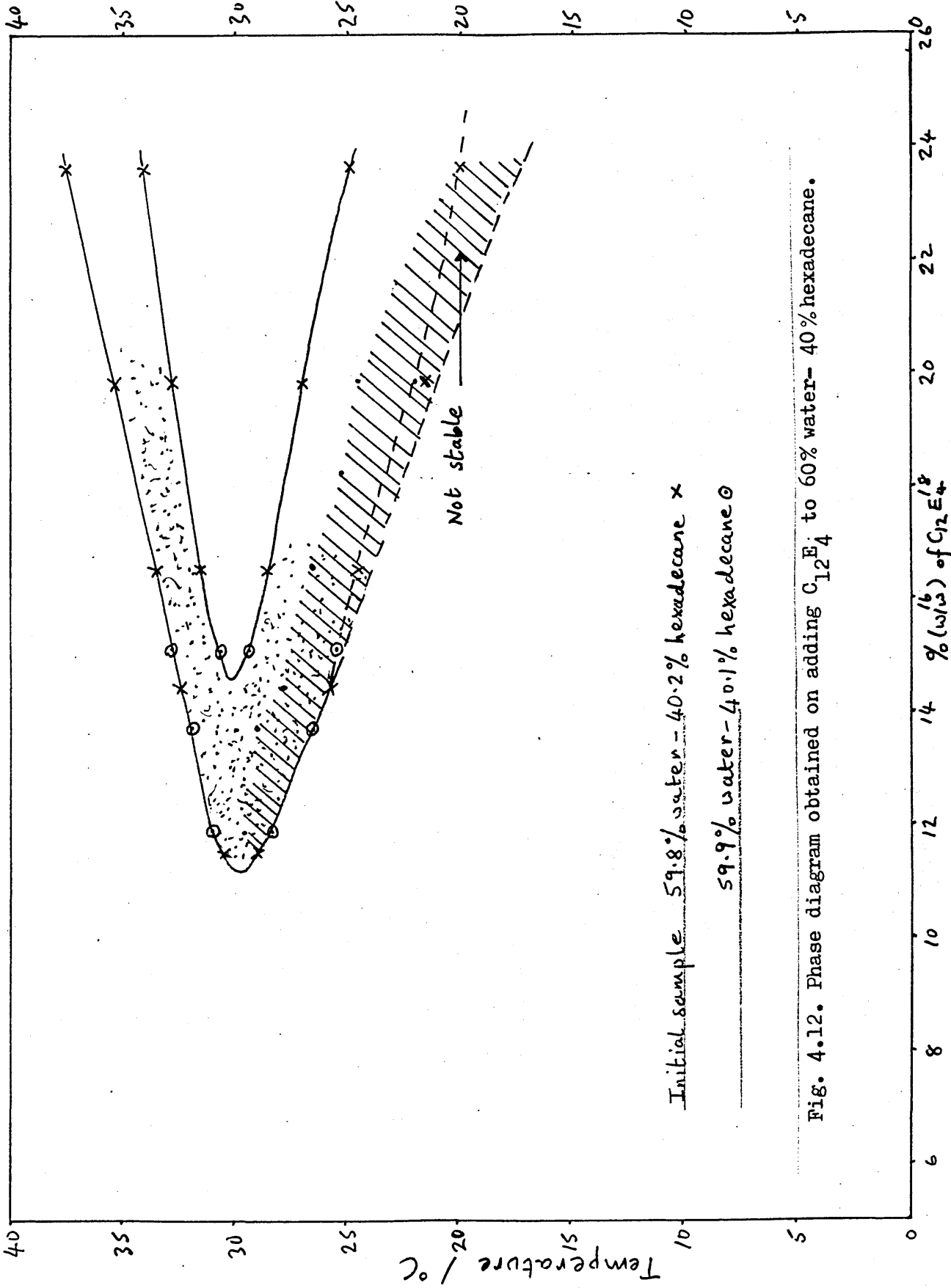


Fig. 4.11. Phase diagram obtained on adding  $C_{12}E_4$  to 60.0% water-40.0% decane.





Initial sample 59.8% water - 40.2% hexadecane x

59.9% water - 40.1% hexadecane o

Fig. 4.12. Phase diagram obtained on adding C<sub>12</sub>E<sub>4</sub> to 60% water - 40% hexadecane.

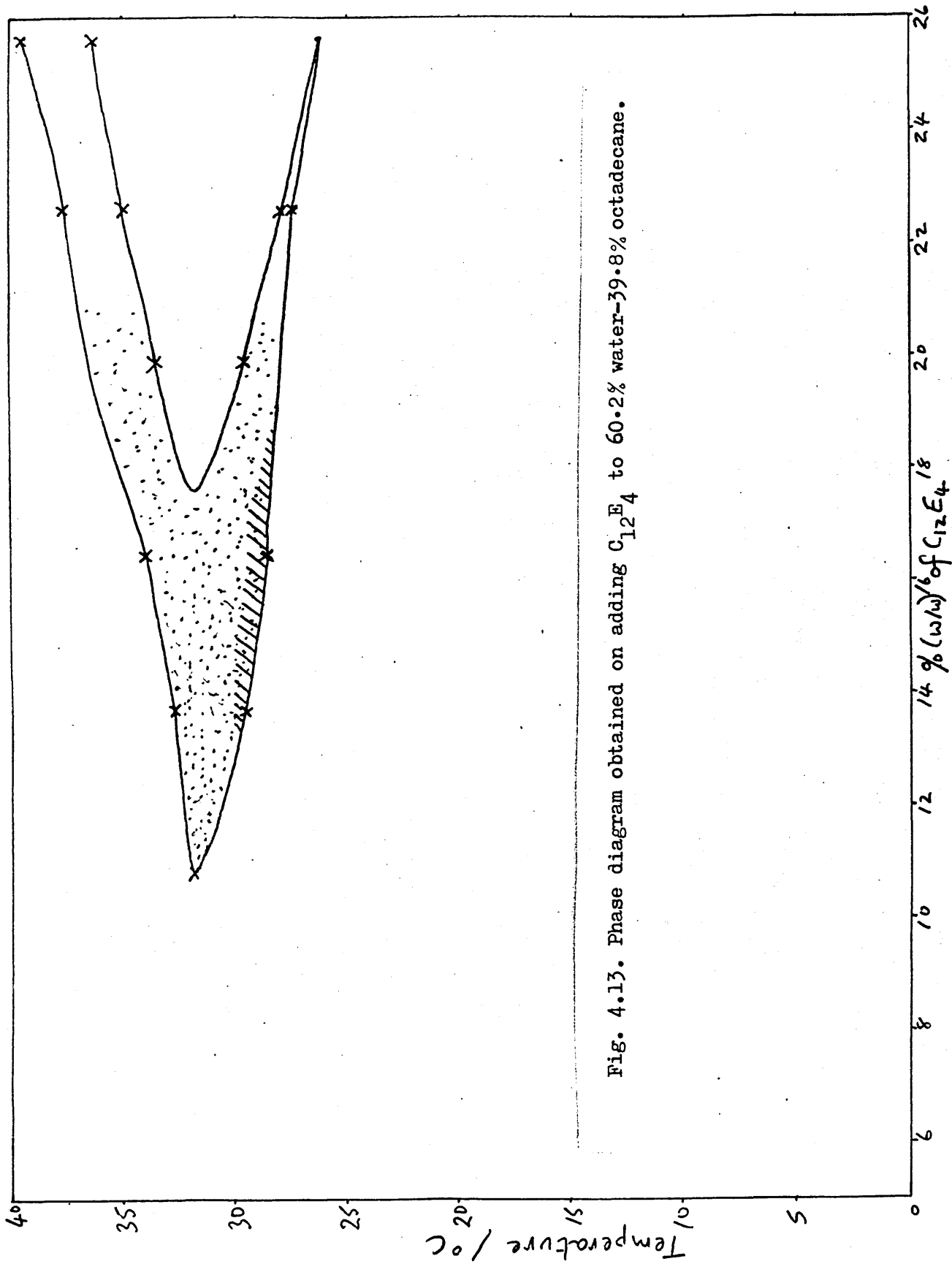


Fig. 4.13. Phase diagram obtained on adding C<sub>12</sub>E<sub>4</sub> to 60.2% water-39.8% octadecane.

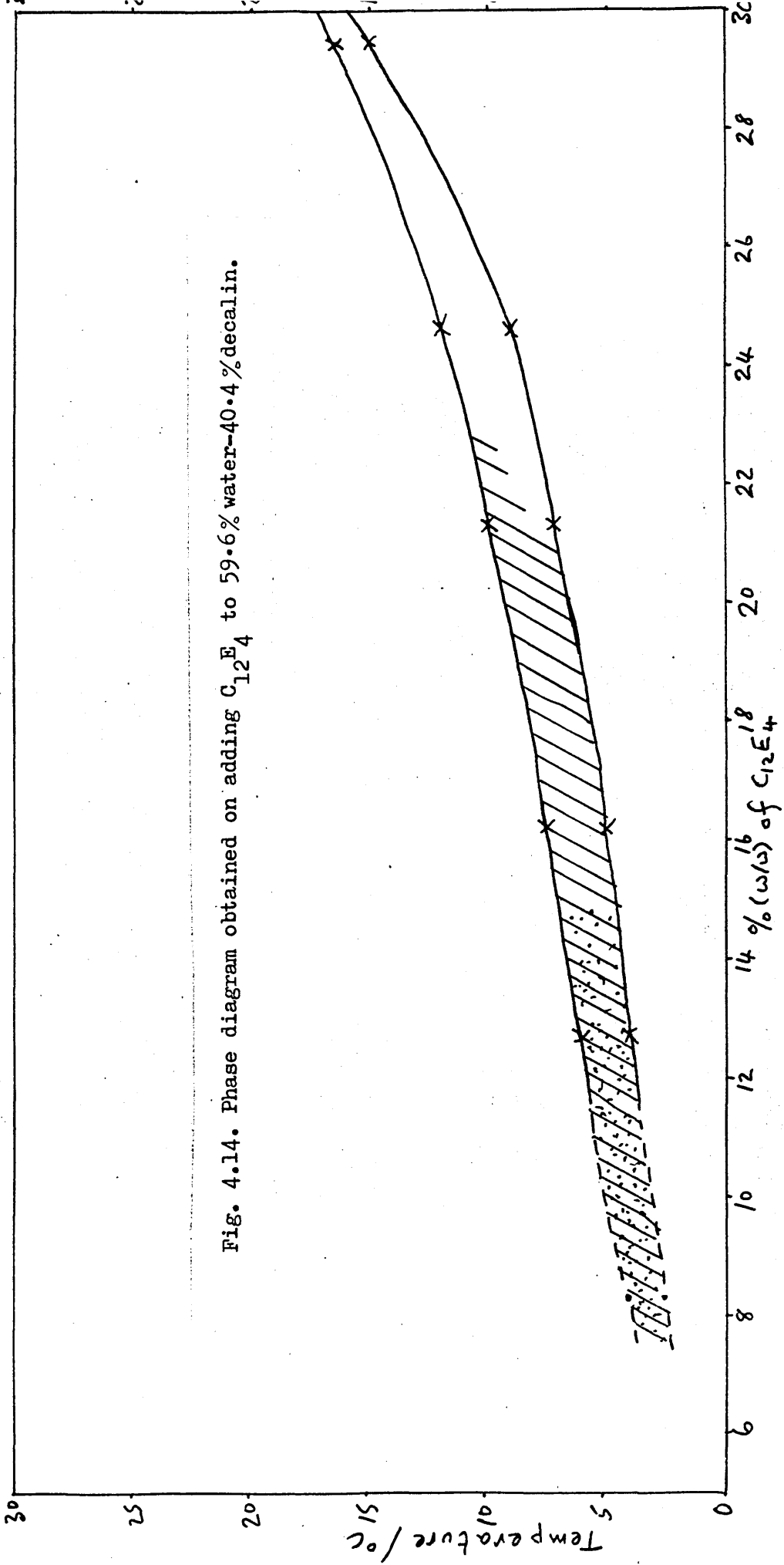


Fig. 4.14. Phase diagram obtained on adding C<sub>12</sub>E<sub>4</sub> to 59.6% water-40.4% decalin.

Fig. 4.15. Phase diagrams obtained on adding heptane to 30.0% and 35.3%  $C_{12}E_4$ -water.

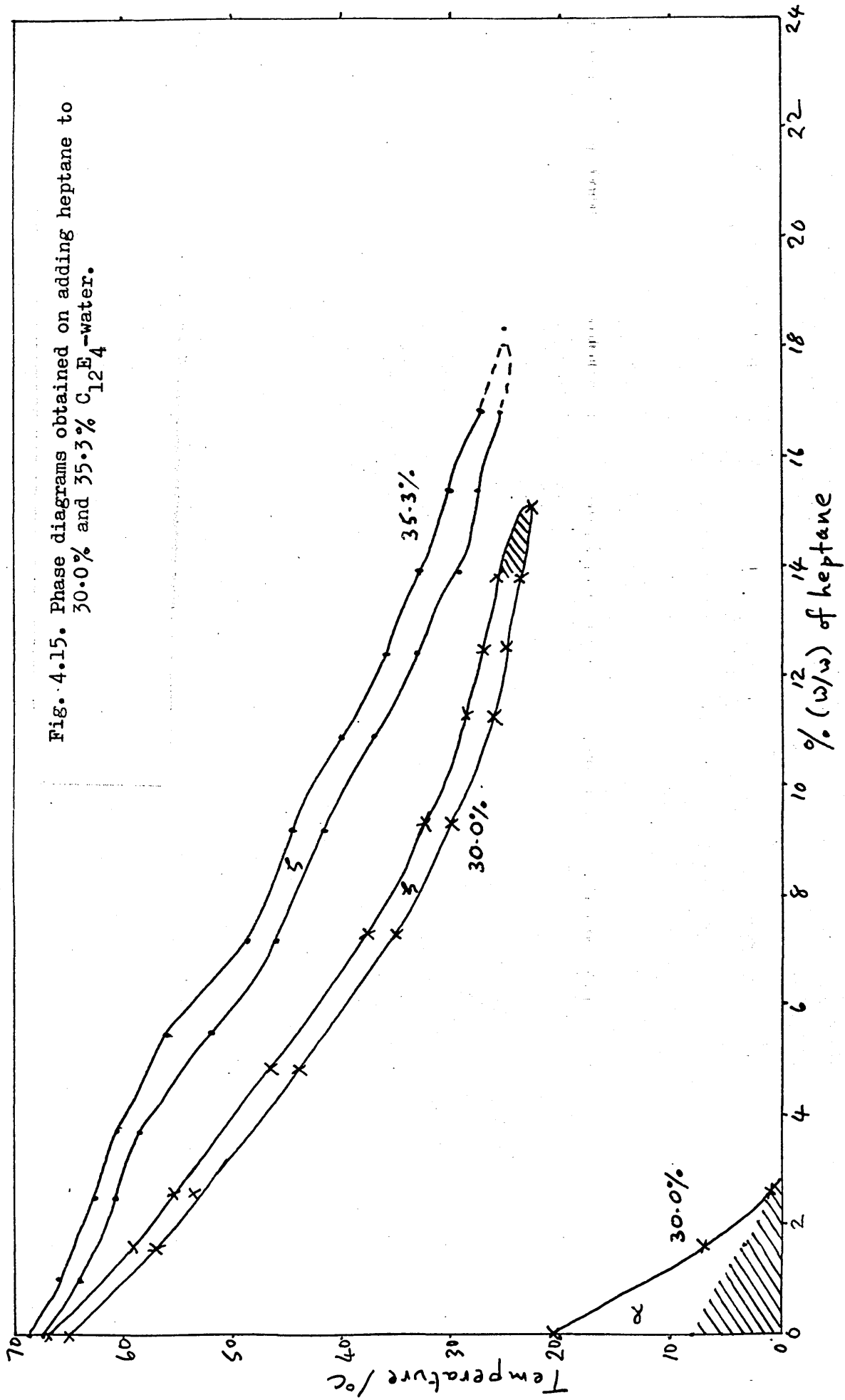


Fig.4.16. Phase diagram obtained on adding decalin to 34.9%  $C_{12}E_4$ -water.

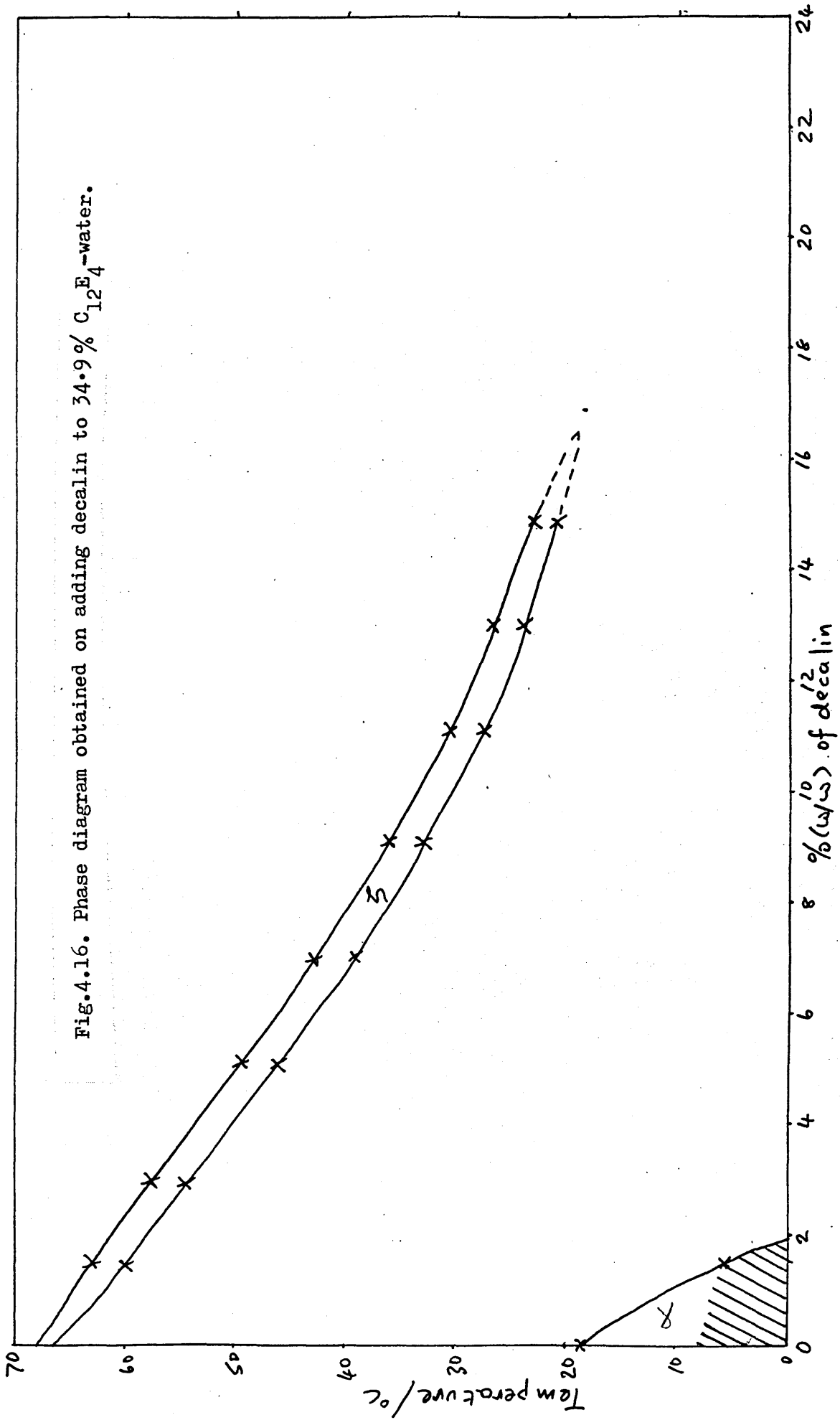
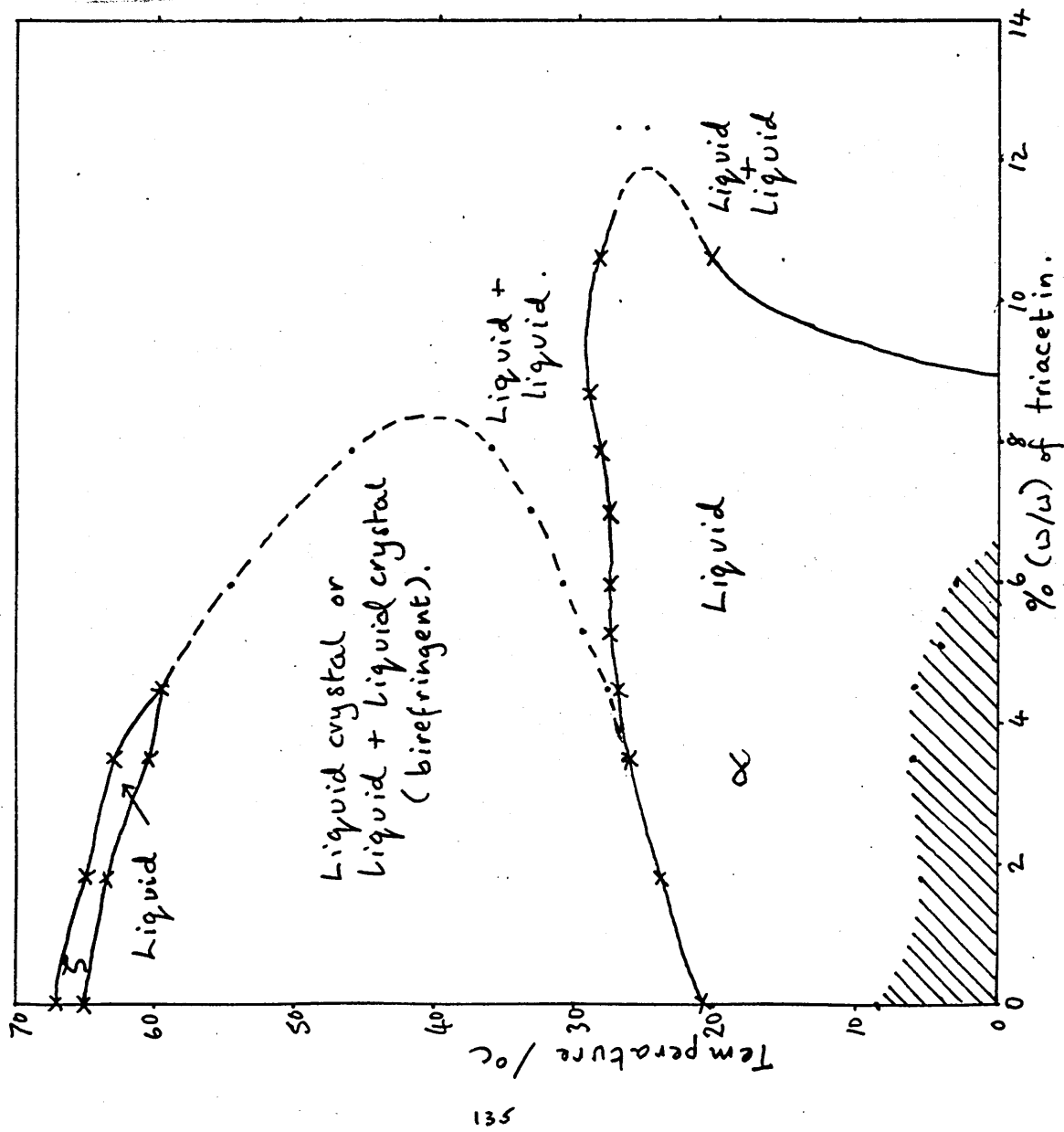


Fig. 4.17. Phase diagram obtained on adding triacetin to 29.9% C<sub>12</sub>E<sub>4</sub>-water.



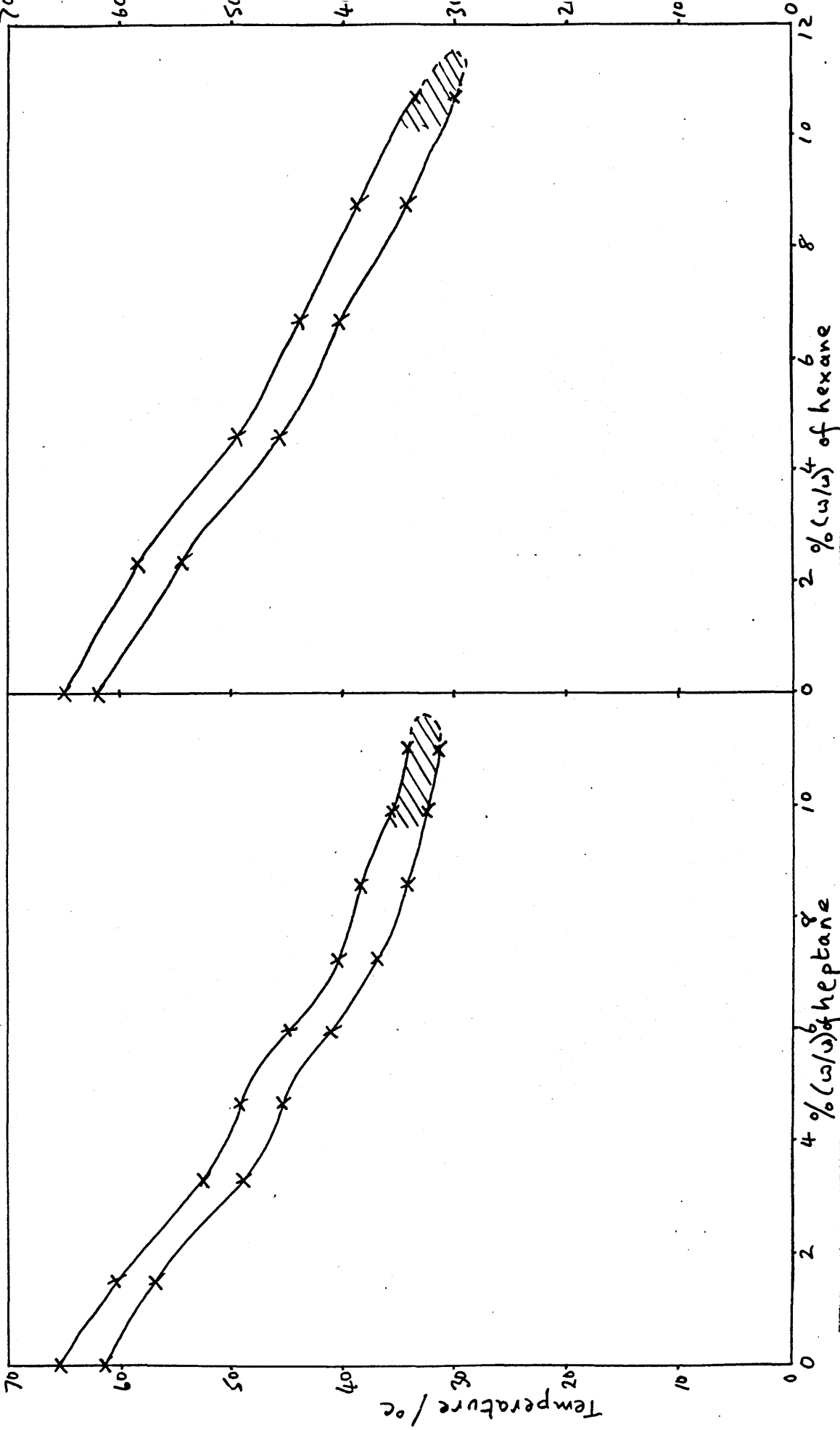


Fig. 4.18. Phase diagram obtained on adding heptane to 35.3% Brij-water.

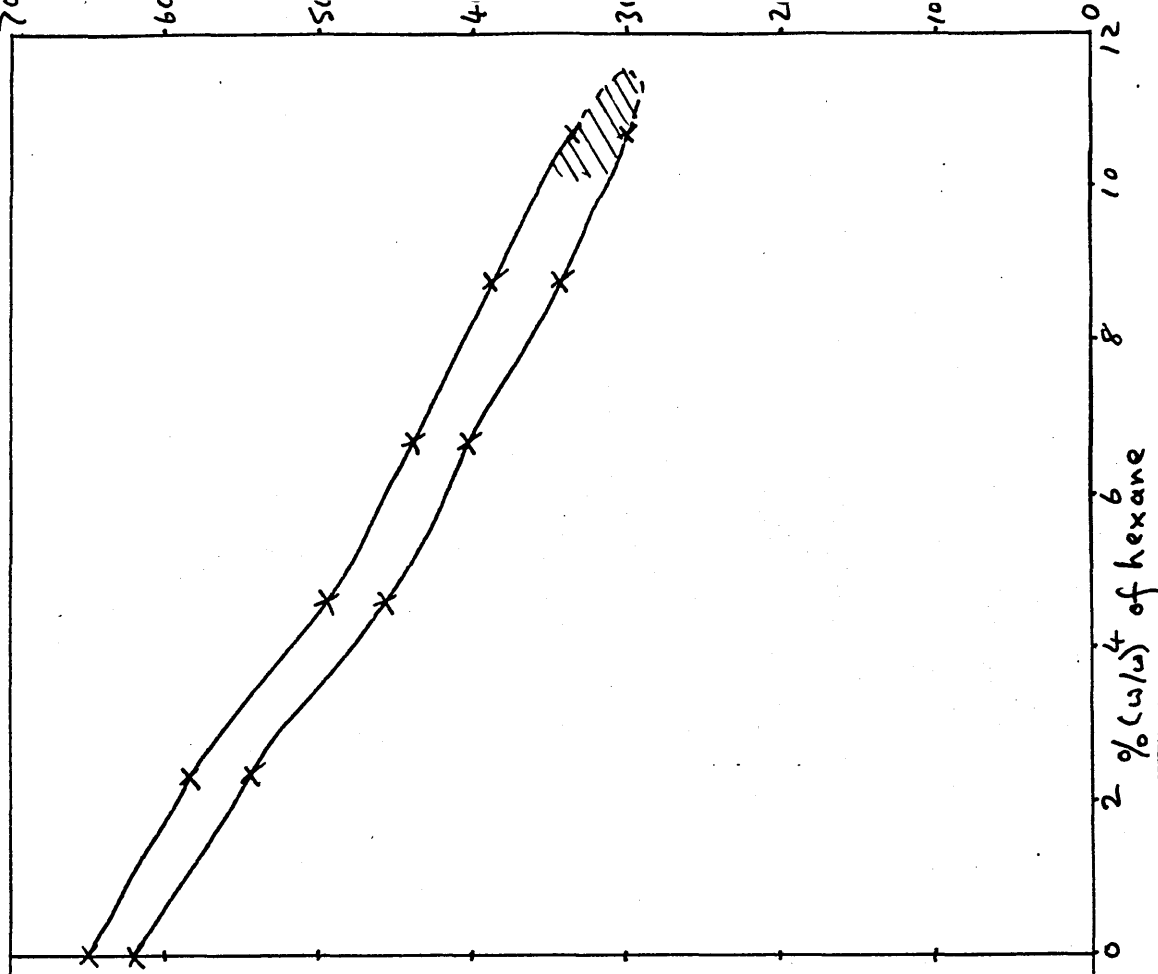


Fig. 4.19. Phase diagram obtained on adding hexane to 35.4% Brij-water.

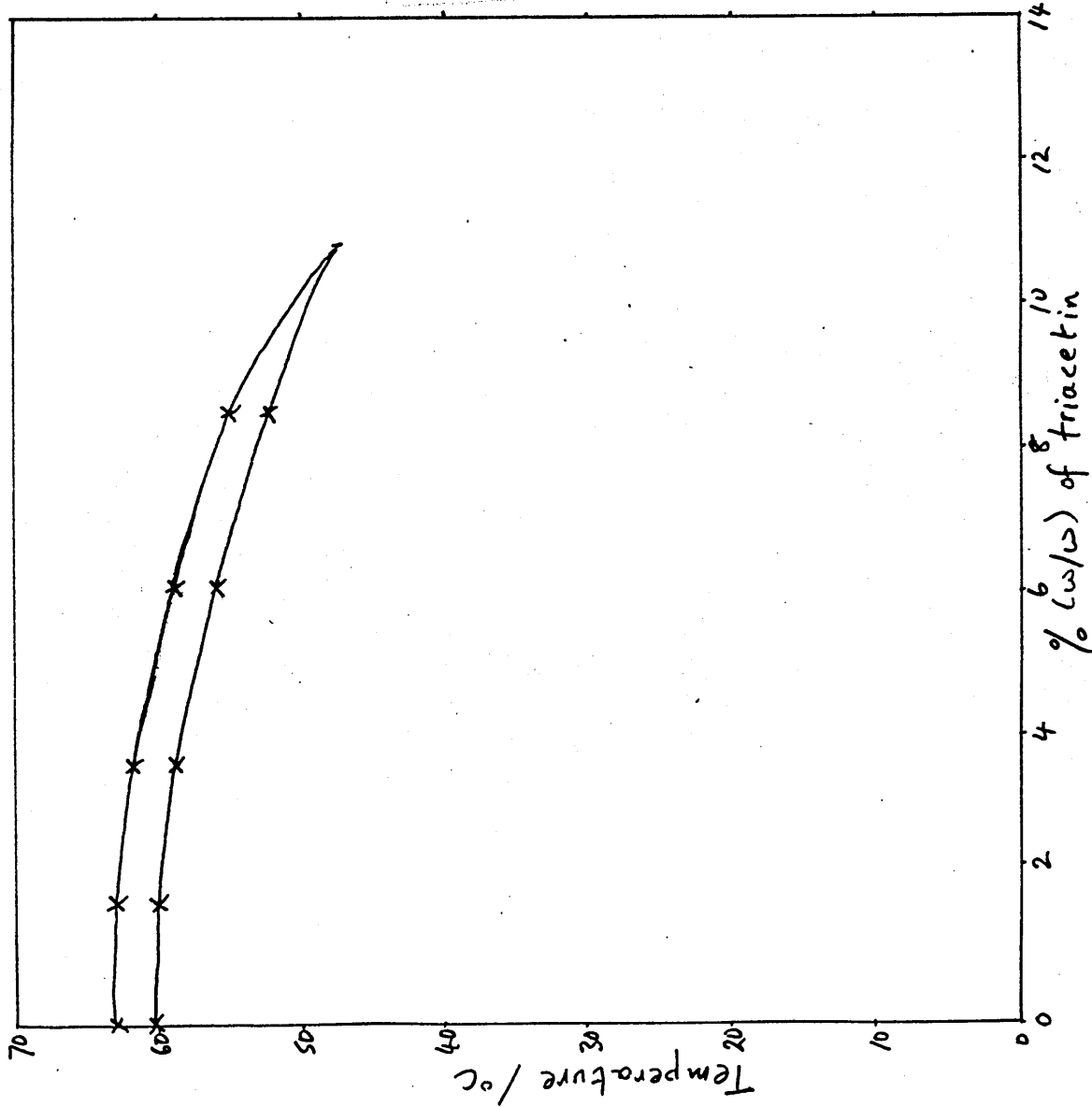


Fig. 4.20. Phase diagram obtained on adding triacetin to 30.1% Brij-water.

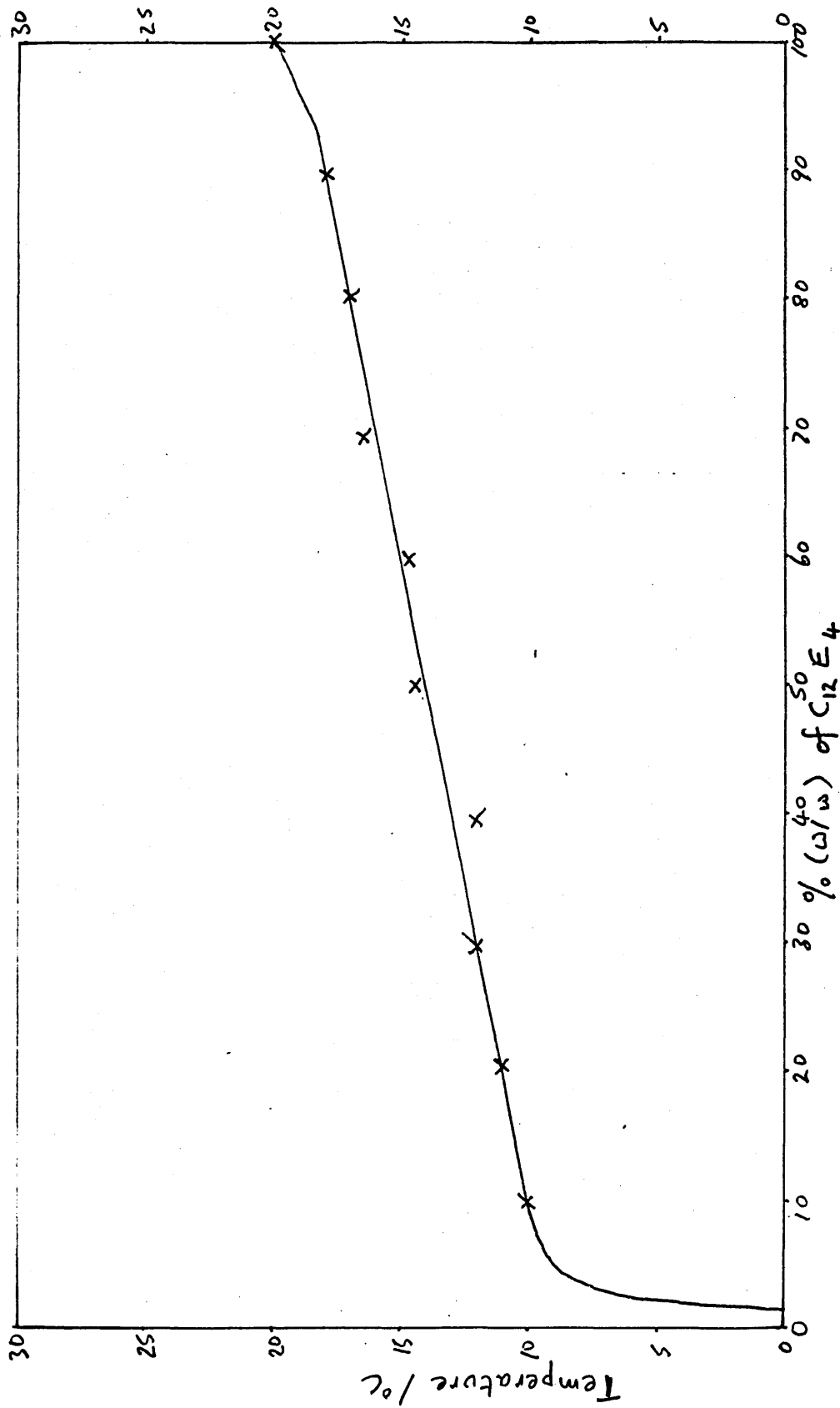


Fig. 4.21. Phase diagram of C<sub>12</sub>E<sub>4</sub>-triacetin.

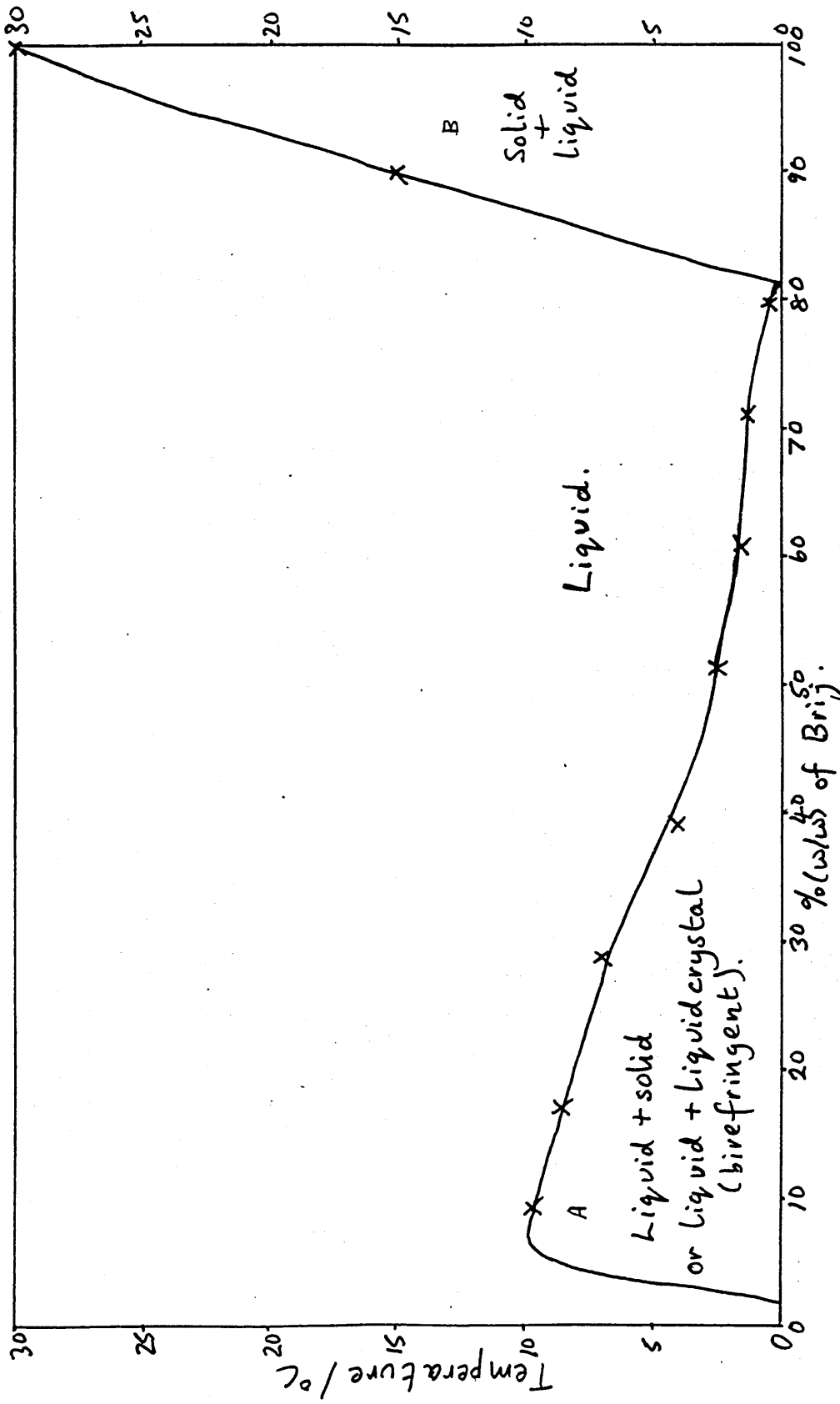


Fig. 4.22. Phase diagram of Brij-triacetin.

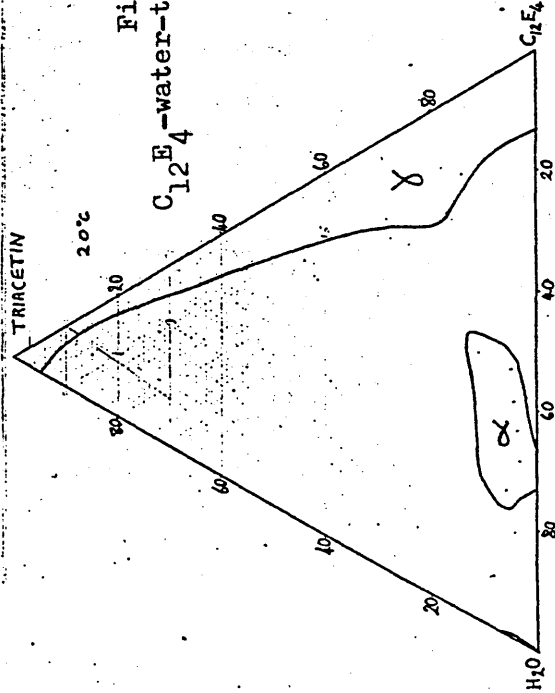
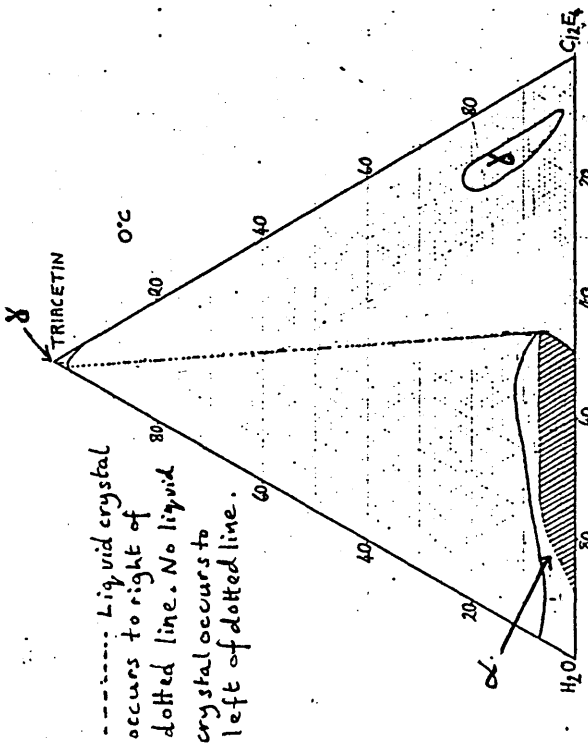
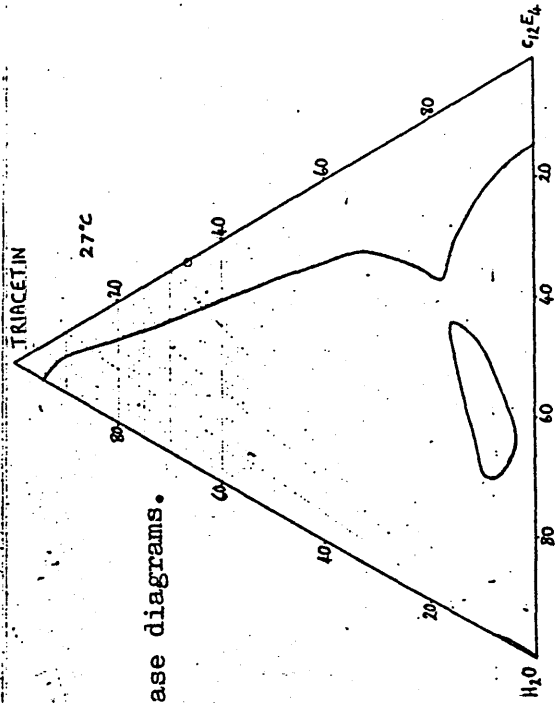
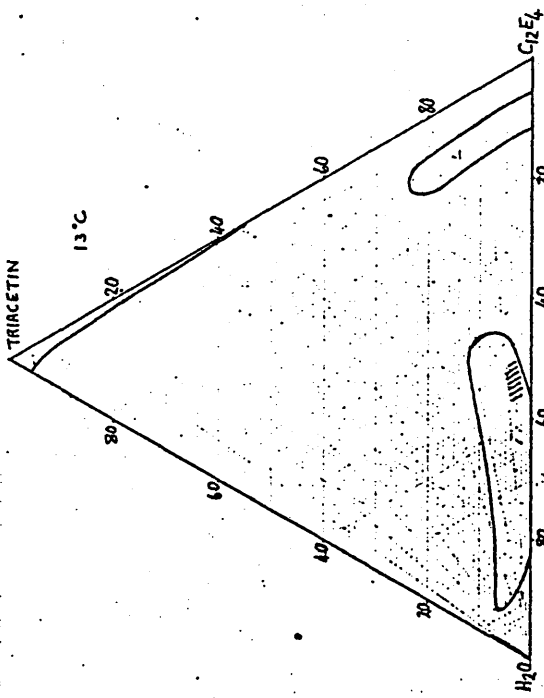


Fig. 4.23.  
C<sub>12</sub>E<sub>4</sub>-water-triacetin phase diagrams.



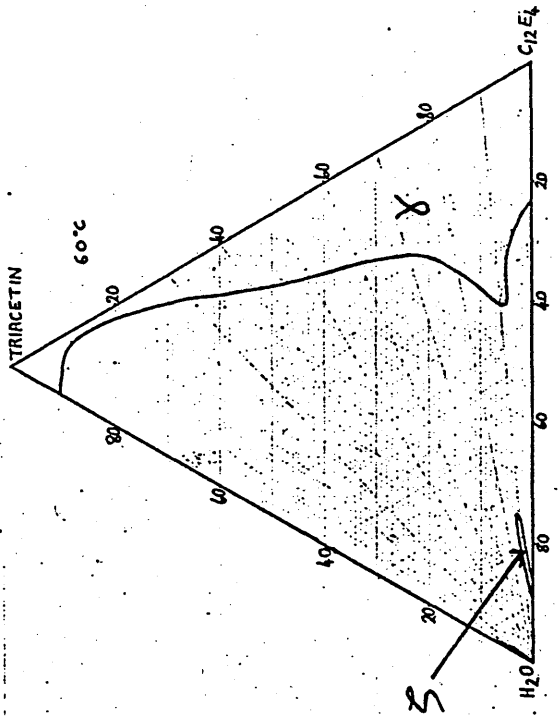
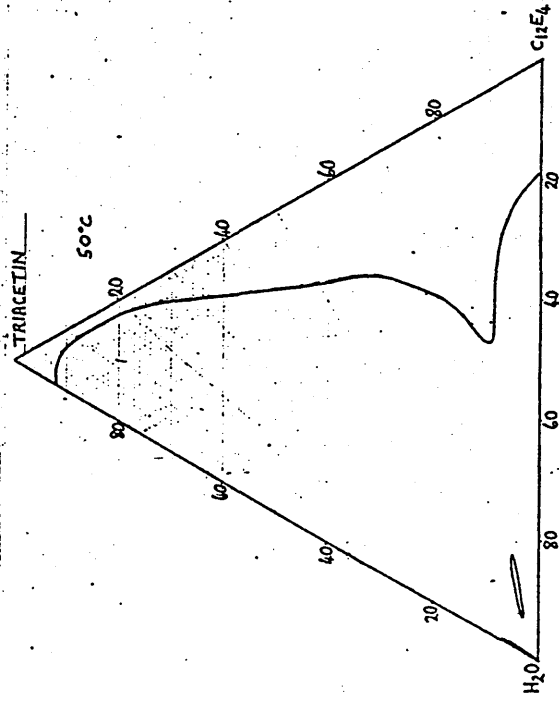
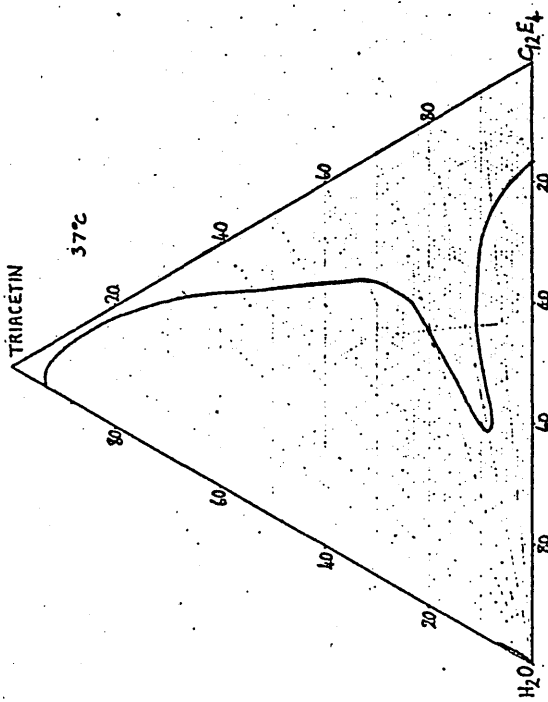


Fig. 4.24.  
C<sub>12</sub>E<sub>4</sub>-water-triacetin phase diagrams.

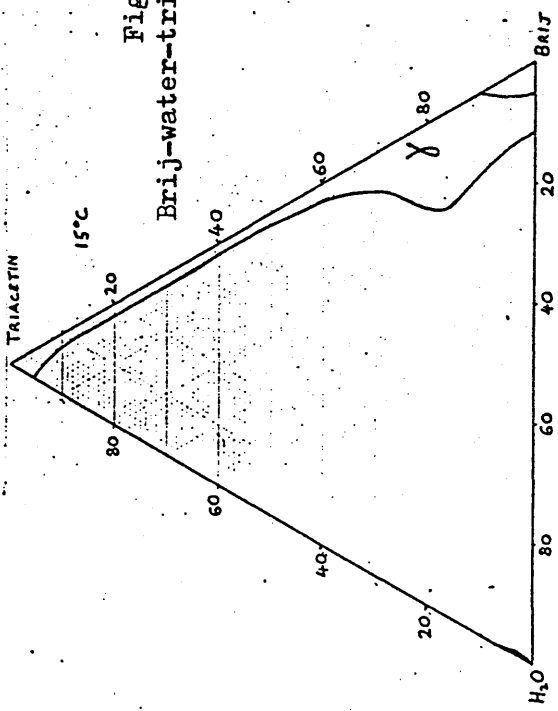
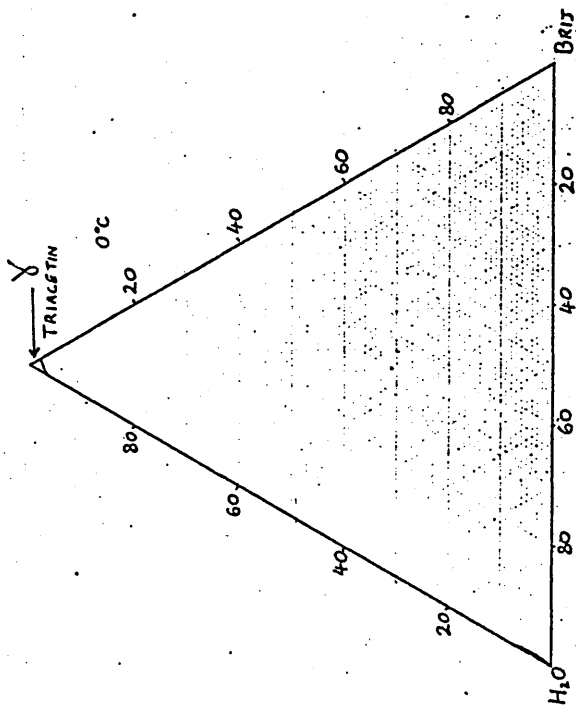
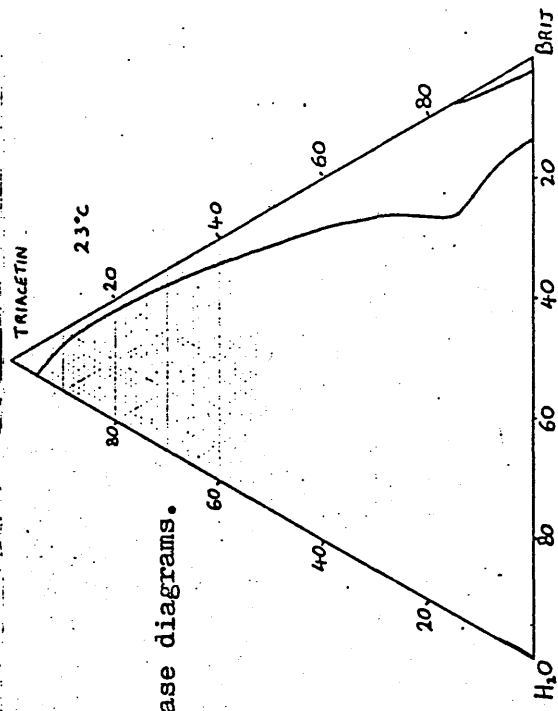
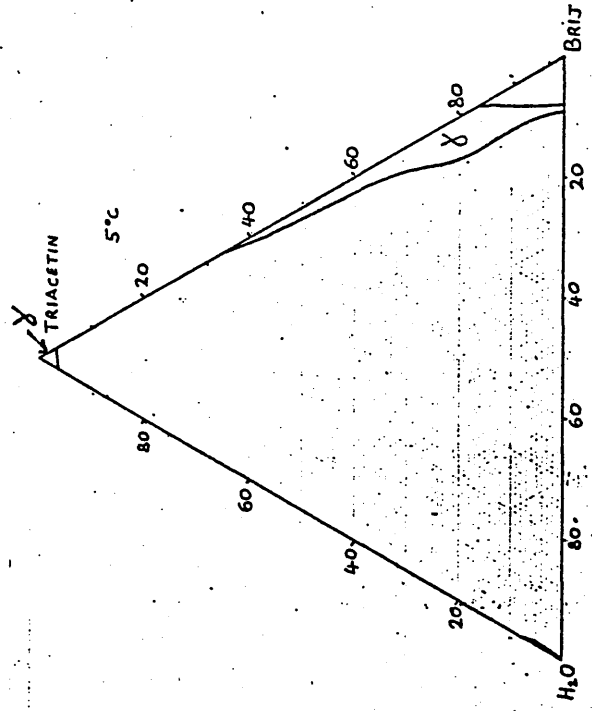


Fig. 4.25.  
Brij-water-triacetin phase diagrams.



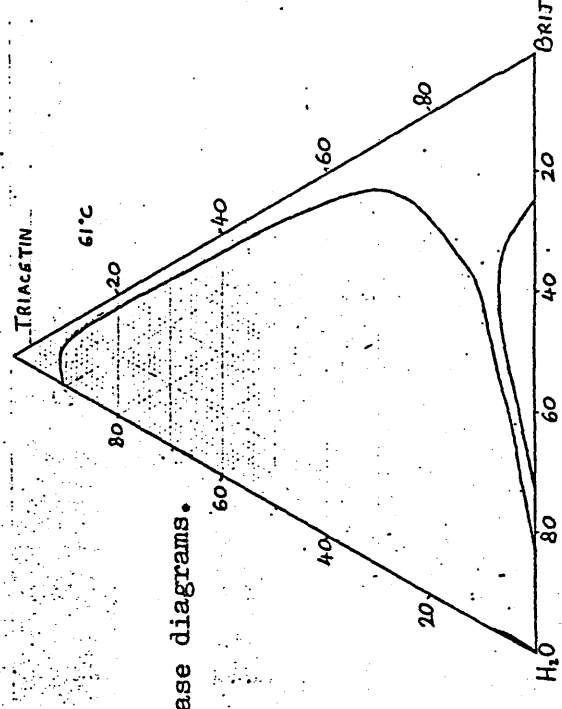
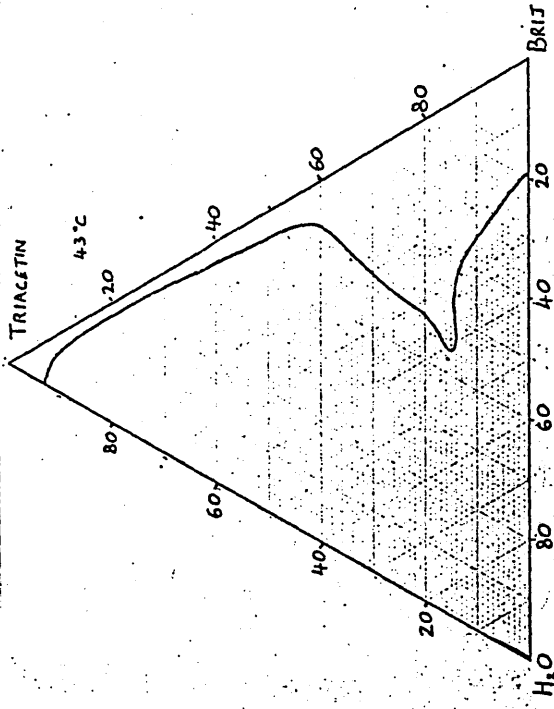


Fig. 4.26.  
Brij-water-triacetin phase diagrams.

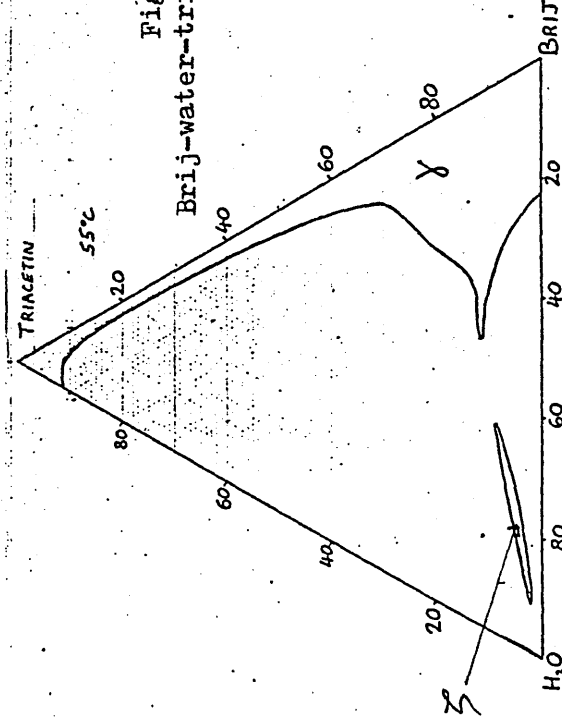
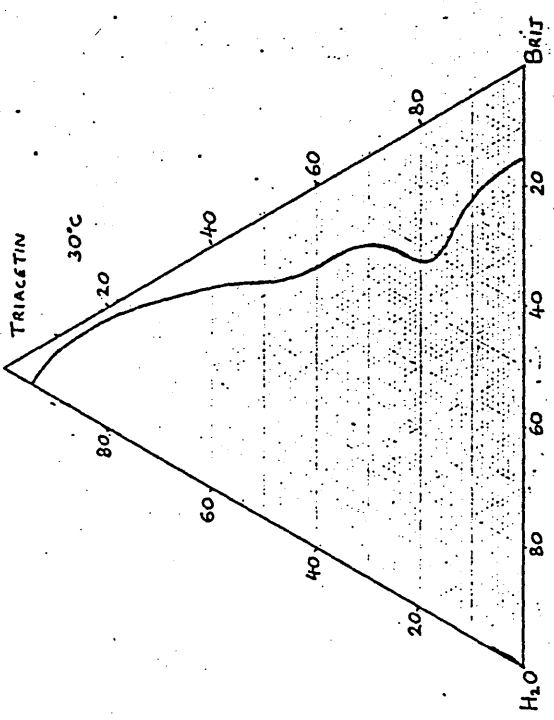
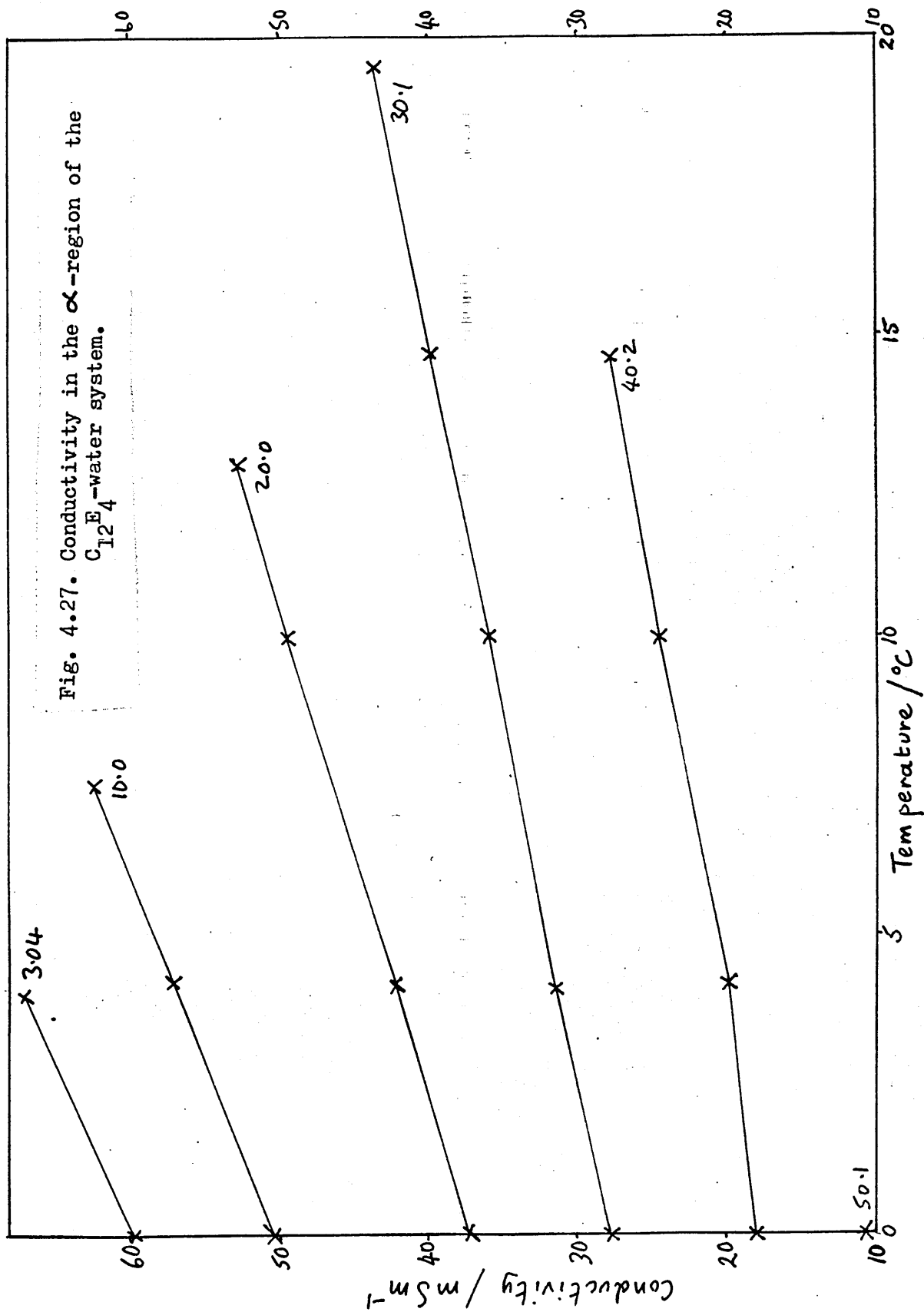


Fig. 4.27. Conductivity in the  $\alpha$ -region of the  $C_{12}E_4$ -water system.



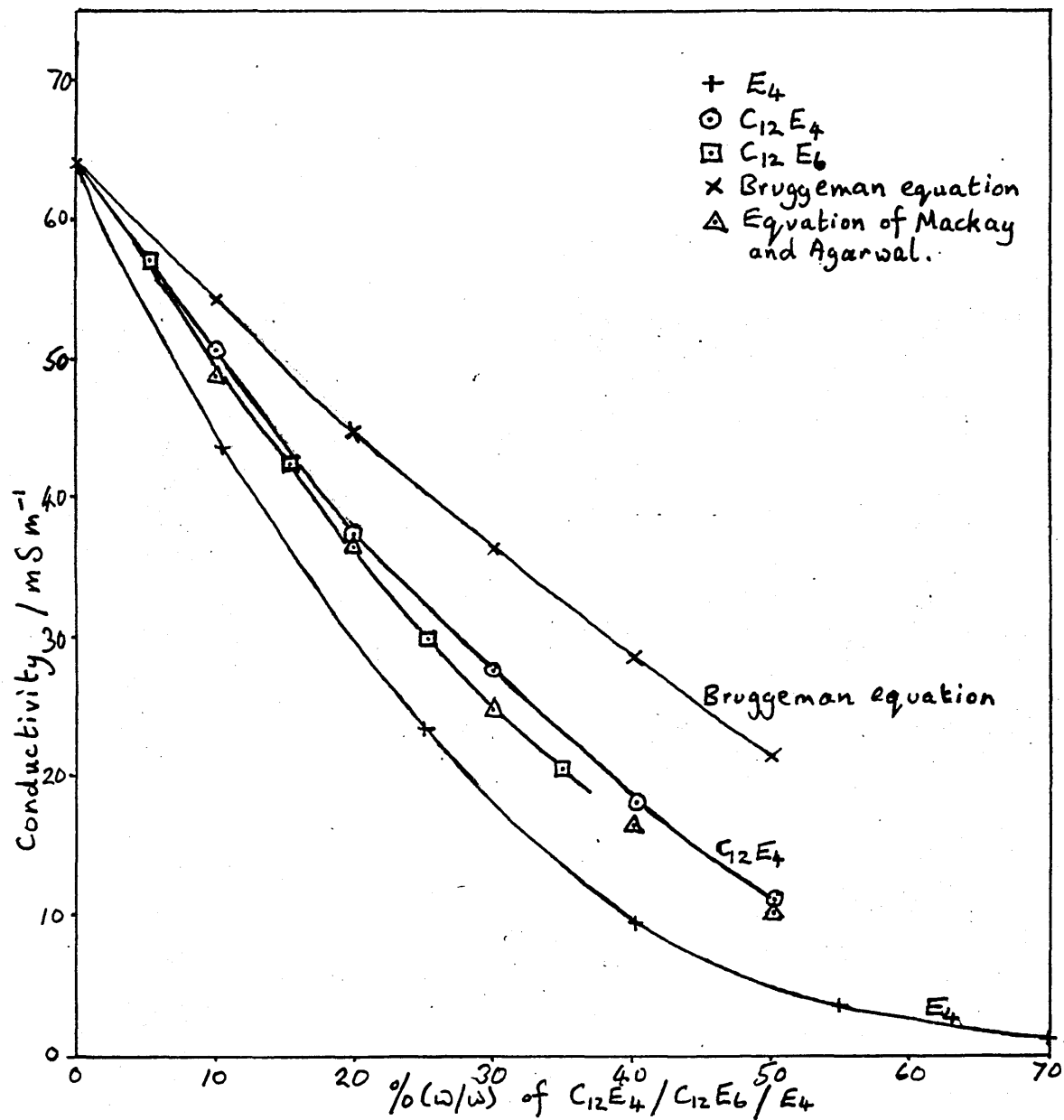


Fig.4.28. Variation of conductivity with composition in the C<sub>12</sub>E<sub>4</sub>-water and C<sub>12</sub>E<sub>6</sub>-water systems at 0°C. Samples doped with sodium chloride.

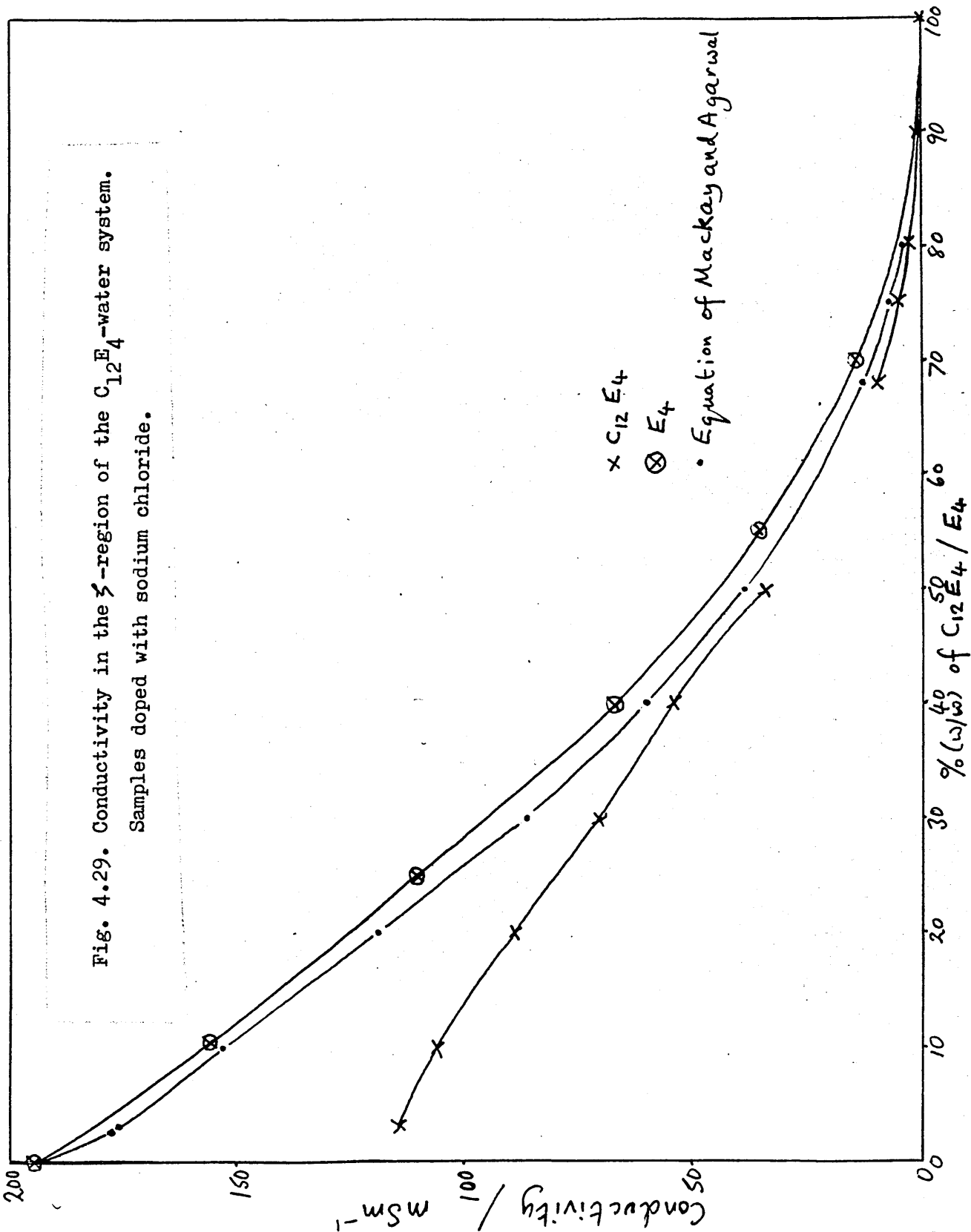


Fig. 4.29. Conductivity in the  $\zeta$ -region of the  $C_{12}E_4$ -water system. Samples doped with sodium chloride.

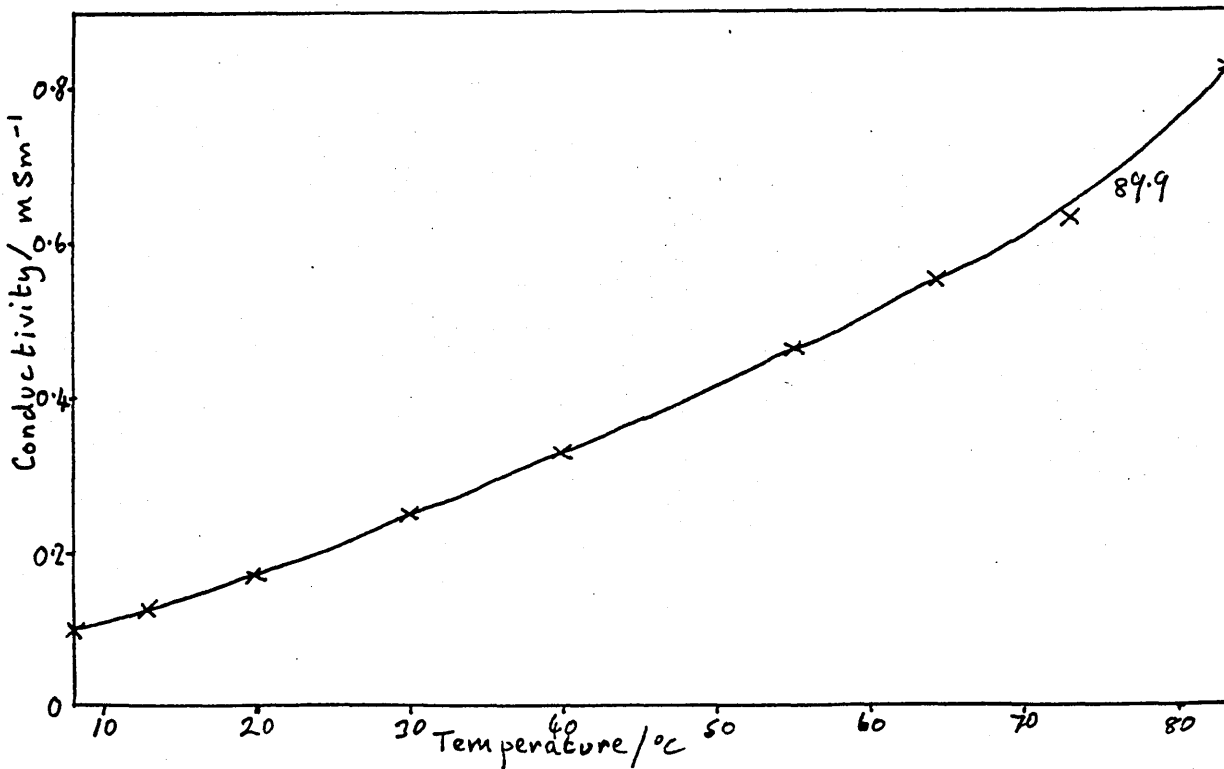
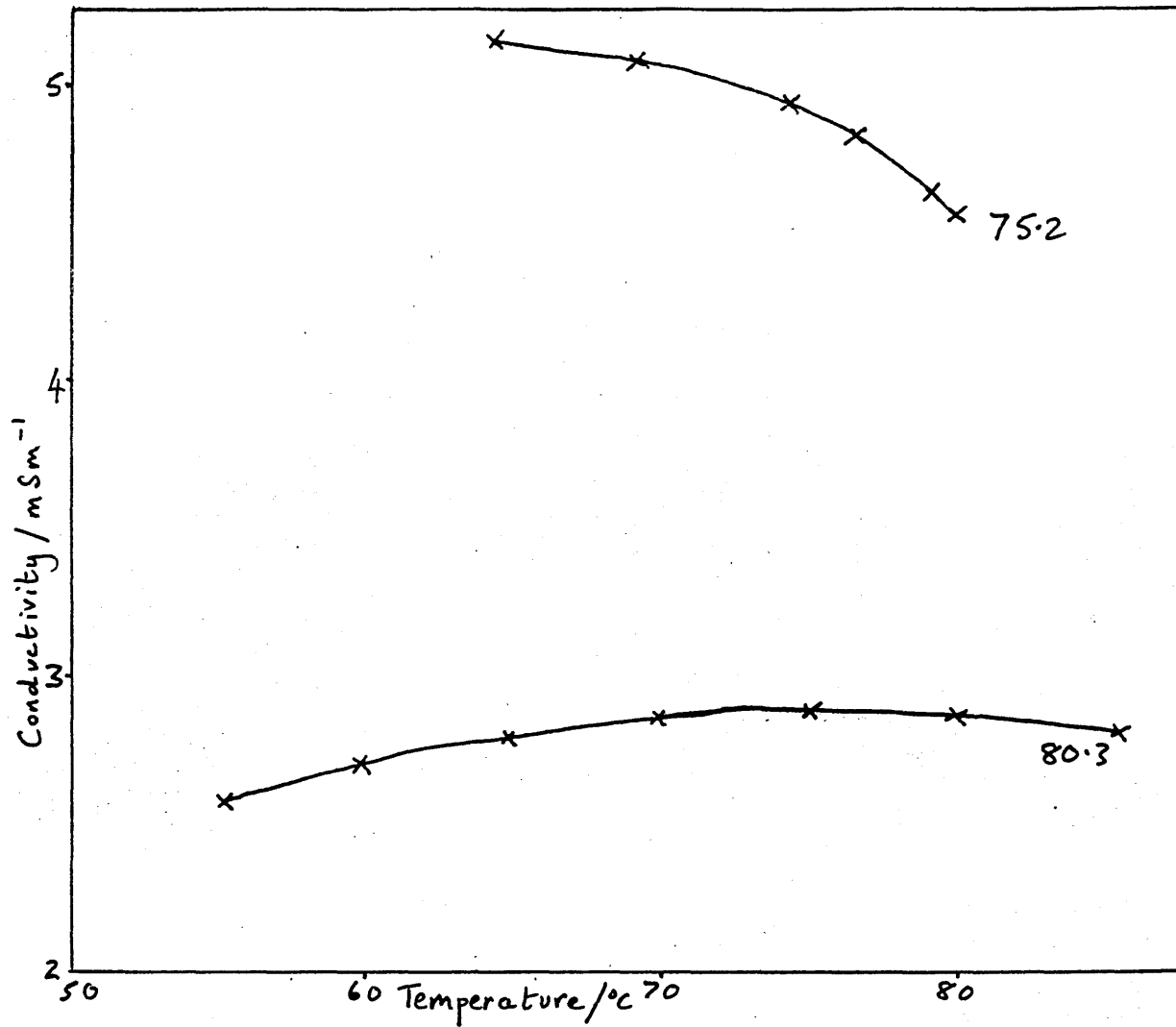


Fig.4.30. Variation of conductivity with temperature in  $\text{C}_{12}\text{E}_4$ -water samples, doped with sodium chloride.

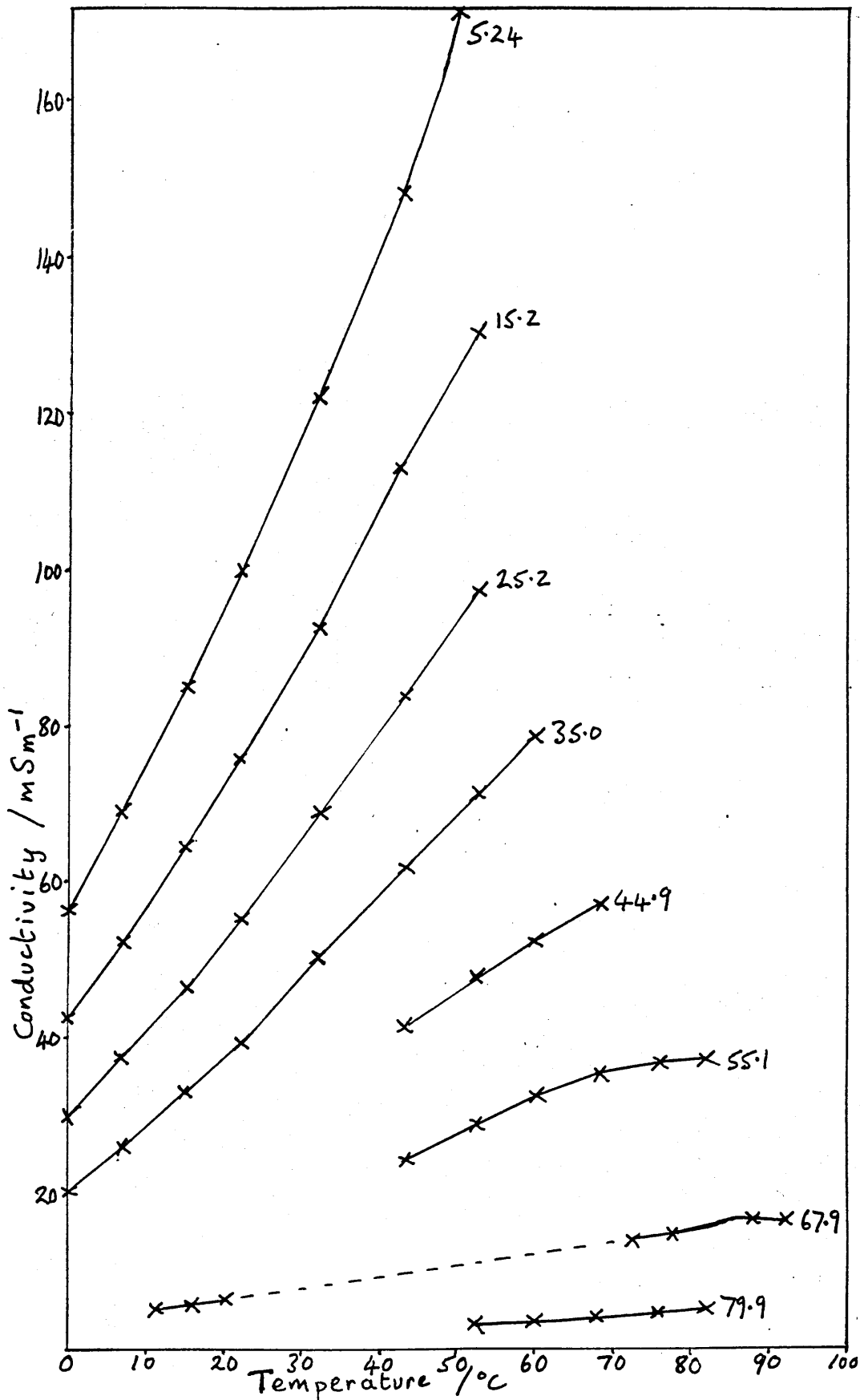


Fig.4.31. Variation of conductivity with temperature in C<sub>12</sub>E<sub>6</sub>-water samples, doped with sodium chloride.

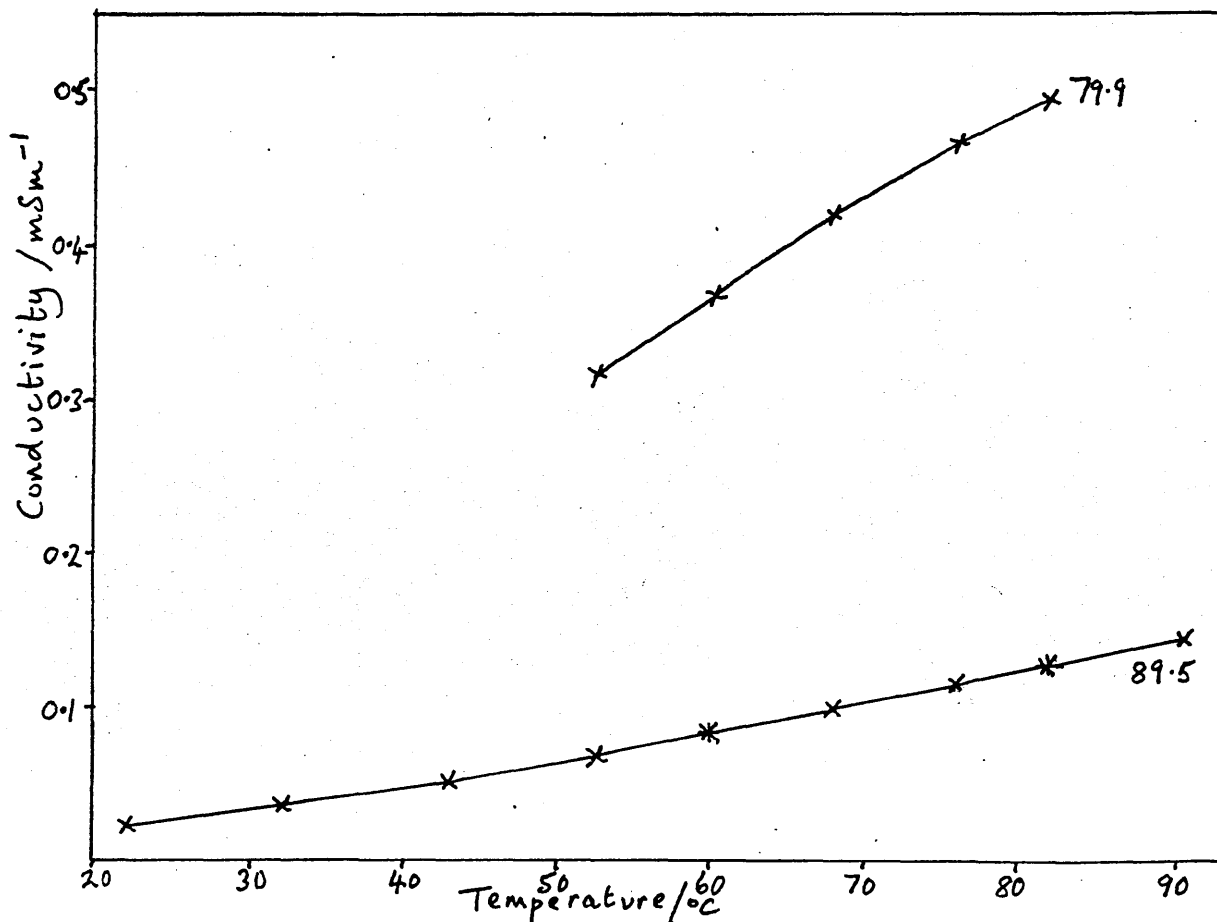
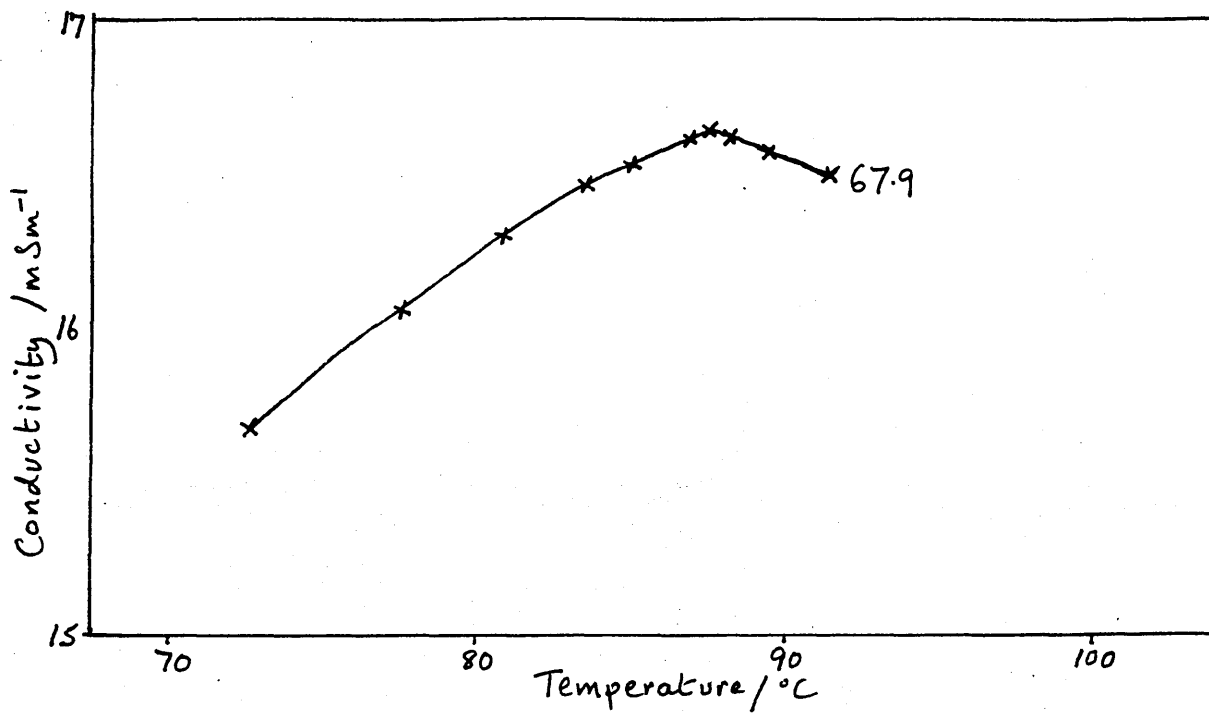


Fig.4.32. Variation of conductivity with temperature in C<sub>12</sub>E<sub>6</sub>-water samples. Samples doped with sodium chloride.

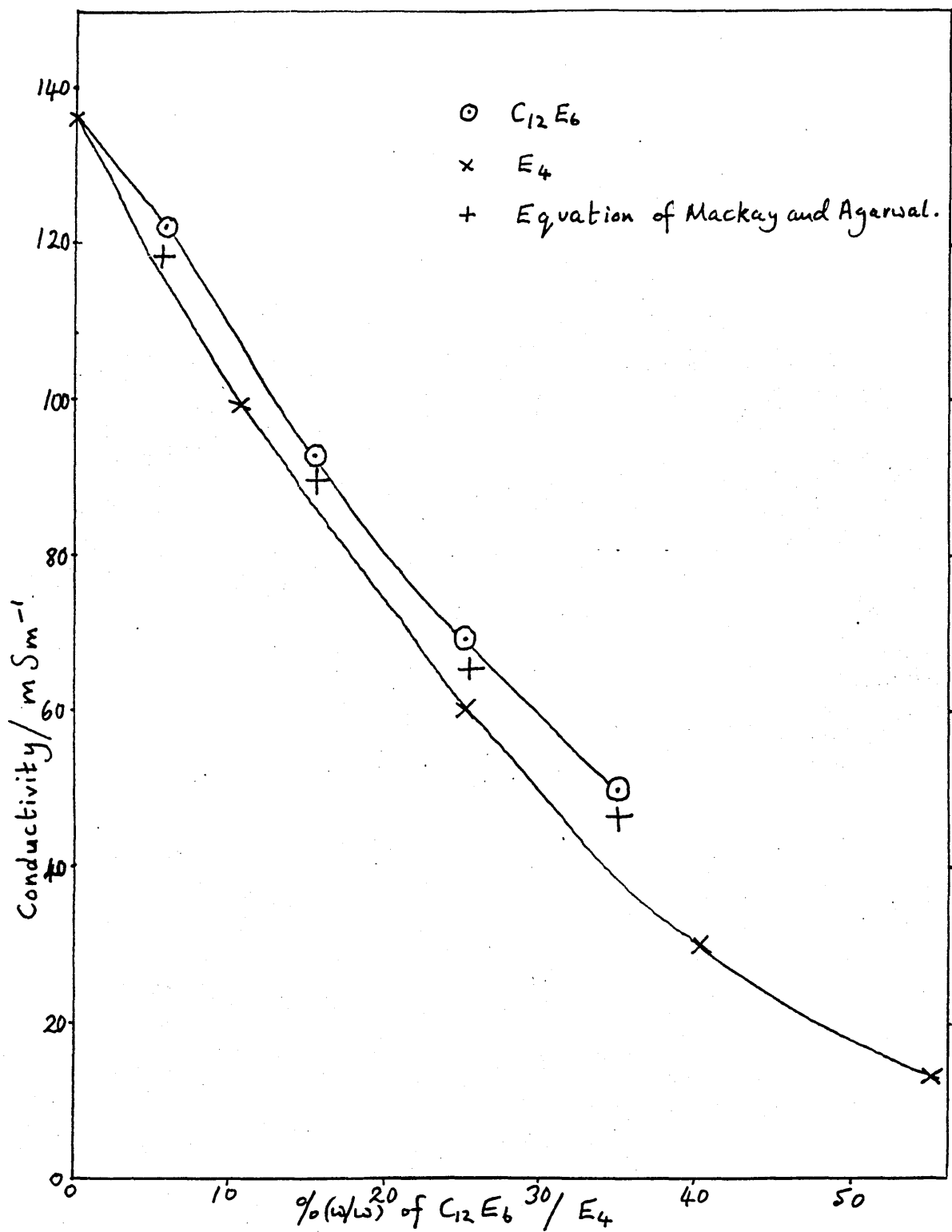


Fig.4.33. Conductivity in the  $C_{12}E_6$ -water system as a function of composition at  $32^\circ C$ . Samples were doped with sodium chloride.

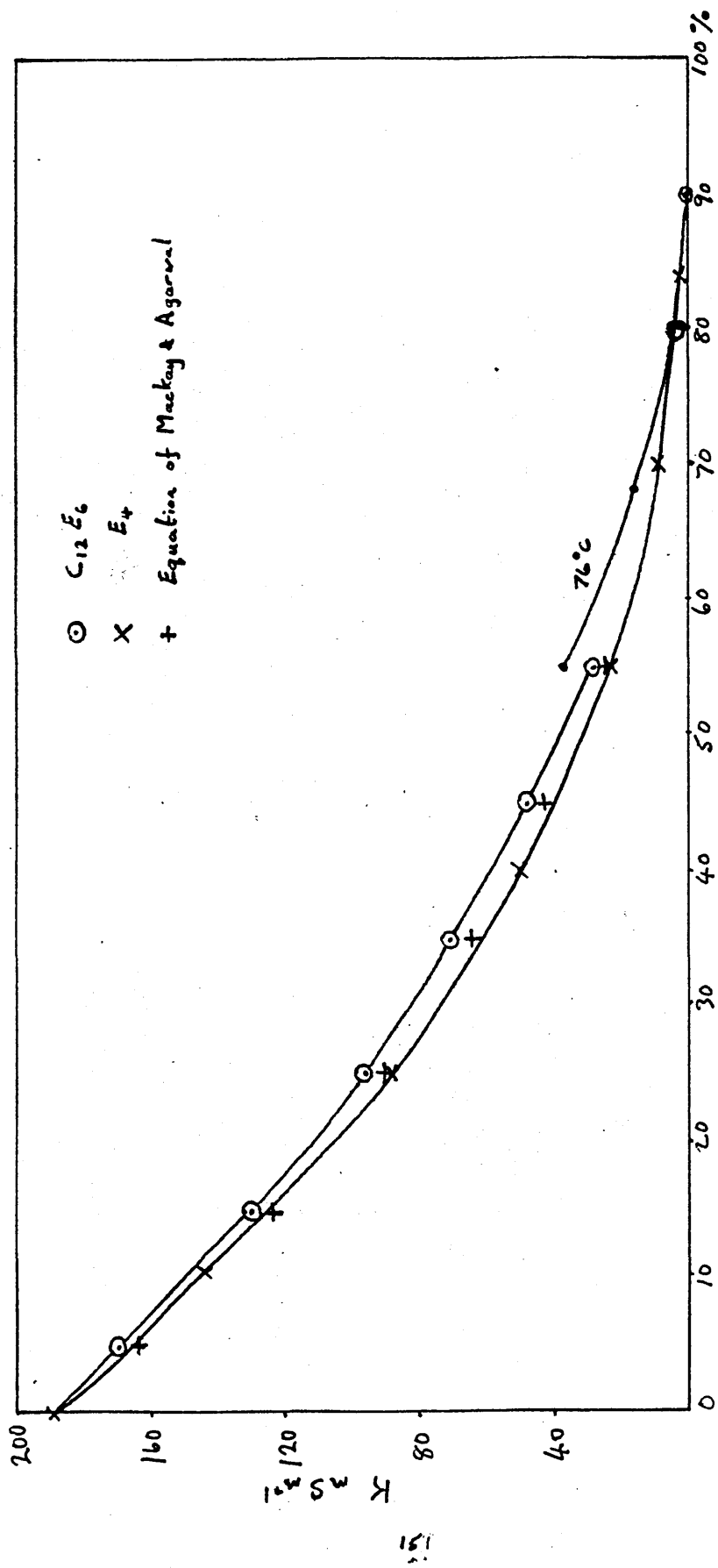


Fig. 4.34. Conductivity in the C<sub>12</sub>E<sub>6</sub>-water system at 52.5°C, as a function of composition. Samples doped with sodium chloride.

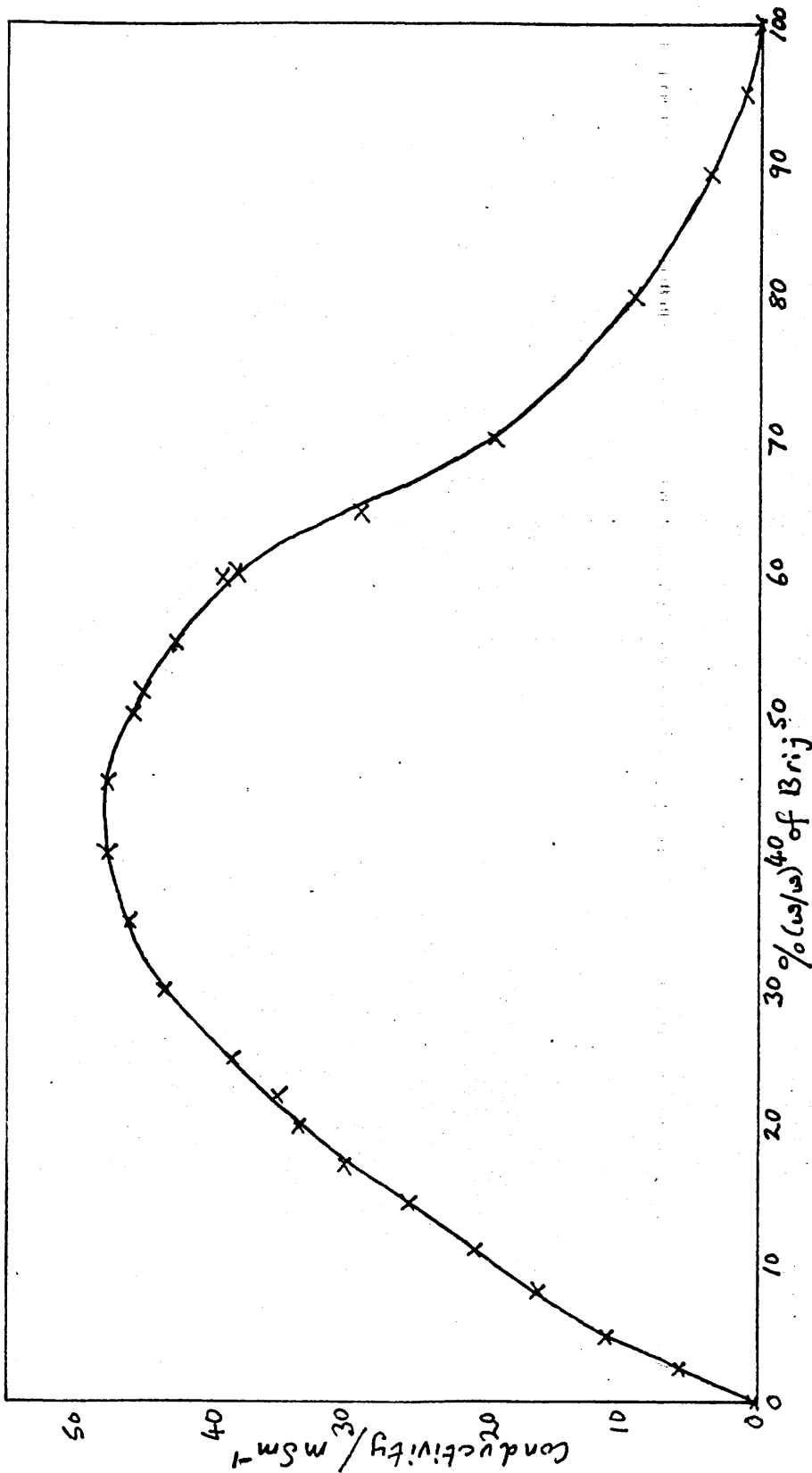


Fig. 4.35. Conductivity in the Brij-water system as a function of concentration. The temperature varied from 57.5°C at 5% to 69°C at 55%; above 55% it was maintained at 69°C.

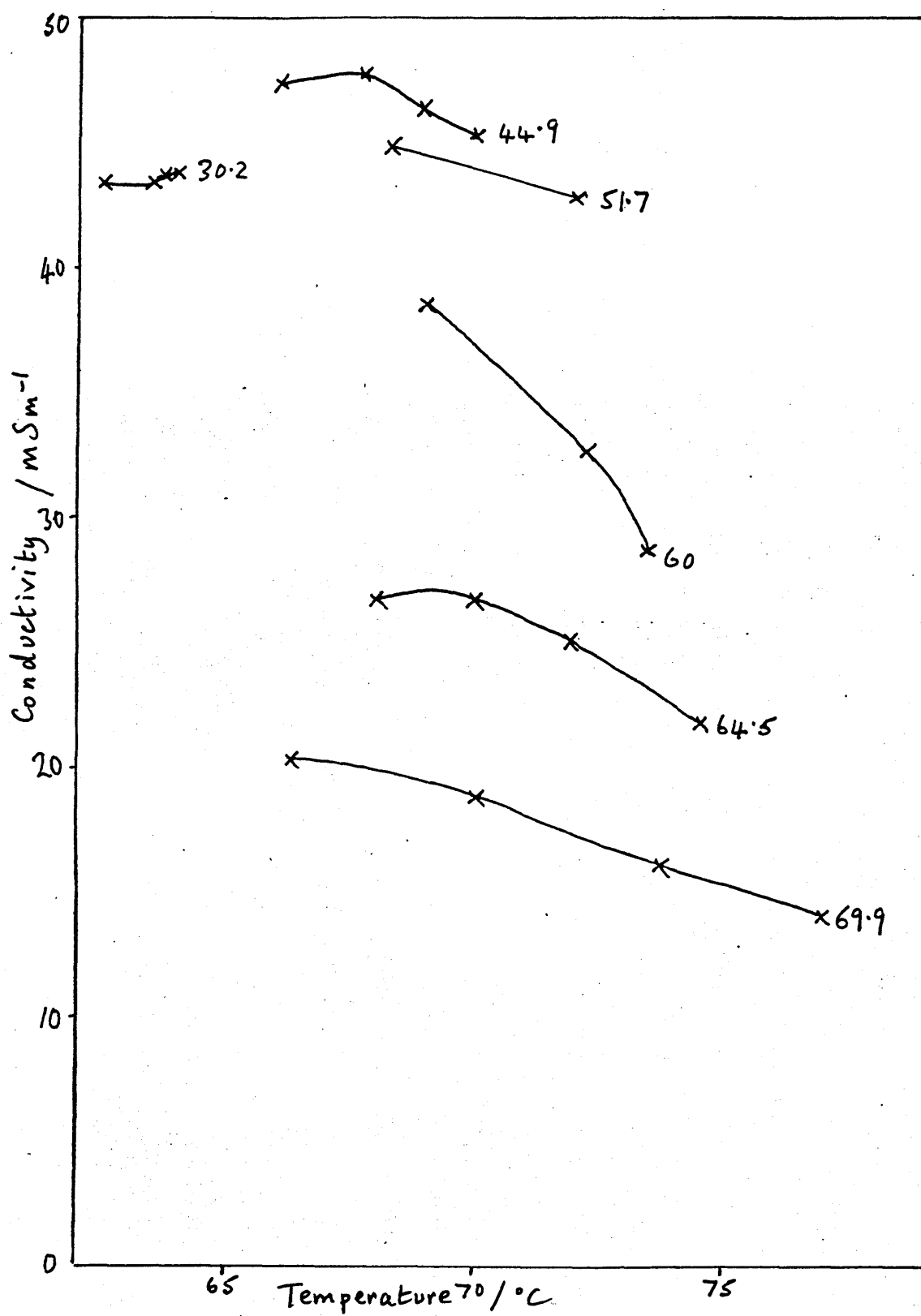


Fig.4.36. Variation of conductivity with temperature in Brij-water samples.

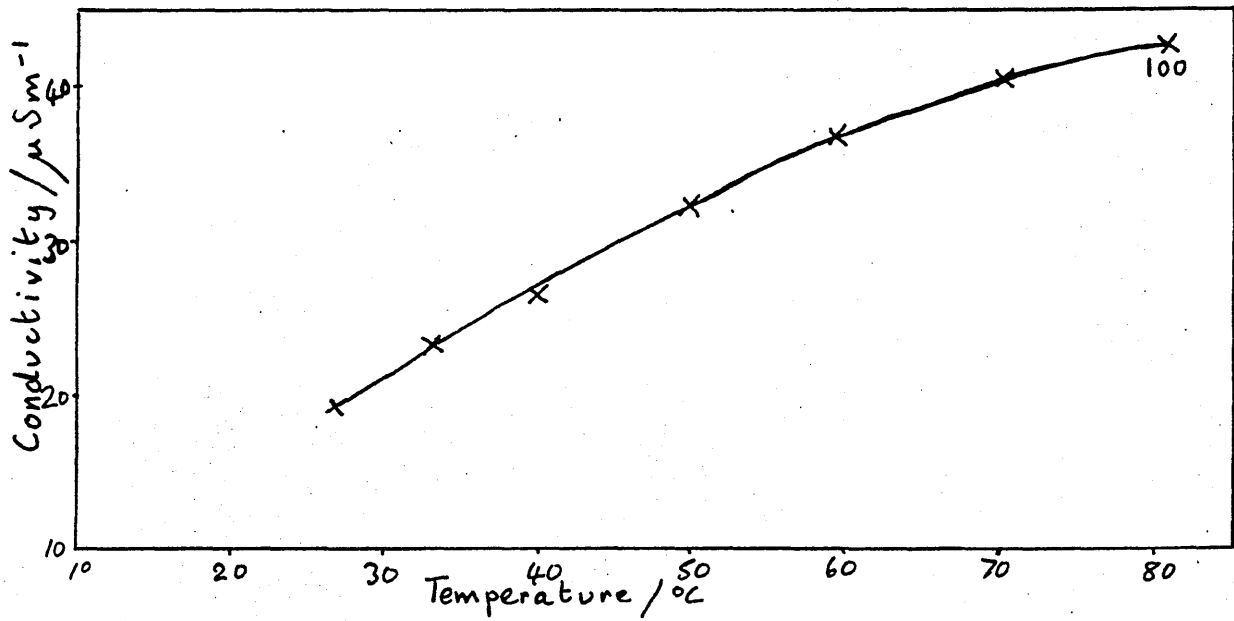
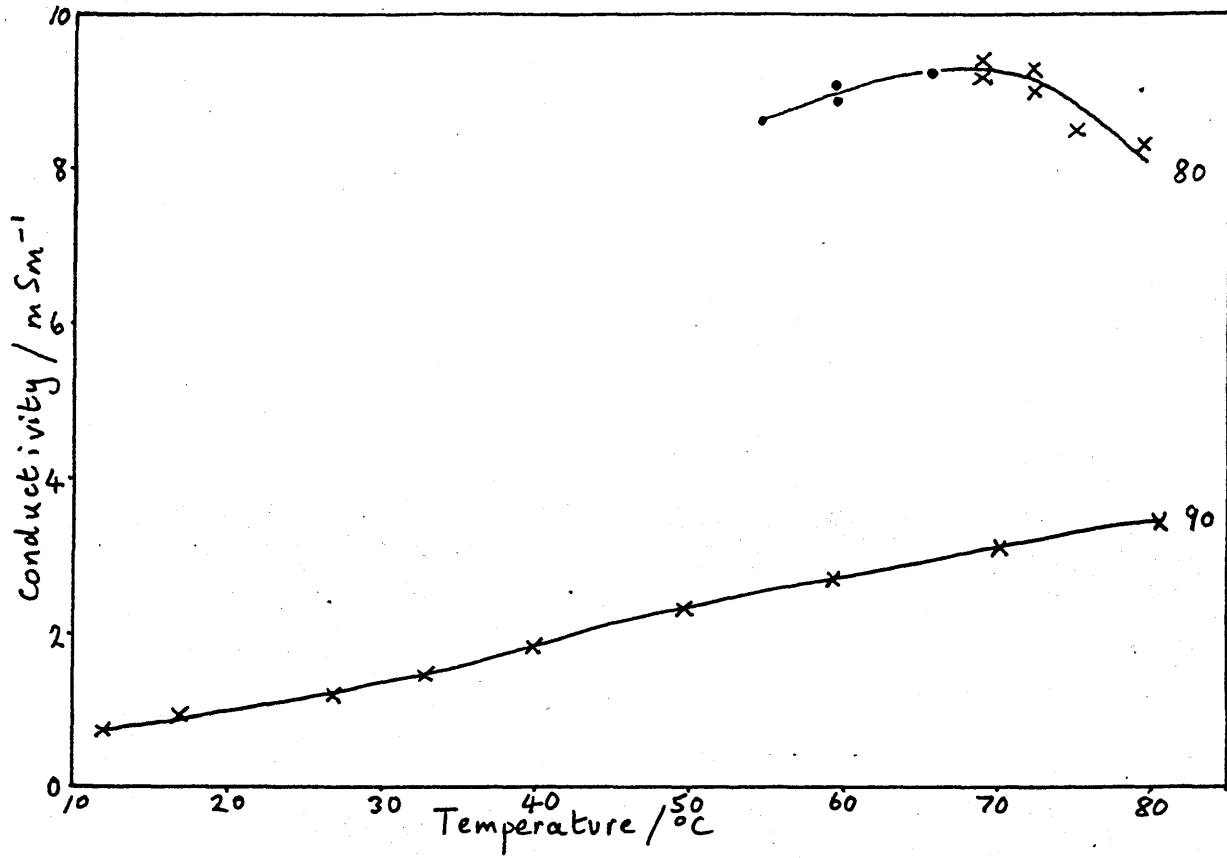


Fig.4.37. Variation with temperature of the conductivity of Brij and Brij-water samples.

At 80% Brij a correction has been made to allow for a difference of 1.1% in the water content of the two samples measured.

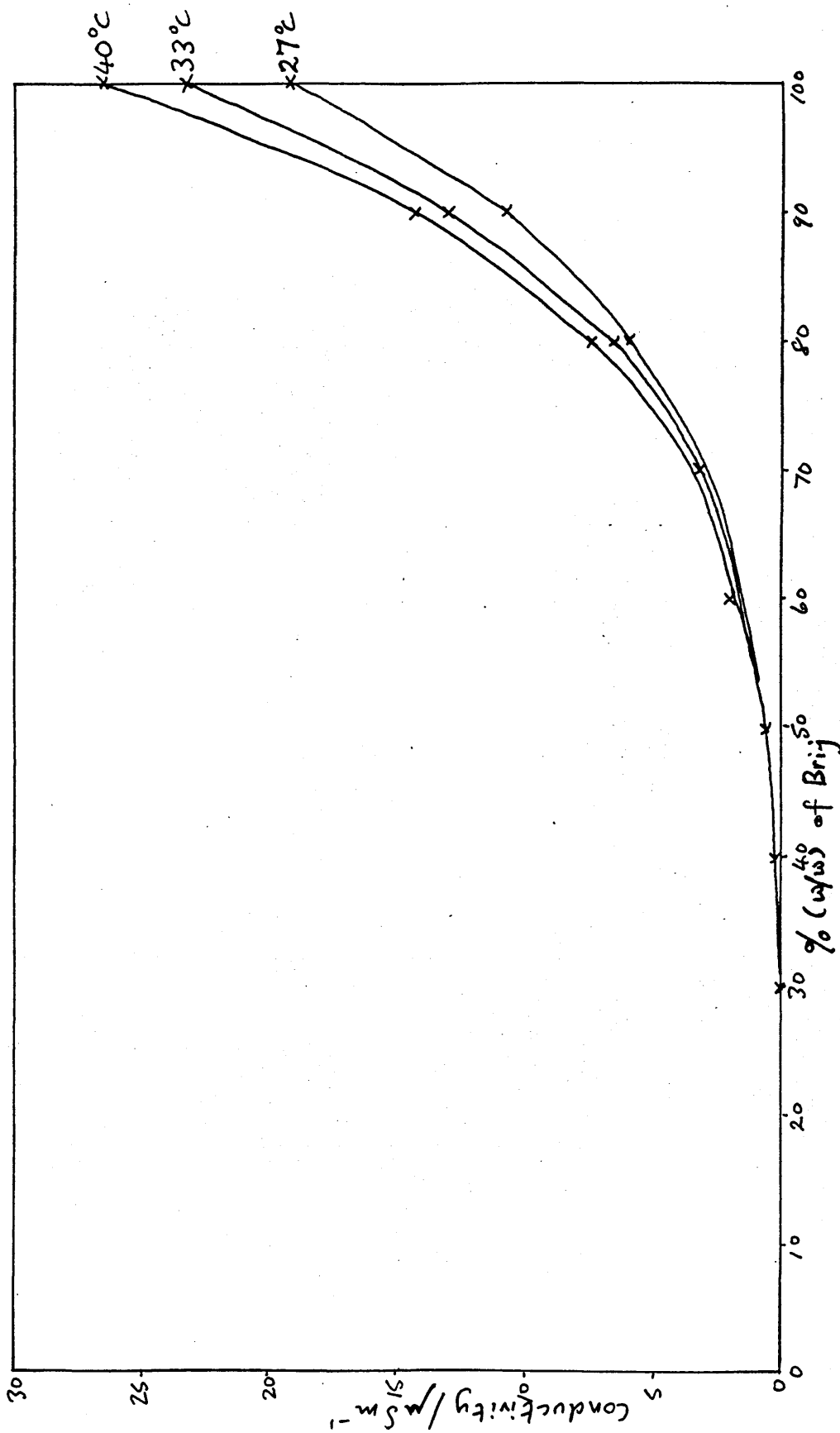


Fig. 4.38. Conductivity of Brij- hexane mixtures.

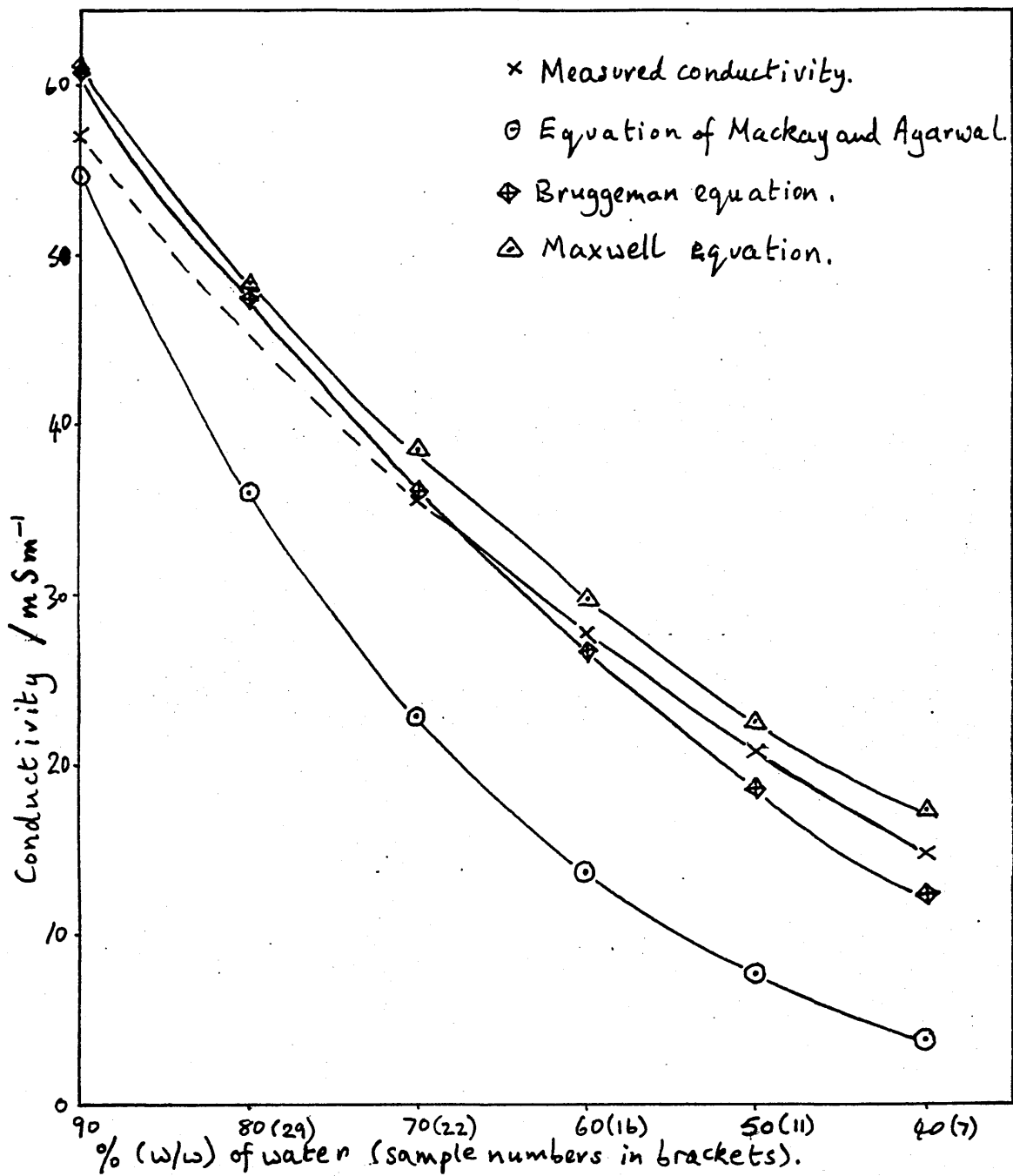
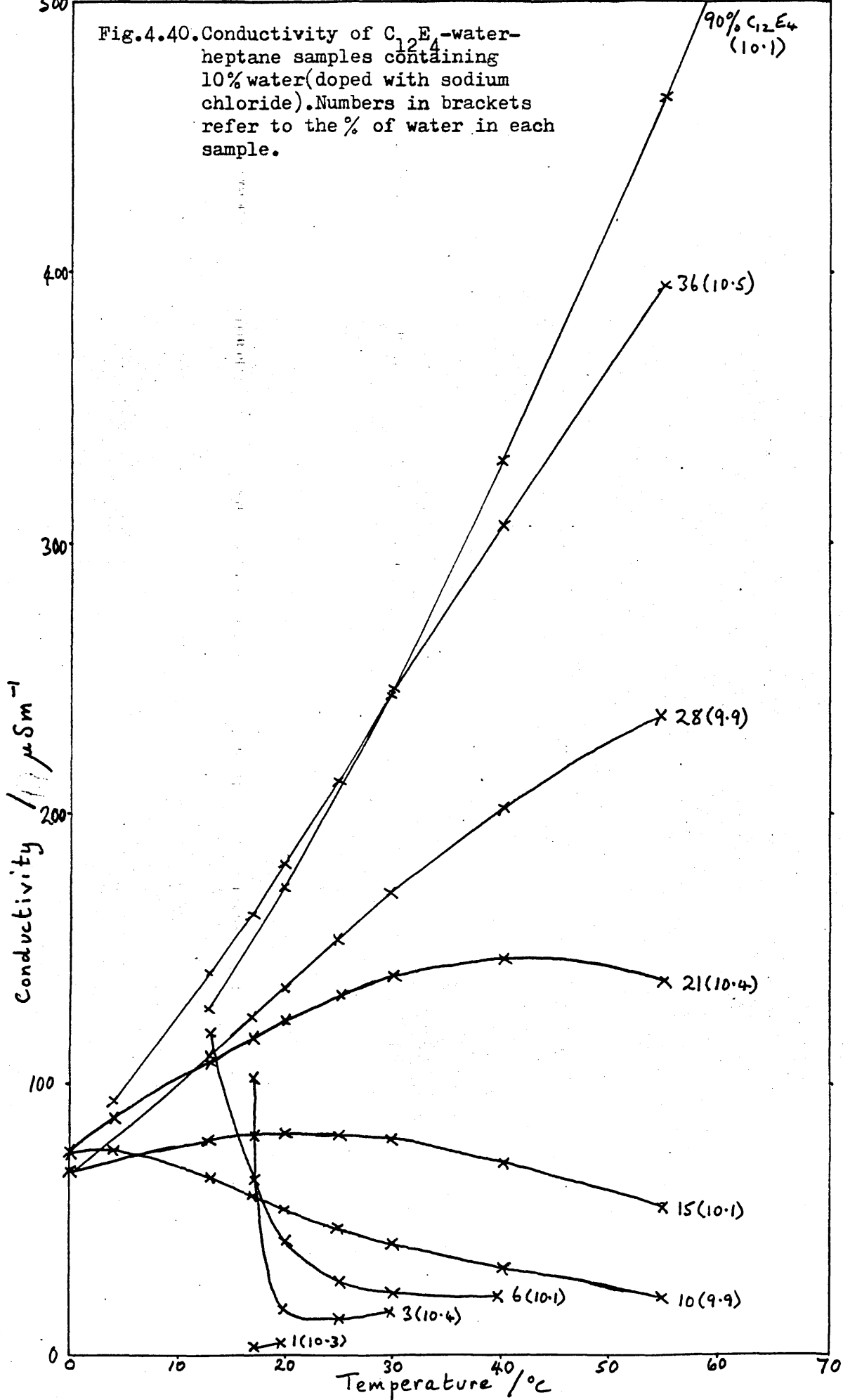


Fig.4.39. Conductivity in the  $\delta$ -region of the  $C_{12}E_4$ -water-heptane system. (samples doped with sodium chloride).

Fig.4.40. Conductivity of  $C_{12}E_4$ -water-heptane samples containing 10% water (doped with sodium chloride). Numbers in brackets refer to the % of water in each sample.



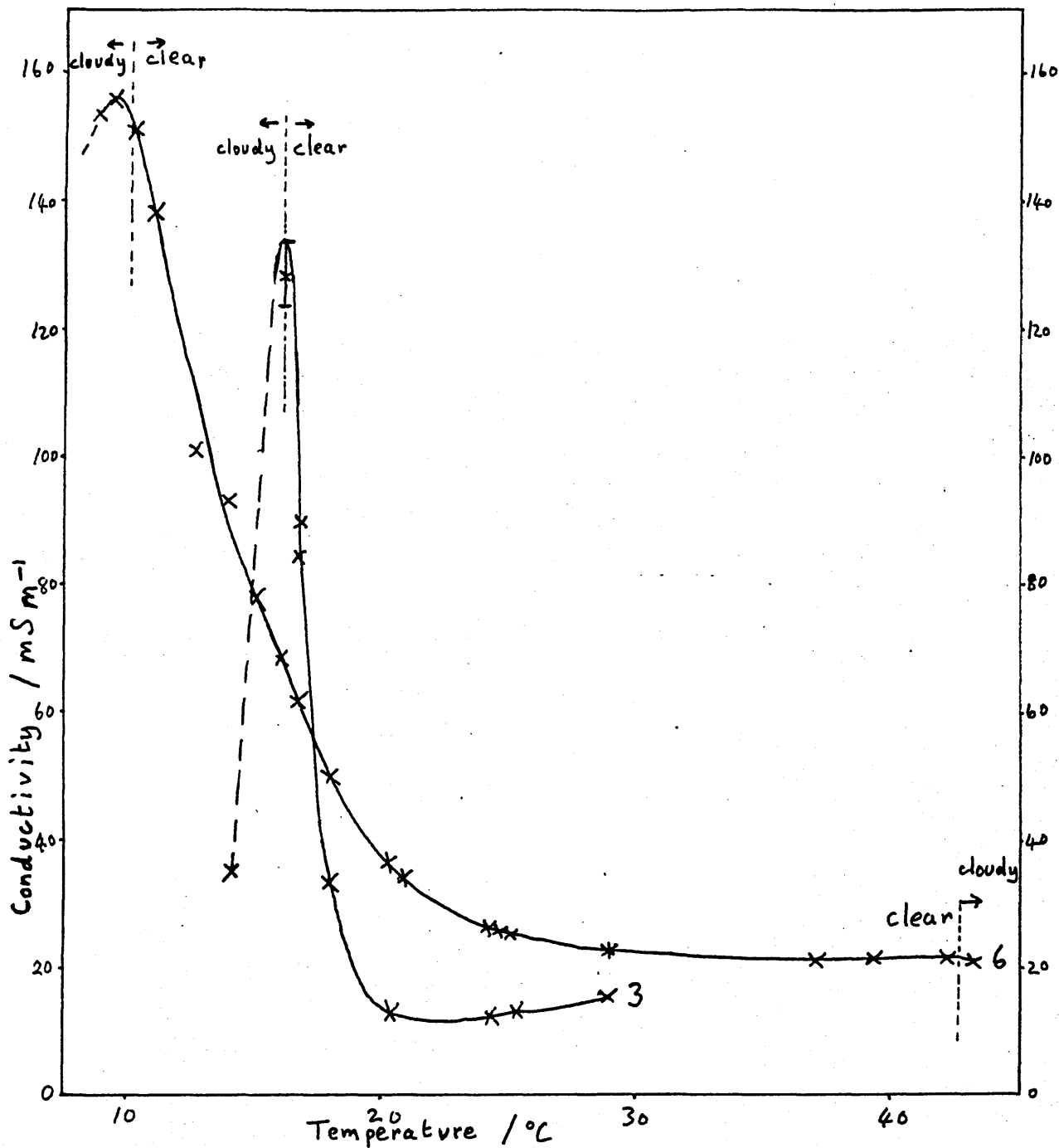


Fig.4.41. Conductivity of 20.1%  $C_{12}E_4$ -10.2% sodium chloride solution-69.7% heptane (sample 3), and of 30.0%  $C_{12}E_4$ -10.0% sodium chloride solution-59.9% heptane (sample 6), as a function of temperature.

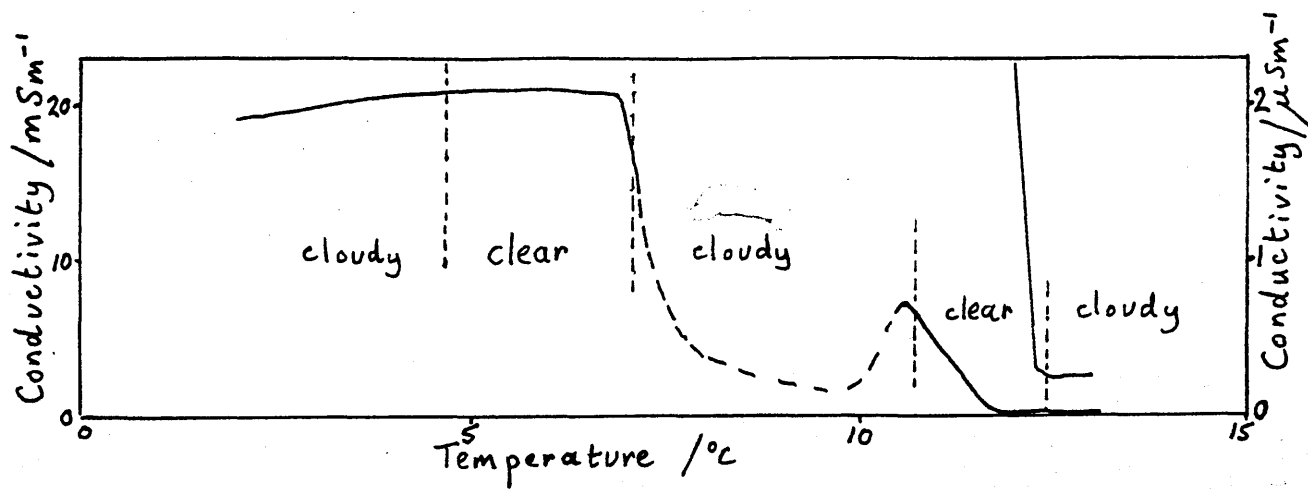


Fig.4.42. Conductivity of an initial mixture of 55.2% sodium chloride solution and 44.8% heptane to which 10.0%  $C_{12}E_4$  was added. (Sample 11).

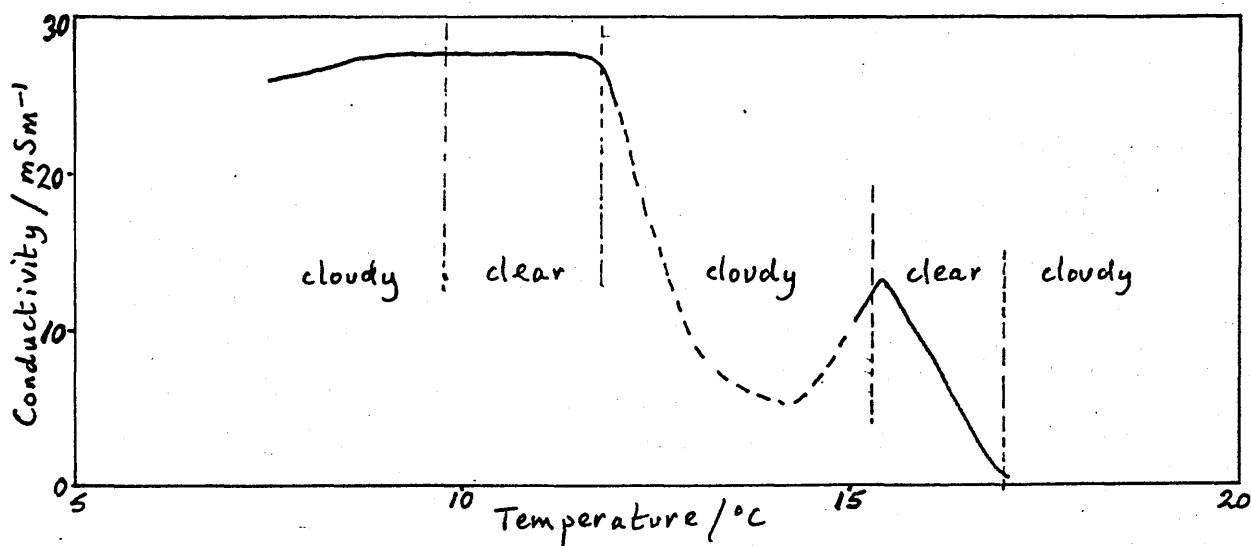


Fig.4.43. Conductivity of an initial mixture of 60.2% sodium chloride solution and 39.8% decane to which 9.8%  $C_{12}E_4$  was added.

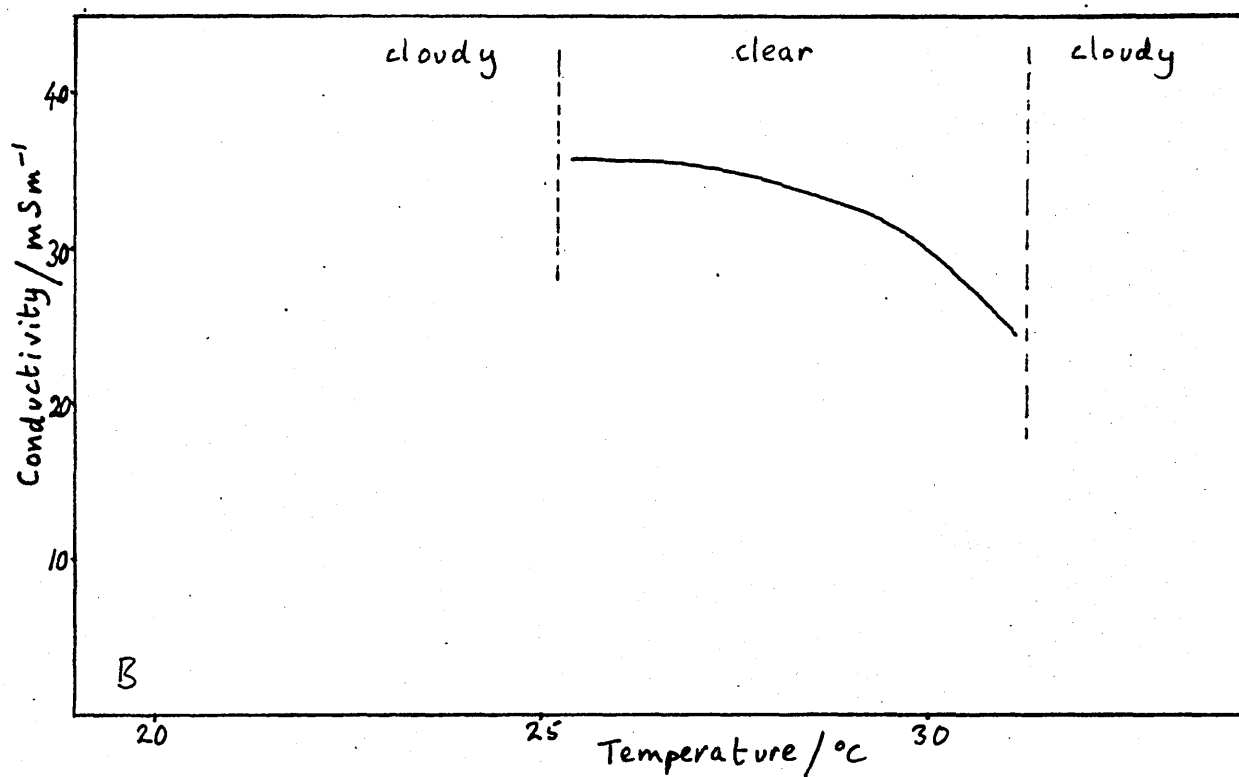
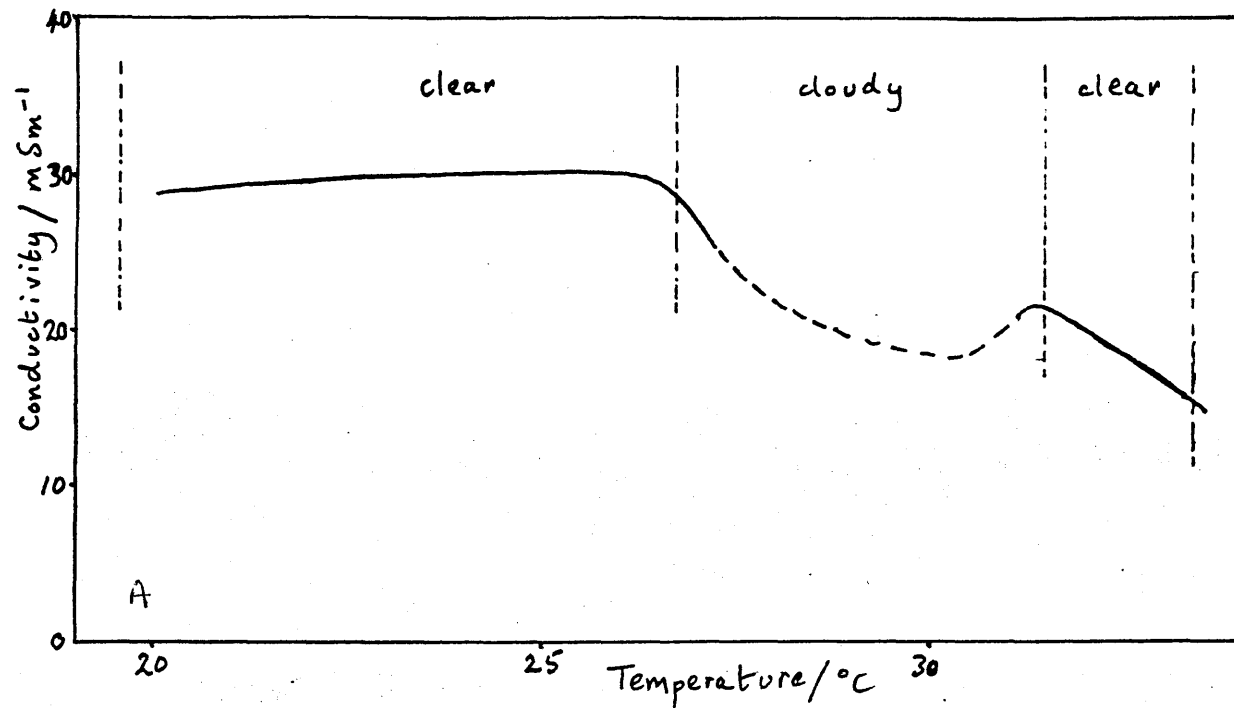


Fig.4.44. Conductivity of:

- A - an initial mixture of 60.0% sodium chloride solution and 40.0% hexadecane to which 18.0%  $C_{12}E_4$  was added.
- B - an initial mixture of 60.1% sodium chloride solution and 39.9% hexadecane to which 14.0%  $C_{12}E_4$  was added.

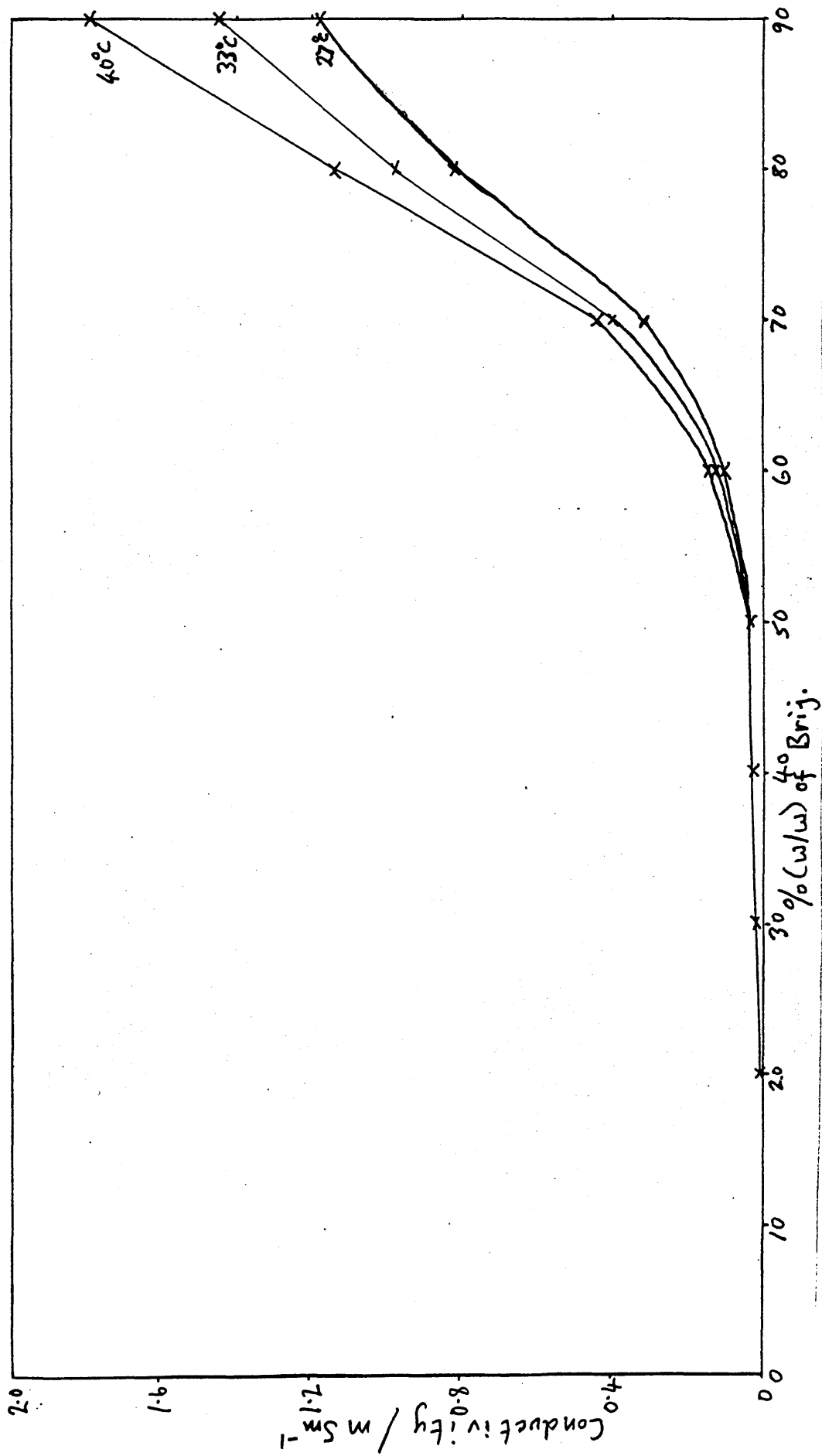


Fig. 4.45. Conductivity of Brij- water- hexane mixtures containing 10% water.

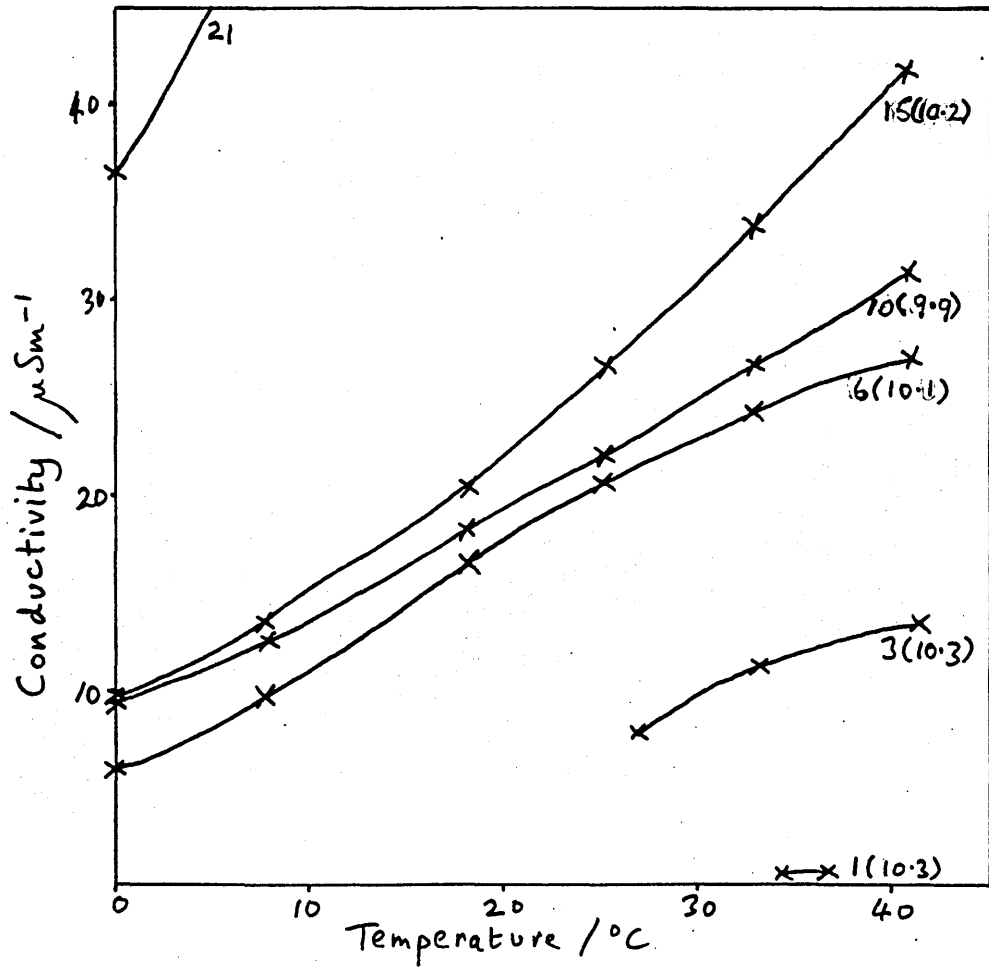
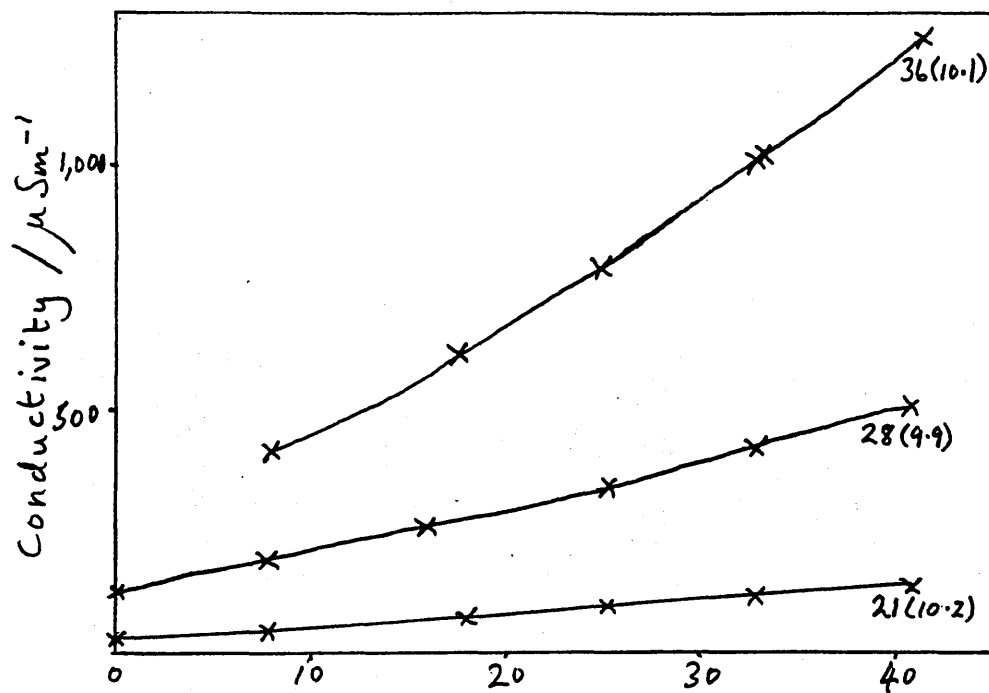
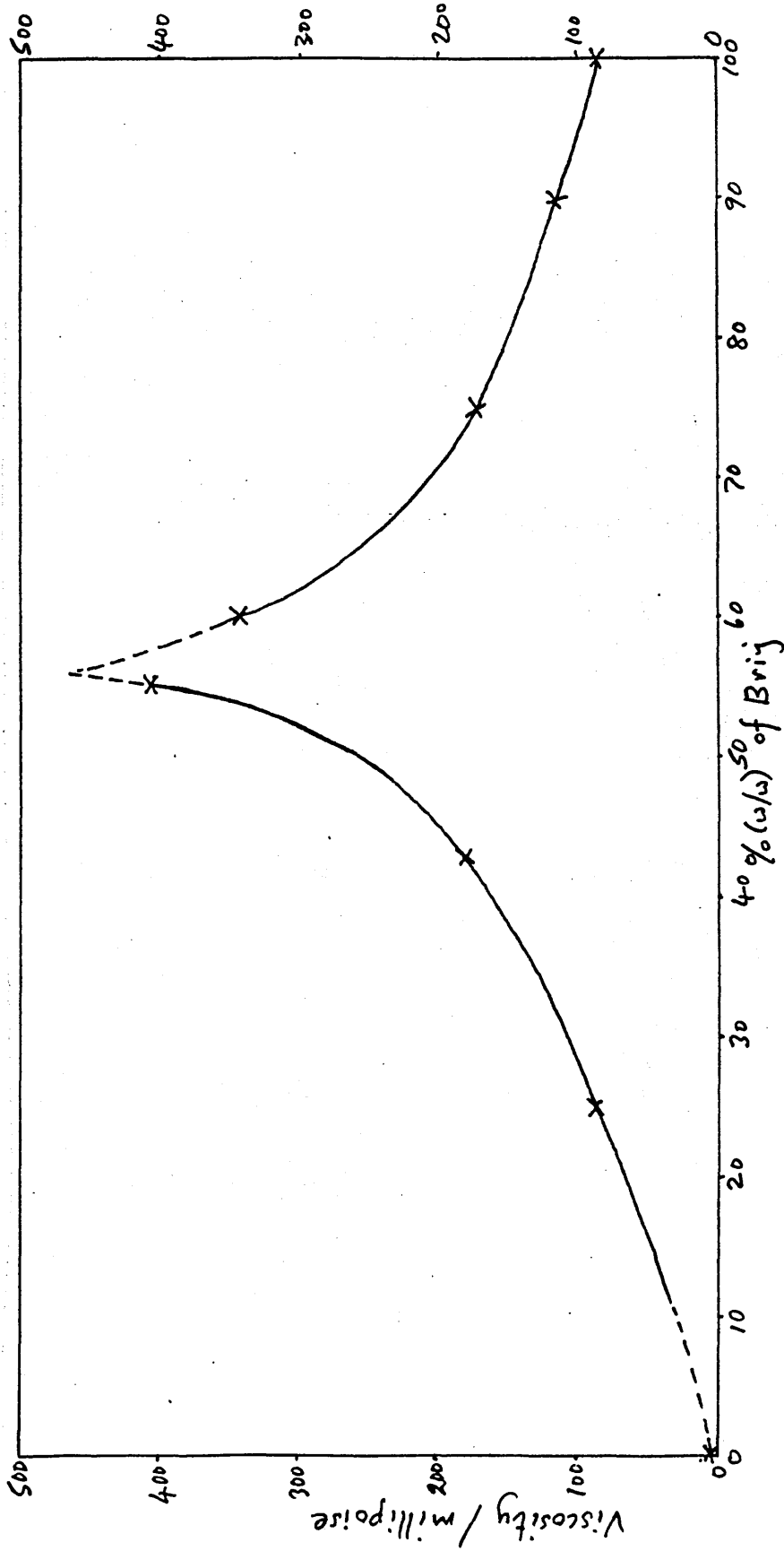


Fig.4.46. Variation in conductivity of Brij- H<sub>2</sub>O- hexane samples containing approximately 10 % H<sub>2</sub>O. Numbers in brackets give the % of H<sub>2</sub>O in each sample.

Fig. 4.47. Variation of viscosity with composition in the Brij- water system. Measurements were made at the lowest temperature at which each sample was clear for samples containing less than 70 % Brij and at 67° for more concentrated samples.



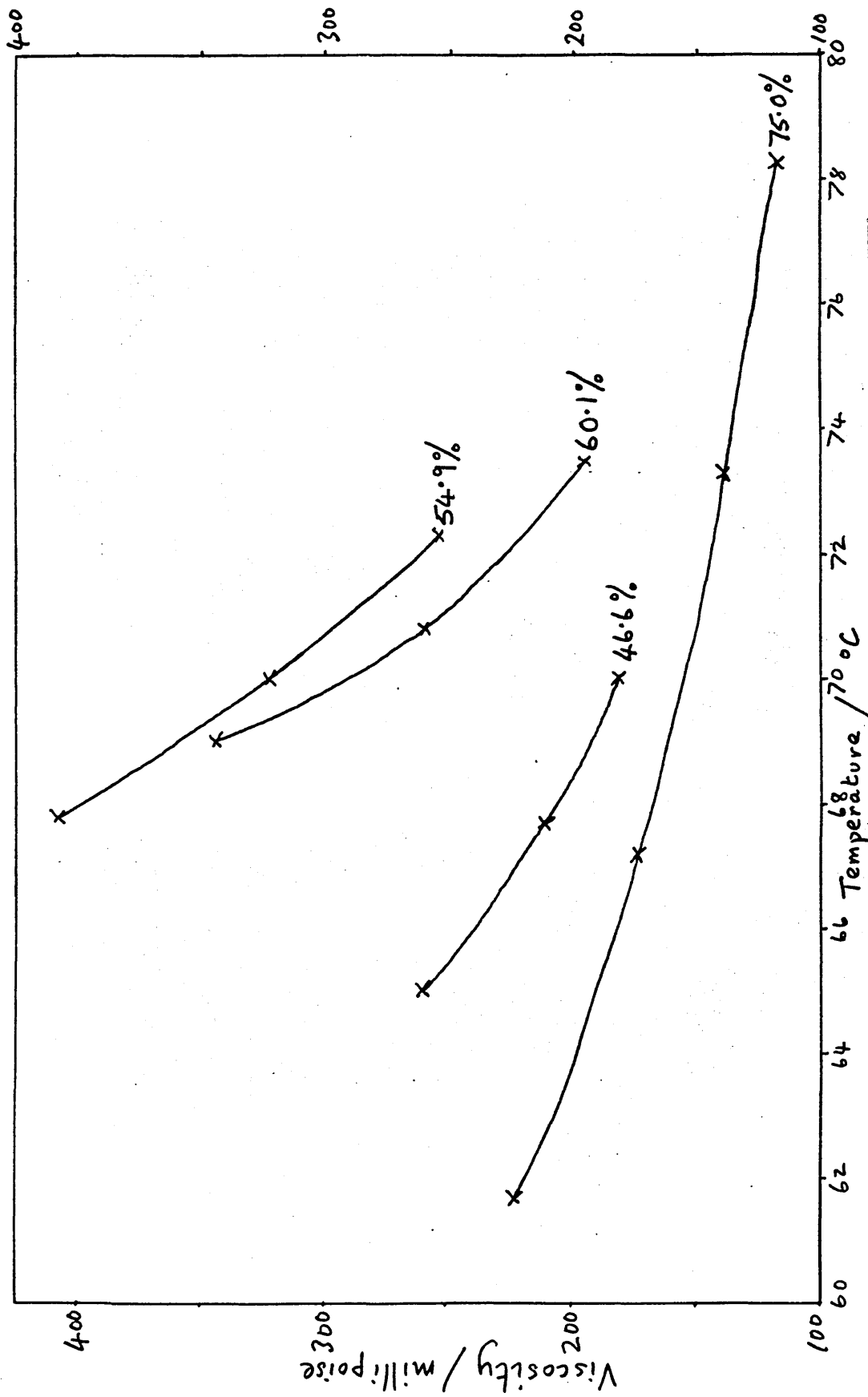


Fig. 4.48. Variation of viscosity with temperature in Brij- water samples.

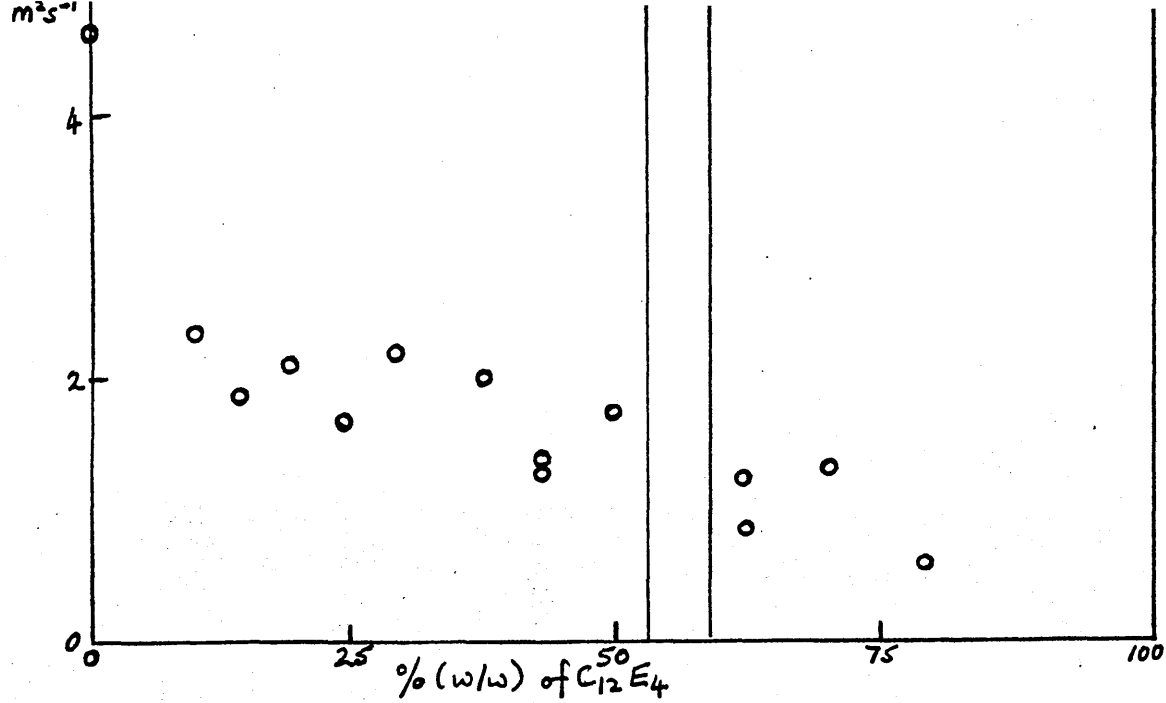


Fig.4.49. Water diffusion coefficients in the  $\zeta$ -region and  $\beta$ -region of the  $C_{12}E_4$ -water system.

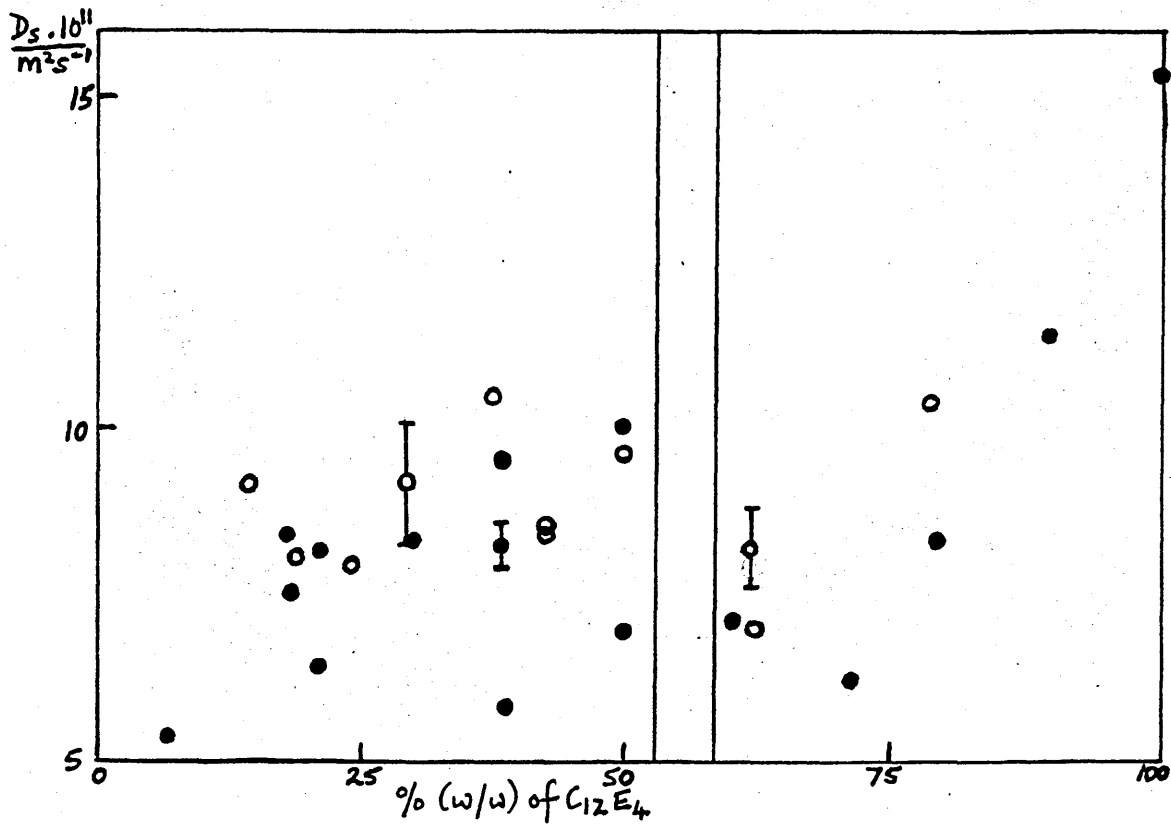


Fig.4.50. Surfactant diffusion coefficients in the  $\zeta$ -region and  $\beta$ -region of the  $C_{12}E_4$ -water system.

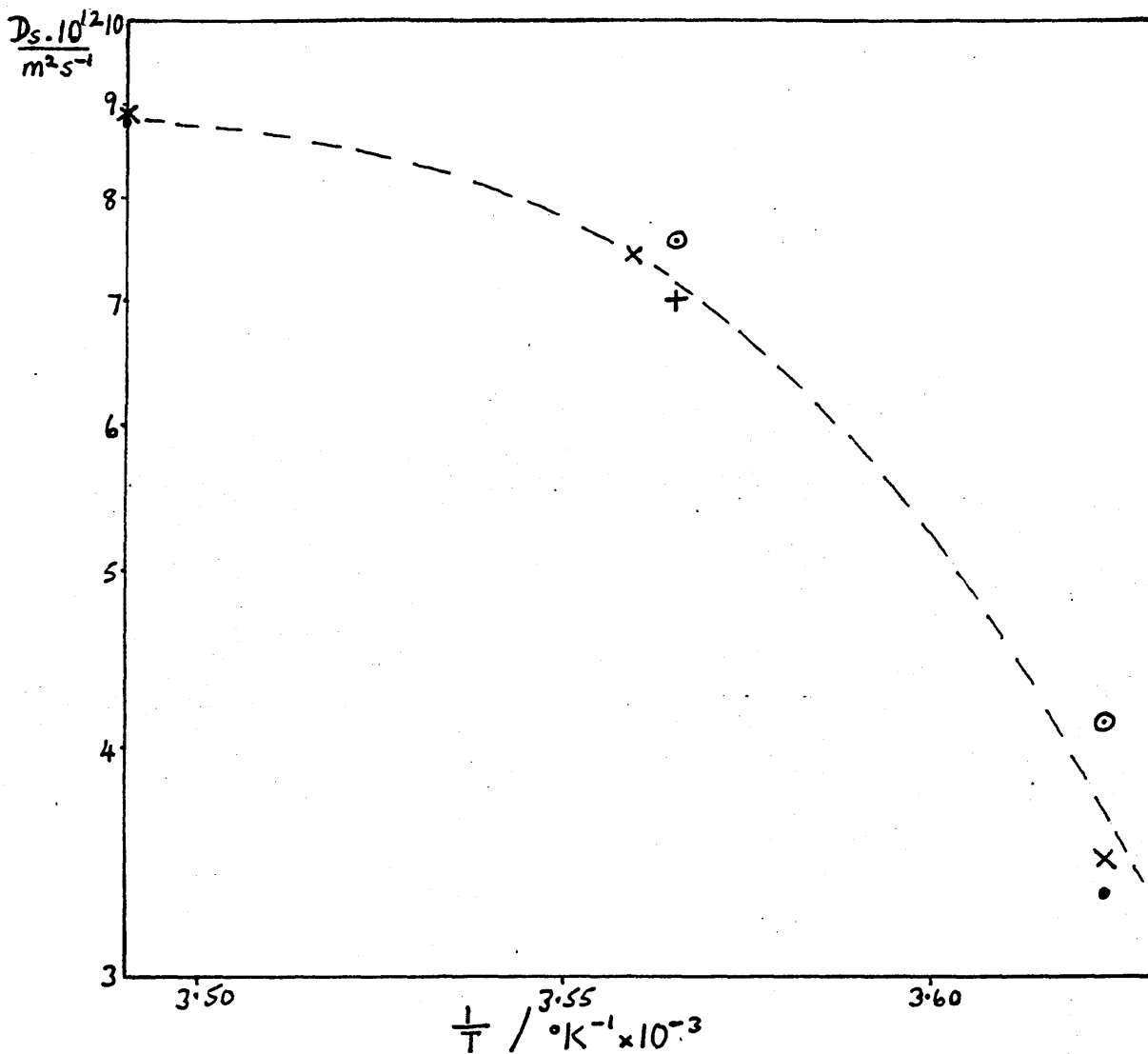


Fig. 4.51. Surfactant diffusion coefficients in the  $\alpha$ -region of the  $C_{12}E_4$ -water system (activation energy plot).

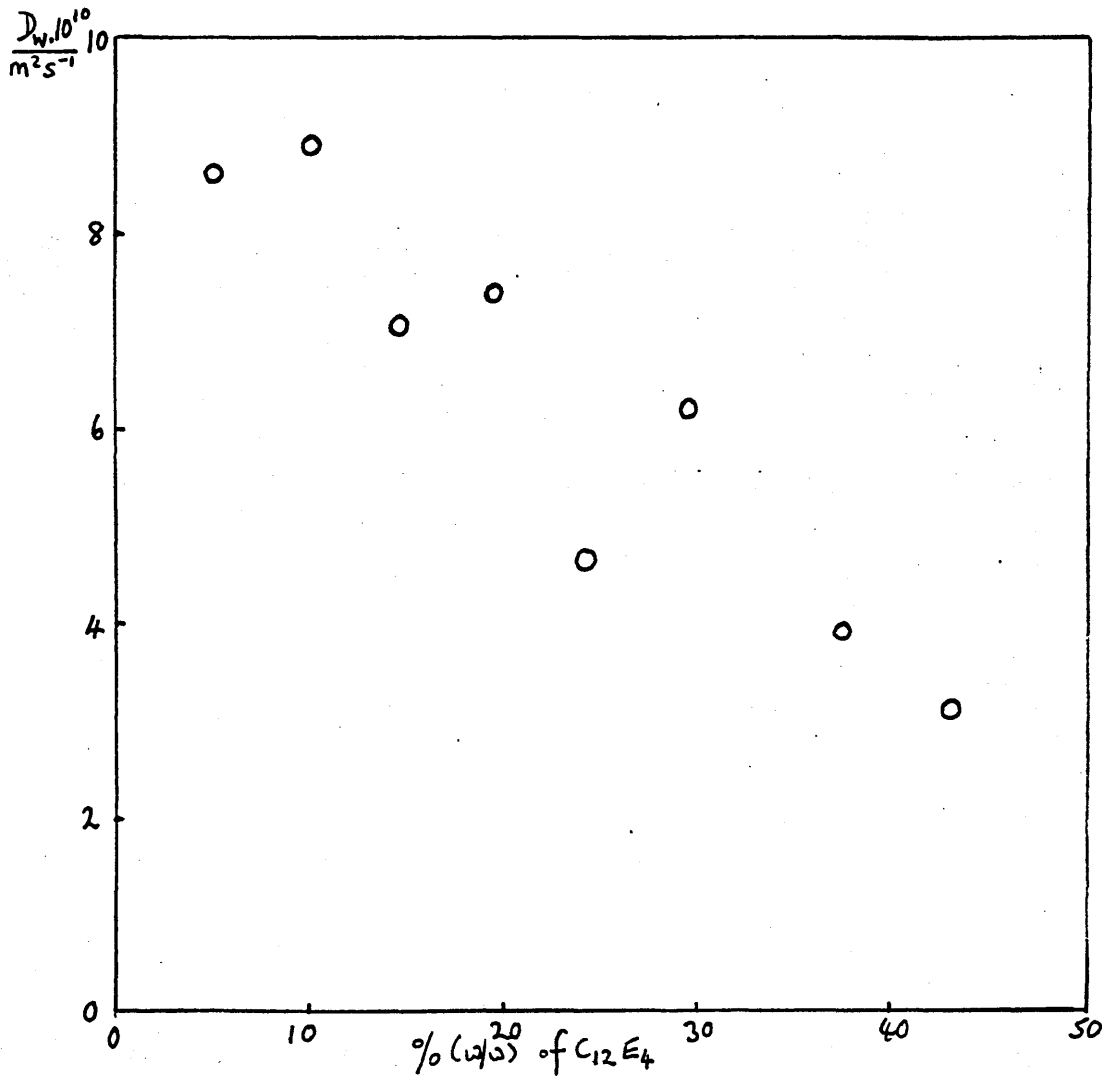


Fig.4.52. Water diffusion coefficients in the  $\alpha$ -region of the C<sub>12</sub>E<sub>4</sub>- water system.

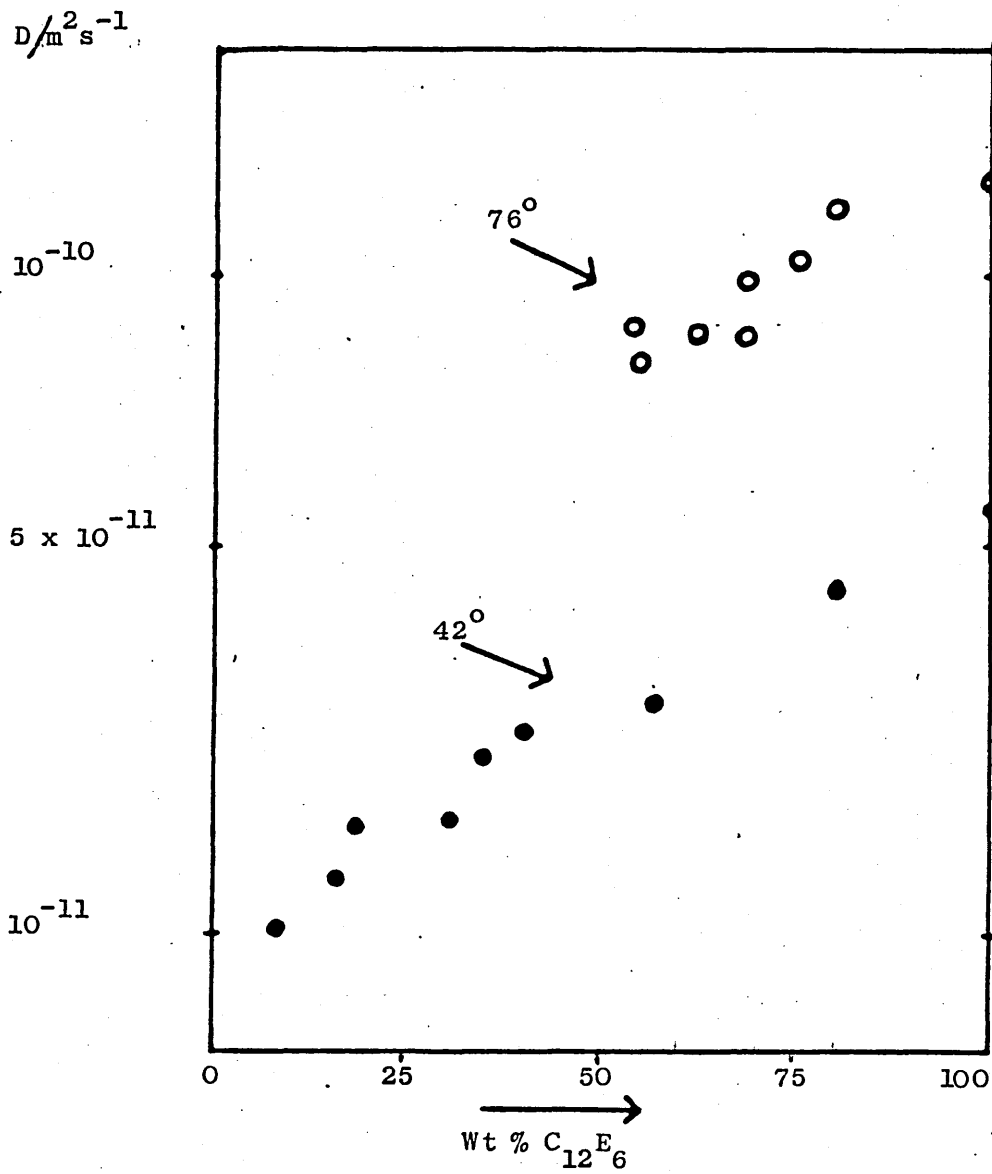


FIG 4.53. Surfactant diffusion coefficients in  $C_{12}E_6$  - water solutions.

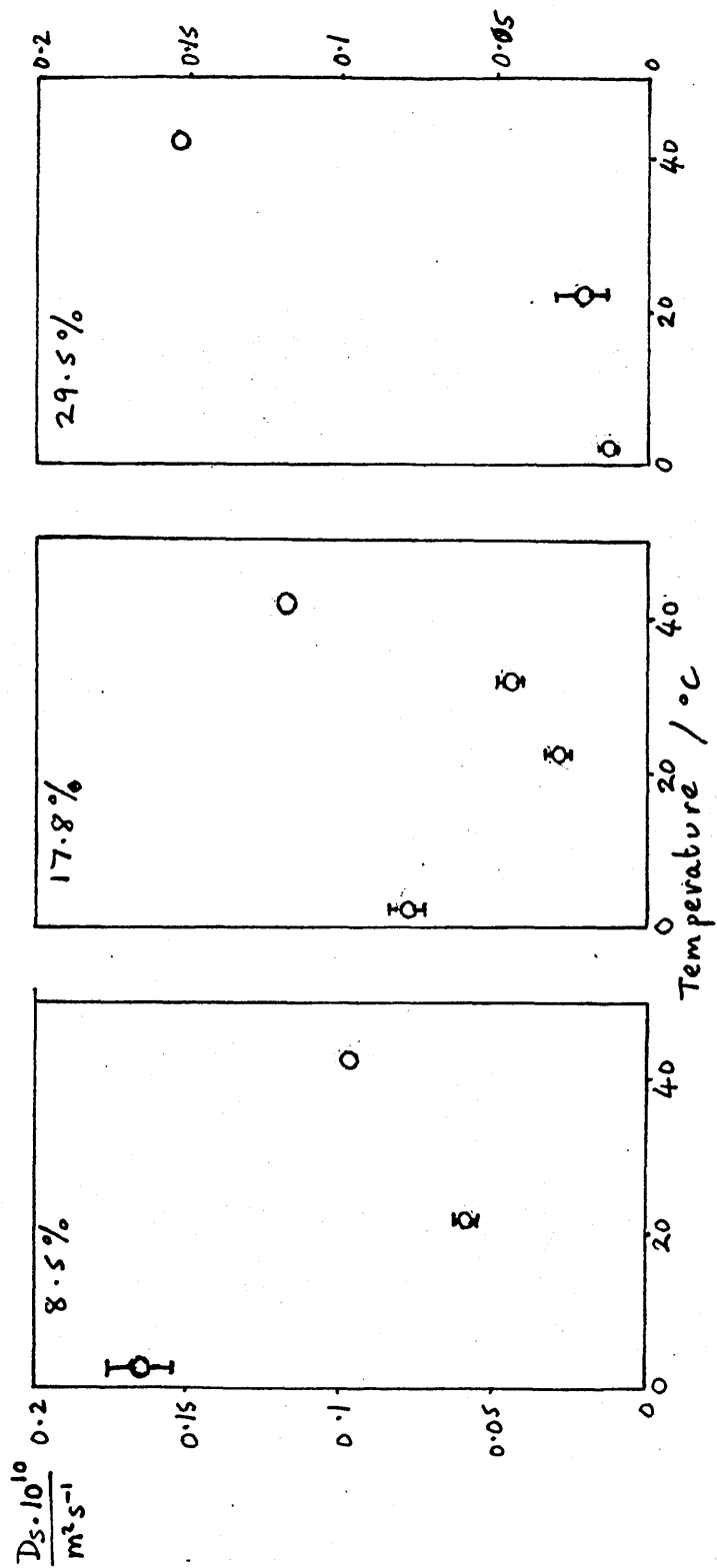


Fig. 4.54. Surfactant self-diffusion coefficients in the C<sub>12</sub>E<sub>6</sub>-water system at low temperature and high water content.

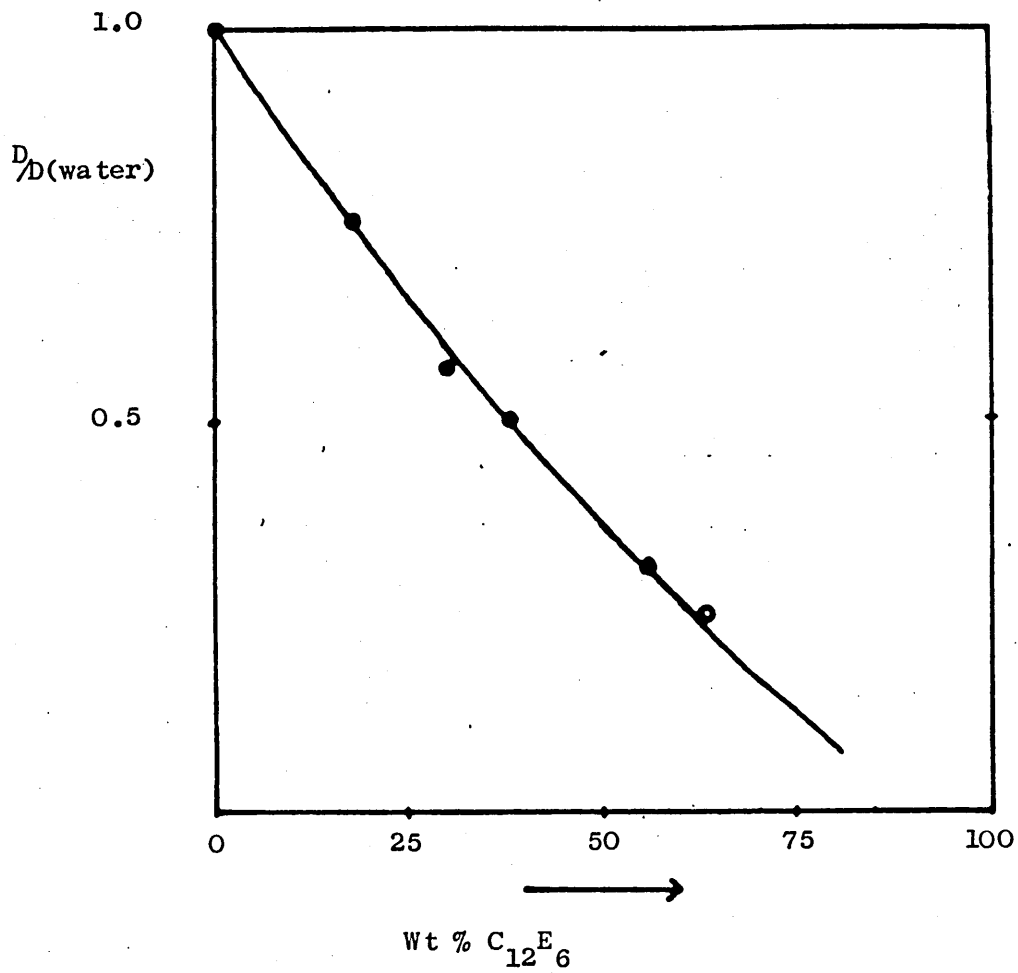


Fig. 4.55. Self-diffusion coefficient of water in solutions with  $C_{12}E_6$  at  $42^\circ\text{C}$ . The value at 62% is extrapolated.

In the following tables of conductivity results  $K_{calc}$  is the value calculated from the equation of Mackay and Agarwal:

$$\frac{K}{K_0} = (1-\phi)^{2.5}$$

The disperse phase volume,  $\phi$ , was assumed to be the same as the volume fraction of surfactant.

TABLE 4.1 CONDUCTIVITY IN THE  $C_{12}E_4-H_2O$  SYSTEM

Sample $C_{12}E_4$ %(W/W)	Composition NaCl solution %(W/W)	Temp. /°C	K /m <sup>-1</sup>	K calc. /m <sup>-1</sup>
2.55	97.45	53.6	114.6mS	177mS
3.04	96.96	53.9	113.4mS	176mS
		4.1	67.2mS	66.3mS
		0.0	59.7mS	59.0mS
10.0	90.0	58.5	106mS	153mS
		7.6	62.6mS	59.7mS
		4.2	57.0mS	54.4mS
		0.0	50.6mS	48.4mS
20.0	80.0	62.5	88.5mS	117.9mS
		12.9	52.9mS	50.5mS
		10.0	49.4mS	46.9mS
		4.2	42.2mS	39.9mS
		0.0	37.3mS	35.5mS
30.1	69.9	66.2	70.0mS	86.5mS
		19.5	43.7mS	40.5mS
		14.7	39.9mS	36.8mS
		10.0	35.9mS	32.9mS
		4.1	31.3mS	28.1mS
		0.0	27.7mS	24.9mS
40.2	59.8	69.4	54.3mS	59.7mS
		14.7	27.7mS	24.5mS
		10.0	24.6mS	21.9mS
		4.2	19.9mS	18.7mS
		0.0	17.98mS	16.6mS
50.1	49.9	71.2	33.1mS	38.2mS
		0.0	11.06mS	10.4mS
67.9	32.1	72.7	8.88mS	12.6mS
		71.6	9.01mS	12.4mS
75.2	24.8	79.9	4.56mS	7.00mS
		79.1	4.62mS	6.96mS
		76.5	4.82mS	6.78mS
		74.2	4.93mS	6.62mS
		69.1	5.08mS	6.27mS
		64.2	5.15mS	5.93mS

Table 4.1 Cont'd.

80.3	19.7	85.4	2.805mS	4.09mS
		80.0	2.867mS	3.88mS
		75.1	2.885mS	3.70mS
		Maximum of 2.88-		
		2,89mS between 70 and 75°C		
		69.9	2.864mS	3.50mS
		64.9	2.79mS	3.30mS
		59.9	2.698mS	3.12mS
		55.3	2.586mS	2.93mS
		55.2	2.577mS	2.93mS
89.9	10.1	83.0	831μS	755μS
		72.7	636μS	681μS
		64.3	555μS	620μS
		55.1	465μS	554μS
		40.1	331μS	445μS
		30.0	247μS	373μS
		20.0	173.5μS	304μS
		13.0	128.6μS	260μS
		8.1	102.8μS	228μS
100		72.7	1.13μS	
		64.4	818nS	
		55.5	784nS	
		40.1	588nS	
		30.1	453nS	
		30.0	435nS	
		25.0	397nS	

TABLE 4.2 CONDUCTIVITY IN THE  $C_{12}E_6-H_2O$  SYSTEM

Sample $C_{12}E_6$ %(W/W)	Composition NaCl solution %(W/W)	Temperature /°C	K /m <sup>-1</sup>	K calc /m <sup>-1</sup>
5.24	94.76	52.5*	170.5mS	163.9mS
		43	148.3mS	142.9mS
		32.0	121.9mS	118.4mS
		22.1	99.8mS	97.5mS
		15.0	85.1mS	83.0mS
		7.1	69.4mS	68.2mS
		0.0	56.7mS	55.9mS
15.2	84.8	52.5	129.9mS	124.1mS
		42-43	113mS	108mS
		32.0	92.6mS	89.7mS
		22.1	75.6mS	73.8mS
		15.0	64.5mS	62.9mS
		7.1	52.3mS	51.6mS
		0.0	42.4mS	42.4mS
25.2	74.8	52.5	96.7mS	90.8mS
		43.0	83.7mS	79.1mS
		32.1	68.9mS	65.6mS
		22.1	55.3mS	54.0mS
		15.0	46.6mS	46.0mS
		7.1	37.4mS	37.8mS
		0.0	30.1mS	31.0mS
35.0	65.0	60.0	78.3mS	70.4mS
		52.5	71.0mS	63.9mS
		43.0	61.5mS	55.8mS
		32.1	49.9mS	46.2mS
		22.1	39.5mS	38.0mS
		15.0	32.9mS	32.4mS
		7.1	25.9mS	26.6mS
44.9	55.1	68.3	56.8mS	51.1mS
		60.1	52.4mS	46.5mS
		52.4	47.6mS	42.2mS
		43.3	41.3mS	36.9mS

Table 4.2 Cont'd.

55.1	44.9	82.0	37.1mS	35.4mS		
		76.0	36.8mS	33.3mS		
		68.3	35.0mS	30.7mS		
		60.1	32.6mS	27.9mS		
		52.4	28.9mS	25.3mS		
		43	24.6mS	22.1mS		
		67.9	32.1	91.5	16.50mS	16.6mS
89.5	16.56mS			16.3mS		
88.2	16.61mS			16.2mS		
maximum of 16.64mS between 87 and 88°C						
86.9	16.61mS			16.0mS		
85.0	16.53mS			15.7mS		
83.5	16.47mS			15.5mS		
80.8	16.29mS			15.1mS		
77.5	16.05mS			14.6mS		
72.6	15.66mS			13.9mS		
20.2 †	4.83mS			6.25mS		
15.4 †	3.97mS			5.63mS		
10.9 †	3.31mS			5.02mS		
79.9	20.1			82.0	4.94mS	4.75mS
				76.0	4.67mS	4.79mS
		68.0	4.20mS	4.09mS		
		60.1	3.68mS	3.74mS		
		52.5	3.17mS	3.40mS		
		89.5	10.5	90.5	1.45mS	1.01mS
82.1	1.27mS			0.936mS		
82.0	1.29mS			0.936mS		
76.0	1.16mS			0.881mS		
68.0	1.00mS			0.807mS		
60.1	825μS			738μS		
60.0	842μS			738μS		
52.5	696μS			670μS		
52.5	699μS			670μS		
43.0	533μS			584μS		
32.1	361μS			484μS		
22.0	238μS			397μS		

Table 4.2 Cont'd.

100	-	74.6	11.50 $\mu$ S
(sample possibly wet)		65.1	9.64 $\mu$ S
		54.2	7.90 $\mu$ S
		44.3	6.30 $\mu$ S
		34.1	4.75 $\mu$ S
		24.8	3.47 $\mu$ S

\*5.24% C<sub>12</sub>E<sub>6</sub> at 52.5°C slightly cloudy

†Conductivity of viscous isotropic liquid crystal

TABLE 4.3 Conductivity in the Brij 30-H<sub>2</sub>O System

Approximate results obtained with copper cell.

Sample Brij 30 %(W/W)	Composition H <sub>2</sub> O %(W/W)	Temperature /°C	K /mSm <sup>-1</sup>
2.52	97.48	57.7	6.1*
4.90	95.10	57.5	10.9*
8.05	91.95	57.6	15.8*
11.1	88.9	57.9	20.8
14.2	85.8	58.3	25.5
17.3	82.7	59.9	30.1
20.0	80.0	60.2	33.9
22.1	77.9	60.0	35.2
25.0	75.0	61.3	38.3
		61.3	39.0
		61.5	37.9
30.2	69.8	62.5	43.3
		63.5	43.3
		63.7	43.7
		64.0	43.7
35.0	65.0	65.3	46.0
39.9	60.1	66.6	47.7
44.9	55.1	66.1	47.4
		67.7	47.7
		68.9	46.4
		70.0	45.3
45.1	54.9	67.5	47.8
49.9	50.1	68.7	45.7
51.7	48.3	68.3	44.9
		72.0	42.7
55.1	44.9	69.0	42.4
59.8	40.2	69.0	38.8
		69.0	39.3
59.9	40.1	72.3	32.9
		72.3	32.2
		73.4	28.6
60.2	39.8	69.0	38.1
64.5	35.5	68.0	26.6
		70.0	26.6
		71.9	25.0
		74.6	21.7
64.5	35.5	69.0	29.8
69.9	30.1	66.3	20.2
		70.0	18.7
		73.7	16.0
		76.9 <sup>+</sup>	14.0
70.1	29.9	69.0	19.5
79.3	20.7	54.8	9.4
		59.7	9.7
		59.7	9.8
		65.8	10.0
		79.5	9.1

Table 4.3 Cont'd.

80.4	19.6	69.0	9.2
		69.0	9.4
		72.3	9.3
		72.3	9.0
		75.0	8.5
		79.6	8.3
89.1	10.9	69.0	3.98
90	10	12.0	0.76
		17.1	0.92
		27	1.18
		33.0	1.45
		40.0	1.80
		49.7	2.31
		59.3	2.66
		70.3	3.11
		80.5	3.4
94.9	5.1	69.0	1.29
100	-	27	0.0192
		33.0	0.0233
		40.0	0.0265
		49.7	0.0323
		59.3	0.0369
		70.3	0.0404
		80.5	0.0428

\*The isotropic liquid region in these samples is not stable.

†Sample just cloudy at this temperature.

Abbreviations used in tables 4.4-4.7 to describe the sample appearance

- c - cloudy or hazy
- bft - birefringent

All samples were clear unless otherwise stated.

TABLE 4.4 Conductivity in the  $C_{12}E_4-H_2O$ -heptane system

A Sample number	Samples containing 10% NaCl solution			Temp. /°C.	$K$ $\mu S m^{-1}$	Sample appearance
	Sample $C_{12}E_4$ %(W/W)	NaCl solution %(W/W)	Composition heptane %(W/W)			
1	10.1	10.3	79.6	17.0	2.06	
				19.8	3.91	
3	20.1	10.4	69.5	17.0	102.4	
				19.8	15.9	
				24.9	13.0	
				29.8	15.7	
				14.1	35	c, bft
				Maximum - 16.0	134	just c, bft
				16.1	120-130	
				16.7	84.3	
				16.7	89.4	
				18.0	33.0	
				20.4	12.62	
				24.2	12.58	
				25.2	13.4	
28.9	15.3					
6	30.0	10.1	59.8	13.1	119.0	
				17.0	64.4	
				20.0	41.1	
				24.9	26.3	
				29.9	22.5	
				39.8	21.4	
				8.8	150	c, bft
				9.5	159	
				10.2	151.4	
				11.0	138.3	
	12.7	111.1				
	14.0	93.1				
	15.1	78.0				
	16.0	68.2				
	16.7	61.3				
	18.0	50.0				
	20.4	36.6				
	21.0	34.2				
	24.2	26.5				
	24.8	25.7				
25.1	25.3					
28.9	21.5					
29.0	22.7					
37.1	21.3					
39.4	21.5					

TABLE 4.4 Cont'd.

				42.3	21.3	
				43.3	21.1	c
10	40.0	9.9	50.1	0.0	74.6	
				0.0	75.1	
				4.0	75.0	
				13.1	64.9	
				17.0	58.6	
				20.0	53.6	
				24.9	46.6	
				29.9	40.6	
				40.2	31.7	
				55.1	21.0	c
15	49.8	10.1	40.1	0.0	67.2	
				13.0	78.6	
				17.0	80.7	
				19.9	81.4	
				24.9	81.2	
				29.8	79.0	
				40.2	69.8	
				55.0	54.6	
21	59.6	10.4	30.0	0.0	75.9	
				4.0	87.5	
				13.0	107.9	
				17.0	117.4	
				20.1	124.2	
				24.9	133.4	
				29.9	140.0	
				40.2	146.4	
				55.1	138.3	
28	70.0	9.9	20.1	0.0	68.2	
				13.0	110.6	
				17.0	124.8	
				20.0	135.7	
				24.9	153.6	
				29.8	171.0	
				40.2	201.9	
				55.0	236.1	
36	79.3	10.5	10.2	4.2	94.3	
				13.1	141.5	
				16.9	163.4	
				20.0	181.7	
				24.9	212.5	
				29.8	244.0	
				40.0	307	
				55.0	396	

Cont'd..

TABLE 4.4 Cont'd.

11 (cont'd)				7.9-8.0	3.3-5.5mS	c, bft
				8.8	3.8 mS	c, bft
				9.5	3.2 mS	c, bft
				9.7-9.8	1.4-1.6mS	c, bft
				10.3	5.0 mS	c
				10.65	7.26mS	just c.
				10.8-10.9	5.2-5.5mS	
				11.1	4.24mS	
				11.35	2.31mS	
				11.75	246 $\mu$ S	
				12.3	582 nS	
				12.6	264 nS	just c
				13.1	287 nS	c
12	20.2	39.9	39.9	17.0	2.86 $\mu$ S	
				20.1	1.15 $\mu$ S	
13	30.1	29.9	40.1	20.0	398 $\mu$ S	
				24.9	9.87 $\mu$ S	
14	40.0	19.9	40.1	25.0	385 $\mu$ S	
				29.8	12.95 $\mu$ S	
				40.3	32 $\mu$ S	just c
16	10.0	59.9	30.1	4.0	27.7mS	
				12.1	3.7-3.9 $\mu$ S	
17	20.0	50.0	30.0	17.0	2.20-2.24 $\mu$ S	
18	29.8	40.1	30.1	20.0	792 $\mu$ S	
				24.8	8.01 $\mu$ S	
19	40.1	29.9	30.0	25.0	1.57mS	
				29.9	329 $\mu$ S	
20	50.1	19.8	30.1	25.0	1.102mS	
				29.9	859 $\mu$ S	
				40.2	399 $\mu$ S	
22	10.0	69.9	20.1	0.0	32-33 mS	just c
				4.0	35.4 mS	
26	50.1	29.8	20.1	40.0	2.41mS	
27	59.9	20.2	19.9	40.0	1.546mS	
				55.0	907 $\mu$ S	
34	59.9	30.2	10.0	55.0	6.04mS	
35	69.9	20.2	10.0	55.3	2.19mS	

Cont'd.

TABLE 4.4 Cont'd.

B Samples containing more than 10% NaCl solution

Sample number	Composition C <sub>12</sub> E <sub>4</sub> %(W/W)	NaCl Solution %(W/W)	heptane %(W/W)	Temp. /°C	K /m <sup>-1</sup>	
2	10.1	19.9	70.0	15.7	1.15 μS	
				15.8	1.16 μS	
4	10.0	30.0	60.0	13.1	16 μS	
5	19.8	20.2	60.1	17.0	201 μS	
				19.9	4.95 μS	
				24.8	7.12 μS	
7	9.9	40.2	49.8	5.8	15.7 mS	
				13.1	379 nS	
7	11.0	40.0	49.0	4.1	14.68 mS	
				5.1	14.07 mS	
				5.7	15.08 mS	
				6.0	14.49 mS	
				6.0	14.61 mS	
				6.1	13.82 mS	
				6.3	13.87 mS	
				6.4	13.35 mS	
				7.0	10.40 mS	just bft
				11.5	4.21 mS	
				11.7	3.88 mS	
				11.85	2.54 mS	
				11.9	2.92 mS	
				12.3	520 μS	
				12.65	11.4 μS	
13.0	1.2-1.5 μS					
13.6	359 nS					
14.0	771 nS					
14.1	361 nS	just c.				
8	19.8	30.4	49.9	17.0	8.32 μS	
				20.0	2.58 μS	minimum in K between 17.0 & 20.0°C
9	30.0	19.6	50.4	20.0	295 μS	
				24.8	22.7 μS	
				29.9	14.4 μS	
11	10.2	49.8	40.1	4.0	20.7 mS	
				12.1	41 μS	
				12.5	600-1000 nS	
	10.0	49.7	40.3	2.0	19.08 mS	c
				3.0	19.73 mS	c
				4.0	20.38 mS	c
				4.4	20.18 mS	c
				5.1	20.91 mS	
				6.0	20.92 mS	
				6.8	20.77 mS	
7.1	14.47 mS					
7.4	9.3 mS	c, bft				

TABLE 4.4 Cont'd.

C Conductivity in the  $\zeta$ -region

Initial composition $C_{12}E_4$ %(W/W)	Sample composition NaCl Solution %(W/W)	Heptane added	Temperature / $^{\circ}C$	$K$ / $mSm^{-1}$
50.1	49.9	-	71.2	33.1
		✓	54.7	23.2
40.2	59.8	-	69.4	54.3
		✓	39.9	32.0
		✓	30.0	17.13
30.1	69.9	-	66.2	70.0
		✓	55.0	59.6
		✓	40.0	45.7
		✓	30.0	35.9
		✓	25.0	25.6
20.0	80.0	-	62.5	88.5
		✓	55.0	79.6
		✓	40.0	61.6
		✓	30.0	50.7
		✓	25.0	44.2

TABLE 4.5

Conductivity in the  $C_{12}E_4-H_2O$ -decane system

Sample composition $C_{12}E_4$ %(W/W)	NaCl Solution %(W/W)	Decane %(W/W)	Temperature / $^{\circ}C$	$K$ / $m^{-1}$
8.9	54.8	36.2	7.5	25.9mS c
			8.6	26.7mS c
			9.2	27.55mS c
			9.6	27.48mS just c
			9.95	27.53mS
			10.0	27.53mS
			10.7	27.49mS
				27.72mS
			11.4	27.55mS
				27.61mS
			12.0	24.2mS c, bft
			12.7	12-15 mS c, bft
			13.25	7.60mS c, bft
			14.25	5.19mS c, bft
			14.95	10.06mS c, bft
			15.15	11.16mS c, bft
			15.45	13.08mS
15.75	10.72mS			
16.0	8.36mS			
16.4	5.03mS			
16.5	3.645mS			

			16.75	1.649mS	
			16.85	1.043mS	
			17.05	400 $\mu$ S	c
13.1	52.0	34.8	0.0	18.17mS	†
			2.45	19.56mS	†
			5.25	21.32mS	
			7.3	22.57mS	
			9.7	23.21mS	
			16.85	6.85mS	c, bft
			17.25	8.56mS	c, bft
			17.8	9.17mS	
			17.75	9.68mS	
			17.9	8.79mS	
			18.2	7.29mS	
			18.65	5.01mS	
			18.8	4.25mS	
			19.15	2.53mS	
			19.7	523 $\mu$ S	
			19.95	144.6 $\mu$ S	
			20.2	35.7 $\mu$ S	Just c
			20.85	5.08 $\mu$ S	c

† Sample clear during measurement but metastable

TABLE 4.6

Conductivity in the  $C_{12}E_4-H_2O$ -hexadecane system

Sample composition			Temperature /°C	k /mSm <sup>-1</sup>	
$C_{12}E_4$ %(W/W)	NaCl solution %(W/W)	Hexa- decane %(W/W)			
15.3	50.8	33.9	20.05	28.86	
			21.0	29.27	
			21.1	29.29	
			22.15	29.58	
			23.4	29.9	
			24.5	30.08	
			25.4	30.12	
			26.25	30.01	
			26.9	27.26	c, bft
			27.1	26.53	c, bft.
			27.6	23.22	c, bft
			27.7	23.81	c, bft
			28.65	20.43	c, bft
			29.5	18.98	c, bft
			30.55	18.6	bft
			31.1	21.89	just bft

Cont'd.

TABLE 4.6 Cont'd.

			31.7	20.9	
			32.1	19.68	
			32.5	18.53	
			33.05	16.61	
			33.55	14.65	c
17.4	49.5	33.1	16.05	24.41	†
			16.8	24.88	†
			18.4	25.64	
			14.45	26.02	
			20.65	26.38	
			21.5	26.63	
			22.5	26.91	
			23.5	27.17	
			24.55	27.41	
			25.6	24.73	just c
			30.4	4.48	c, bft
			30.9	5.58	bft
			31.35	8.27	bft
			31.8	16.03	bft
			32.25	18.72	just bft
			32.6	18.14	
			32.9	17.30	
			33.35	16.19	
			33.95	14.74	
			34.35	13.62	
			34.95	11.70	
			35.35	10.68	c
12.3	52.7	35.0	25.4	35.5	
			26.25	35.3	
			26.9	35.2	
			27.6	34.6	
			27.7	34.5	
			28.65	33.1	
			29.5	31.4	
			30.55	27.1	
			31.1	24.4	Just c

† Sample clear during measurement but metastable

TABLE 4.7

Conductivity in the Brij 30-H<sub>2</sub>O-hexane system

A Measurements made with the platinum cell with samples containing 10% water.

Sample number	Sample Brij 30 %(W/W)	Composition		Temperature		
		H <sub>2</sub> O %(W/W)	hexane %(W/W)	/°C	K /μSm <sup>-1</sup>	
1	10.0	10.3	79.7	33.2	0.7	slight haze
				34.1	0.8	slight haze
				34.4	0.8	slight haze
				34.4	0.5	slight haze
				35.8	0.7	slight haze
				37.2	0.7	slight haze
				39.0	-	c
6	30.1	10.1	59.8	0.0	5.90	
				7.7	9.72	
				18.2	16.5	
				25.2	20.6	
				32.7	24.3	
				40.7	26.9	
10	40.6	9.9	49.5	0.0	9.34	
				7.7	12.6	
				18.2	18.1	
				25.2	22.1	
				32.7	26.8	
				40.7	31.6	
15	50.2	10.2	39.6	0.0	9.45	
				7.7	13.4	
				18.0	20.6	
				25.2	26.8	
				32.8	33.9	
				40.7	41.9	
21	59.1	10.2	30.7	0.0	36.5	
				7.7	51.3	
				18.0	76.0	
				25.2	95.5	
				32.8	116.4	
				40.7	139.0	
28	69.9	9.9	20.2	0.0	134.1	
				7.7	190.6	
				16.1	258	
				25.2	344	
				32.8	418	
				40.7	497	

36	79.6	10.1	10.3	7.8	411
				17.5	615
				24.9	796
				33.2	1020
				41.4	1251

B Approximate results obtained with the copper cell with samples containing more than 10% water.

	Approximate composition			Temp. /°C	K /μSm <sup>-1</sup>
	Brij 30 %(W/W)	H <sub>2</sub> O %(W/W)	hexane %(W/W)		
2	10	20	70	33	2
				40	1.7
4	10	30	60	33	1.3
				27	6
5	20	20	60	33	5.2
				27	0.6
7	10	40	50	27	7
				27	5
8	20	30	50	22	7.5
				27	9.5
9	30	20	50	33	5
				18	1-2
12	20	40	40	20	2
				22	2
13	30	30	40	20	2
				22	2
14	40	20	40	27	3
				18	8
17	20	50	30	20	6
				22	~4
18	30	40	30	27	6
				33	7.6
19	40	30	30	40	10
				16	0.7
20	50	20	30	20	0.4
				22	0.4-0.8
25	40	40	20	27	2
				33	1.7
26	50	30	20	27	17
				33	21
27	60	20	20	33	5.4
				40	63
35	70	20	10	40	730
				33	4.4x10 <sup>3</sup>
				40	4.6x10 <sup>3</sup>

Cont'd.

TABLE 4.7 Cont'd.

C Approximate results obtained with the copper cell in the narrow salient ( $\xi$ -region)

Sample composition			Temperature	K
Brij 30	H <sub>2</sub> O	hexane	/°C	/mSm <sup>-1</sup>
%(W/W)	%(W/W)	%(W/W)		
20.0	76.0	4.0	32.9	19.6
22.0	73.5	4.5	31.5	19.8
27.0	66.9	6.1	33.0	17.1
20.1	77.4	2.5	38.7	22.0
29.2	65.3	5.5	37.0	24.1
40.1	50.3	9.6	38.7	7.98

TABLE 4.8

Conductivity in the E<sub>4</sub>-H<sub>2</sub>O system

E <sub>4</sub>	NaCl	Temperature	K
%(W/W)	Solution	/°C	/m <sup>-1</sup>
	%(W/W)		
9.9	90.1	25.0	85.9mS
19.9	80.1	25.0	60.3mS
30.0	70.0	25.0	40.1mS
40.0	60.0	25.0	24.8mS
50.0	50.0	24.9	13.83mS
60.4	39.6	24.9	6.85mS
70.3	29.7	24.9	3.14mS
80.4	19.6	24.9	1.24mS
89.9	10.1	24.9	404 μS
"	"	24.9	241 μS
10.4	89.6	0.0	43.3mS
		9.7	58.2mS
		20.4	76.4mS
		30.0	94.7mS
		39.5	113.3mS
		50.8	139.4mS
		59.9	159.1mS
25.0	75.0	0.0	23.3mS
		9.7	32.5mS
		20.4	44.7mS
		30.0	56.7mS
		39.4	69.7mS
		50.8	86.6mS
		59.9	101.7mS
40.2	59.8	0.0	9.92mS
		9.7	14.70mS
		20.1	21.12mS
		30.1	28.33mS
		39.4	36.2mS
		50.1	47.3mS
		59.9	56.2mS

TABLE 4.8 Cont'd.

55.0	45.0	0.0	3.46mS
		9.7	5.49mS
		20.1	8.44mS
		30.1	12.05mS
		39.3	16.14mS
		51.0 <sup>±0.3</sup>	21.97mS
		59.9	27.02mS
70.1	29.9	0.0	880 $\mu$ S
		9.7	1.54mS
		18.9	2.44mS
		29.8	3.94mS
		39.4	5.69mS
		50.7	8.01mS
		59.9	10.20mS
		69.7	12.94mS
		80.5	16.3mS
		88.1	18.9mS
84.8	15.2	0.0	182 $\mu$ S
		9.7	343 $\mu$ S
		18.9	578 $\mu$ S
		29.8	985 $\mu$ S
		39.4	1.45mS
		50.7 <sup>±0.1</sup>	2.18mS
		54.9	2.80mS
		69.7	3.70mS
		80.5	4.76mS
		88.1	5.60mS
100.0	-	0.0	5.69 $\mu$ S
		20.6	16.16 $\mu$ S
		39.4	30.8 $\mu$ S
		59.6	55.2 $\mu$ S

TABLE 4.9

Conductivity of the sodium chloride solution used

Temperature /°C	$k/\text{mSm}^{-1}$
0.0	63.9, 64.0
4.0	71.6
12.1	88.9
17.0	100.0
19.7	106.0
24.8	118.0
25.0	117.8, 117.8
29.7	131.8
29.8	132.0
29.9	130.2
40.3	156.7
54.5	194.5
60.5	208
64.4	217
69.2	238
72.7	238
76.0	244
81.9	260
82.9	264

$C_{12}E_{14}$ °C	6.8	18.0	21.6	30.0	38.3	50.1	60.3	71.7	79.6	89.6	100
2.5											
3			.033	.035	.041						
7.5		.070			.076						
8				.074							
13.5			.088	.089							
21.5										.190	
22											.283 .307 .322
40										.495	
41											.725
52	.534										
54									.569		
55		.833 .833									
56		.753									
56.5		.433	.809								
57.5			.627								
60				.828						1.27	1.29
61					.836						
62					.945						
62.5					.586						
64						.996					
64.5						.692	.696	.608			
79.5											2.32
80								1.28	1.74	2.28	
100										2.57	3.53

Table 4.11. Self-diffusion coefficients of  $^{12}\text{C}_2\text{H}_4$  in  $\text{H}_2\text{O}$  samples.  $710 \text{ m}^3$

Upper figure in square refers to surfactant diffusion,  
lower figure to water diffusion.

$\frac{C_2E_4}{\text{°C}}$	4.9	10.0	14.5	19.0	24.3	29.4	37.65	42.9	49.8	62.15	69.3	79.1
2	8.61	8.95	7.05	7.37		6.23		3.11				
2.5					4.65		.939 3.90					
7				1.12 9.36		6.58	3.40					
8				9.89								
10						7.76						
12						7.76						
52.5												.780 4.45
53		23.0										
53.5												.769 5.70
54.5			.937 18.9									
56				.799 20.7								
57.5					.793 17.1							
60						.910 21.4						
60.5												.924 5.38
62.5							.867 13.2					
63							1.04 19.9					
63.5							.861 13.8					
65										.693 .807 12.0 8.52		1.28 10.2
65.5										1.50 13.1		
66								.958 17.6				1.09 6.56
70.5												1.37 11.5
72												1.27 11.5
72.5												1.76 1.49 10.3
75.5												1.42 9.31
78.5												1.52 8.99

Table 4.12. Self-diffusion coefficients of  $C_{12}E_6-D_2O$  samples.  $/10^{-10}m^2s^{-1}$

$\begin{matrix} C_{12}E_6 \\ \text{\%} \\ \text{\textcircled{C}} \end{matrix}$	8.5	17.8	29.5	33.2	34.5	55.2	61.8	65.1	67.9	69.2
2.5	.165	.084	.013							
5.5									.035 <sup>V</sup>	
20								.080 <sup>V</sup>		
22	.059									
22.5		.029	.022				.099 <sup>V</sup>			
32		.044								
42			.153			.222				
42.5	.097	.118			.184					
60				.489						
75.5						.856				
76.5										1.02

'V' indicates results obtained for the viscous isotropic liquid crystal. (Also Table 4.13.)

Table 4.13. Self-diffusion coefficients of  $C_{12}E_6-H_2O$  samples.  $/10^{-10} m^2 s^{-1}$

Upper figure in square refers to surfactant diffusion,  
lower figure to water diffusion.

$C_{12}E_6$ % °C	18.1	29.9	38.2	55.8	61.8	68.5	69.8	76.5	81.8	100
2.5	8.51									
10						.035 2.22				
22		16.6								
22.5	.054 15.9									
23.5										.207
32.5					.203 7.53					
42	25.0	18.7	15.3	.220 10.4						
42.5	.154		.208	.243 11.5					.327	.469
55		22.2								
60				.843 18.2						
60.5										.851
62								.589 9.55		
70								.935 13.2		
76					.842 11.2			1.08 7.78		1.42
76.5				.798 17.1		.872 13.1			1.33	
85								1.21 15.9		2.08
95								1.72 18.3		

TABLE 4.14

NMR linewidths in the  $\alpha$ -region of the  $C_{12}E_4-H_2O$  system

Sample % $C_{12}E_4$ (W/W)	Temp- erature /°C	Linewidth at half height	
		oxyethylene chain /Hz	hydrocarbon chain /Hz
20	$1\frac{1}{2}$	6	broad
	$5\frac{1}{2}$	$5\frac{1}{2}$	broad
	$10\frac{1}{2}$	4	21
	$14\frac{1}{2}$	3	15
	$17\frac{1}{2}$	4	12
	25	very broad	very broad
30	$\frac{1}{2}$	6	broad
	4	$4\frac{1}{2}$	29 approx.
	$8\frac{1}{2}$	$4\frac{1}{2}$	27
	$12\frac{1}{2}$	3	$14\frac{1}{2}$
	$17\frac{1}{2}$	3	$10\frac{1}{2}$
	$21\frac{1}{2}$	very broad	very broad
40	$1\frac{1}{2}$	$5\frac{1}{2}$	broad
	$5\frac{1}{2}$	$4\frac{1}{2}$	30 approx.
	$10\frac{1}{2}$	4	21
	$15\frac{1}{2}$	4	$16\frac{1}{2}$
	$19\frac{1}{2}$	3	13
	25	very broad	very broad

TABLE 4.15

Comparison of the Brij 30- $H_2O$ -hexane and Brij 30- $H_2O$ -heptane systems

Sample number	<u>Temperature range of the isotropic liquid region</u>	
	Heptane °C	Hexane °C
12	19 - 28	18 - 27
13	20 - 36	20 - 34
14	$18\frac{1}{2}$ - 43	16 - 41
17	no clear region	17 - 22
18	$20\frac{1}{2}$ - 29	18 - 28
19	25 - 38	$22\frac{1}{2}$ - 34
20	19 - 47	19 - 47
25	33 - $34\frac{1}{2}$	31 - 34
26	$41\frac{1}{2}$ - $46\frac{1}{2}$	41 - 44
32	37 - 41	36 - 41
33	42 - 48	42 - 50
34	42 - $58\frac{1}{2}$	46 - above 55

TABLE 4.16      Tie Lines

Temperature /°C	Initial Composition		hexadecane %(W/W)	Final Composition				
	C <sub>12</sub> E <sub>4</sub> %(W/W)	H <sub>2</sub> O %(W/W)		Upper Layer C <sub>12</sub> E <sub>4</sub> %(W/W)	Lower layer H <sub>2</sub> O %(W/W)			
28°	10.2	29.7	60.1	-	100	14	43	43
4	6.3	20.2	heptane	C <sub>12</sub> E <sub>4</sub>	heptane	C <sub>12</sub> E <sub>4</sub>	H <sub>2</sub> O	heptane
12	3.7	12.4	84.0	trace	100	8	35	56
				3	97	5	28	67

5.1 SURFACTANT-WATER SYSTEMS5.1.1 C<sub>12</sub>E<sub>6</sub> - WATER5.1.1.1 THE PHASE DIAGRAM

Fig. 4.2 shows the phase diagram of C<sub>12</sub>E<sub>6</sub> and water. A continuous isotropic liquid region extends from 0% to 100% C<sub>12</sub>E<sub>6</sub>, though its temperature of occurrence varies and its range of stability with temperature (0-60°C at 2% by weight; 70-above 95°C at 65%). Hexagonal and lamellar liquid crystalline phases occur, separated by a cubic liquid crystalline phase, the hexagonal appearing first at lowest surfactant concentrations. At concentrations below that at which the hexagonal phase occurs an isotropic liquid region exists which shows streaming birefringence, evidence of anisotropic aggregates; this occurs between about 31% and 37% surfactant and about 5 and 35°C. The viscosity in this region is slightly greater than in the regions not exhibiting streaming birefringence.

The phase diagram is essentially the same as that of Clunie, Goodman and Symons (77), except for the cubic phase which these authors describe as a fluid isotropic phase continuous with the large isotropic liquid region. The cloud point is about 5°C higher in the present work; this is most probably due to differences in the small amounts of impurities present. The narrow two-phase regions bordering the liquid crystalline phases are not shown in the present work, nor are the solid hydrates which are not of interest here.

### 5.1.1.2 CONDUCTIVITY

The solutions used for conductivity measurements were made up from  $C_{12}E_6$  and 0.01M sodium chloride solution. The presence of this concentration of sodium chloride had no significant effect on the  $C_{12}E_6-H_2O$  phase diagram, or on any of the phase diagrams of the  $C_{12}E_4$  systems studied.

Figs. 4.31 and 4.32 shows the conductivity of different compositions in the  $C_{12}E_6-H_2O$  system as a function of temperature. The curves are of a similar form up to and including 35.0%  $C_{12}E_6$ . In this sample conductivity measurements were carried out in the region exhibiting streaming birefringence but there is no evidence of any discrepancy in the conductivity of this region.

Above 44.9%  $C_{12}E_6$  the shape of the curve changes; below 44.9%  $d^2K/dT^2$  is just positive- $K$  is almost linear with  $T$ ; at 55.1%  $d^2K/dT^2$  is negative. Fig. 4.32 shows the conductivity of samples containing 67.9%, 79.9% and 89.5%  $C_{12}E_6$  in greater detail than can be shown on the scale of Fig. 4.31. At 67.9% there is a maximum in  $K$ : above  $87^\circ C$   $K$  decreases. Further discussion of behaviour of this type is given in section 5.1.2.2. At 79.9%  $d^2K/dT^2$  is probably just negative whilst at 89.5% it is probably just positive.

The alternative to the above treatment is to consider the conductivity as a function of composition at a given

### 5.1.1.2 Cont'd.

temperature. It is not possible to take a line across the phase diagram such that an isotropic liquid phase exists from 0% to 100%  $C_{12}E_6$  at a given temperature. At  $52\frac{1}{2}^{\circ}C$  of the compositions used only 67.9%  $C_{12}E_6$  is not liquid. Fig. 4.34 shows that  $K$  at  $53^{\circ}C$  plotted as a function of composition gives a smooth curve indicating that any major structural change, such as phase inversion, takes place gradually. It is possible to plot  $K$  at  $76^{\circ}C$  from 44.9% to 100%  $C_{12}E_6$ ; again no discontinuity is observed.

Figs. 4.34 and 4.28 show  $K$  at  $53^{\circ}C$  and  $0^{\circ}C$  as a function of composition for both  $C_{12}E_6-H_2O$  and tetraethylene glycol ( $E_4$ ) -  $H_2O$ .  $E_4$  was used for comparison; it is soluble in water from 0% to 100% and does not form micelles or liquid crystals; ether oxygens will be hydrogen bonded in the water as are those of the ethylene oxide chain of  $C_{12}E_6$ . The curve for  $C_{12}E_6$  falls above that for  $E_4$  at both temperatures and also at  $32^{\circ}$  (Fig. 4.33). At  $53^{\circ}$  the curves are indistinguishable on the scale shown beyond 80%. At 85% at this temperature  $K$  is virtually the same for  $C_{12}E_6$  and  $E_4$ . Pure  $C_{12}E_6$  has a conductivity lower than that of  $E_4$  ( $K$  of  $C_{12}E_6 = 7.7 \mu Sm^{-1}$ ,  $K$  of  $E_4 = 47 \mu Sm^{-1}$  at  $53^{\circ}$ ). At the lower concentrations the magnitude of  $K$  for both solutions is typical of water continuous solutions. In the case of  $E_4$  the complete miscibility with water and absence of any tendency to form micelles indicates that the low concentration water continuous solution changes continuously to an  $E_4$  continuous solution. The

5.1.1.2 Cont'd.

$C_{12}E_6$  appears to behave similarly though micelles are known to be present at the lower concentrations in the water continuous medium. The presence of the hydrocarbon chains in the pure  $C_{12}E_6$  can explain at least qualitatively, the lower conductivity than that of  $E_4$  (88). If the hydrocarbon micelle cores are considered as an excluded volume and the oxyethylene chains are dissolved in the water, the concentration of oxyethylene chains in the water is equivalent to a lower concentration of  $E_4$ . Thus the conductivity of 25% (W/W)  $C_{12}E_6$  might be compared with the conductivity of 20% (W/W)  $E_4$ , or the conductivity of 25% (W/W)  $C_{12}E_4$  might be compared with that of 15% (W/W)  $E_4$ :

	$K$ at $0^\circ C$		$K$ at $0^\circ C$
25% $C_{12}E_6$	$30mSm^{-1}$	20% $E_4$	$29mSm^{-1}$
25% $C_{12}E_4$	$32mSm^{-1}$	15% $E_4$	$36mSm^{-1}$

The excluded volume has been based on the hydrocarbon chain length but the inner part of the oxyethylene micellar mantle may also be regarded as part of the excluded volume since there can be little movement of ions in this region; thus the  $E_4$  concentrations used for comparison are only approximate.

Fig. 4.28 shows plots of the Bruggeman and Maxwell equations compared with the results for  $C_{12}E_6$ ,  $C_{12}E_4$  and

### 5.1.1.2 Cont'd.

$E_4$  at  $0^\circ\text{C}$ . These equations are applicable to macro-emulsions with spherical droplets, (Section 2.1.1). The solid line represents the semi-empirical equation of Mackay and Agarwal (71) (Sections 1.5.6 and 2.11):

$$\frac{k}{k_0} = (1 - \phi)^{2.5} \quad 5.1$$

where  $k$  is the measured conductivity,  $k_0$  the conductivity of the continuous phase and  $\phi$  the disperse phase volume. The weight fraction of  $C_{12}E_6$  has been used for  $\phi$  here; the density of  $C_{12}E_6$  ( $0.97\text{gcm}^{-3}$  at  $29^\circ\text{C}$  (96)) is such that this is close to the volume fraction. This is not necessarily the same as the effective volume fraction since water is hydrogen bonded to the oxyethylene chains of the micellar mantle and trapped between them. Movement of ions is likely to occur to some extent in the outer part only of this mantle. The effective volume fraction may also change slightly with temperature. However, this appears to be a good approximation to the effective value of  $\phi$ , since there is good agreement between this equation and the experimental results. This good agreement with equation 5.1 extends to the conductivity results for almost the whole of the isotropic region of the  $C_{12}E_6$ - $H_2O$  phase diagram Table 4.2. The discrepancies occur at 90%  $C_{12}E_6$  which has measured values of  $k$  considerably lower than those predicted by the equation at the lower temperatures of its existence ( $k/k_0 = 0.0021$  compared to the theoretical value of  $0.0032$  at  $22^\circ\text{C}$ ) and too high at the higher temperatures

studied ( $k/k_o = 0.0047$  at  $76^\circ$ ) so that there is only agreement in the middle of its temperature range at about  $50^\circ\text{C}$ .

The other sample showing some discrepancy is 68%  $\text{C}_{12}\text{E}_6$  which has the anomolous conductivity versus temperature curve. Even here the discrepancy is not great;  $k/k_o$  is 0.064 at  $76^\circ\text{C}$  and 0.061 at  $85.5^\circ\text{C}$  whereas the theoretical value is 0.058.

It is remarkable that the equation developed by Mackay and Agarwal for their four component micro-emulsion system should fit the two component surfactant-water system so well. The fact that it fits over so much of the phase diagram suggests that no major structural changes occur over most of the isotropic liquid region. Mackay and Agarwal suggest that the principal factor responsible for lower values of the exponent ( $n$ ) at higher oil content in their O/W system (section 1.5.6) is an increase in mean droplet size leading to polydispersity. As  $n$  decreases in their system it tends to the value in the Bruggeman equation. Thus the constancy of  $n$  may suggest that the system is monodisperse and/or of small droplet size.

Self-diffusion measurements have been made for both the water and the surfactant in this system.

At high water content the diffusion coefficient of the water is slightly less than that of pure water whilst the diffusion coefficient of the surfactant is a factor of 100 smaller. This agrees with the existence of  $C_{12}E_6$  as micelles in a water continuous medium with very little monomeric  $C_{12}E_6$  (monomers would tend to increase the diffusion coefficient); the surfactant monomer concentration in this region is approximately the same as the cmc ( $\sim 4 \times 10^{-2} \text{ gdm}^{-3}$  (89)). As the concentration of  $C_{12}E_6$  is increased, at constant temperature, the diffusion coefficient of the water decreases gradually and continuously. It was not possible to measure it beyond 80%  $C_{12}E_6$  because the signal due to the surfactant protons swamped that due to the water protons. We have analysed the self-diffusion coefficients of water at  $42^\circ\text{C}$  as a function of  $C_{12}E_6$  concentration as follows (90):

The self-diffusion of molecules in an isotropic liquid which contains a number of different sites,  $i$ , is given by:

$$D = \sum_i p_i D_i \quad 5.2$$

where  $p_i$  is the fraction of molecules in site  $i$ . In the present system we have two sites for water (free

### 5.1.1.3. Cont'd.

or associated with surfactant), and two sites for surfactant (monomer or micelle). We anticipate that water diffusion will be much faster than micelle diffusion. For water molecules, the volume occupied by the hydrophobic part of the micelle, the hydrocarbon core, will represent a barrier to diffusion. In this case water diffusion is given by:

$$D = (1-V_m)(p_f D_f + p_s D_s) \quad 5.3$$

where  $V_m$  is the volume fraction occupied by the micelle core and subscripts f and s refer to free and surfactant (micellar) associated water. A third term, involving surfactant monomers is neglected because it is small. The surfactant bound water fraction is given by  $p_s = Kc_s$  where  $c_s$  is the weight fraction of surfactant, and K is the weight of water bound per unit weight of surfactant. Equation (5.3) can be arranged:

$$\frac{D}{D_f} = (1-hc_s)(1-Kc_s(1-\frac{D_s}{D_f})) \quad 5.4$$

$V_m$  has been replaced by  $hc_s$  with h representing the fraction of nonionic surfactants volume occupied by the hydrocarbon core. This can be determined from known densities. Values of water diffusion were measured at 42°C, where from the phase diagram (Fig. 4.2) a large range of compositions form isotropic solutions. The

### 5.1.1.3 Cont'd.

self-diffusion coefficients are given in Fig. 4.55 (points) together with a curve calculated from equation 5.4. A good agreement between the calculated line and experimental points is obtained with  $h=0.43$  and  $K(1-D_s/D_f) = 1.1$ . The value of  $h$  was estimated assuming equal densities for ethylene oxide groups and water and a density of 0.9 for the alkyl groups. A change in this value by  $\pm 10\%$  has only slight effect on the calculated values. The value of  $D_s$ , for the local diffusion of surfactant <sup>associated water</sup> within the micelle is likely to be of the order of  $5 \times 10^{-10} \text{ m}^2 \text{ s}^{-1}$  or lower, so  $(1-D_s/D_f) \sim 0.9-1$ . This implies that the fraction of water associated with the micelle is approximately equal to the weight of surfactant. The amount of water involved is far higher than that required to hydrogen-bond to ether oxygen atoms, and suggests that a proportion of the water is 'trapped' within the polyethylene oxide network.

Insufficient results were obtained at other temperatures for a similar analysis to be carried out.

Fig. 4.53 shows surfactant diffusion at 42 and 76°C. At high water content the monomer concentration is approximately the same as the cmc ( $\sim 4 \times 10^{-2} \text{ gdm}^{-3}$ ); assuming a monomer diffusion coefficient of  $10^{-9} \text{ m}^2 \text{ s}^{-1}$ , the contribution of monomer to the observed diffusion coefficients is less than  $4 \times 10^{-13} \text{ m}^2 \text{ s}^{-1}$ . Since this is

### 5.1.1.3 cont'd.

far smaller than the measured values it can be neglected (90). Thus at high water content the measured diffusion coefficient is that of the micellar surfactant.

At high surfactant concentrations interactions between micelles are expected to lead to a reduction in the surfactant self-diffusion coefficient. However,  $D$  increases with surfactant concentration. Thus either the monomer contribution to the self-diffusion increases or the micellar size decreases. The latter appears more likely; the pure surfactant is thought to consist of small aggregates, the aggregation number being between about 2 and 20 (91). For pure surfactant the plot of  $\ln D$  versus  $T^{-1}$  (where  $T$  is the temperature in degrees Kelvin) from which the activation energy  $(30 \pm 1 \text{ kJ K}^{-1} \text{ mol}^{-1})$  may be determined, is a good straight line, indicating no change in aggregate state with increasing temperature.

At high surfactant concentrations the  $D$  values of water (Table 4.13) are at least an order of magnitude higher than those of the surfactant indicating that the water is located in the continuous phase, presumably consisting of water plus oxyethylene chains. The highest concentration at which the water self-diffusion was measured was 76.5%. At this concentration therefore the surfactant would be expected to exist as normal micelles with water plus oxyethylene chains forming the continuous

### 5.1.1.3 Cont'd.

phase. The ratio of the surfactant hydrocarbon and oxyethylene chains would tend to favour this: the hydrocarbon chain length: oxyethylene chain length ratio is very approximately 12:19 (by counting the number of atoms in the chains).

The surfactant self-diffusion increases continuously beyond 76.5%. There is no sudden change which might occur if inversion occurred, other than by some very gradual process. The results are consistent with the conductivity measurements which did not indicate inversion to a hydrocarbon continuous system.

Fig. 4.54 shows surfactant diffusion for samples containing less than 30%  $C_{12}E_6$ . The hexagonal phase does not occur at these compositions and the clear region extends to lower temperature. At 2.5°C the surfactant self diffusion coefficient decreases markedly with increasing surfactant concentration, by more than a factor of 10 between 8.5% and 29.5%  $C_{12}E_6$ . At 22°C the rate of decrease is much less (less than a factor of 3 between 8.5% and 29.5%  $C_{12}E_6$ ), and the diffusion coefficient is lower than at 2.5°C at both 8.5% and 17.8%  $C_{12}E_6$ ; at 29.5% it is slightly higher. By 42°C the surfactant again diffuses faster than at 22°C though at 8.5%  $C_{12}E_6$  the diffusion is still slower at 42°C than it is at 2.5°C. Further results are required to confirm those already obtained in this region and to fill in the gaps, so that

### 5.1.1.3 Cont'd.

only tentative suggestions can be made concerning the behaviour of the surfactant in this region.

Most of the work on  $C_{12}E_6$  micelles in aqueous solution concerns dilute solutions. Balmbra et al (92) found, from light scattering measurements that the micellar molecular weight of  $C_{12}E_6$  in water at concentrations below 2% (W/W) increased exponentially from 15 to 45°C (they found the cloud point to be 48°C). They deduced that micelles of the size to be found above 25°C could not be spherical and suggested a rod shape. From more recent work (8) it appears that their experimental results are due to micellar aggregation. Ottewill et al (93), working with  $D_2O$  solutions at concentrations of 1% or less, found from sedimentation velocity and intrinsic viscosity, that at 5°C the micellar molecular weight was not concentration dependent. Their results corresponded to heavily hydrated spherical micelles with a radius of  $26\text{\AA}$ . In the temperature range 15-35°C the micellar molecular weight increased considerably. The results suggested that the spherical micelles were aggregating to form larger units and that the aggregation processes were both temperature and concentration dependent. Corkill and Walker (94) also found a transition temperature of 15°C, which coincided with a change from the formation of a single micelle to the formation of a distribution of micelle sizes - later work suggests micellar

### 5.1.1.3 Cont'd.

aggregation rather than a size distribution. At 5°C they found considerable evidence for monodisperse micelles. Tanford et al (4) made sedimentation and gel chromatography measurements at 25°C. They found small micelles only at the very lowest concentration employed, larger micelles occurring at higher concentrations (still below about 3%). The equilibration between the initially formed small micelles and the larger micelles was a relatively slow process suggesting that the larger micelles were formed by a mechanism differing from that of the formation of the initial small micelles; this would agree with a process of micellar aggregation. At 5°C where no secondary aggregation occurs Tanford (95) concluded that they are of a disc-like shape.

Thus at 8.5%  $C_{12}E_6$  at 2.5°C the system may consist of monodisperse micelles which are not aggregated and hence the surfactant self-diffusion coefficient is relatively high ( $0.165 \times 10^{-10} \text{ m}^2 \text{ s}^{-1}$ ). At 17.8% and 2.5°C  $D$  is less than at 8.5% and at 29.5% it is reduced still further; if aggregation does not occur at this temperature and at these concentrations this decrease in  $D$  is likely to be due to some combination of increasing micellar size and increasing micellar concentration (leading to more interaction between micelles) as the surfactant concentration is increased. At 35%  $C_{12}E_6$  streaming birefringence is not observed at 2.5°C, whereas it is observed at higher temperatures, suggesting that the aggregates are not

### 5.1.1.3 Cont'd.

markedly anisotropic at this temperature.

At 8.5%  $C_{12}E_6$  at  $22^\circ C$  the surfactant self-diffusion coefficient is less than half its value at  $2.5^\circ C$ .  $22^\circ C$  is above the threshold temperature for micellar aggregation ( $15^\circ C$ ) in more dilute solutions, so that this decrease in  $D$  is likely to be due to micellar aggregation. The same is true at 17.8%  $C_{12}E_6$ . At 29.5%  $C_{12}E_6$  although  $D$  at  $22^\circ C$  is less than that of 17.8% at the same temperature, it has increased from its value at  $2.5^\circ C$ . 29.5% at  $22^\circ C$  is on the verge of the region exhibiting streaming birefringence. Anisotropic aggregates would be expected to start developing at a concentration below that at which the streaming birefringence is first observed by the method used here. Since the region exhibiting streaming birefringence is adjacent to the hexagonal liquid crystal phase the anisotropic aggregates are likely to be cylindrical..

By  $42^\circ C$  the rate of surfactant diffusion has increased. At 8.5%  $C_{12}E_6$   $D$  at  $42^\circ C$  is still below that at  $2.5^\circ C$ , presumably because of the considerable effect of secondary aggregation and possibly a larger micelle size.

A few measurements have been made in the viscous isotropic phase which occurs between the lamellar and hexagonal phases. Only two values for water diffusion have been obtained in this region at 68.5%  $C_{12}E_6$  and  $10^\circ C$ , where  $D_{\text{water}}$  ( $2.2 \times 10^{-10} \text{ m}^2 \text{ s}^{-1}$ ) is one tenth of the value for pure

### 5.1.1.3 Cont'd.

water at room temperature, and at 61.8% and 32.5°C where  $D_{\text{water}}$  ( $7.5 \times 10^{-10} \text{ m}^2 \text{ s}^{-1}$ ) is rather higher, the increase being mainly due to the increase in temperature. The water diffusion is of the same order of magnitude as that in the water oxyethylene chain continuous structure at high surfactant content and higher temperature. The surfactant self-diffusion coefficients in this region range from 0.03 to  $0.09 \times 10^{-10} \text{ m}^2 \text{ s}^{-1}$  (Tables 4.10 and 4.11) which are of the same order of magnitude as those of the surfactant in the water-continuous micellar system below 35%  $\text{C}_{12}\text{E}_6$ . These results suggest that this phase consists of surfactant micelles in a water-oxyethylene chain continuum, or a bicontinuous structure (section 1.4.7).

## 5.1.2 C<sub>12</sub>E<sub>4</sub> - WATER

### 5.1.2.1 THE PHASE DIAGRAM

The C<sub>12</sub>E<sub>4</sub>-water phase diagram (Fig. 4.1) shows three separate isotropic liquid regions, labelled for convenience  $\alpha$ ,  $\beta$  and  $\zeta$ . The  $\alpha$ -region shows streaming birefringence, evidence of anisotropic aggregates, at concentrations of surfactant above about 10% by weight and at temperatures below 9°C. The  $\beta$  and  $\zeta$  regions approach each other but are not connected, there being a gap between about 54% and 62% C<sub>12</sub>E<sub>4</sub>. The lower phase boundary of the  $\beta$  region above 90% surfactant is not shown in detail; the occurrence of crystal hydrates might be expected here as in the C<sub>12</sub>E<sub>6</sub> - H<sub>2</sub>O system (section 5.1.1). The  $\zeta$ -region has a very narrow temperature range of between 1°C and 2°C over most of its compositions. Below about 16% surfactant it appears blue translucent becoming increasingly so with decreasing surfactant concentration. This is an indication of the presence of particles or aggregates large enough to scatter light (~100nm) in the visible range.

Only a lamellar liquid crystal occurs in this system above 0°C; the smaller oxyethylene group is less favourable for the formation of cylindrical aggregates. A hexagonal liquid crystal phase has been found below 0°C (91). The phase diagram shown in ref.88 is essentially the same as that shown in Fig. 4.1, though its temperature

#### 5.1.2.1 Cont'd.

of occurrence is about  $5^{\circ}\text{C}$  lower. The melting point of the surfactant itself is about  $4^{\circ}\text{C}$  lower. The gap between the  $\zeta$  and  $\beta$  regions ~~is about 6%~~ is about 6% compared to 10% in the present work (Fig. 4.1). These differences are likely to be due to impurities in the surfactant which differ between batches.

#### 5.1.2.2. CONDUCTIVITY IN THE $\text{C}_{12}\text{E}_4\text{-H}_2\text{O}$ SYSTEM

Fig. 4.27 shows the conductivity of compositions in the low temperature clear region,  $\alpha$ . The curves are indistinguishable from linear. At 40%  $\text{C}_{12}\text{E}_4$  there appears to be an inflexion but further results would be required to show whether this is merely due to experimental error. The presence or absence of streaming birefringence does not appear to be related to any change in the conductivity.

Fig. 4.28 shows the variation of conductivity with composition at  $0^{\circ}\text{C}$ . At  $4^{\circ}\text{C}$  the behaviour is similar. The curve at  $0^{\circ}\text{C}$  is very close to that for the  $\text{C}_{12}\text{E}_6\text{-H}_2\text{O}$  system at the same temperature; the conductivity is greater than that of  $\text{E}_4\text{-H}_2\text{O}$  samples of the same percentage (by weight) composition. The same considerations (in particular the excluded volume effect of the hydrocarbon) apply as were discussed in section 5.1.1.2. There is a marked increase in the viscosity of the samples with increasing  $\text{C}_{12}\text{E}_4$  content, as observed on stirring in the tube with the thermometer. However, the conductivity

#### 5.1.2.2 Cont'd.

does not appear to reflect this.  $E_4-H_2O$  samples do not show the same increase in viscosity; the  $C_{12}E_4-H_2O$  curve remains above that of  $E_4-H_2O$  by an amount which changes only slightly from 10% to 50%.

Fig. 4.30 shows conductivity in the  $\beta$ -region. At 67.9%  $C_{12}E_4$  it was possible to make two measurements at 71.6 and 72.7°C; the decrease in  $K$  with increasing temperature, from  $9.01\text{mSm}^{-1}$  to  $8.88\text{mSm}^{-1}$ , was greater than the experimental error. At 75.2%  $C_{12}E_4$ ,  $K$  again decreases with increasing temperature; at 80.3% there is a maximum at 75°C; at 89.9%  $K$  increases with temperature and  $d^2K/dT^2$  is positive; at 100%  $C_{12}E_4$  (not shown)  $K$  increases with temperature. In the pure  $C_{12}E_4$  the rapid absorption of water by the sample tended to increase the conductivity further.

The decrease in conductivity with increasing temperature occurs only over a very limited part of the phase diagram, in the  $\beta$ -region, at high temperature and close to the phase boundary between  $\beta$  and  $\beta$ +water, and in the narrow salient below 70%  $C_{12}E_4$ . At 89.9%  $C_{12}E_4$  the conductivity measurements were not made at a sufficiently high temperature (because of practical considerations above 80°C) to show whether a decrease in conductivity or a change in  $d^2K/dT^2$  to negative from positive occurs at above 82°C, though the increasing

#### 5.1.2.2. Cont'd.

gradient of the graph suggests that  $K$  is not about to decrease at a temperature just a few degrees higher. The decrease in  $K$  with temperature is presumably due to some structural change in the system. This may be related to the inability of the system to retain the quantity of water present and hence the separation of water at a temperature several degrees higher. Localisation of some of the water as very small droplets (still within the one-phase system) would reduce the conductivity. At these compositions  $K$  is very sensitive to the percentage of water present; from a graph of  $K$  versus composition at  $72^{\circ}\text{C}$  it is possible to estimate that at 30%  $\text{C}_{12}\text{E}_4$  a reduction in the quantity of water present from 20.0 to 19.5% produces a reduction of  $0.2\text{mS}\text{m}^{-1}$  in  $K$ . At 75.2%  $\text{C}_{12}\text{E}_4$  an effective reduction by a maximum of about 2.5% (i.e. from 24.8 to 22.3%) in the water in the continuous phase is required to account for the decrease in conductivity over the complete temperature range ( $64.2\text{-}79.9^{\circ}\text{C}$ ). The systems contain sodium chloride so that if there is a tendency for the ions to be preferentially located in the isolated water "droplets" the above effect will be accentuated. Thus isolation of small amounts of water several degrees below the temperature of phase separation may account partially if not completely for this anomolous behaviour of the conductivity.

### 5.1.2.2 Cont'd.

Since the  $\xi$  region is so narrow, series of measurements at varying temperature and fixed composition could not be made. Also the temperature of the individual measurements across the region is not the same, because the temperature of occurrence of the region changes. The values for the  $E_4$  system plotted for comparison are at the same temperatures as the  $C_{12}E_4$  system so that the  $E_4$  line can be compared directly without regard to the varying temperature. The  $C_{12}E_4-H_2O$  line is lower than that of  $E_4-H_2O$ . Below 40%  $C_{12}E_4$  the discrepancy is large and increases with increasing dilution to over  $60\text{mSm}^{-1}$  at 3%  $C_{12}E_4$ . Above 40%  $C_{12}E_4$  the discrepancy is less - about  $10\text{mSm}^{-1}$ . The  $C_{12}E_4$  curve continues to fall below that of  $E_4$ , in the  $\beta$  region.

Regardless of the behaviour of  $E_4$  and the problems of comparison outlined previously (section 5.1.2) the conductivity of the  $\xi$  region is exceptionally low. Extrapolating the curve back to the axis at 0%  $C_{12}E_4$  would give a value for  $k$  nearly  $80\text{mSm}^{-1}$  below that of sodium chloride solution at a similar temperature. One reason for this behaviour could be large micelles of some shape such that they tend to obstruct the flow of charge, or aggregates of smaller micelles. Both of these possibilities could account for the blue translucence of the system below about 16%  $C_{12}E_4$  which is evidence of light scattering by bodies in the solution.

Tanford et al (4) investigated micelle shape in the  $C_{12}E_X$  series and concluded that disc-like micelles occurred in such systems except for very high values of  $x$  (at least 32) where spherical micelles occurred. However, these disc-like micelles were only proposed for systems where  $x \gg 8$ .

The systems were also considerably more dilute than those at present under discussion ( $\leq 1\%$ ) and the temperatures were  $35^\circ\text{C}$  or below.

Boyle (96,97) has used dielectric measurements to study the present system. The  $\alpha$ - and  $\beta$ -regions agree well with a theoretical equation for an oil phase dispersed, as spherical droplets, in a continuous aqueous phase. The equation converted for conductivity instead of dielectric results is:

$$\frac{K}{K_0} = (1 - \phi) \frac{1}{1-A} \quad 5.5$$

where  $\phi$  is the disperse phase volume and 'A' is  $\frac{1}{3}$  for spherical droplets so that the equation reduces to the Bruggeman equation for spherical droplets. 'A' is the depolarising factor which can be calculated for prolate or oblate ellipsoids for different axial ratios. Boyle found that the results for the  $\zeta$  region could be fitted if oblate ellipsoidal micelles (i.e. disc-like micelles) were present the axial ratio increasing with increasing dilution.

#### 5.1.2.2. Cont'd.

In the regions ( $\alpha$  and  $\beta$ ) where Boyle suggested spherical micelles the Bruggeman equation does not fit the present conductivity results. Equation 5.1 fits well in the  $\alpha$ -region but not in the  $\beta$ -region where the results are rather lower than this equation would suggest (Table 4.1).  $\phi$  in equation 5.1 was calculated using a value of  $0.94\text{gcm}^{-3}$  for the density of  $\text{C}_{12}\text{E}_4$  (the density at  $23^\circ\text{C}$  (96)).

In the  $\zeta$ -region the results are considerably lower especially at lower concentrations. It is possible that axial ratios for ellipsoidal micelles could be calculated using equation 5.1 and a factor similar to the 'A' in equation 5.2. Equation 5.2 does not fit the conductivity results when the values of 'A' derived from Boyle's dielectric results are used: e.g. at 10%  $\text{C}_{12}\text{E}_4$  the axial ratio was found to be 3.6 for oblate spheroids, with an 'A' value of 0.68; the calculated conductivity at  $58.5^\circ\text{C}$  is  $145\text{mSm}^{-1}$  whereas the measured conductivity was  $105\text{mSm}^{-1}$ .

The alternative to ellipsoidal micelles in  $\zeta$  is aggregates of micelles, possibly spherical micelles. Tanford et al (4) suggested that micelles formed by n-alkyl polyoxyethylene surfactants might aggregate where the polyoxyethylene chain length falls below a critical level. They confirmed the phenomenon of concentration - dependent growth of particle size for  $\text{C}_{12}\text{E}_6$ . They suggested that the large particles might be formed from

#### 5.1.2.2. Cont'd.

small micelles by association between polyoxyethylene groups. Staples and Tiddy (8) have shown by nmr that for  $C_{12}E_6$ , small micelles aggregate to form larger units as the cloud point is approached. They propose a looser association than Tanford et al based on the balance between the Van der Waal's attraction force and a hydration-repulsion force arising from the attraction between surfactant head groups and water which gives a repulsive force between micelles. This force decreases with increasing temperature as the hydration decreases with increasing temperature. However in samples in the  $C_{12}E_6-H_2O$  system where secondary aggregation is known to occur, no evidence of a reduction in conductivity, which could be ascribed to this, was found. The maximum in conductivity with increasing temperature at 67.9%  $C_{12}E_6$  is more likely to be due to isolation of small amounts of water prior to phase separation. The type of secondary aggregation proposed by Staples and Tiddy for the  $C_{12}E_6-H_2O$  system is a loose association which would tend to present little barrier to the movement of charge. Thus secondary aggregation of this type does not seem a likely explanation of the low conductivities recorded in the  $\zeta$ -region of the  $C_{12}E_4-H_2O$  system.

### 5.1.2.3. SELF-DIFFUSION IN THE $C_{12}E_4-H_2O$ SYSTEM

The self-diffusion coefficient of water in  $C_{12}E_4-H_2O$  mixtures is shown as a function of composition for the  $\zeta$ -region and  $\beta$ -region in Fig. 4.49. It decreases steadily with increasing surfactant concentration from values approximately half that of pure water at 10.0%  $C_{12}E_4$  to something less than a quarter of that value at 79.1%  $C_{12}E_4$ . These values tend to confirm the conductivity measurements and indicate that the water (water plus oxyethylene chain at high  $C_{12}E_4$  concentration) is the continuous phase and that its self-diffusion is hindered by the surfactant micelles. At low  $C_{12}E_4$  concentration extrapolation of the curve back to the axis at 0%  $C_{12}E_4$  would give a value close to half of that for pure water; this is similar to the behaviour of the conductivity at these concentrations (Fig. 4.29); the reduction in the conductivity and the self-diffusion of the water at the low-surfactant end of the  $\zeta$ -region is larger than would be expected on the simple excluded volume basis and hence the proposal of some sort of secondary aggregates of ellipsoidal or lamellar micelles. That very large ellipsoidal or lamellar micelles are not present is indicated by the fact that self-diffusion measurements were possible by the technique used. If the nmr line were very broad, as in the case of large ( $\sim 100$ nm) micelles, (8) this technique could not be used. The light scattering (causing the blue translucence in the

### 5.1.2.3. Cont'd.

$\zeta$ -region at lower concentrations) must be due to aggregates of micelles rather than the micelles themselves. The behaviour of the water diffusion coefficient in the  $\zeta$ -region of the  $C_{12}E_4-H_2O$  system is different to that in the isotropic liquid region of the  $C_{12}E_6-H_2O$  system where the water diffusion coefficient decreases smoothly and continuously from the value for pure water (section 5.1.1.3).

The water diffusion coefficient continues to decrease in the  $\beta$ -region of the  $C_{12}E_4-H_2O$  system. No discontinuity (beyond the limits of experimental error) is observed at the gap between the  $\zeta$ - and  $\beta$ -regions. The system is still water - oxyethylene chain continuous.

Measurements of the water diffusion coefficient have been made in the  $\alpha$ -region and show a decrease with increasing surfactant concentration (Fig. 4.52). The results are in agreement with the system being water-continuous and the decrease in the diffusion coefficient with increasing concentration is likely to be due to the increasing excluded volume of the surfactant micelles and to the increasing amount of water hydrogen bonded to the increasing number of ether oxygens. Only one measurement was obtained for water at a comparable temperature and composition in the  $C_{12}E_6-H_2O$  system; this is of the same order of magnitude, which is consistent with the phase structure being similar.

Surfactant self-diffusion has been measured in the  $\zeta$ -region (Fig. 4.50). The results show considerable scatter which may partly be due to changes in surfactant aggregation occurring over the narrow temperature range of the region in addition to the experimental problems outlined in section 3.6. For  $C_{12}E_4$ - $D_2O$  samples the lower surfactant D values in the  $\zeta$ -region tend to occur at fractionally higher temperatures (Table 4.10).

Viscosity results in the Brij system (5.1.3.2 and 5.1.3.3) indicate that significant changes may occur over this narrow temperature range. At high water content such changes might have less effect on the water-diffusion than on the surfactant. In the  $\zeta$ -region there is probably a slight rise in the surfactant diffusion coefficients with increasing concentration. In the  $\beta$ -region there is a pronounced rise as in the  $C_{12}E_6$  system at these concentrations. This may be due to decreasing micelle size as a result of packing considerations as in the  $C_{12}E_6$  system. The magnitude of the surfactant self-diffusion coefficient indicates that the surfactant is aggregated. Measurements of the water diffusion coefficient up to 79.1%  $C_{12}E_4$  indicate that water or water plus oxyethylene chain is the continuous phase. Beyond this surfactant concentration there is no discontinuity in surfactant D values versus concentration which might indicate inversion. Thus it would appear that the surfactant exists as small aggregates even in the pure

surfactant.

The activation energy graph for self-diffusion in pure  $C_{12}E_4$  is a good straight line indicating that no structural change occurs; the value obtained for the activation energy  $(27 \pm 1 \text{ kJ K}^{-1} \text{ mol}^{-1})$  is close to that for  $C_{12}E_6$ . Values for the activation energy for surfactant self-diffusion in 89.6%  $C_{12}E_4$ - $D_2O$  and 79.1%  $C_{12}E_4$ - $H_2O$  are similar, which is in agreement with the structure being similar.

The surfactant diffusion coefficient is higher in pure  $C_{12}E_4$  than it is in pure  $C_{12}E_6$ . This may reflect a smaller aggregate size for  $C_{12}E_4$ ; an increase in the proportion of monomers present could also have the same effect.

The surfactant self-diffusion coefficient has been measured in the  $\alpha$ -region in  $C_{12}E_4$ - $D_2O$  samples (Table 4.10) and is consistent with the system being surfactant micelles in water. The surfactant diffusion coefficient shows little change with concentration, within the limited number of measurements made, suggesting that there is little change in micelle size. The large increase in viscosity (determined qualitatively only by stirring with a glass rod) on increasing the  $C_{12}E_4$  concentration, is presumably due to increasing interactions between micelles. Streaming birefringence indicates the presence of anisotropic micelles or aggregates of micelles at the lower temperatures; it decreases with increasing

temperature indicating a decrease in the anisotropy of the micelles or aggregates. This change in structure is reflected in the non-linear activation energy plot (Fig. 4.51.) for the surfactant diffusion. Secondary aggregation of the type occurring in the  $C_{12}E_6-H_2O$  system (8) may also be involved as the temperature is increased and cause deviation of this plot from linearity. Surfactant diffusion values for different compositions fall on the same curve.

High resolution nmr spectra of 20%, 30% and 40%  $C_{12}E_4-H_2O$  show line-broadening of the surfactant peaks as the temperature is lowered (Table 4.14). The changes are gradual. The hydrocarbon chain peak broadens considerably; the oxyethylene chain peak broadens only slightly. This indicates that the motion of the hydrocarbon chains in the anisotropic micelles is restricted considerably more than that of the oxyethylene chains which extend into the water continuous phase.

### 5.1.3. BRIJ 30 - WATER

#### 5.1.3.1 THE PHASE DIAGRAM

Brij 30 is a commercial surfactant having an average oxyethylene chain length of four units; higher and lower oxyethylene chain lengths will certainly be present. The hydrocarbon chains are nominally  $C_{12}$  but probably include some  $C_{10}$  and  $C_{14}$ .

The Brij-water system (Fig. 4.3) contains some of the features present in the  $C_{12}E_4$ -water system. The  $\zeta$  and  $\beta$ -regions have apparently joined, and this region starts to widen above about 25% surfactant so that its range increases from about  $2^\circ\text{C}$  at 25% to about  $6^\circ\text{C}$  at 60%. Below about 16% Brij the liquid is blue-translucent as in the  $C_{12}E_4$ -water system; below about 10% it is unstable. A lamellar liquid crystal occurs at similar compositions to that in the  $C_{12}E_4$ -water system. The  $\alpha$  region is absent.

The fact that the phase diagram differs from that of  $C_{12}E_4$  is due to the mixture of chain lengths present and other impurities present.

#### 5.1.3.2. CONDUCTIVITY

Conductivity measurements were made in the isotropic liquid region. In order that conductivity could be measured as a function of composition, measurements had to be made at slightly different temperatures below 55% Brij; the temperatures were chosen so as to be near the

### 5.1.3.2. Cont'd.

middle of the clear region for each sample. Differences in conductivity due to slightly different temperatures of measurement were small compared to the differences due to changes in composition (Figs. 4.35-4.37).

At low Brij concentrations the conductivity increases with increasing Brij concentration. This is not unexpected since the liquid would be expected to be water continuous and increasing the Brij concentration increases the number of ions, as these are present as an impurity in the Brij. Calculations show, however, that the conductivity is lower than would be expected for a fully dissociated sodium salt at the concentration known to be present, from atomic emission determinations. For example, a 8.85% Brij-water solution has a conductivity of  $17\text{mSm}^{-1}$  at  $58^{\circ}\text{C}$  and a sodium concentration of  $5\text{m mol}/1000\text{g}$ ; the conductivity of a 5m molar solution of sodium chloride at  $60^{\circ}\text{C}$  is approximately  $110\text{mSm}^{-1}$ . Similarly a 3.5% Brij solution (not a stable solution) has a conductivity of  $8\text{mSm}^{-1}$  at  $57^{\circ}$ , whereas a sodium chloride solution of a similar sodium concentration of  $2\text{m mol dm}^{-3}$ , has a conductivity of approximately  $45\text{mSm}^{-1}$  at  $60^{\circ}\text{C}$ . There are at least two factors which may be responsible for this. Firstly, the anion in Brij is not known; there may be several different anions present. If any of these anions are included in the micelles then the sodium ions will be present as counter ions and the

### 5.1.3.2 Cont'd.

contributions of these sodium ions to the conductivity, will be much reduced. Secondly, the  $C_{12}E_4-H_2O$  system shows exceptionally low conductivity in the  $\zeta$ -region especially at the lowest concentrations. The Brij system may be structurally very similar to the  $C_{12}E_4$  system in this region, so that the conductivity may be reduced in the same way. This second factor would only account for part of the discrepancy unless the lamellar micelles or aggregates of micelles are very much bigger in the impure system. The above figures at 8.85% and 3.5% Brij do not allow for the excluded volume of the Brij itself which causes an effectively higher salt concentration in the aqueous phase but produces some barrier to conduction at the same time.

As the phase diagram is traversed the conductivity increases until 45% Brij when it starts to decrease. At this point the effect of the increasing phase volume of the surfactant becomes greater than the effect of the increasing number of ions present. There is no discontinuity in the conductivity across the phase diagram indicating that any structural changes are gradual.

Measurements of conductivity as a function of temperature at fixed compositions (Figs. 4.36 and 4.37) give results similar to those in the  $C_{12}E_4-H_2O$  system (Fig. 4.30). At 100% and 90% Brij the conductivity

### 5.1.3.2. Cont'd.

increases with temperature. At 80% Brij the changes in conductivity over a range of 25°C are only slightly greater than experimental error; there is a maximum at about 67°C. At 70% Brij there is a decrease in conductivity with increasing temperature. At 60% the temperature range is smaller (69° to 73°C) and there is a greater decrease in  $K$  ( $12\text{mSm}^{-1}$ ). At lower concentrations of Brij it was still possible to make some measurements as a function of temperature because of the wider temperature range of the isotropic region. The changes in conductivity with temperature were small - less than about 6% over temperature ranges of about 4°C or less.

### 5.1.3.3. VISCOSITY IN THE BRIJ SYSTEM

Fig. 4.47 shows the viscosity of Brij-H<sub>2</sub>O samples across the high temperature clear region as a function of sample composition. There is a maximum at about 56% Brij. Whilst the impure nature of the Brij renders it impossible to draw any firm conclusions concerning this maximum in the viscosity, it is of interest that at 56% C<sub>12</sub>E<sub>4</sub>-H<sub>2</sub>O the lamellar liquid crystal melts directly to a two-phase liquid-liquid mixture. This gap between  $\zeta$  and  $\beta$  in the C<sub>12</sub>E<sub>4</sub>-H<sub>2</sub>O system extends from about 54% to 73% C<sub>12</sub>E<sub>4</sub>. Possibly the Brij system in this region contains large lamellar micelles. Streaming birefringence was not observed in this region, however.

Fig. 4.48 shows viscosity as a function of temperature at four compositions, two on each side of the peak. There is a decrease in viscosity with increasing temperature which is greater in the samples closer to the composition of peak viscosity. The compositions showing larger decreases in viscosity with increasing temperature are similar to those showing marked decreases in conductivity with increasing temperature, presumably due to a structural change which affects both properties. A breakdown of lamellar micelles into smaller units could have this effect.

#### 5.1.4 CONCLUSIONS CONCERNING THE $C_{12}E_n$ -WATER SYSTEMS

The  $C_{12}E_6$ -water system has one extensive isotropic liquid region which is water continuous at high water concentrations and water-oxyethylene chain continuous at low water concentrations. Normal micelles at low surfactant content decrease in size as the solution becomes more concentrated, until in the pure surfactant they are more properly described as small aggregates. At surfactant concentrations below that at which the hexagonal liquid crystalline phase occurs surfactant self-diffusion results reflect changes in micellar size shape and aggregation, whilst the conductivity is apparently unaffected by these changes (equation 5.1 would not fit throughout this region if factors other than the surfactant concentration were involved). Below about 5°C the micelles are possibly spherical; at higher temperatures and concentrations approaching 38% at which

#### 5.1.4 Cont'd.

the hexagonal phase occurs, streaming birefringence and self diffusion results are consistent with rod shaped micelles. Approaching the cloud point there is secondary aggregation of micelles.

Fig. 1.1 shows the  $C_{12}E_5$ -water system (7). Hexagonal and lamellar liquid crystalline phases occur, separated by a viscous isotropic phase as in the  $C_{12}E_6$ -water system (91). The high surfactant content isotropic liquid phase, the  $\beta$ -region, is now separated from the low surfactant content isotropic liquid phase, the  $\alpha$ -region, by the lamellar liquid crystalline phase. On the basis of results from the  $C_{12}E_6$  - and  $C_{12}E_4$  - water systems it seems probable that the  $\alpha$ -region is water-continuous with normal surfactant micelles, whose shape may vary with temperature and concentration, possibly being rod-like in the vicinity of the hexagonal liquid crystalline phase, and which exhibit secondary aggregation as the cloud point is approached. The  $\beta$ -region is likely to be water-oxyethylene chain continuous with normal micelles decreasing in size to small aggregates in the pure surfactant. As the temperature is increased water-oxyethylene chain interactions become less favourable resulting in the formation of collections of water molecules prior to phase separation. In the  $C_{12}E_4$ -water system this results in decreasing conductivity with increasing temperature as the phase boundary is

approached. In the  $C_{12}E_6$ -water system this behaviour was only observed at 67.9%. The longer oxyethylene chain enables the system to retain more water to higher temperatures at high surfactant content. This results in phase separation into water plus the  $\beta$ -phase occurring at lower surfactant concentration at a given temperature for the longer oxyethylene chain. In the  $C_{12}E_6$ -water system 67.9% is the only sample where this phase boundary was approached sufficiently closely for the decrease in  $k$  to be observed. At the lower concentrations studied too much water was present for this behaviour to be observed.

The  $C_{12}E_5$ -water system exhibits double cloud points, a  $\zeta$ -phase occurring at high water content as in the  $C_{12}E_4$ -water system. The  $\zeta$ -phase occurs about  $10^\circ\text{C}$  higher in the  $C_{12}E_5$ -water system, but as in the  $C_{12}E_4$ -water system it is immediately above the highest temperature of occurrence of the lamellar liquid crystalline phase (either as a single phase or with water). Its structure is likely to be similar in both surfactant-water systems, possibly some sort of large aggregates of lamellar or disc-like micelles which reduce the water self-diffusion coefficient and the conductivity to a significantly greater extent than the excluded volume effect would do alone. These effects are most pronounced at high water content, where the large aggregates scatter light causing the solutions to appear

#### 5.1.4. Cont'd.

blue-translucent. The factors producing this phase are so delicately balanced that it has only a narrow temperature range of existence.

The  $\alpha$ -region in the  $C_{12}E_4$  system is smaller than in the  $C_{12}E_5-H_2O$  system extending only to about  $21^\circ C$  rather than  $50^\circ C$ . This phase is water continuous and the conductivity follows the equation of Mackay and Agarwal (equation 5.1). The changes in the micelle structure with decreasing temperature, indicated by the appearance of streaming birefringence and the line broadening of the hydrocarbon chain resonance in high resolution nmr, are not reflected in any marked deviation from this equation.

The hexagonal liquid crystal phase is absent, above  $0^\circ C$ , in the  $C_{12}E_4$ -water system. The shorter oxyethylene chain length is less favourable for the formation of this phase which occurs in the  $C_{12}E_5$ -water system and to a greater extent in the  $C_{12}E_6$ -water system.

The Brij 30-water system bears considerable resemblance to the  $C_{12}E_3$ -water system (Fig. 5.1)(9)), a reflection of the polydispersity of this commercial surfactant, in particular of lower oxyethylene chain lengths than the nominal four units and of possibly some longer hydrocarbon chain lengths than the nominal 12-carbon chain. The wider  $\xi$ -region now joined to the  $\beta$ -region makes measurements within this region possible.

#### 5.1.4. Cont'd.

It appears to be similar in structure to the  $\zeta$ -region in the  $C_{12}E_4$ -water systems; it occurs just above the lamellar phase. The  $\alpha$ -region is absent, lamellar liquid crystal and lamellar liquid crystal plus water occurring in this part of the phase diagram. Again this is similar to the  $C_{12}E_3$ -water system. There is sufficient  $C_{12}E_3$  or perhaps  $C_{14}E_4$  to form a lamellar liquid crystal at these compositions.

## 5.2 SURFACTANT-HYDROCARBON SYSTEMS

### 5.2.1 C<sub>12</sub>E<sub>4</sub>-HEPTANE

#### 5.2.1.1 THE PHASE DIAGRAM

The phase diagram of C<sub>12</sub>E<sub>4</sub>-heptane is shown in Fig. 4.4. Above the surfactant melting point the surfactant and hydrocarbon are completely miscible. On cooling C<sub>12</sub>E<sub>4</sub> crystallises out until the C<sub>12</sub>E<sub>4</sub> content is reduced to 2%, by weight, or less, when the system is still an isotropic liquid at 0°C.

Polyoxyethylene alkyl ethers have been reported to form reversed or "inverted" micelles in hydrocarbon solvents, the polyoxyethylene chains forming the interiors of the micelles. Miura and Nakamura<sup>(107)</sup> used heats of mixing to study the series C<sub>12</sub>E<sub>n</sub>, where n= 1 to 5, in dodecane; they found that these surfactants exhibited a well defined cmc (shown as a discontinuity in the ΔH versus concentration curve) ranging from 1.4 to 0.26 mol<sub>m</sub><sup>-3</sup>. Below the cmc they deduced that the oxyethylene chains were in a cyclic state, the terminal -OH group being intramolecularly hydrogen bonded to an ether oxygen.

Tiddy et al (98) using vapour pressure measurements on the C<sub>12</sub>E<sub>n</sub> series plus heptane at 35°C, have found no well defined cmc's for the lower members of the series. They found a cmc of about 2% for C<sub>12</sub>E<sub>12</sub>. For C<sub>12</sub>E<sub>4</sub> there was a gradual association (dimers, trimers etc.) at about 8%. C<sub>12</sub>E<sub>8</sub> formed larger aggregates (about 20 units)

### 5.2.1.1 Cont'd.

at about 4%.  $C_{12}E_4$  exhibited a lower association concentration in hexadecane.

At high surfactant concentration the heptane is expected to be solubilised in the surfactant in the hydrocarbon cores of surfactant aggregates.

### 5.2.1.2. CONDUCTIVITY IN THE $C_{12}E_4$ -HEPTANE SYSTEM

The conductivity of heptane itself is very low; conductance measurements made with the platinum cell were so low that they were on the limit of what was measurable with the Wayne Kerr conductance bridge.

Results obtained in this system are given below:

Sample	Conductivity/ $nSm^{-1}$		
	20°	30°	55° C
Heptane		$2 \pm 1$	$6 \pm 1$
$C_{12}E_4$ (see also section 5.1.2.2)		$470 \pm 10$	
$C_{12}E_4$ /heptane (50% by wt)	$19 \pm 1$	$22 \pm 1$	$27 \pm 1$

## 5.2.2. BRIJ 30 - HEXANE

### 5.2.2.1 THE PHASE DIAGRAM

The polydispersity of Brij resulted in such ill-defined phase boundaries that no phase diagram has been drawn for this system. Brij itself does not have a very well defined melting or clearing point. As the volume of added hexane is increased the clearing point becomes even less well defined. The low solubility in hexane of components with long oxyethylene chains and the presence of ionic impurities and traces of water result in small amount of solid material remaining even at higher temperatures (e.g. 40°C at 20% Brij).

### 5.2.2.2 CONDUCTIVITY IN THE BRIJ-HEXANE SYSTEM

Fig. 4.38 shows the conductivity in this system measured as a function of composition. Many of the samples on which measurements were made contained traces of solid material. The decrease in conductivity with increasing hexane content shows no discontinuity which might indicate an inversion of the system from ethylene oxide continuous to oil continuous. Since some water is present in the Brij, the situation is more complex than the  $C_{12}E_4$ -heptane system. The effect of added water is discussed in section 5.3.1.2 - The  $\gamma$ -region. Since the ions in the system come from the Brij itself, the effect of a decreasing number of ions is superimposed on the effect due to structural change.

## 5.3 SURFACTANT-WATER-HYDROCARBON SYSTEMS

### 5.3.1 C<sub>12</sub>E<sub>4</sub>-H<sub>2</sub>O-HEPTANE

#### 5.3.1.1 THE PHASE DIAGRAM

Figs. 4.5 - 4.7 show the phase diagrams of C<sub>12</sub>E<sub>4</sub>-H<sub>2</sub>O-heptane at various temperatures. The isotropic liquid regions are shown, and in some diagrams the approximate boundary of the lamellar liquid crystalline phase is shown. Another clear liquid region exists (sample number 1 is clear between about 10 and 2°C) at high heptane content but is not shown; on observing the sample between crossed polars birefringence is observed. Such "solutions" have been observed near the boundary of a lamellar liquid crystalline phase in the sodium dodecyl sulphate-pentanol-water-benzene system (56), (Section 1.4.8).

#### The $\alpha$ -region

At 0°C the  $\alpha$ -region is at its most extensive, with regard to the temperatures studied. This region is an extension of the  $\alpha$ -region in the binary system (Fig.4.1). The extent of the  $\alpha$ -region is reduced as the temperature increases; it does not occur at temperatures above 21°C, its maximum temperature of occurrence in the binary system. The heptane is presumably solubilized in the hydrocarbon cores of the micelles. Their structure is such that they are unable to take more than a small amount of heptane and remain stable. About 3% of heptane in 30% C<sub>12</sub>E<sub>4</sub>-H<sub>2</sub>O is sufficient to cause phase separation (Fig.4.15).

The  $\mathcal{D}$ -region

The  $\mathcal{D}$ -region is also at its most extensive at  $0^{\circ}\text{C}$  (studies were not made below  $0^{\circ}\text{C}$ ). It appears to join the  $\alpha$ -region close to the water corner at  $0^{\circ}\text{C}$ ; the problems encountered in investigating this region, particularly at the lower temperatures are discussed in section 4.14. At the lowest temperatures studies many of the samples in this region are highly viscous although isotropic. As the temperature is increased the  $\mathcal{D}$ -region definitely becomes detached from the water corner; its extent decreases until by  $8^{\circ}\text{C}$  it has disappeared.

Samples in parts of this region exhibit streaming birefringence indicating the presence of anisotropic aggregates or easily deformable particles. The higher surfactant content side of the region is adjacent to a part of the phase diagram where a lamellar liquid crystalline phase is one of the phases present. If the structure of this region is heptane droplets surrounded by a surfactant monolayer, in water, then as two droplets approach each other closely the surfactant monolayers on coming together will tend to form a liquid crystalline layer which will be a barrier to coalescence of the droplet. The position of the phase relative to the lamellar liquid crystalline phase ensures this, because close approach of the droplets locally increases the surfactant concentration. Thus the system will be stabilized. This has been found to occur in emulsions (99).

### 5.3.1.1 Cont'd.

This may also account for the appearance of streaming birefringence, as the "streaming" brings the droplets close together, especially if they are relatively easily deformed.

The low surfactant content side of the region exhibits blue-translucence indicating the present of large aggregates. This phase boundary follows approximately a constant surfactant: oil ratio; in view of the difficulty in locating the phase boundary precisely (Section 4.14) deviations from the straight line shown in the phase diagrams could easily be due to experimental error. It is possible to estimate the droplet diameter at this surfactant: oil ratio (about 12:88) using the value of  $4400 \text{ nm}^2$  for the surface area per molecule, a value obtained by Tiddy and Lyle (100) for the lamellar liquid crystal. A value of about 90nm is obtained which is consistent with the light scattering observed. As the surfactant concentration decreases across the region (taking a constant heptane: water ratio) the heptane droplets need to increase in size in order to reduce the total surface area and decrease the surfactant requirement. Such an increase in droplet size with decreasing surfactant concentration can explain the gradual appearance of blue translucence and then cloudiness. There appears to be a gradual change to macro-emulsion.

The limit of the  $\mathcal{J}$ -region at high heptane content is determined by the amount of water required to fill the

interstices between droplets and to hydrate the oxyethylene chains.

That the  $\delta$ -region or at least part of it, is thermodynamically stable is indicated by the tie line shown in Table 4.16, though ideally a repeat determination is required.

#### The $\gamma$ -region

The  $\gamma$ -region occurs at a surfactant-water ratio of 9:1 (wt:wt), and a little above and below this. It does not join the surfactant-water axis until the temperature is increased to  $8^{\circ}\text{C}$  when it joins the extension of the  $\beta$ -region of the  $\text{C}_{12}\text{E}_4\text{-H}_2\text{O}$  system. The solubility of  $\text{C}_{12}\text{E}_4$  in heptane increases with increasing temperature so that the  $\gamma$ -region extend along the heptane-surfactant axis as the temperature is increased.

#### The $\epsilon$ -region

At  $13^{\circ}\text{C}$  another isotropic liquid region ( $\epsilon$ ) is present and part of it overlaps the  $\delta$ -region which occurred at lower temperatures. The  $\epsilon$ -region is not connected to the  $\delta$ -region. A three-phase system containing liquid crystalline material occurs in this part of the phase diagram at intervening temperatures. The  $\epsilon$ -region is blue translucent at lowest surfactant content; this can be ascribed to large aggregates. The low-surfactant phase boundary tends to follow a line of constant surfactant: water ratio particularly at the lower temperatures of occurrence of the region (e.g.  $13^{\circ}\text{C}$ ). If it is assumed that the structure is of water droplets

#### 5.3.1.1 Cont'd.

surrounded by a surfactant monolayer, in heptane, the droplet size can be estimated as above for the  $\delta$ -region. A value of about 50nm is obtained for the diameter. As in the  $\delta$ -region on decreasing the surfactant content at a given heptane: water ratio, the system becomes gradually blue translucent and then cloudy; again this may be explained by increasing droplet size in order to reduce the surfactant requirement. There appears to be a gradual change to a macro-emulsion.

Part of this region at the high water content end and at the lowest temperatures of occurrence, shows streaming birefringence, evidence of anisotropic aggregates or easily deformable aggregates. Further discussion of the structure of this region is given in sections 5.3.1.2 and 5.3.2.2.

As the temperature is increased the  $\epsilon$ -region joins the  $\gamma$ -region close to the heptane corner. The two regions merge completely at higher temperatures. Behaviour of this type is exhibited by the  $C_{12}E_4-H_2O$ -hexane system reported by Friberg and Lapczynska (29). Since they do not record the behaviour of the system below  $10^\circ C$ , the presence or absence of a  $\delta$ -type region is not shown.

#### The $\zeta$ -region

The  $\zeta$ -region appears as a narrow isolated region initially. It is in fact an extension of the  $\zeta$ -region in the  $C_{12}E_4-H_2O$  system (Fig. 4.1). Heptane added to this

### 5.3.1.1 Cont'd.

region reduces its temperature of occurrence without appreciably altering its narrow temperature range (about 2°C). Where the  $\zeta$ -region contains the highest heptane concentration it exhibits streaming birefringence. At higher temperatures this region joins up with the  $\gamma$ -region. In the  $C_{12}E_4$ -water system there is a gap between the  $\zeta$ - and  $\beta$ -regions (the  $\beta$ -region joints the  $\gamma$ -region). It requires very little heptane (2-3%) to remove this gap so that the  $\zeta$ - and  $\beta$ -regions join.

The  $\zeta$ -region occurs in the  $C_{12}E_4$ -H<sub>2</sub>O-hexane system of Friberg and Lapczynska, and they show how it moves towards higher surfactant content with increasing temperature, but since the highest temperature they record is 35°C no amalgamation with the  $\gamma$ -region is shown.

### 5.3.1.2. CONDUCTIVITY IN THE $C_{12}E_4$ -H<sub>2</sub>O-HEPTANE SYSTEM

Figs. 4.5-4.7 show conductivity in the  $C_{12}E_4$ -H<sub>2</sub>O- heptane system on the phase diagrams.

#### The $\delta$ -region

These results indicate that the  $\delta$ -region is water continuous. The conductivity decreases with increasing heptane concentration as expected. Since the region is water continuous presumably the heptane exists in the interiors of the micelles, surrounded by a layer of surfactant. As the heptane content of the system is increased the excluded volume is increased so that the conductivity decreases. Application of the equation of Mackay and Agarwal (equation 5.3) to the series of samples

### 5.3.1.2. Cont'd.

containing 10%  $C_{12}E_4$  at  $4^\circ C$  shows little agreement (Fig. 4.39).

$$k = k_m (1 - \phi)^{2.5} \quad 5.3$$

The Bruggeman equation (equation 5.4) shows much better agreement (Fig. 4.39)

$$k = k_m (1 - \phi)^{1.5} \quad 5.4$$

Above 20% (W/W) heptane the results lie between the Bruggeman and Maxwell (equation 5.5) equations, and are closer to the Maxwell equation at the highest heptane concentration.

$$k = k_m \left( \frac{2(1 - \phi)}{2 + \phi} \right) \quad 5.5$$

The phase volume,  $\phi$ , has been calculated on the basis of the densities of the components so is open to some error in that slight changes may occur when the components are mixed e.g. heptane in micelles may not exactly have the same effective density as the pure component. A much larger source of error is the fact that the volume of the disperse phase has been taken as the volume of heptane plus the volume of  $C_{12}E_4$ . The Volume assumed for the disperse phase is discussed in section 5.1.1.2. It appears that the conductivity in the  $\beta$ -region shows a much greater resemblance to the conductivity in a normal emulsion than it does to the conductivity in the  $\alpha$ -region of the binary system, or to Mackay and Agarwal's microemulsion (section 1.5.6).

### 5.3.1.2 Cont'd.

The conductivity of monodisperse O/W emulsions generally lies between that predicted by the Bruggeman and Maxwell equations whilst that of a polydisperse system generally follows the Bruggeman equation (section 2.1.2). If the assumptions mentioned above are valid then from 30% (W/W) heptane to 50% the system is showing conductivity behaviour typical of a monodisperse macro-emulsion.

#### The $\epsilon$ -region

The  $\epsilon$ -region shows very low conductivity over most of its range, of the order of  $1 \mu\text{Sm}^{-1}$ . This is so low that the system cannot be water continuous. It is of the same order of magnitude as the conductivity of the pure surfactant and rather higher than that of heptane.

Some higher values of conductivity are recorded on the edge of the region. The reasons for these higher values are discussed below and in section 5.3.2.2.

#### The $\gamma$ -region

In this region conductivity has been measured for the series of samples containing 10% water, at varying temperature (Fig. 4.40 and 4.41).

90%  $\text{C}_{12}\text{E}_4$ -10%  $\text{H}_2\text{O}$  consists of surfactant aggregates in an oxyethylene chain-water continuum. The conductivity of sample number 36 behaves in a similar manner as a function of temperature, suggesting a similar structure; now that heptane has been added this will be localised in the cores of the surfactant aggregates while the oxyethylene

### 5.3.1.2. Cont'd.

chains and water form the continuous phase as before. The presence of heptane would be expected to reduce the conductivity, since it increases the volume of the cores of the aggregates and so reduces the volume available for conduction. This is seen at higher temperatures, though apparently not below about 30°C. However, the nominally 90% C<sub>12</sub>E<sub>4</sub>-H<sub>2</sub>O sample contained 10.1% water whilst sample number 36 contained 10.5% water. It can be deduced, from measurements of conductivity in the  $\beta$ -region of the binary system, that, in the region of 90% C<sub>12</sub>E<sub>4</sub>-10% H<sub>2</sub>O, a difference of 0.5% in the water content can produce a difference of as much as 50  $\mu\text{Sm}^{-1}$  in the conductivity at 60°C. This difference would decrease with decreasing temperature as the measured conductivities themselves decrease. Thus the slightly different amounts of water in the 90% sample and sample number 36 combined with the slightly different slopes of the conductivity versus temperature graphs lead to the crossing of these graphs. The graph of sample number 21 crosses that of sample number 28 at about 11°C for the same reason; sample number 21 containing 10.4% water whilst sample number 28 contains 9.9% water.

The conductivity of sample number 28 behaves similarly to that of sample number 36. The conductivity of sample 28 is lowered as would be expected considering the increased volume of heptane present, presumably within the surfactant micelles as in sample number 36.

### 5.3.1.2 Cont'd.

At the opposite end of this series of samples are those containing large proportions of heptane and 10% water. Water can have a considerable effect on the micelle formation of polyoxyethylene alkyl ethers in nonaqueous solvents. The water becomes associated with the polyoxyethylene chains so converting them to more hydrophilic species; the micelles, therefore, grow with the water solubilized in the micellar core (101). Sample number 1 must either be oil-continuous with surfactant micelles containing solubilized water, or some sort of "molecular" solution, since it contains 80% heptane by weight (more than 80% by volume) which is an impossibly large proportion to disperse in the surfactant and water unless the heptane droplets are polydisperse as in certain types of emulsion. There is more water present than is required to hydrate the oxyethylene chains even on the basis of two water molecules for each oxygen, so that "free" water must be present in the system. On this basis and also in view of the evidence (101) for micelles containing solubilized water in this type of system, it seems highly improbable that the system consists of anything other than reversed surfactant micelles containing solubilized water in a heptane continuum. Some of the water in the micelles is hydrogen-bonded to the surfactant ether oxygens and the rest exists as water "pools" (sections 1.4.2 and 1.5.4).

The above structure would be expected to have an extremely low conductivity, about twice that of pure heptane if it obeyed the Bruggeman equation for an oil-continuous emulsion (equation 2.3), even allowing for the presence of the sodium chloride. The measured conductivity of  $2.06 \mu\text{Sm}^{-1}$  at  $17.0^\circ\text{C}$ , and  $3.91 \mu\text{Sm}^{-1}$  at  $19.8^\circ\text{C}$ , is far in excess of this (the conductivity of heptane is about  $2\text{nSm}^{-1}$ ). In oil-continuous systems abnormally high conductivities may be due to percolation (sections 1.5.7 and 2.1.3). The disperse phase volume of sample 1 is 15% if all the surfactant is included in the disperse phase, this is well below theoretical and experimental threshold values for percolation (section 2.1.3). Lagues et al (73) have suggested that in their microemulsion system the non-zero conductivity below the percolation threshold was due to electrophoresis, the microemulsion droplets having a small charge (estimated to be one ion per 600 molecules of soap in the interfacial film). They report that this conductivity below the threshold was much greater than that of the continuous phase (cyclohexane) ranging from 1 to  $100 \mu\text{Sm}^{-1}$ . An ionic surfactant was used in combination with an alcohol in contrast to the present nonionic surfactant. Ions would be expected to be located in the aqueous interior of the micelles in the present case and not in the interfacial film as in the system of Lagues et al. Conductivities of samples thought to be heptane-continuous fall in the lower part of the above range ( $< 25 \mu\text{Sm}^{-1}$ , say)

except close to phase boundaries (this is discussed below). Non-zero conductivity below the percolation threshold has also been observed by Lagourette et al (76). Electrophoretic movements of the disperse globules was suggested as a possible explanation; the system again contained an ionic surfactant plus a cosurfactant. Peyrelasse et al (102) suggested that droplet electrophoretic movement could contribute to microemulsion bulk conductivity.

If electrophoresis is the explanation for the surprisingly high conductivity of the oil-continuous phase, factors affecting the micelle size in the high-heptane content part of the  $\gamma$ -region would be expected to have some effect on the conductivity. Larger particles will be less mobile and so unless there is an equivalent increase in their charge or their number, the conductivity of the system will be less. It has been found that the micellar weight of polyoxyethylene nonyl phenols in cyclohexane solutions increases linearly with the mole ratio of added water (103). Thus sample 2 might be expected to have a lower conductivity than sample 1. However, although the conductivity is lower ( $1.2 \mu\text{Sm}^{-1}$  at  $15.8^\circ\text{C}$ ) compared to  $2.06 \mu\text{Sm}^{-1}$  at  $17.0^\circ\text{C}$  for sample 1) this may be due entirely to the temperature difference; extrapolation from the two results for sample 1 suggests this. Where the volume of water is increased to a greater extent relative to the surfactant

### 5.3.1.2 Cont'd.

the expected drop in conductivity occurs as in samples 7 and 11 in the  $\epsilon$ -region, in the upper part of their temperature range (section 5.3.2.2).

Where the quantity of water remains constant whilst the surfactant is increased some increase in conductivity might be expected as long as there is sufficient water present. A larger number of smaller micelles will be produced provided that there is sufficient water to hydrate the surfactant chains. If electrophoresis forms the major part of the conduction mechanism, the conductivity is likely to rise because the aggregates are smaller. Sample 3 does appear to show this effect with respect to sample 1, at the upper end of its temperature range.

The conductivity of samples 3 and 6 is recorded in greater detail ~~of~~ over their complete temperature range in Fig. 4.41. Both samples show a considerable increase in conductivity with decreasing temperature at the lower ends of their temperature ranges. No such increase was observed in the case of sample number 1; the lower temperature of measurement is  $1.2^{\circ}\text{C}$  above phase separation, so any increase in conductivity can only occur over a very limited temperature range within the clear phase.

The maximum in the conductivity is very close to the lower phase boundary for both sample 3 and sample 6.

As decreasing temperature leads to phase separation the conductivity falls. One of the phases which separates is a liquid crystalline phase.

To exclude any possibility of the presence of sodium chloride causing this conductivity behaviour, measurements were made on sample 6, using distilled deionised water instead of 0.010 M sodium chloride solution. The presence of 0.010 M sodium chloride has not been found to affect phase boundaries significantly. The form of the conductivity versus temperature curve was the same; the measured conductivities were appreciably lower:  $3\mu\text{Sm}^{-1}$  at  $30^{\circ}\text{C}$  as opposed to  $22.5\mu\text{Sm}^{-1}$  at  $29.9^{\circ}\text{C}$ , and  $8\mu\text{Sm}^{-1}$  at the maximum close to the phase transition, as opposed to  $159\mu\text{Sm}^{-1}$ . The effect of the sodium chloride is much larger where the conductivity increases close to the phase transition. There is nevertheless a significantly greater conductivity in sample 6 at the higher temperatures, where it is likely to be an oil-continuous micellar system. This increase due to the presence of sodium chloride is likely to exist to some extent throughout the oil-continuous region.

Boyle et al (104) have made dielectric measurements in the  $\text{C}_{12}\text{E}_4\text{-H}_2\text{O}$ -heptane system. For samples 1,2,4 and 5 their results for the high temperature ends of the isotropic liquid regions are consistent with a W/O structure. At the lower ends of the temperature ranges

they suggest that large lamellar aggregates are present and that these change to inverted micelles with increasing temperature. For samples 3 (in this case 16%  $C_{12}E_4$ , 10%  $H_2O$  and 74% heptane) and 6, where the surfactant: water ratio is higher, their results at the high temperature ends of the clear regions agree with calculated values for a W/O + S structure (in these cases the calculated permittivities are based on water dispersed in an ideal mixture of oil plus surfactant). At the low temperature ends of the clear regions the permittivities increase towards values for O/W structures though they do not reach these magnitudes. This behaviour is similar to that of samples 1, 2, 4 and 5 in which lamellar aggregates were proposed.

The low temperature phase transitions of samples 1 to 6 are to mixtures containing lamellar liquid crystal as one component. Thus the occurrence of lamellar aggregates prior to the phase transition is not unreasonable. Some streaming birefringence might be expected in the region where these lamellar aggregates are thought to occur. Slight streaming birefringence was observed only in sample number 2. However, the factors such as particle size and the viscosity of the medium which determine whether streaming birefringence is observed by the crude method used, are not known.

The mere presence of lamellar aggregates in samples 3 and 6 at their lower temperatures of occurrence would not be sufficient to account for the increase in conductivity.

### 5.3.1.2. Cont'd.

Some mechanism for conduction is required since the continuous phase is still heptane. It has been suggested that percolation occurs in oil-continuous micro-emulsion systems and accounts for unexpectedly high conductivities (sections 1.5.7 and 2.1.3); in the systems studied ionic surfactants plus cosurfactants were used and the conduction was thought to take place through the droplet interfaces (73, 76). With nonionic surfactants this cannot occur; the sodium chloride ions added to the present system are located in the aqueous interiors of droplets or micelles, surrounded by a barrier of nonionic surfactant. Collision of the droplets does not normally allow charge transfer to take place. This can explain why some oil-continuous phases observed in the present work do not exhibit conductivity indicative of the occurrence of percolation although the disperse phase volume is above the threshold for percolation (section 2.1.3) (e.g. samples 5 at its highest temperature of occurrence and samples 7 and 11 at the highest temperature of occurrence of the  $\epsilon$ -region). However, the situation may be different when the aggregates are lamellar: if collisions allow contact of the aqueous layers there is the possibility of charge transfer. If there is a dynamic situation in which the aggregates break up and recombine the means of charge transfer is improved.

### 5.3.1.2 Cont'd.

Such a structure could account for the high conductivities observed in samples 3 and 6 at the lower ends of their temperature ranges. The structure becomes most favourable for charge transfer as the phase boundary is approached on decreasing the temperature, and then as lamellar liquid crystalline material phase separates, the means of charge transfer is lost and the conductivity falls. The fact that sodium chloride increases the conductivity close to the lower phase boundary to a greater extent than at the high temperature end of the region agrees with a conduction mechanism of this type.

The disperse phase volume of sample 3 is below the theoretical percolation threshold ( $\phi = 0.29$  in section 2.1.3); that of sample 6 (0.32 approx) is close to it, if all the surfactant (as well as the water) is included in this volume. However, this theoretical percolation threshold is based on a static hard sphere model. If the disperse phase is in the form of disc-like micelles or lamellar aggregates in a dynamic system the percolation threshold may be lowered considerably. Sample 1 has a disperse phase volume of about 0.15; this may be too low for percolation to occur, if similar structures to those suggested for samples 3 and 6, are formed close to the phase boundary as the temperature is reduced. This may account for the fact that no evidence of a rise in conductivity was found in sample 1.

The high and rapidly changing conductivities observed elsewhere on the edges of this oil-continuous region (the  $\epsilon$ -region and the  $\gamma$ -region both at high heptane content), may be attributed to the same structural changes e.g. the following values of conductivity were measured for sample number 5:

Temperature/ $^{\circ}\text{C}$	Conductivity/ $\mu\text{Sm}^{-1}$
17.0	201
19.9	4.95
24.8	7.12

17.0 $^{\circ}\text{C}$  is only just above the temperature of the lower phase boundary.

The disperse phase volume (0.16 approx.) of sample 3 is too low for phase inversion to occur. That of sample 6 (0.21 approx) is also too low since only the oxyethylene chains of the surfactant can be included with the water in the calculation of the aqueous phase volume. A minimum of 0.26 by volume is required to fill the interstices of a system of close-packed spheres. The conductivities of samples 3 and 6 do approach those of samples in which the oxyethylene chains form the continuum (samples 28 and 36). However, the hydrogen-bonding of all the water to the oxyethylene chains in samples 28 and 36 (at least over most of the temperature range studied) results in a continuous phase with a relatively low conductivity, although it is water

oxyethylene chain continuous.

Fig. 4.40 shows the variation of conductivity versus temperature for the series of samples containing 10% water.  $d^2k/dT^2$  changes from positive (90%  $C_{12}E_4-H_2O$ ) to negative (sample 28 above about  $30^\circ C$ ); in sample 21 the trend is continued so that  $k$  exhibits a maximum at about  $40^\circ C$ . Sample 15 shows a maximum in  $k$  between  $21$  and  $22^\circ C$ . In sample 10 there is very little change in  $k$  between  $0$  and  $4^\circ C$  and a decrease above  $4^\circ C$ . Within this region (the  $\gamma$ -region) the continuous phase changes, with no discontinuity from oil to oxyethylene chain plus water. In the low surfactant content samples some "free" water remains whilst in the high surfactant content samples it is all hydrogen-bonded to the oxyethylene chains. The hydration of the oxyethylene chains has been reported to vary widely; Schott(6) reports values ranging from 0.4 to 6.3 water molecules per ether oxygen whilst El Eini et al (5) report values ranging from 5.2 to 10.6 for a range of commercial surfactants from  $C_{16}E_{17}$  to  $C_{16}E_{63}$ . These values were for normal micelles and include water which is "trapped" between the polyoxyethylene chains as well as that actually hydrogen-bonded to them, hence the values in excess of the theoretical 2 molecules of water per ether oxygen. Kumar and Balasubramanian (65) studied inverse micelles of Triton X-100 plus hexanol in cyclohexane and

### 5.3.1.2. Cont'd.

found much lower values; a limiting value of one molecule of water per ether oxygen was found as water was added. Geometrical factors are involved in the degree of hydration and also temperature since hydrogen-bonding is reduced at higher temperatures.

Where the surfactant: water ratio at the given temperature is such that all the water can be accommodated by bonding to the oxyethylene chains the system is unlikely to invert to oil-continuous provided that the phase volumes are appropriate for oil to remain as the disperse phase. Boyle et al (104) suggested that when the hydrogen-bonding breaks down on increasing temperature and the entropy of mixing is insufficient, the water becomes encapsulated. The continuous phase becomes oil plus surfactant hydrocarbon chains. In sample 10 there are five water molecules for each surfactant molecule (i.e. four ether oxygens plus one alcohol oxygen). This is a little in excess of the limiting value for hydration found in inverse micelles by Kumar and Balasubramanian (65). The volume of the heptane phase (50% by weight) is about 60%. Thus inversion is likely to occur at compositions around that of sample 10. The conductivity is in agreement with the system containing oil-cored micelles at the lowest temperatures and water-cored micelles in heptane at the highest temperatures (Fig. 4.40) when the hydrogen-bonding has decreased.

The dielectric results of Boyle et al indicate this type of behaviour. Between the two extremes there is a continuous change presumably within a surfactant matrix. Both oil-cored and water-cored micelles may be present at the same time or polydisperse small aggregates or some sort of bicontinuous structure may occur, with surfactant at the interface separating oil and water (section 1.4.7).

Boyle et al report that sample 10 was the sample with the lowest water: surfactant ratio to display a W/O+S structure as indicated by dielectric results, (i.e. the results agreed with calculated values based on a dispersion of water in an ideal mixture of oil plus surfactant. The conductivity of sample 15 at the higher temperatures measured is not as low as that of sample 10 but the fact that it decreases above 22°C may be an indication that the sample is starting to invert by the same mechanism as sample 10, though it never reaches complete inversion at the temperatures studied. This behaviour is also observed in the conductivity of sample 21 at higher temperature (above about 40°C). At the higher surfactant contents and lower heptane contents a higher temperature is needed before the inversion process starts. In sample number 28 the only indication that inversion may occur at a temperature above the range studied is the change in slope of the  $K$  versus temperature curve ( $d^2K/dT^2$  becomes negative with increasing temperature).

### 5.3.1.2. Cont'd.

In sample number 36 there is no indication of the beginning of an inversion process.

There is a similarity between this inversion process and the changes occurring in the binary  $C_{12}E_4$ -water samples at 68 to 80%  $C_{12}E_4$ , where small aggregates of water form with increasing temperature prior to phase separation and the conductivity is reduced (section 5.1.2.2).

#### Conductivity in the $\epsilon$ -region

Conductivity in this region indicates that it is oil-continuous. Only about 10% of surfactant is necessary to solubilize large amounts of water (up to at least 50% by volume) at the lowest temperatures leading to relatively large droplets-the solutions are blue-translucent at the lowest surfactant contents. The large droplet size may account for the extremely low conductivities recorded,  $0.38\mu\text{Sm}^{-1}$  in sample 7 and  $0.58\mu\text{Sm}^{-1}$  in sample 11; these are lower than the conductivities recorded in the oil-continuous part of the  $\gamma$ -region, the lowest being  $2.1\mu\text{Sm}^{-1}$  in sample 1. As in samples 3 and 6 at the low temperature end of the clear region a rapid rise in conductivity with decreasing temperature was found up to the phase boundary when the system became cloudy and birefringent due to the presence of lamellar liquid crystal. This conductivity behaviour was found on the higher surfactant content edge

### 5.3.1.2. Cont'd.

of the region where the phase transition is from isotropic liquid to a system containing liquid crystalline material; this is essentially the same as the low temperature phase boundary, because of the way the  $\epsilon$ -region moves across the phase diagram with temperature. This behaviour was ascribed to the formation of lamellar aggregates as in samples 3 and 6. It is discussed for samples 7 and 11 in section 5.3.2.2.

As the  $\epsilon$ -region moves across the phase diagram with increasing temperature, and becomes continuous with the  $\gamma$ -region, conductivity measurements on the samples involved indicate behaviour intermediate between that of the oil-continuous region with the lamellar aggregates at its lowest temperatures, and the surfactant plus water continuous region which inverts as in sample 10.

#### Conductivity in the $\zeta$ -region

This is an extension of the  $\zeta$ -region in the binary system, and is water continuous. The conductivity decreases with added heptane as would be expected if it is going into the interiors of the micelles and either their size or their number is increasing. As heptane is added to samples containing 20% and 30%  $C_{12}E_4$  the conductivity decreases almost linearly with the decreasing temperature of the narrow clear region. The temperature of occurrence of the clear region decreases almost linearly

### 5.3.1.2 Cont'd.

with added weight of heptane (Fig. 4.15). Both the increasing heptane volume fraction and the decreasing temperature (assuming no structural change with temperature) will cause  $K$  to decrease.

The region is joined to the  $\gamma$ -region at higher temperatures. The conductivity was measured at fixed temperatures and compositions; within these limitations no discontinuity was observed in the conductivity where the regions joined. The high water content end of the  $\xi$  region where water is the continuous medium merges continuously into the water plus oxyethylene chain continuous part of the  $\gamma$ -region.

### 5.3.2. WATER-HYDROCARBON MIXTURES WITH ADDED SURFACTANT C<sub>12</sub>E<sub>4</sub>-WATER-HEPTANE

#### 5.3.2.1. THE PHASE DIAGRAM

Fig. 4.10 shows the phase diagram obtained on adding C<sub>12</sub>E<sub>4</sub> to a mixture of 59.7% water plus 40.3% heptane. This shows the  $\mathcal{J}$  and  $\epsilon$ -regions as a function of temperature for this water: heptane ratio. Between these regions there is a three-phase region, which has the lamellar liquid crystal as one component. The regions diverge with increasing surfactant content, the water-continuous  $\mathcal{J}$ -phase occurring at lower temperature whilst the oil-continuous  $\epsilon$ -phase occurs at higher temperature. The  $\mathcal{J}$ - and  $\epsilon$ -regions are discussed in section 5.3.1.1.

5.3.2.2. THE CONDUCTIVITY OF SAMPLES 7 and 11 IN THE  
C<sub>12</sub>E<sub>4</sub>-H<sub>2</sub>O-HEPTANE SYSTEM

Sample 11 is close to the composition shown in the segmental phase diagram described above (Fig. 4.10) at 10% C<sub>12</sub>E<sub>4</sub>. The conductivity as a function of temperature is shown in Fig. 4.42. The high conductivity in the water-continuous  $\delta$ -region changes little with temperature. The sample is blue-translucent and exhibits streaming birefringence in this region. The conductivity decreases sharply at the phase transition when the sample becomes cloudy and birefringent. The conductivity decreases about a factor of ten. At least the middle part of the region between the  $\delta$  and  $\epsilon$ -regions is 3-phase; lamellar liquid crystal is present throughout. The conductivities measured here varied considerably (by a factor 2 or 3) depending on how the inhomogeneous material was mixed.

The conductivity rises again before the phase transition to the  $\epsilon$ -region and then starts to fall rapidly close to the phase boundary. The conductivity of the  $\epsilon$ -region close to the phase boundary is about  $\frac{1}{3}$  of that of the  $\delta$ -region. It falls from  $7\text{mSm}^{-1}$  to  $500\text{nSm}^{-1}$  within the  $\epsilon$ -region.

That this conductivity behaviour is not due to the presence of sodium chloride was shown by measurements made on a sample made up with distilled deionised water instead of sodium chloride solution. The magnitude of

### 5.3.2.2. Cont'd.

the conductivity was reduced throughout but the form of the conductivity versus temperature curve remained the same.

Sample 7 behaves similarly to sample 11, though the higher heptane content causes some reduction in  $k$  throughout.

Conductivity in the  $\delta$ -region has been discussed (section 5.3.1.2 - The  $\delta$ -region). The conductivity of the  $\epsilon$ -region at the high temperature end of its range of existence is characteristic of an oil-continuous system as discussed in sections 5.3.1.2 and 5.3.2.2. As the temperature is reduced the conductivity increases continuously by a factor of  $10^4$ . It is possible to explain this by a percolation mechanism combined with changes in aggregate structure and interactions.

As the temperature is reduced the spherical droplets of the oil-continuous microemulsion change, by some gradual process, to lamellar aggregates. The interactions of these aggregates enable conduction to occur by a percolation mechanism as in samples 3 and 6: breaking up and recombination of the aggregates enables charge transfer to occur. In the present case the conductivity rises far more than in samples 3 and 6. The disperse phase volume of samples 3 and 6 is less, so that there are less aggregates via which charge can be

### 5.3.2.2. Cont'd.

transferred. Also phase separation may curtail the process which proceeds much further in sample 11 (and also sample 7). Close to the phase boundary of sample 11 a dynamic situation exists with the aqueous phase within lamellar aggregates formed by the surfactant, which rapidly break up and recombine. It is suggested that phase inversion has not occurred (as we suggested previously (88)) but that the system is still oil-continuous. According to equation 2.7 the conductivity of a percolating system with the disperse phase volume of sample 11 would be about  $12\text{mSm}^{-1}$  (assuming that half the surfactant is included in the disperse phase and that the conductivity of the disperse phase is the same as that of the 0.01 M sodium chloride solution at the same temperature) compared to the  $7\text{mSm}^{-1}$  observed and the  $21\text{mSm}^{-1}$  in the  $\mathcal{J}$ -region. Thus it would appear possible for the system to still be oil-continuous. Both samples 7 and 11 show streaming birefringence in the region where these lamellar aggregates are proposed. At the high temperature end of the clear region streaming birefringence is absent, but on cooling it appears and increases in intensity so that it is strong just above the phase transition. This is consistent with the proposed structure of the system. The samples were blue in the region suggesting relatively large aggregates.

### 5.3.2.2. Cont'd.

The surfactant monolayer curvature is concave towards the oil in the  $\mathcal{J}$ -region. In the intervening 3-phase region it is planar. Then as the system passes into the  $\epsilon$ -region it changes from planar to convex towards the oil within the  $\epsilon$ -region. If the system inverted completely within the  $\epsilon$ -region, the surfactant monolayer, planar in the 3-phase region, would then return to concave before becoming convex towards the oil, with increasing temperature.

### 5.3.3 WATER-HYDROCARBON MIXTURES WITH ADDED SURFACTANT -

#### $C_{12}E_4$ -WATER-n-decane

##### 5.3.3.1 THE PHASE DIAGRAM

The phase diagram for 60.0%  $H_2O$ -40.0% n-decane as  $C_{12}E_4$  is added, is shown in Fig. 4.11. It does not differ markedly from the analogous diagram with heptane as the hydrocarbon. The  $\mathcal{J}$ -region is probably a little wider, though the lower boundary could not be determined very precisely. The  $\mathcal{J}$ - and  $\epsilon$ -regions occur at slightly higher temperatures. Friberg and Lapczynska (29) have determined the triangular phase diagrams for this system above  $15^\circ C$  (Fig. 5.1); the  $\mathcal{J}$ -region occurs below  $15^\circ C$  and so is not shown. The isolated  $\epsilon$ -region extends to higher water contents than in the heptane case; on increasing the temperature it then joins the  $\gamma$ -region close to the decane corner as in the heptane system. On further increase in temperature it rapidly amalgamates

5.1

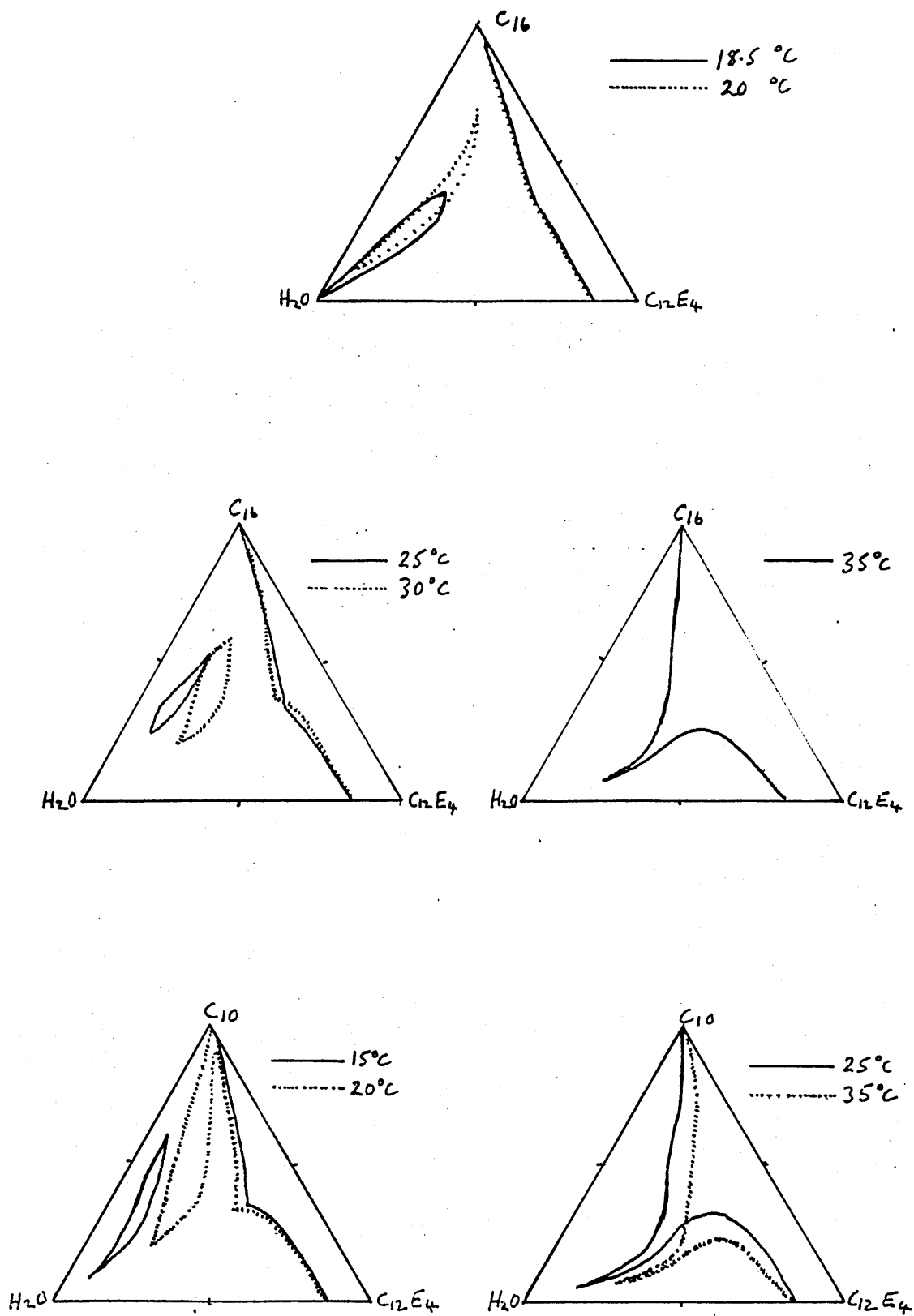


Fig. 5.1. Phase diagrams of the systems C<sub>12</sub>E<sub>4</sub>-water-hexadecane and C<sub>12</sub>E<sub>4</sub>-water-decane. From ref. 29.

### 5.3.3.1 Cont'd.

completely with the  $\gamma$ -region and a narrow salient pointing to the water corner, has already formed by 25°C. In the heptane case the formation of this narrow salient is by linking with the  $\zeta$ -region and occurs between 30 and 39°C.

### 5.3.3.2 THE CONDUCTIVITY OF SAMPLES OF 60% n-decane-40% WATER PLUS C<sub>12</sub>E<sub>4</sub>

Fig.4.43 shows the conductivity of 60.2% water-39.8% decane plus 9.8% added C<sub>12</sub>E<sub>4</sub>. The  $\mathcal{J}$ -region appears to be water-continuous. The  $\epsilon$ -region shows decreasing conductivity as in the heptane case but the conductivity never reaches the very low values that it reaches for heptane.  $1\text{mSm}^{-1}$  is the lowest value for this sample within the clear region. 59.9% water - 40% decane plus 15.1% C<sub>12</sub>E<sub>4</sub> shows similar behaviour. The lowest value of  $K$  in the  $\epsilon$ -region is  $0.5\text{mSm}^{-1}$ . At 9.8% C<sub>12</sub>E<sub>4</sub> the  $\epsilon$ -region is blue and shows streaming birefringence; at 15.1% C<sub>12</sub>E<sub>4</sub> it is no longer blue but still shows streaming birefringence.

This behaviour could be attributed to large lamellar aggregates as in the heptane system, inversion having occurred in the intervening region (between the  $\mathcal{J}$ - and  $\epsilon$ -regions) where lamellar liquid crystal is one of the phases present. Complete inversion, to the oil-continuous system with spherical water droplets and the surfactant monolayer preventing percolation, never takes place, however.

C<sub>12</sub>E<sub>4</sub>-WATER-n-hexadecane5.3.4.1 THE PHASE DIAGRAM

The phase diagram of 59.8% H<sub>2</sub>O-40.2% hexadecane + C<sub>12</sub>E<sub>4</sub> is shown in Fig. 4.12. The  $\mathcal{J}$ - and  $\epsilon$ -regions have been shifted to higher temperature and now join at their low surfactant content ends. The clear region is blue at the lower surfactant contents and shows streaming birefringence only in the lower half of the  $\mathcal{J}$ -region. Friberg and Lapezynska (29) have determined the triangular phase diagrams for this system. There is a marked difference from the heptane and decane systems in that the  $\mathcal{J}$ -region, which joins the water corner at low temperatures, moves away from the water corner and towards lower surfactant content and then becomes the  $\epsilon$ -region (ie. the  $\mathcal{J}$ -region is continuous with the  $\epsilon$ -region). This  $\epsilon$ -region then moves towards higher surfactant content and joins the  $\gamma$ -region near the middle of the phase diagram, between 30 and 35°C.

5.3.4.2. THE CONDUCTIVITY OF SAMPLES OF 60% WATER - 40% -  
n hexadecane plus C<sub>12</sub>E<sub>4</sub>

Conductivity was determined for 14.0%, 18.0% and 21.0% of added C<sub>12</sub>E<sub>4</sub> as a function of temperature. Fig. 4.44 shows the results for 14.0% and 18.0%; the results at 21.0% of added C<sub>12</sub>E<sub>4</sub> were virtually the same as those for 18.0%. At 18.0% and 21.0% the  $\mathcal{J}$ -region appears to

be water continuous. Conductivity in the  $\epsilon$ -region remains high; although it shows some decrease with increasing temperature the lowest values recorded in the clear region were  $17\text{mSm}^{-1}$  at 18.0%  $\text{C}_{12}\text{E}_4$  and  $12\text{mSm}^{-1}$  at 21%  $\text{C}_{12}\text{E}_4$  compared to  $30\text{mSm}^{-1}$  and  $27\text{mSm}^{-1}$  respectively in the water-continuous  $\delta$ -region.

At 14%  $\text{C}_{12}\text{E}_4$  the conductivity decreases from  $35.5\text{mSm}^{-1}$  to  $24.4\text{mSm}^{-1}$  over the clear region. This sample appears to be water continuous at the low temperature end of the clear region.

The  $\epsilon$ -region joins the  $\gamma$ -region near the middle of the phase diagram where the surfactant:water ratio favoured inversion via a surfactant continuous phase in the samples with only 10% water, as in sample 10. The conductivity data for the  $\epsilon$ -region is consistent with some sort of disordered bicontinuous structure both oil and water continuous in which surfactant forms the interfacial film.

Further information on this system is available: Lindman et al (70) have made self-diffusion measurements in this system. Their results showed that in the  $\delta$ -region at high water content ( $> 50\%$  by weight) normal micelles existed in a water-continuous phase - the hexadecane and surfactant diffusion coefficients were small (they were not measured separately) and approximately the same whilst the water diffusion was reduced from that of pure

water by less than a factor of 2. This is in agreement with the conductivity results.

In the  $\gamma$ -region Lindman et al measured self-diffusion for samples in which the surfactant:hexadecane ratio was kept about 45:55 and the water content varied, and also at one point with a much higher hexadecane content. The hexadecane diffusion was rapid in all these samples. In the water-rich part of the  $\gamma$ -region, close to where it joins the  $\epsilon$ -region at slightly higher temperature, the water diffusion was slower by a factor of about 10, than in pure water; this is still a relatively high value compared to that of water in inverted micelles. The surfactant diffusion was about the same as that of the pure surfactant in all the samples measured in the  $\gamma$ -region, except in the absence of water when it was considerably higher (by a factor of 2.4).

In the  $\epsilon$ -region, referred to as the surfactant phase by Lindman et al, they found that both water and hexadecane diffusion were relatively rapid, demonstrating that the phase is both water and hydrocarbon continuous.

They also found an increased  $C_{12}E_4$ -hexadecane diffusion coefficient in the  $\mathcal{J}$ -region for two samples at the lowest water contents where the region is closest to the  $\epsilon$ -region and the  $\gamma$ -region. These might reflect

the approaching changes from water continuous to the bicontinuous structure. The high values for water diffusion in the water rich part of the  $\gamma$ -region might again be an indication of a bicontinuous structure here.

The results of Lindman et al are consistent with the conductivity results. To summarize, the water continuous  $\delta$ -region changes to the bicontinuous  $\epsilon$ -region at low surfactant content. The bicontinuous  $\epsilon$ -region joins the  $\gamma$ -region where this is inverting from surfactant-water continuous to surfactant-oil continuous.

The bicontinuous structure does not show the streaming birefringence associated with the lamellar aggregates proposed in the oil-continuous  $\epsilon$ -region in the  $C_{12}E_4$ - $H_2O$ -heptane system. The low surfactant content parts of the  $\epsilon$ -region and the  $\delta$ -region and particularly the part of the system where these two regions join show the blue-translucence associated with large aggregates of some form.

The bicontinuous structure suggested is a disordered bicontinuous structure in which the interface in this case is formed by the  $C_{12}E_4$  so that water and hexadecane are not incontact. The system can change continuously to a water or oil continuous phase via changes in curvature of the surfactant interface. Such a bicontinuous structure appears to be closely related to the large lamellar aggregates of surfactant and water dispersed in the hydrocarbon which were proposed in the decane system.

This is not unreasonable - a little more linkage of the lamellar aggregates could lead to a bicontinuous structure.

The bicontinuous structure proposed for the  $\epsilon$ -region changes continuously to the structure of the  $\gamma$ -region where inversion occurs. This may also be a bicontinuous structure (section 5.3.1.2. - The  $\gamma$ -region) but of a rather different form, there being much less water present.

#### 5.3.5. THE IMPORTANCE OF THE HYDROCARBON IN THE FORMATION OF BICONTINUOUS STRUCTURES IN TERNARY SYSTEMS

The hydrocarbon appears to determine the ternary phase behaviour. Figs. 4.13 and 4.14 show the section through the phase diagram at 60% water plus 40% hydrocarbon with added  $C_{12}E_4$  for n-octadecane and decalin. The octadecane diagram is similar to that of hexadecane except that the  $\mathcal{J}$ -region is not as extensive because of the separation of crystalline material. The decalin diagram is quite different and without further phase studies it is not possible to say exactly what is happening, but the single phase region which is shown, appears to be from its shape and temperature dependence, the  $\epsilon$ -region shifted to lower temperature. The shape of the decalin molecule (two fused cyclohexane rings) is very different from the straight chain n-alkanes discussed above.

In the  $C_{12}E_4-H_2O$ -heptane system water continuous and oil-continuous microemulsions exist, at low surfactant content. As the temperature is increased inversion from the water-continuous to the oil-continuous system occurs via an intervening 3-phase region containing lamellar liquid crystal. When the hydrocarbon is changed to decane which is still just shorter than the surfactant hydrocarbon chain, the water continuous and oil-continuous microemulsions still exist though the oil-continuous microemulsion shows a trend towards the bicontinuous structure. When the hydrocarbon chain length is increased to 16, which is longer than the surfactant hydrocarbon chain, the water continuous microemulsion changes at low surfactant content with no phase boundary into a bicontinuous structure which can then change to an oil continuous structure at much higher surfactant content. For octadecane the situation appears to be similar to hexadecane though more evidence would be required to substantiate this. Thus the hydrocarbon chain length determines whether a low surfactant-content oil-continuous microemulsion will be formed or whether a bicontinuous phase will be formed. Decalin with its oddly shaped molecule would not fit in between surfactant hydrocarbon chains in the same way and so changes the phase behaviour.

5.3.6.1 THE PHASE DIAGRAM OF BRIJ 30-H<sub>2</sub>O-HEXANE

Figs. 4.8 and 4.9 show the Brij-H<sub>2</sub>O-hexane phase diagrams. At 1°C the  $\alpha$ -region present in the C<sub>12</sub>E<sub>4</sub>-H<sub>2</sub>O-heptane system is absent (it is also absent from the Brij-H<sub>2</sub>O phase diagram) and also the  $\delta$ -region. These regions were not observed at higher temperatures. Thus it appears that Brij is unable to produce an O/W microemulsion at low surfactant content. The  $\gamma$ -region is present at 1°C; its low water content boundary is too ill-defined to be shown.

As the temperature is increased no new isotropic liquid phases are observed until 16°C when a small isolated region occurred around 20% Brij-45% H<sub>2</sub>O - 35% hexane. This appears to be a remnant of the  $\epsilon$ -region (see conductivity results 5.3.6.2) which is much more extensive in the C<sub>12</sub>E<sub>4</sub>-H<sub>2</sub>O-heptane system. As the temperature is increased this joins the  $\gamma$ -region in the middle where the surfactant and hexane proportions are similar.

The  $\gamma$ -region then extends and a narrow salient appears pointing towards the water corner. By 27°C a small narrow isolated region has appeared close to the water corner; this is an extension of the narrow high-temperature clear region in the binary system, the  $\zeta$ -region (Fig. 4.3). As the temperature is increased further the  $\zeta$ -region joins up with the salient of the

$\gamma$ -region. Both ends of these regions exhibit streaming birefringence before the union takes place; this may reflect the presence of lamellar aggregates. Streaming birefringence was not observed where the  $\zeta$ -region joined the  $\beta$ -region in the Brij-water system; the joining of the  $\zeta$ -region to the  $\gamma$ -region is an extension of this in the presence of hexane (the  $\beta$ -region joins the  $\gamma$ -region). Streaming birefringence was observed at 40°C whereas it was not at 70°C; the anisotropic aggregates may be larger.

The  $\zeta$ -region first appears at a similar temperature in both the  $C_{12}E_4$ -H<sub>2</sub>O-heptane and Brij-H<sub>2</sub>O-hexane systems. However, in the Brij system the  $\gamma$ -region also extends at this temperature to include compositions of relatively high water and hexane content with low surfactant content. This is due to different fractions of the polydisperse oxyethylene chains assuming importance at temperatures different to those of the tetraoxyethylene system. At the lowest surfactant content, around 50% hexane, 40% water and 10% Brij, the liquid is blue-translucent indicating large aggregates. This is likely to be due to the same factors producing blue-translucence in the  $C_{12}E_4$  system at low surfactant content, i.e. larger aggregates are produced because of the small amount of surfactant available to form the interfacial film (section 5.3.1.1 the  $\delta$ -region and the  $\epsilon$ -region).

As the temperature is increased further this extension of the  $\gamma$ -region moves to higher hexane content and then recedes, though at 50°C the  $\gamma$ -region in the Brij-H<sub>2</sub>O-hexane system remains more extensive at high hexane content than the  $\gamma$ -region in the C<sub>12</sub>E<sub>4</sub>-H<sub>2</sub>O-heptane system.

### 5.3.6.2. THE PHASE DIAGRAM OF THE BRIJ 30-H<sub>2</sub>O-HEPTANE SYSTEM

A detailed study has not been made of this system. Table 4.15 gives the temperature ranges of samples with isotropic liquid regions and sample numbers greater than 11 (i.e. the high hydrocarbon content samples are not included). Figs. 4.18 and 4.19 show the behaviour of the  $\zeta$ -region at 35.3% Brij in the presence of heptane and 35.4% Brij with added hexane. There are small temperature differences (mostly 3°C or less) between the isotropic liquid regions in the heptane and hexane systems but no significant differences in the general behaviour; no comparison has been made at high hydrocarbon content and low surfactant content.

If as suggested in section 5.3.5, C<sub>12</sub>E<sub>4</sub>-H<sub>2</sub>O-heptane, the difference between the hydrocarbon chain length and the length of the surfactant hydrocarbon chain is important then no qualitative change might be expected in replacing hexane by heptane since both are considerably shorter than the dodecyl chain.

Figs. 4.8 and 4.9 show the conductivity measured at discrete points in the phase diagram.

The conductivity indicates that the  $\epsilon$ -region is oil continuous - hence the designation. At 20.1% Brij; 44.9% H<sub>2</sub>O and 35.0% heptane the conductivity in this region at 18.6°C is  $0.39 \mu\text{Sm}^{-1}$  which is as low as the lowest values obtained in the  $\epsilon$ -region of the C<sub>12</sub>E<sub>4</sub>-H<sub>2</sub>O-heptane system. Throughout the temperature range of clarity of this sample the conductivity changed very little (Table 4.7). A similar sample in which heptane replaced the hexane behaved in the same way. No trace of the very rapid increase in conductivity close to the lower (with respect to temperature) "phase boundary" was found. However, some of the components of the poly-disperse Brij may separate before others so that the observed phase boundary (at the separation of the first components) is not the same as in the system with the pure surfactant.

The behaviour of the conductivity in the  $\gamma$ -region looks rather different to that in the C<sub>12</sub>E<sub>4</sub>-H<sub>2</sub>O-heptane system in Figs. 4.5-4.7. Samples 36, 28 and 21 appear to be water- $\alpha$ -xyethylene chain continuous. The conductivities are relatively high and increase steeply with increasing temperature. The situation is more complex than with the pure surfactant, because, not only are there impurities

### 5.3.6.3. Cont'd.

present in the Brij, including ionic impurities (section 4.7) and a distribution of oxyethylene chain lengths, both of which factors affect the structure of the system but also the quantity of ions varies according to the quantity of Brij present instead of with the quantity of water present. Since there is some water present in the Brij there is slightly more than 10% water in the samples nominally containing this amount of water. As in the  $C_{12}E_4-H_2O$ -heptane system small differences ( $\sim 0.1\%$ ) in the amount of water have a significant effect on the conductivity.

Sample 21 shows no decrease in conductivity at higher temperatures, but  $41^\circ C$  is the maximum temperature of measurement and in the  $C_{12}E_4-H_2O$ -heptane system the decrease in  $K$  for sample 21 occurred above  $40^\circ C$ . The behaviour of samples 15 and 10 suggests that such a decrease is unlikely to occur. The conductivities of samples 15, 10 and 6 all increase with increasing temperature up to  $41^\circ C$  (again measurements were not made above this temperature). Whilst  $d^2K/dT^2$  is positive for samples 10 and 15, for sample 6 it changes from probably just positive to negative. Sample 3 exhibits significantly lower conductivity;  $K$  increases with temperature;  $d^2K/dT^2$  is negative.

The conductivities of samples 6, 10 and 15 are surprisingly close (Fig. 4.4.6) considering that the differences in the quantities of Brij present result

in equivalent differences in the number of ions present. Either the number of ions present has only a small effect on the measured conductivity or structural changes take place with increasing Brij concentration which if the concentration of ions could be maintained constant would actually reduce the conductivity. The conductivities of samples 3, 6 and 10 are of the same order of magnitude as those of the equivalent samples, at the upper ends of their temperature ranges, in the  $C_{12}E_4$ - $H_2O$ -heptane system. These samples were regarded as oil-continuous at the upper ends of their temperature ranges (section 5.3.1.2 - the  $\gamma$ -region). The conductivity of sample 15 is considerably lower than that of the equivalent sample in the  $C_{12}E_4$ - $H_2O$ -heptane system (at  $0^\circ C$   $K$  is  $9.4\mu Sm^{-1}$  compared to  $67.2\mu Sm^{-1}$ ; at  $40^\circ C$   $K$  is  $42\mu Sm^{-1}$  compared to  $70\mu Sm^{-1}$ ). If samples 6, 10 and 15 are oil-continuous this could account for the surprisingly close values of their conductivities. The number of ions present would have little effect on the conductivity of systems where percolation does not occur. Some discussion of the conduction mechanism in such systems has been given previously (section 5.3.1.2 - the  $\gamma$  -region). Sample 3 exhibits a lower conductivity which could be explained by a larger droplet size. Sample 1 barely cleared at around  $34^\circ C$ . It showed a very low conductivity ( $0.78\mu Sm^{-1}$ ) which is considerably lower than that of sample 1 in the  $C_{12}E_4$ - $H_2O$ -heptane system at  $17^\circ C$  ( $2.06\mu Sm^{-1}$ ) and is comparable with the lowest values of

conductivity measured in both systems. This suggests a relatively large droplet size (approaching that of samples appearing blue-translucent due to light scattering). In the Brij system the droplet size in the oil-continuous samples with 10% water appears to increase with decreasing surfactant content, to a far greater extent than in the  $C_{12}E_4$  system.

Sample 6 is clear at  $0^{\circ}C$  unlike that in the  $C_{12}E_4$ - $H_2O$ -heptane system. Sample 3 has its isotropic liquid range about  $10^{\circ}C$  higher than in the  $C_{12}E_4$  system. In sample 6 the lower phase boundary is below the temperatures investigated. The absence of the rapid rise in conductivity at the lower end of the temperature range of sample 3 may be due to the nature of the lower phase boundary as described previously with regard to the  $\epsilon$ -region in the Brij system.

When conductivity is plotted versus composition (for the samples containing 10% water)(Fig. 4.45) there is an ill defined break in the curve at the composition corresponding to sample 15. Between sample 15 and sample 21 the system appears to change continuously from oil-continuous to water-oxyethylene chain continuous, presumably via a similar structure to that occurring in the  $C_{12}E_4$ - $H_2O$ -heptane system. The change seems to occur over a shorter composition range than in the  $C_{12}E_4$ - $H_2O$ -heptane system. Also there is no evidence of inversion from oil-

continuous to water-oxyethylene chain continuous with temperature as in the  $C_{12}E_4$ - $H_2O$ -heptane system.

As the  $\gamma$ -region extends to low surfactant content at  $27^\circ C$  the conductivity decreases with decreasing surfactant content. This accords with increasing droplet size (as in the  $C_{12}E_4$  system); the blue translucence on the low surfactant edge of this region suggests larger droplets here. Drifting readings of conductivity obtained on the low surfactant boundary of this region may be an indication of rapid changes occurring in conductivity as a function of temperature close to the phase boundary, or to the limitations of the copper cell when used to measure very low conductivities (section 3.3.1).

The behaviour of conductivity in the  $\zeta$ -region is very similar to that in the  $C_{12}E_4$  system. Since the maximum temperature at which measurements were made was  $40^\circ C$  the conductivity in the narrow salient of the  $\gamma$ -region was still considerably lower than that in the  $\zeta$ -region. This is also similar to the  $C_{12}E_4$  system below the temperature at which the two regions unite, suggesting that similar structures occur in both systems.

The differences between the isotropic liquid regions of the Brij -  $H_2O$ -hexane system and the  $C_{12}E_4$ - $H_2O$ -heptane system stem from the impurities present in the Brij and the polydispersity of the oxyethylene chains. The Brij-water phase diagram bears considerable resemblance to the  $C_{12}E_3$ -water phase diagram. If a significant proportion of  $C_{12}E_3$  is present in the Brij this will tend to favour W/O

rather than O/W emulsions to a greater extent than  $C_{12}E_4$ . The longer chain homologues present will tend to favour O/W rather than W/O. The binary phase diagram and the absence of the  $\delta$ -region in the ternary system combined with the extension of the  $\gamma$ -region at higher temperatures are a reflection of this. That the  $\epsilon$ -region is so reduced though a W/O system is produced at higher temperature is a indication of different oxyethylene chain length component assuming importance at higher temperature.

#### 5.4 SURFACTANT-TRIACETIN SYSTEMS

##### 5.4.1. $C_{12}E_4$ - TRIACETIN

Fig 4.21 shows the  $C_{12}E_4$ -triacetin phase diagram. Above the melting point of  $C_{12}E_4$  the two are completely miscible. At lower temperatures crystalline material ( $C_{12}E_4$ ) separates out; the temperature at which it does so, decreases with increasing triacetin concentration.

##### 5.4.2. BRIJ 30- TRIACETIN

Fig. 4.22 shows the Brij-triacetin system. Above the clearing point of the Brij the two are completely miscible. At lower temperatures the system becomes two-phase (or multi-phase) as solid (or liquid crystalline-no distinction was made during the determination) material separates out. The peculiar shape of this lower phase boundary is due to the impure nature of the Brij; the diagram shown is not strictly a binary phase diagram because Brij is not a single

component but a mixture. In region B the solid material which separates out is  $C_{12}E_4$  and other homologues. In region A the solid or liquid crystalline material which separates may be ionic impurities possibly with any water present (it is not  $C_{12}E_4$  as this would be against the phase rule).

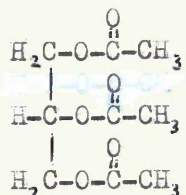
## 5.5 SURFACTANT-WATER-TRIACETIN SYSTEMS

### 5.5.1 $C_{12}E_4$ -H<sub>2</sub>O-TRIACETIN

The triangular phase diagrams of this system are shown in Figs. 4.23 and 4.24

#### The $\alpha$ -region

At 0°C the  $\alpha$ -region is much more extensive than when the third component is heptane. Very little heptane could be accommodated in the  $C_{12}E_4$  micelles of the  $\alpha$ -region. The structure of the  $\alpha$ -region can accommodate much more triacetin, though not necessarily within the micelles as in the case of heptane. The structure of triacetin:



is likely to lead to partitioning with the oxyethylene chains rather than with the hydrocarbon chains forming the micellar core. This is apparently possible with the  $\alpha$ -region micelle structure.

As the temperature is increased the  $\alpha$ -region moves away from the triacetin in water solution (at 0°C about 7% of triacetin is soluble in water). The extensive region

showing streaming birefringence is much diminished at 13°C. The origins of the streaming birefringence are presumably the same as in the  $C_{12}E_4-H_2O$   $\alpha$ -region. By 27°C the streaming birefringence is no longer observed. The  $\alpha$ -region has moved to higher surfactant content, is rather smaller in extent and no longer extends to the surfactant-water axis since the  $\alpha$ -region in the binary system does not occur at this temperature. At 37°C the  $\alpha$ -region has joined the  $\gamma$ -region. This behaviour is quite different to that in the ternary system with heptane. It bears more resemblance to the  $C_{12}E_6-H_2O$  system where the  $\alpha$ -region and  $\beta$ -region are joined to form a single extensive isotropic liquid region. If the triacetin is located with the oxyethylene chains this will tend to extend the water-oxyethylene chain medium (heptane extends the hydrocarbon medium) so that it is possible to maintain the normal micellar structure from high water content to high surfactant content with no break. Also triacetin does not favour the formation of the lamellar liquid crystalline phase. At 0°C the extent of the region exhibiting birefringence and therefore containing either liquid crystalline material or solid crystalline material (with or without other phases) is shown on the phase diagram (Fig. 4.23). In the heptane system the liquid crystalline phase occurred as one component of the system at much lower surfactant concentrations. This difference was also observed at higher temperatures.

### 5.5.1. Cont'd.

In the  $C_{12}E_4-H_2O$  system the lamellar liquid crystalline phase separates the  $\alpha$ - and  $\beta$ -regions.

#### The $\gamma$ -region

At  $0^\circ C$  the  $\gamma$ -region extends nearly to the  $C_{12}E_4-H_2O$  axis but only as far as 20% triacetin. This is quite different from the  $C_{12}E_4-H_2O$ -heptane system. As the temperature is increased the  $\gamma$ -region joins the  $\beta$ -region of the binary system. The tiny isotropic liquid region at the triacetin corner (water is slightly soluble in triacetin at  $0^\circ C$ ) (as is  $C_{12}E_4$ ) extends along the triacetin- $C_{12}E_4$  axis as the solubility of  $C_{12}E_4$  in triacetin increases with increasing temperature. Presumably triacetin and  $C_{12}E_4$  form some sort of molecular solution at higher triacetin content. At low triacetin content the normal micelles or smaller aggregates of  $C_{12}E_4$  plus around 10% water still exist with the triacetin in the continuous phase.

By  $20^\circ C$  the two parts of the  $\gamma$ -region have joined. The region still does not include many of the 10% water samples which are included in the  $\gamma$ -region in the  $C_{12}E_4-H_2O$ -heptane system. Sample 15 is just included in the  $\gamma$ -region at  $20^\circ C$ ; at higher temperatures sample 10 is included also. Samples 15 and 10 in the  $C_{12}E_4-H_2O$ -heptane system, are those that are thought to invert from water-oxyethylene chain continuous to oil-continuous

### 5.5.1. Cont'd..

with increasing temperature. Samples with lower  $C_{12}E_4$  content are thought to be oil-continuous and these do not give clear regions in the system with triacetin as third component. The  $C_{12}E_4$  does not appear to form inverted micelles with water as the core in triacetin. Since triacetin is likely to have little affinity with the dodecyl chain this seems reasonable.

In samples 10 and 15 either the triacetin is able to fit into the inverting structure (possibly bicontinuous) or the system does not invert and the surfactant remains as some sort of normal micelle with oxyethylene chains, water and triacetin forming the continuous phase. This phase can transform continuously to the molecular solutions of triacetin and  $C_{12}E_4$ .

#### The $\epsilon$ -region

This region is completely absent as might be expected from the above discussion, that is if the conclusions drawn from the  $C_{12}E_4$ -H<sub>2</sub>O-heptane system are correct. The  $\epsilon$ -region is thought to be an oil-continuous microemulsion. The equivalent triacetin system would consist of water in the droplets surrounded by surfactant with the oxyethylene chains in the water and the hydrocarbon chains in the continuous phase of triacetin; its occurrence was not observed.

The  $\delta$ -region

This is thought to be a water continuous micro-emulsion phase in the  $C_{12}E_4$ - $H_2O$ -heptane system. Again it was not found to occur in the triacetin system. The equivalent structure in the  $C_{12}E_4$ - $H_2O$ -triacetin system would be normal micelles with triacetin in the interior of the micelles with the hydrocarbon chains which is not likely. Triacetin is more likely to be localised with the oxyethylene chains as probably occurs in the extended  $\alpha$ -region. That the  $\alpha$ -region does not extend further to cover compositions of the  $\delta$ -region is probably due to the fact that sufficient surfactant oxyethylene chains would be required with which the triacetin could be associated: the  $\delta$ -region is of low surfactant content.

The  $\zeta$ -region

This first appears at much higher temperature than in the  $C_{12}E_4$ - $H_2O$ -heptane system and by  $60^\circ C$  it is still widely separated from the  $\gamma$ -region. Fig. 4.17 shows the effect of adding triacetin to 34.9%  $C_{12}E_4$ - $H_2O$ . The phase can accommodate very little triacetin; it can accommodate very much more heptane (Fig. 4.15) with an associated drop in its temperature of occurrence. Although the  $\zeta$ -phase is water continuous its structure remains unclear; it is thought to consist of aggregates of lamellar micelles in the water. Just as triacetin is not readily taken into the lamellar liquid crystalline

### 5.5.1 Cont'd.

phase but heptane is, so it is not readily taken into the  $\zeta$ -phase whilst heptane is. Perhaps the same factors are operating in the  $\zeta$ -phase as in the lamellar liquid crystalline phase. This behaviour tends to strengthen the evidence for some sort of lamellar micelle in the  $\zeta$ -region, associated with the lamellar liquid crystalline phase which occurs at slightly lower temperature than the  $\zeta$ -phase.

### 5.5.2 THE BRIJ 30-H<sub>2</sub>O-TRIACETIN SYSTEM

The only extensive isotropic liquid regions occurring in this system are the  $\gamma$ - and  $\zeta$ -regions (there is a small isotropic liquid region on the H<sub>2</sub>O-triacetin axis due to the solubility of triacetin in water)(Figs. 4.25 and 4.26).

#### The $\gamma$ -region

At 0°C only a tiny part of this region exists at the triacetin corner. There is no clear region near the Brij as in the case of C<sub>12</sub>E<sub>4</sub>, because of the higher melting point of components of the Brij.

By 5°C this high Brij content part of the  $\gamma$ -region has appeared. It joins the Brij-triacetin axis in a different manner because of the different binary phase diagram

The  $\gamma$ -region in the Brij-H<sub>2</sub>O-heptane system extends to low surfactant content sample numbers and relatively high water and oil content. This part of the  $\gamma$ -region is thought to be oil-continuous from the conductivity measurements. With triacetin as the third component this part of the  $\gamma$ -region was not observed. The same factors which prevent the oil-continuous phases occurring in the C<sub>12</sub>E<sub>4</sub>-H<sub>2</sub>O-triacetin system are likely to be operative here.

As the temperature is increased a salient develops pointing towards the water corner. This eventually joins the  $\zeta$ -region.

#### The $\zeta$ -region

This again occurs at higher temperature than in the equivalent system with heptane as the third component. Fig. 4.20 shows the effect of adding triacetin to 32.2% Brij-H<sub>2</sub>O. Although rather more triacetin can be accommodated than in the C<sub>12</sub>E<sub>4</sub> system it is still not nearly as large as the quantity of heptane which can be accommodated and the temperature of occurrence of the  $\zeta$ -region drops only slightly.

At 61°C the  $\zeta$ -region has joined the  $\gamma$ -region. In the Brij system the impurities and the mixture of oxyethylene chain lengths appear to enable more triacetin to be taken in to the  $\zeta$ -region. The gap between the

$\zeta$ -region and the  $\beta/\gamma$ -region in the  $C_{12}E_4$  system is not closed at  $60^\circ\text{C}$  in the presence of triacetin. In the Brij system no such gap exists and by  $61^\circ\text{C}$  the isolated  $\zeta$ -region has joined the  $\gamma$ -region.

#### The $\alpha$ -, $\delta$ - and $\epsilon$ -regions

The  $\alpha$ -region does not occur in the binary system or the ternary system with heptane; it was not observed in the ternary system with triacetin.

The  $\delta$ -region does not occur in the ternary system with heptane or in the  $C_{12}E_4$ - $\text{H}_2\text{O}$ -triacetin system so it is not expected in the present system.

Only a trace of the  $\epsilon$ -region exists in the ternary system with heptane. From the behaviour of the  $C_{12}E_4$ - $\text{H}_2\text{O}$ -triacetin system it would not be expected to occur in this system.

Only the  $\gamma$ -region is shown in the system Emu 09- $\text{H}_2\text{O}$ -tricaprylin (31) presumably at room temperature; Emu 09 is a commercial polyoxyethylene alkyl-aryl ether. The phase diagram is similar to that of Brij- $\text{H}_2\text{O}$ -triacetin at similar temperatures. Isotropic liquid regions occurring at high water content were not investigated by these authors. The 1-monocaprylin- $\text{H}_2\text{O}$ -tricaprylin system at  $20^\circ\text{C}$  (105) bears more resemblance to the Brij- $\text{H}_2\text{O}$ -triacetin system between  $30$  and  $40^\circ\text{C}$ .

In this system 1-monocaprylin is taking the place of a more usual surfactant. At 20°C the  $\gamma$ -region is beginning to extend into a narrow salient at this temperature though whether this develops at higher temperature or was connected to an  $\alpha$ -region at lower temperature, is not shown. There is a difference from the Brij-H<sub>2</sub>O-triacetin system, along the tricaprylin - monocaprylin axis because at 20°C the two do not form an isotropic liquid below 40% tricaprylin. Apart from the  $\gamma$ -region there is only a very small isotropic liquid region at the water corner.

## 5.6 CONCLUSIONS

The C<sub>12</sub>E<sub>4</sub>-H<sub>2</sub>O system has a low-temperature liquid region consisting of surfactant micelles in water. At high surfactant content the system is shown, by self-diffusion and conductivity measurements to be water-oxyethylene chain continuous; the aggregate size decreases with decreasing water content to small aggregates in the pure surfactant. A high-temperature water-continuous isotropic liquid region with a very narrow temperature range also exists above the melting point of the lamellar liquid crystal and extends to low surfactant content (2.5%). The structure of the surfactant aggregates remains unclear; it is such that both water self-diffusion and conductivity are reduced to a significantly greater extent, particularly at the

## 5.6 Cont'd.

lowest surfactant content, than would be expected if the surfactant formed normal micelles. In the  $C_{12}E_6-H_2O$  system the low temperature water-continuous micellar solution changes continuously to the high surfactant content system with smaller aggregates. The narrow high temperature region is absent.

In the Brij- $H_2O$  system the oxyethylene chain length distribution and impurities result in the low temperature water continuous region being absent. The high surfactant content region appears similar to that of the  $C_{12}E_4-$  and  $C_{12}E_6-H_2O$  systems. The narrow high temperature liquid region is wider and is continuous with the high surfactant content region. The structure of the narrow high temperature region appears to be similar to that of the narrow high temperature region in the  $C_{12}E_4-H_2O$  system; the variation in the concentration of the ions as the Brij concentration varies, and the unknown anion, renders interpretation of the conductivity results more difficult.

The  $C_{12}E_4-H_2O$ -hydrocarbon system produces an O/W microemulsion at low surfactant content and low temperature containing up to 60% (W/W) hydrocarbon. At higher temperature and similarly low surfactant content W/O microemulsions and bicontinuous phases occur depending on the hydrocarbon used, the longer hydrocarbon chain favouring bicontinuous structures. When the hydrocarbon

is hexadecane the O/W microemulsion changes continuously to a bicontinuous structure. The self-diffusion results of Lindman et al (70) indicate that both water and hydrocarbon are continuous; whilst the conductivity results are in agreement with this it is not possible to distinguish, on the basis of conductivity alone, systems which are water continuous with some restriction of conductivity, bicontinuous systems and oil-continuous systems where conduction takes place by a percolation mechanism. When the hydrocarbon is heptane the low temperature O/W microemulsion is not continuous with the higher temperature microemulsion for which conductivity results provide unequivocal evidence of an oil-continuous structure at its highest temperatures of occurrence; at similarly low surfactant content to the O/W microemulsion, the W/O microemulsion extends to 60% water. As the temperature is reduced the conductivity of the W/O microemulsion increases to a similar order of magnitude to that of a water-continuous or bicontinuous structure. It is possible to explain this abnormally high (for an oil-continuous system) conductivity by a percolation mechanism, occurring when the aggregate structure changes without invoking phase inversion within the isotropic liquid phase. When the hydrocarbon is decane the behaviour is intermediate between that of the systems containing hexadecane and heptane: the two microemulsion regions are separate but the conductivity at

the highest temperatures of the upper region does not decrease to the very low values observed at the highest temperatures of the oil-continuous microemulsion of the heptane system.

The narrow high temperature clear region of the  $C_{12}E_4-H_2O$  system extends into the ternary system as heptane is added, occurring at lower temperature with increasing heptane content, but remaining narrow with respect to both composition and temperature. The low temperature water-continuous micellar system can only take a small amount of heptane ( $< 3\%$ ) before phase separation occurs.

At low water content the  $C_{12}E_4-H_2O$ -heptane system changes continuously from water-oxyethylene chain continuous at high surfactant content, to oil-continuous at high hydrocarbon content. Whilst these changes are reflected in the conductivity results, evidence from other methods of investigation is needed to elucidate the structures involved.

Replacement of  $C_{12}E_4$  by Brij results in the loss of the water-continuous microemulsion at low surfactant content and a severe reduction in the W/O microemulsion, a remnant of which occurs at slightly higher surfactant content. The W/O phase is more extensive at high oil-content. These differences can be ascribed to the mixture of chain lengths in the Brij and the impurities

## 5.6 Cont'd.

present. At low water content there is again a continuous evolution from water-oxyethylene chain continuous to oil-continuous with increasing oil content (in this case hexane); conductivity results suggest that the structural changes do not follow exactly the same pattern as in the case of the pure surfactant. The narrow high temperature clear region behaves similarly to that in the  $C_{12}E_4-H_2O$ -heptane system, remaining slightly wider than in the pure surfactant system, as it does in the binary system.

When the third component is triacetin, which is more likely to partition with the oxyethylene chains than with the hydrocarbon chains, the O/W and W/O micro-emulsions at low surfactant content do not occur. The oil-continuous regions do not occur except for essentially molecular solutions of triacetin plus surfactant containing little water. The narrow high temperature region is much reduced in the pure surfactant system but not in the Brij system. The low-temperature water-continuous micellar solution of the  $C_{12}E_4-H_2O$  system is extended by the addition of triacetin and joins the high surfactant content region.

Without further information from other methods of investigation it is not possible to make more than tentative suggestions concerning the structures of many of the isotropic liquid phases. Conductivity results may

## 5.6 Cont'd.

show whether oil or water is the continuous phase but this is not always the case. Where self-diffusion measurements are also available the continuous phase or phases can be determined but detailed structures are still not known.

## REFERENCES

1. S. Friberg, L. Rydhag and T. Dea Lyotropic Liquid Crystals, Symposium Proceedings - Stockholm (A.C.S. Advances in Chem., No. 152, Washington D.C., 1976) Chap. 3.
2. K. Shinoda, T. Nakagawa, B.J. Tamamushi and T. Isemura, Colloid Surfactants, ed. K. Shinoda (Academic Press, New York, 1963), chap. 1.
3. H-G Elias, J. Macromol. Sci - Chem., 1973, A7(3),601
4. C. Tanford, Y. Nozaki and M.F. Rohde J. Phys. Chem., 1977, 81 (16), 1555.
5. D.I.D. El Eini, B.W. Barry and C.T. Rhodes J. Colloid Interface Sci., 1976, 54 (3), 348
6. H. Schott, J. Colloid Interface Sci., 1967 24 193
7. F. Harusawa, S. Nakamura and T. Mitsui Colloid Polm. Sc., 1974, 252, 613.
8. E. J. Staples and G.J.T. Tiddy, J. Chem., Soc. Far. Trans. I, 1978, 74, 2530
9. G.J.T. Tiddy Phys. Rep., 1980, 57 (1).
10. G.J.T. Tiddy (Unilever Research, Port Sunlight Laboratory). Private communication.
11. P. Becher and S. Tahara, Chem. Phys. Chem. Anwendungstech Grenzflachenaktiven Stoffe, Ber.Int.Kongr. 6th, 1972 (Carl Hauser Verlag, Munich, 1973) vol. 2, part 2, p519.
12. K. Shinoda and H. Arai J. Phys. Chem. 1964 68 (12) 3485
13. K. Shinoda and H. Takeda J. Colloid Interface Sci., 1970 32 (4) 642

REFERENCES Cont'd.

14. J. H. Schulman, W. Stoeckenius and L.M. Prince  
J. Phys. Chem., 1959, 63, 1677.
15. L. M. Prince, Microemulsions, ed. L.M. Prince,  
(Academic Press, New York 1977), Chap. 2.
16. T. P. Hoar and J. H. Schulman, Nature 1943, 52, 102
17. L. M. Prince, ref. 15, chap. 1.
18. V. K. Bansal and D.O. Shah, ref. 15, chap 7.
19. S. Friberg, Chem. Tech., 1976, 124.
20. K. Shinoda and H. Kunieda  
J. Colloid Interface Sci., 1973, 42, 381
21. G. D. Smith, C.E. Donelan and R.E. Barden  
J. Colloid Interface Sci., 1977, 60 (3) 488
22. G. Gillberg, L. Eriksson and S. Friberg,  
Emulsions, Latices and Dispersions, eds. Becher and  
Yudenfreund (Marcel Dekker, New York, 1978)
23. T. Nakagawa, Nonionic Surfactants, ed. M.J. Schick  
(Edward Arnold, London, 1967).
24. H. Saito and K. Shinoda,  
J. Colloid Interface Sci., 1967, 24, 10.
25. K. Shinoda and H. Kunieda, ref. 15, chap. 4.
26. K. Shinoda and H. Saito, J. Colloid Interface Sci.,  
1968, 26, 70.
27. K. Shinoda and H. Sagitani  
J. Colloid Interface Sci., 1978, 64 (1), 68.
28. K. Shinoda and S. Friberg  
J. Colloid Interface Sci., 1975, 4, 281.
29. S. Friberg and I. Lapczynska  
Prog. Colloid Polym. Sci., 1975, 56, 16.

REFERENCES Cont'd.

30. L. M. Prince, ref. 15, p48.
31. S. Friberg and L. Rydhag  
J.Am.Oil Chem. Soc., 1971, 48, 113.
32. J.H. Schulman and J.A. Friend,  
J.Soc. Cosmet Chemists, 1949, 1, 381.
33. J.B. Brown, I. Lapczynska and S. Friberg,  
Proc. Int. Conf. Colloid Surf. Sci., ed. Wolfram  
(kiado, Budapest, 1975) vol. 1, p.507.
34. M. Zulauf and H-F Eicke  
J.Phys.Chem., 1979, 83(4), 480.
35. M. Baviere,  
Revue L Institut Francais du Petrole, 1974, XXIX, 41.
36. K. Shinoda and S. Friberg  
Adv. Colloid Interface Sci., 1975, 4, 281.
37. L. M. Prince, ref. 15, chap. 5.
38. T. Okazawa and J. Bron,  
J. Colloid Interface Sci., 1979, 69 (1), 86.
39. L. M. Prince, ref. 15, p106.
40. e.g. E. Ruckenstein and J. C. Chi,  
J. Chem. Soc. Faraday 2, 1975, 71 (10), 1690
41. H-F Eicke  
J. Colloid Interface Sci., 1977, 59 (2), 308
42. E. Ruckenstein, Micellization, Solubilization and  
Microemulsions, ed. K.L. Mittal, (Plenum Press, New  
York, 1977) vol. 2, p.755.
43. M. L. Robbins, ibid, p713.
44. Y. Talman and S. Prager,  
Nature, 1977, 267, 333.

REFERENCES Cont'd.

45. R.N. Healy, R.L. Reed and D.G. Stenmark  
Soc. Petrol. Engng. J., 1976, 16, 147.
46. W. Gerbacia, H. L. Rosano and J.H. Whittam,  
Proc. 50th Colloid and Surface Science Symposium,  
Puerto Rico, 1976, ed. M. Kerker, (Academic Press  
Inc., 1976) vol. 2, p245.
47. H.L. Rosano,  
J. Soc. Cosmet. Chem., 1974, 25, 609.
48. W. Gerbacia and H.L. Rosano,  
J. Colloid Interface Sci., 1973, 44(2), 242.
49. J. Th. G. Overbeek,  
Faraday Disc. Chem. Soc., 1978, 65, 7.
50. M. Rosoff and A. Giniger  
ref. 46, Vol. V, p.475.
51. L. E. Scriven  
Nature, 1976, 263, 123.
52. P. Lalanne, J. Biais, B. Clin, A-M Bellocq and  
B. Lemanceau, C.R. Acad., Sci., Paris, Ser.C  
1978, 286, 55.
53. F. Larche, J. Rouviere, P. Delord, B. Brun and  
J.L. Dussosoy.  
J. Phys. Lett., 1980, 41(18), 437.
54. A. Skoulios and D. Guillon  
J. Phys. Lett., 1977, 38, 137.
55. A. A. Giniger,  
Ph.D. Thesis, Columbia University, Univ.Microfilms,  
75-27,416.

REFERENCES Cont'd..

56. S.I. Ahmad, K. Shinoda and S. Friberg,  
J. Colloid Interface Sci., 1974, 47 (1), 32.
57. L. M. Prince, ref. 15, p10.
58. S. Ballara, F. Mallamace and F. Wanderlingh,  
Optics Comms., 1978, 25 (2), 144.
59. J. W. Falco, R.D. Walker, Jr., and D.O. Shah.  
A.I.Ch.E. J., 1974, 20(3), 510.
60. C. Kumar and D. Balasubramanian,  
J. Colloid Interface Sci., 1979, 69(2), 271.
61. G.D. Smith, C.E. Donelan and R.E. Barden,  
J. Colloid Interface Sci., 1977, 60(3), 488.
62. R.N. Hwan, C.A. Miller and T. Fort Jr.,  
J. Colloid Interface Sci., 1979, 68(2), 221.
63. M. Dvolaitzky, M. Guyot, M. Lagues, J.P. Le Pesant,  
R. Ober, G. Sauterey and C. Taupin, J. Chem.Phys.,  
1978, 69 (7), 3279.
64. C. Kumar and D. Balasubramanian,  
J. Colloid Interface Sci., 1980, 74, (1), 64.
65. C. Kumar and D. Balasubramanian  
J. Phys. Chem. 1980, 84, 1895.
66. B.A. Keiser, D. Varie, R.E. Barden and S.L. Holt,  
J. Phys. Chem., 1979, 83 (10), 1276
67. D.O. Shah, Ann.N.Y. Acad. Sci., 1973, 204, 125.
68. D.O. Shah, A. Tamjeedi, J.W. Falco and  
R.D. Walker, Jr., A.I. Ch.E. J., 1972, 18(6), 1116.
69. D.O. Shah and R.M. Hamlin, Jr., Science 1971, 171, 483.

REFERENCES Cont'd.

70. B. Lindman, N. Kamenka, T-M Kathopoulos, B. Brun  
and P.G. Nilsson,  
J. Phys. Chem. 1980, 84 (19), 2485.
71. R.A. Mackay and R. Agarwal  
J. Colloid Interface Sci., 1978, 65 (2), 225.
72. G. Roux and A. Viallard  
J. Colloid Interface Sci., 1977, 62(2), 295.
73. M. Lagues, R. Ober and C. Taupin,  
J. Phys. Lett. 1978, 39 (24), 487
74. S. Kirkpatrick,  
Rev.Mod.Phys., 1973, 45 (4), 574
75. M. Lagues and C. Sauterey  
J. Phys. Chem. 1980, 84, 3503.
76. B. Lagourette, J. Peyrelasse, C. Bøned and  
M. Clause, Nature 1979, 281, 60.
77. J.S. Clunie, J.F. Goodman and P.C. Symons  
Trans. Faraday Soc., 1969, 65, 287.
78. R.M. Fuoss,  
J. Solution Chem., 1978, 7 (10), 771.
79. P. Sherman, Emulsion Science, ed. P. Sherman  
(Academic Press, London, 1968) p.320.
80. T. Hanai, ref. 79, p379.
81. T. Hanai, ref. 79, p417.
82. I.D. Chapman,  
J. Phys. Chem., 1968, 72, 33.
83. M. Clause, P. Sherman and R.J. Sheppard,  
J. Colloid Interface Sci., 1976, 56 (1), 123.

REFERENCES Cont'd.

84. I. Webman, J. Jortner and M. H. Cohen,  
Phys. Rev. B., 1975, 11 (8), 2885.
85. E.O. Stejskal  
Advan. Mol. Relaxation Processes 1972, 3, 27.
86. A. Wieslander, L. Rilfors, L.B.A. Johansson and  
G. Lindblom Biochemistry, 1981, 20, 730.
87. G.J.T. Tiddy, J.B. Hayter, A.M. Hecht and  
J.W. White.  
Bev. Bunsen. P.C., 1974, 78 (9), 961.
88. T.A. Bostock, M.P. McDonald, G.J.T Tiddy and L.  
Waring. Surface Active Agents Symp. (Soc. Chem.  
Ind. Nottingham, 1979, p181).
89. J.M. Corkill, J.F. Goodman and R.H. Ottewill,  
Trans. Faraday Soc., 1961, 57, 1627.
90. T.A. Bostock, M.P. McDonald and G.J.T. Tiddy,  
Chem. Soc. - Faraday Div., Colloid Interf Sci Group,  
Informal discussion, Hull, 1978.
91. G.J.T. Tiddy,  
Unilever Research, Port Sunlight Laboratory, Private  
communication.
92. R. R. Balmbra, J.S. Clunie, J.M. Corkill and  
J. F. Goodman, Trans. Faraday Soc. 1962, 58, 1661.
93. R.H. Ottewill, C.C. Storer and T. Walker,  
Trans. Faraday Soc., 1967, 63, 2796.
94. J.M. Corkill and T. Walker  
J. Colloid Interface Sci., 1972, 39 (3), 621.
95. C. Tanford  
J.Phys. Chem. 1974, 78 (24), 2469.

REFERENCES Cont'd.

96. M. H. Boyle, Sheffield City Polytechnic,  
Private communication.
97. T.A. Bostock, M.H. Boyle, M.P. McDonald and  
R.M. Wood,  
J. Colloid Interf. Sci., 1980, 73, 368.
98. G.J.T. Tiddy, Unilever Research, Port Sunlight  
Laboratory, P. Jones and E. Wyn-Jones, Salford  
University unpublished results.
99. S. Friberg and I. Wilton  
Am. Perfumer Cosmetics, 1970, 85, 27.
100. I.G. Lyle and G.J.T. Tiddy, Unilever Research, Port  
Sunlight Laboratory, unpublished results.
101. I. Lo, F. Madsen, A.T. Florence, J-P Treguier,  
M. Seiller and F. Puisieux, ref. 42, Vol. 1, p455.
102. J. Peyrelasse, V.E.R. McClean, C. Boned, R.J.  
Sheppard and M. Clause  
J. Phys. D.: Appl. Phys., 1978, 11, L117.
103. Ref. 23, p513.
104. M. H. Boyle, M.P. McDonald, P. Rossi and R.M. Wood,  
to be published.
105. S. Friberg and L. Mandell  
J. Am. Oil Chemists' Soc. 1970, 47, 149
106. J.S. Murday and R.M. Cotts, J. Chem. Phys. 1970,  
53, 4724.
107. T. Miura and M. Nakamura, Bull. Chem. Soc. Japan, 1977,  
50 (10), 2528.

## ACKNOWLEDGEMENTS

I would like to thank my supervisor, Dr. M. P. McDonald for his assistance throughout the course, also my industrial supervisor, Dr. G. J. T. Tiddy, for assistance with the work carried out at Port Sunlight and many helpful discussions. I would like to thank Unilever Research for the use of their facilities at the Port Sunlight Laboratory, in particular the Bruker NMR spectrometer. Finally I would like to thank my husband without whose assistance in this thesis would never have been written.

This work was supported by an S.R.C. CASE award.

Lecture courses attended.

Sheffield City Polytechnic

Liquid Crystals - Dr. M. P. McDonald

Sheffield University

Interfaces - Dr. I. A. McLure and Dr. R. N. Young

NMR and ESR Theory - Prof. N. M. Atherton